PAPER NO: IAF-90-292

DYNAMICS AND CONTROL OF MULTIPAYLOAD PLATFORMS: THE MIDDECK ACTIVE CONTROL EXPERIMENT (MACE)

David W. Miller
Space Engineering Research Center
Massachusetts Institute of Technology
Cambridge, MA USA

Javier de Luis
Payload Systems Inc.
Cambridge, MA USA

Edward F. Crawley
Space Engineering Research Center
Massachusetts Institute of Technology
Cambridge, MA USA

41st CONGRESS OF THE INTERNATIONAL ASTRONAUTICAL FEDERATION

October 6-12, 1990/Dresden, GDR

DYNAMICS AND CONTROL OF MULTIPAYLOAD PLATFORMS: THE MIDDECK ACTIVE CONTROL EXPERIMENT (MACE)

David W. Miller*
Space Engineering Research Center
Massachusetts Institute of Technology
Cambridge, MA USA

Javier de Luis+
Payload Systems Inc.
Cambridge, MA USA

Edward F. Crawley#
Space Engineering Research Center
Massachusetts Institute of Technology
Cambridge, MA USA

ABSTRACT

A flight experiment entitled the Middeck Active Control Experiment (MACE) proposed by the Space Engineering Research Center (SERC) at the Massachusetts Institute of Technology is described. The objective of this program is to investigate and validate the modeling of the dynamics of an actively controlled flexible, articulating, multibody platform free floating in zero gravity. A rationale and experimental approach for the program are presented. The rationale shows that on-orbit testing, coupled with ground testing and a strong analytical program, is necessary in order to fully understand both how flexibility of the platform affects the pointing problem, as well as how gravity perturbs this structural flexibility causing deviations between 1- and 0-gravity behavior. The experimental approach captures the essential physics of multibody platforms, by identifying the appropriate attributes, tests, and performance metrics of the test article, and defines the tests required to successfully validate the analytical framework.

INTRODUCTION

Large spacecraft have become the focus of intense scientific and engineering research in recent years. Beginning with Space Station Freedom, spacecraft will no longer be restricted to the mass and volume limits imposed by a single launch vehicle. Instead, they can be assembled on-orbit, using astronauts on EVA or telerobotic equipment. These Large Space Structures (LSS) will have increasingly stringent pointing or shape requirements, and a simultaneous reduction in their structural mass and associated stiffness. It will often be impossible to fully test such a structure on the ground before its operational deployment. Therefore, the question that must be dealt with is how can confidence in the designer's ability to predict the on-orbit structural dynamic behavior of such spacecraft be increased in order to assure operational success of its mission? The answer implies the development of an effective and efficient LSS *qualification* procedure.

Figure 1 shows the possible *qualification* tests that can be performed on a spacecraft in order to characterize its on-orbit open and closed-loop structural dynamic behavior. Each cell in the matrix corresponds to a test or accurate analysis which the designer must be capable of performing before *qualifying* the operational vehicle. The least expensive test, a scaled test of a spacecraft component performed in atmosphere on the ground, is in

---

* Research Associate, Member AIAA
+ Staff Scientist, Member AIAA
# Professor of Aeronautics and Astronautics, Member AIAA

the upper left corner. The most expensive test, a full scale 0-g test performed in vacuum, is in the lower right corner. The goal is to develop the most efficient sequence of tests and analyses, in this matrix, which leads to a high level of confidence in the performance of the operational vehicle.

The goal of the Middeck 0-gravity Dynamics Experiment (MODE) family of flight experiment facilities, conducted by the MIT Space Engineering Research Center, is to explore the gravity-dependent aspects of this matrix in order to *develop* the analytical tools and test sequences necessary to conduct an effective and efficient spacecraft *qualification* procedure. This *development* is accomplished through a series of small, relatively inexpensive flight experiments conducted in the interactive shirtsleeve environment of the Space Shuttle Middeck.

		1 - g		0 - g	
		Component	Ensemble	Component	Ensemble
1 Atmos.	Subscale	MODE	MODE	MODE	MODE
	Fullscale	Contractor Tests	May Not Be Practical	May Not Be Practical	Not Practical
Vacuum	Subscale				
	Fullscale	May Not Be Practical	Not Practical		Operational Vehicle

Figure 1   Qualification test matrix for structural dynamic characterization of spacecraft

MODE-1, which is to be flown in August 1991, will conduct a series of open-loop dynamic experiments on fluid tanks, deployable and erectable trusses, flexible appendages, and rotary joints typical of future spacecraft.[1] MODE-1 is funded under the NASA OAET In-Step program.

MODE-2, which is to be flown in September 1993, is a reflight of the MODE-1 instrumentation with the new Middeck Active Control Experiment (MACE) test article.[2] It will continue the work begun in MODE-1 but will extend it to include structures utilizing Controlled Structures Technology (CST). CST uses active control

CONTENTS

OVERVIEW

The Space Engineering Research Center (SERC) at MIT, started in July 1988, has completed two years of research. The Center is approaching the operational phase of its first testbed, is midway through the construction of a second testbed and is in the design phase of a third. We presently have seven participating faculty, four participating staff members, ten graduate students and numerous undergraduates.

This report reviews the testbed programs, individual graduate research, other SERC activities not funded by the Center, interaction with non-MIT organizations, and SERC milestones. Published papers made possible by SERC funding are included at the end of the report.

Testbed Program

OPTICAL INTERFEROMETER TESTBED

The first of the MIT SERC testbeds is based on a design for a 35 meter space-based optical interferometer, chosen for the stringent alignment and structural control requirements placed on such a structure by scientific mission objectives. At the time of the last report, a scaled 3.5 meter tetrahedral truss frame had been assembled and suspended in the laboratory, and optical component design was underway for an internal laser metrology system capable of measuring structural misalignment to an accuracy of 10 nanometers. At the time of this writing, the construction and integration of testbed optics, sensors, real time computer, and support hardware is well underway, and preliminary tests have been performed on the structure. The reader is referred to a full description of the state of the testbed in the publication *MIT's Interferometer Testbed* (included at the back of this report), prepared in August for inclusion in the proceedings of the JPL Workshop on Technologies for Space Interferometry, which two students attended in April. A brief summary is presented here to highlight the areas of activity for the testbed.

Optics: Hardware for a six-axis laser metrology system has been installed in the tetrahedral truss to measure internal pathlength changes due to structural flexibility. A 670 μWatt HP laser and beam steering optics are mounted to a truss vertex and powers optical measurement legs to three (cat's eye) retroreflectors at distant locations in the truss. Ambient laboratory disturbances measured by one optical leg are approximately 20 nm rms (broadband) which is 2-3 times below the desired closed-loop stability level (in the presence of scaled disturbances) dictated by our performance metric.

Control Hardware: Three piezoelectric struts have been integrated to the truss with a suite of collocated sensors. Active piezoelectric mounts are under construction for the three cat's eye retroreflectors, which will be used for output compensation in the range of +/- 5 μm. Software is being written for a VME based real time control computer capable of handling 32+ states at sample rates of up to 2 kHz; the hardware for this system is complete and can handle a total of 16 inputs and 10 outputs.

System Identification: A multichannel spectrum analyzer and a suite of 32 accelerometers has been integrated to the testbed and used to perform a system identification of the "naked truss" frame. The data indicates very low damping (.1% and lower) and tightly spaced modes occuring in clumps.

Finite Element Model: A 228 node finite element model predicts a frequency of the first mode that is in 10% error with results of the system ID test. The model is being updated, and is being utilized for controllability and observability studies used for sensor and actuator placement.

Passive Damping: Several truss members have been constructed with viscoelastic material and will be installed in the truss to establish a nominal level of damping in the testbed. The struts are being tested in a axial component tester constructed during the summer.

Control Experiments: Local analog loops using velocity feedback have been closed around active members with acceptable results.

During the next six months, the interferometer testbed will be completed and will enter the research phase of use by graduate students. In particular, the following issues will be addressed:

1) completion of all six legs of the laser metrology system

2) integration and testing of active mirror mounts

3) real time computer software

4) integration of a scaled disturbance source

5) system identification and finite element correlation of the naked truss, followed by a system identification of the completed truss.

6) passive damping treatment

MULTIBODY TESTBED

Work is proceeding on the ground version of the Middeck Active Control Experiment (MACE). For details, see the next section. This experiment is designed to study the behavior of structures that utilize active control to modify their dynamics and whose structural characteristics change between 1- and 0-g environments. SERC has selected a ground based engineering model of the MACE test article as the Center's second testbed. This will function as the basis for a flight experiment on the STS Middeck in 1994.

Structure: This Engineering Model structural bus consists of four flexible Lexan, tubular segments interconnected to the other test article elements at five rigid, metallic nodes. A gimballed payload will be located at each end of the bus. The gimbals rotate in two axes (pitch and yaw but no roll about payload line-of-sight). Rigid body control is supplied by three orthogonally oriented torque wheels located at the center of the bus. The ensemble will be suspended from three CSA zero-g suspension devices. The test article is shown in the figure below.

Sensors: Baseline sensors located along the bus include three 3-axis rate gyro packages and three tri-ax accelerometer units, each of which can be attached to any node of the bus. Four Strain gauges will be bonded to each strut, a load cell will be attached between the test article and each of the suspension devices, and optical encoders will be attached to the gimbal motors.

Types of control tests: Tests on the engineering model will consist of pointing, scanning and multiple control system interaction. Pointing involves active reduction of two-axis stability and jitter of one payload reacting against the flexible structure. Scanning involves active reduction of two-axis angular deviation from a reference scanning profile. Multiple interaction tests involve simultaneous pointing and scanning of both payloads.

Hardware status: All hardware, sensors, and actuators slated to be used on the MACE EM have arrived with the exception of the active bending

segment, the gimbals, and the CSA suspension devices. The active segment will consist of a square Lexan rod with piezoelectric ceramic mounted on its edges. It is in the final design stages and will replace one of the passive segments and provide localized bending in the structure. The first gimbal is currently being assembled at LSMC, and is expected for delivery in mid-December. LSMC is providing support to the MACE over the next two fiscal years in the development of the EM and control methodologies, and in the redesigns of the gimbal actuators. The CSA suspension devices are in the final stages of the manufacturer's testing and are also expected for delivery in mid-December.

Instrumentation and signal conditioning equipment have been acquired and are in the final stages of integration with the AC-100 Real-Time computer we have purchased and received. The AC-100 in conjunction with the CSA suspension devices will serve as a zero-g simulation and real-time digital control facility after its initial responsibility of supporting the MACE program.

Present work: Work is continuing to study control issues involves with the MACE. The attached paper entitled"Dynamics and Control of Multipayload Platforms: The Middeck Active Control Experiment (MACE)" was delivered at the CSI conference in Dresden, GDR in early October. Also included at the back of this report is the set of annotated viewgraphs entitled "The MODE Family of On-Orbit Experiment: The Middeck Active Control Experiment (MACE)" which was presented at the 1990 CSI Conference. A matrix of possible control methodologies has been developed to be included in the sample problem we have issued to various CSI experts for their analysis and input.

Open-loop Identification: Dynamic testing of the MACE EM has been initiated with the results being used to verify a NASTRAN model also being developed. A fully representative model is expected to be completed by the end of January to coincide with expected completion of the EM testbed. At that point closed-loop testing will begin.

Multibody testbed test article.
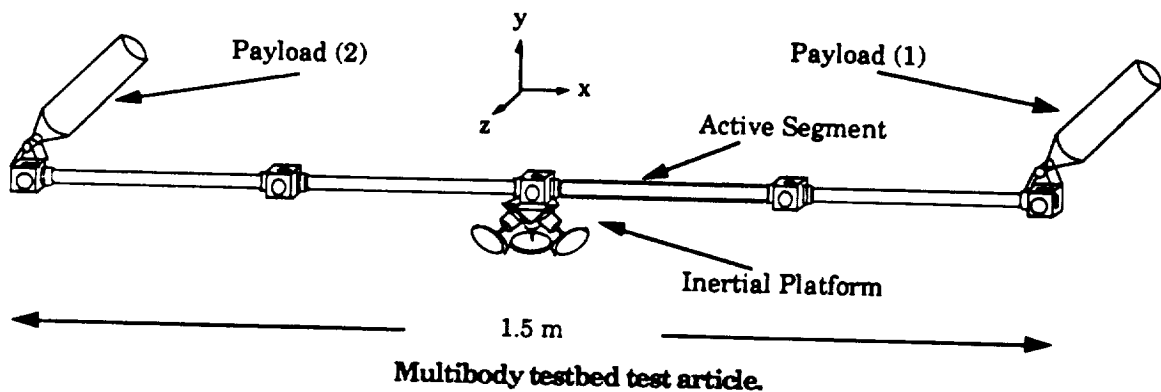
Research Programs

This section gives a discussion of the individual graduate research programs that are funded through the M.I.T. SERC grant. Each discussion is composed of a description of progress made during the last six months and expected progress to be made during the next six months. In addition, a specific testbed affiliation is listed under the researcher's names to indicate the motivation for the research. The phrase *general affiliation* implies that the research is not tied to a specific testbed.

DESIGN OF STRUCTURES FOR CONTROL

Mr. Robert N. Jacques and Dr. David W. Miller

(Interferometer Testbed)

In the past, the design of the structural and control subsystems of spacecraft has been done independently, with control design taking place late in the design process. However, as new space structures become larger, and pointing and alignment requirements become tighter, many flexible modes of the spacecraft will have frequencies inside the needed bandwidth of the controller. The resulting interaction of the structure with the control is very strong and argues against designing these subsystems separately. Currently, the approach to this problem is to use a computer program which iterates over a precisely defined set of structural and control design variables (e.g. sizing of members in a truss, or controller gains) to find a design which optimally meets one or several objectives such as minimum structural mass or RMS motion. The difficulty with this approach is that even when an optimal design is obtained, there is very little insight into why it is optimal. This understanding is crucial in the very early stages of design when many possible design options prohibit formal optimization. Even when a computer program is to be used in the design of the system, engineering insight is needed in selecting the general layout of the system and the design variables. The work done here is an attempt to take a step back from numerical optimization of these systems and develop some "rules of thumb" which can be used in the preliminary design of a controlled structure.

Currently, the approach has proceeded in two parts. In the first part, very simple controlled structures were used to study some of the fundamental aspects of the interaction of the structure with the control. These were simple spring-mass-dashpot systems. The advantage of this simple model is that it is analogous to the interaction of a controller and disturbance with a single mode of a structure, and its simplicity makes it possible to derive the optimal control gains in closed form. This made it possible to obtain analytic expressions for the performance of the system. From analysis of these typical sections, an initial set of design rules of thumb was developed. The second part of the approach used a finite element Bernoulli-Euler beam as a design example. Structural design parameters (such as element thicknesses) and control of this beam were optimized numerically for different problem formulations. The goal was to see if the designs suggested by the typical sections were similar to the numerically optimal designs.

6

Some of the conclusions revealed by this approach have been quite interesting. The first concerns the role of damping in a controlled structure. It was found that in a perfectly modelled system, passive damping is very important when no control is used, however as the level of control is increased, the need for passive damping eventually vanishes. This was because at higher levels of control, the damping tended to resist the control force instead of aiding it. However, when the control is designed for a structure that has unmodelled dynamics, it was found that the damping was extremely important in the unmodelled modes, particularly at high gain. A second conclusion was that the most common way to optimize a structure was to make it less sensitive to disturbances, as opposed to letting the disturbance into the structure and trying to control it out. When the disturbances were step loads, this implied that the structure should be made very stiff to reduce its displacement due to these loads, and when the disturbances were impulses or white noise, the structure should be made to have high inertia where the disturbances are applied. Third, it was found, that the design strategy one should use can depend on the amount of control effort available. Other methods for improving the controlled performance, such as making the structure more sensitive to actuation were found to help only in very special cases.

In the future, several areas still need to be investigated. The beam example used was very simple. It remains to be shown that the rules of thumb can be used on a more complex system. The SERC interferometer testbed is a good candidate for this analysis. Computer models of the structure have been developed. Also, it will be possible to perform experiments on the actual testbed to verify the results of computer analysis. Another area that needs to be investigated is the effect of controller type on design strategy. So far, the controllers used in this research have been optimal LQR/LQG. These controllers work very well in perfectly modelled systems, but have been shown to have some serious short comings in the way of robustness. Actual MIMO controllers used on space structures will probably be based on H∞ methods. Their influence on structural design will be important.

A STATISTICAL MODELLING APPROACH FOR BROADBAND CONTROL OF UNCERTAIN STRUCTURES

Mr. Douglas G. MacMartin and Prof. Steven R. Hall

(Interferometer Testbed)

BACKGROUND

The goal of this research is to develop a methodology for designing optimal active control systems for broadband control of uncertain flexible structures. Thus a control system is required which will give good performance over many modes, while being robust to parametric uncertainties in these modes. Rather than modelling the detailed modal behaviour of the structure using state space based methods, it may be more useful to model only some statistical aspects of the response. One approach that uses this philosophy is Statistical Energy Analysis, and the modelling assumptions from SEA will also be used in this research. It is assumed

that the individual modal amplitudes are not important, and that only the modal energies, averaged over some number of modes, are important. The cost can be related to these energies, and the energy can be related to the power input and dissipation using conservation of energy.

In order to apply this, the power flow from the structure to the control system is required. A power flow model of the structure can be developed using a dereverberated mobility description, which accurately models the local dynamics of the structure near the sensor/actuator pair. This leads to a characterization of the closed loop dynamics via a transfer function H, defined such that $H*H$ is the relative power reflected into the structure, and $I-H*H$ is the relative power dissipated. The transfer function H is analagous to a reflection coefficient in a 1-D waveguide, where the amplitude of the outgoing wave is $H\omega_i$ for an incoming wave ω_i. Since power is quadratic, the outgoing wave has power $H*H$ for an incoming wave of unit power.

Combining this model with the assumptions inherent in Statistical Energy Analysis, the cost functional which reflects the best estimate of the true performance metric of interest is

$$J = \int_{-\infty}^{\infty} C(\omega) tr\left\{\left[(I - H*H)^{-1} H*H\right]\right\} \Pi_{in}(\omega) d\omega$$

where C measures the cost associated with the modes in each frequency band, and Π_{in} measures the power input from external disturbances in each frequency band.

COST FUNCTIONAL MINIMIZATION

This cost functional combines aspects of both the $\mathcal{H}_2$ and $\mathcal{H}_\infty$ problems. Much of the research to date has focused on finding an approach for obtaining compensators that minimize this cost functional. Preliminary results are summarized in [1] which is included at the back of this report.

One approach to optimizing the cost functional is based on finding the necessary conditions using a Lagrange multiplier approach. The cost can be evaluated using a single Riccati and a single Lyapunov equation. For a given, fixed, compensator order, the Riccati and Lyapunov equations required to evaluate the cost can be appended to the cost using Lagrange multipliers, and the first variation of this augmented cost set to zero. The necessary conditions are easily obtained from this approach, but they are difficult to simplify and understand. In the $\mathcal{H}_2$ or LQG problem, the conditions for a fixed-order compensator are simplified greatly by introducing a projection operator [3]. This operator is difficult to identify for this problem due to the structure of the necessary conditions, resulting in what is known as a "double A_c problem." This results because the dynamics of the compensator appear in the problem twice: once in the Riccati equation and once in the Lyapunov equation that is used to evaluate the cost.

There are a number of simpler such "double A_c" optimization problems, and the solution of these should help indicate how to solve the current optimization problem. Three such problems were investigated; these are the multi-model fixed-order approximation, estimation and control problems. One compensator (or estimator, or approximate) is

8

desired, to be applied to a finite set of models. This approach can be applied to give robustness to parametric uncertainty, by choosing a finite number of different models to represent the range of parameter variation. It is also applicable to certain fault tolerance applications, where there may actually be a finite set of models which are possible. The multi-model approximation and estimation problems have been solved by identifying an appropriate projection operator, and in both of these, there is a maximum order for the approximant or estimator that is optimal [2] (also included in the back of this report). For the optimal control problem, there is no *a priori* bound on the order of a compensator which is optimal, and this is directly related to the difficulty in analyzing the necessary conditions. This result is also (apparently) true for our problem.

Another related problem is that of finding a stable compensator that optimizes an $\mathcal{H}_2$ performance. (Note that the optimal compensator for a given system might not be stable.) This problem can be formulated so that it has the same "double A_c" structure as the multi-model control problem, and the cost functional in Equation (2). A variety of researchers have investigated this problem in the past, without obtaining a particularly satisfactory algorithm. One conclusion of this body of research is that for a finite order, rational plant, the optimal compensator may be irrational. A rational (state space) approximation of this compensator must be of arbitrarily high order.

There is, however, reason to believe that in all of these problems, a suboptimal compensator exists with finite order comparable to that of the plant, and with almost the same cost as the optimal, infinite order compensator. The rationale for this belief comes from numrical optimizations that have been carried out using a quasi-Newton algorithm. Both the multi-model problem, and the $\mathcal{H}_2/\mathcal{H}_\infty$ cost functional have been studied in this manner. In both cases, and for several different plants, the optimal fixed order compensator of degree equal to the plant had a cost within a few percent of higher order compensators. With a compensator of twice this order, there was virtually no further improvement in the cost possible.

It may also be possible to minimize the cost by representing it in another form more amenable to different techniques. Along this line, connections have been noted between this $\mathcal{H}_2/\mathcal{H}_\infty$ cost functional, and the work of Zhou *et al.* [4], where the combined $\mathcal{H}_2/\mathcal{H}_\infty$ problem was studied from an input-output induced norm point of view. The cost in [4] is the induced norm of a plant with two inputs. If the second input is restricted to be causal, then the problem is equivalent to the $\mathcal{H}_2/\mathcal{H}_\infty$ problem studied by Bernstein *et al.* [5]. If the restriction is removed, then the problem is equivalent to our $\mathcal{H}_2/\mathcal{H}_\infty$ problem. Zhou *et al.* have not solved this case, but this representation of the problem may lead to solution techniques.

The cost in Equation (2) also has a time domain formulation in terms of a stochastic Stackelberg non-zero sum differential game. The control u minimizes the two norm of z under the influence of a white noise input ω_i and a deterministic but unknown worst case noise ω_j. Once the control Law is chosen, the deterministic noise uses this information and optimizes a modified cost. A set of equations identical to those obtained from the Lagrange multiplier approach can be obtained using this framework instead.

COST FUNCTIONAL INTERPRETATION

The dereverberation procedure can be interpreted as averaging all possible plants over some class of uncertainty. If there is no knowledge of the frequency of the plant poles, then the average plant is the dereverberated model, which has poles on the real axis. If the uncertainly in frequency is smaller, then the appropriate model to use is one where the poles have been left shifted, but not all the way to the real axis. This is again an average of the possible plants.

It is not sufficient to blindly design the control system for this model; the fact that the real structure is conservative must be reintroduced into the problem. This is what the cost functional in Equation (2) is intended to do. The worst case noise in the Stackelberg interpretation of this cost can be thought of as the noise that gives the worst possible conservative system. this can be shown by choosing a control law and a level of left-shift, and finding the optimum noise. The resulting open loop system is conservative,and the frequency is shifted in the direction which increases the cost.

FUTURE WORK

Ultimately, an experimental test of the approach being developed is desired. This will be done on the MIT Space Engineering Research Center interferometer testbed. Some work has already begun in examining the use of an active structural element in this truss for local control. The first experiment will be to perform rate feedback.

An understanding of the optimal solution of the $\mathcal{H}_2/\mathcal{H}_\infty$, multi-model control, and stable $\mathcal{H}_2$ compensator problems is still desired. The numerical algorithm for the $\mathcal{H}_2/\mathcal{H}_\infty$ cost needs to be improved in order to be a viable approach for obtaining the compensator. Once this is done, it can be used to study the robustness that this control design approach offers.

Other goals of the research include formalizing the argument to allow information about lower modes into the model, and comparing the resulting approach with the MEOP approach of Bernstein and Hyland [6]. A generalization for noncollocated sensors and actuators is desired, as is including robustness to time delays, actuator and sensor dynamics and so forth.

REFERENCES

1) MacMartin, D.G., Hall, S.R., and Mustafa, D., "Investigation of a Cost Functional for $\mathcal{H}_2/\mathcal{H}_\infty$ Minimization of Structural Energy," to be presented at the 1990 IEEE Conference on Decision and Control, Honolulu, Hawaii, 1990.

2) MacMartin, D.G., Hall, S.R., and Bernstein, D., "Fixed-Order Multi-Model Estimation and control," submitted to 1991 American Control Conference, Boston, MA, June 1991.

3) Hyland, D.C., and Bernstein, D.S., "The Optimal Projection Equations for Fixed-Order Dynamic Compensation," IEEE Trans. Auto. Contro., Vol. AC-29, No. 11, Nov. 1985, pp 1034-1037.

4) Zhou, K., Doyle, J., Glover and Bodenheimer, B., "Mixed $\mathcal{H}_2$ and $\mathcal{H}_\infty$ Control," Proceedings, 1990 Am. Control Conference, San Diego, Ca 1990, pp 2502-2507.

5) Bernstein, D.S. and Haddad, W.M., "LQG Control with an $\mathcal{H}_\infty$ Performance Bound: A Riccati Equation Approach," IEEE Trans. Auto. Control, Vol. 34, No. 3, March 1989, pp. 293-305.

6) Bernstein, D.S. and Hyland, D.C., "Optimal Projection for Uncertain Systems (OPUS): A Unified Theory of Reduced order, Robust Control Design," in Large Space Structures: Dynamics and Control, Atluri and Amos (ed.), Springer-Verlag, 1988, pp. 263-302.

SYSTEMS ENGINEERING APPROACHES TO THE DESIGN OF CST SPACECRAFT

Prof. Joseph F. Shea

The design of a CST spacecraft must be examined from a systems engineering perspective. The characteristics of a very flexible structure with precision pointing requirements places constraints on the spacecraft design, and the choice of subsystems can strongly interact with the CST tools used for disturbance minimization. There are two research projects investigating the systems engineering approaches to the design of CST spacecraft.

A SYSTEMS ENGINEERING APPROACH TO DISTURBANCE MINIMIZATION FOR SPACECRAFT UTILIZING CST

Mr. Christopher E. Eyerman and Prof. Joseph F. Shea

(Interferometer Testbed)

An MS thesis, completed in June 1990, presented a systems design method for disturbance minimization in the context of a space-based optical interferometer. The thesis first characterizes disturbances due to both environmental and on-board sources to which the spacecraft may be subjected. It then reviews the various CST techniques available for disturbance minimization, and formulates a numerical model of a full-scale version of the SERC interferometer testbed. As examples of the proposed system design method, three of the spacecraft subsystems are examined in detail: the power, attitude control, and interferometer & metrology subsystems. Options for each are examined with respect to performance requirements and disturbance minimization. After the best option is selected, recommendations are made on the use of CST tools to bring the system response to disturbances within performance limits.

VEHICLE DESIGN OF A SPACE-BASED OPTICAL INTERFEROMETER

Mr. Andrew M. Nisbet and Prof. Joseph F. Shea

(Interferometer Testbed)

As a follow-on to the previously described research, and to complement the development of the SERC interferometer testbed, a new

project has been started to complete a full design of an interferometric spacecraft, accepting only the tetrahedral truss structure as a given. Work to date has been in understanding the basic science requirements of the mission and the methods of disturbance minimization available. The next step will be to determine which of several methods for gathering the science data is the best. Methods are differentiated by the number of mirror/detector assemblies required and whether siderostat translation along the truss legs or spacecraft attitude adjustment is used to produce the various baseline lengths and directions. The methods will be measured by their performance, in terms of minimizing disturbances and maximizing science time, and their cost in terms of mass, power, and equipment. The previous research has shown that selection of the science gathering mode will drive the design of the other subsystems, so detailed design of the remaining spacecraft subsystems will come after this initial trade.

ROBUST MULTIVARIABLE CONTROL STUDIES

Prof. Michael Athans

(Interferometer Testbed)

This research deals with the development of concepts, theories, methodologies and techniques for the design of multivariable control systems for large space structures, with special emphasis on the stability and performance robustness characteristics. During this time period the SERC interferometer testbed provided the main vehicle for planning and carrying out the research described in the sequel.

The work is supervised by Professor Michael Athans, assisted by two graduate students research assistants: Joel Douglas of the Electrical Engineering and Computer Science Department, and Leonard Lublin of the Aeronautics and Astronautics Department. Both graduate students are working toward their MS thesis.

Mr. Lublin continued his research related to the development of nominal models, and quantification of unstructured modeling errors, for the interferometer testbed and continues to be a key participant of the interferometer group. During this time period he obtained a higher fidelity finite-element model of the interferometer by explicitly modeling the twelve bay truss structure for each leg of the pyramid using two elements for each strut. The complexity fo the resultant finite-element problem requred the use of a CRAY supercomputer. The new model agrees closely with the simpler beam model developed during the previous reporting period, at least for the low frequency modes.

We seek models of reasonable accuracy for initiating different multivariable control system designs; however, of equal importance is to fully understand the nature of, and bound on, modeling errors. These errors are both parametric due to uncertainties in damping, stiffness, geometry, etc. as well as dynamic in terms of poorly known high-frequency modes and other parasitic dynamic phenomena. However, one of the key findings during this reporting period was that significant modeling errors can also arise in the modeling of the actuators and sensors, which will impart the nominal values and directions of the multivariable

transmission zeros of the transfer function matrix used to model the interferometer structure in control synthesis studies.

Errors associated with the location and directional properties of transmission zeros may have serious impact upon the performance of the control system for disturbance rejection, especially if these are lightly damped zeros, forcing a low bandwidth control system implementation. These issues were investigated by Mr. Lublin, who compared the transfer function matrices of a two-dimensional truss structure with that obtained by a simpler beam approximation, and the models obtained using finite element methods. Although the modes of both systems were very close, the difference between point force and moment controls vs their physical distributed implementation resulted in a very significant modeling error in the transmission zeros and their directions. It is becoming more and more apparent that finite-element models may not be sufficiently accurate to implement a high bandwidth control system. Also, modeling errors in both poles and zeroes may require larger damping than one may have initially suspected. Thus, these models must be refined by empirical data. For these reasons we have started planning for multivariable identification of the interferometer testbed.

Mr. Douglas devoted most of his time in researching design methodologies for stability-robustness and performance-robustness of control systems with significant parametric uncertainty. During this reporting period we were able to derive some new results that can be used to design multivariable control systems using full state feedback strategies. We tested the designs for a simple mass-spring system, which has been used lately as a benchmark for assessing performance robustness for diverse control synthesis methods (Bernstein-Wei in 1990 ACC). We found that our formulation results in remarkable performance robustness in the presence of significant uncertainty in the potential energy stored by the spring (uncertain spring constant). The state variable feedback gains are computed by means of a modified algebraic Riccati equation in which the nature and size of the parameter uncertainties are manifested in two extra terms: one that looks like the term that appears in the $H\infty$ formation, and seems to explain the fact that parameter errors can be partially modeled as extra disturbances in the nominal design; the other term modifies the original state variable penalties, and tries to force the system to move towards operating regimes that minimize the impact of uncertain energy stored in the system. These encouraging results have motivated us to continue our theoretical research along these directions. It should be noted that the present methodology cannot be directly applied to the interferometer

testbed, because we do not measure enough state variables. We must extend the currently available results in a very non-trivial way before they can be used in conjunction with the postulated sensors and actuators in the interferometer testbed.

We have also continued our theoritical effort that may provide us with explicit guidance regarding performance limitations, say in terms of disturbance-rejection, for dynamic systems characterized by lightly-damped stable poles and minimum phase zeros. Such performance limitations are understood for unstable and/or nonminimum phase systems using results from advanced complex variable theory (Poisson integrals, etc.). For the types of structures (e.g. the interferometer testbed)

13

under consideration, in the absence of modeling errors and other nonlinear actuator/sensor effects, the dynamic systems are "stably invertible" so in principle it is possible to obtain excellent disturbance-rejection performance using dynamic multivariable compensators of very high order. However, from a pragmatic point of view, modeling errors, nonlinearities, reduced complexity controllers and decentralized implementation will impose a limit on achievable disturbance-rejection performance while maintaining stability. We seek a theoretical framework that (hopefully) will make these tradeoffs transparent, and reduce the amount of trial and error design iterations that control designers must currently execute. Although the theory is still at its infancy, it confirms the insight gained by von Flotow and his students on single-input single-output systems in that a minimum pole/zero damping may be necessary to ensure stability if there exists significant uncertainty in the location of pole-zero pairs bear the imaginary axis.

BROADBAND INPUT/OUTPUT ISOLATION ON A FLEXIBLE STRUCTURE WITH UNCERTAIN DYNAMICS

Mr. Gary Blackwood and Prof. A. von Flotow

(Interferometer Testbed)

The optical interferometer testbed has several optical mirror components that have small mass compared to the mass of the entire structure. The control task is to maintain the relative pathlength differences between these components to a tolerance of 50 nanometers rms in the presence of scaled space disturbances (primarily a reaction wheel disturbance model, with both broadband and narrowband components). The testbed is representative of a class of space-based optical systems under consideration by astronomers; the relative degree of passive and active control necessary to meet performance objectives is still an open question. In related work, Jim Garcia demonstrated in his MS thesis the feasibility of single-axis broadband positioning of a mirror mounted to a flexible structure. The degree to which a control design could ignore the structural flexibility of the substructure depended on the ratio of the mirror mass to the structure's individual global modal masses, and upon the modal damping ratios.

As an extension to Garcia's MS thesis, three-axis active mirror mounts will be used to position the various optical components in the optical interferometer testbed. Extensions of the theory for the multi-input-multi-output case will be made to develop structural model error bounds for low-order control systems that are designed ignoring selected (perhaps all) flexible modes of the testbed structure. Within this analytical framework, dynamic modifications (both active and passive) will be investigated for their effects in reducing modelling uncertainty and in performance improvement. These approaches will be studied both for the optical output location as well as for disturbance input locations, and will form the basis of Blackwood's PhD dissertation. At the present time, three three-axis mirror mounts using piezoelectric and electrostrictive stacks have been designed and are under construction. Calibration and integration of theses components to the testbed will occur over the next few months, and open loop input-output testing will begin.

14

REFERENCES

1)   *Garcia, J. G., Sievers, L. A., and von Flotow, A. H., "Broadband Positioning Control of 'Small' Payloads Mounted on a Flexible Structure",* Proceedings of the ASME Winter Annual Meeting, Dallas, TX, Nove 28, 1990.

2)   *Laskin, R. A., and San Martin, M., "Control/Structure System Design of a Spaceborne Optical Interferometer",* AAS/AIAA Astrodynamics Specialists Conference, Stowe, VT August 7-10, 1989.

REALIZATION OF IMPEDANCE MATCHING FOR UNCERTAIN STRUCTURES USING PASSIVE ELEMENTS

Mr. Ron Spangler and Prof. Steven Hall

(Interferometer Testbed)

The idea on which this research is based is that it should be possible to constrain any optimal control problem in such a way that the resulting controller can be implemented using strictly passive elements which require no connection to the inertial frame (that is, passive and space-realizable). This is motivated by the results of MacMartin and Hall [1] on power flow control for uncertain structures, in which broadband active impedance-matching is accomplished using a collocated and dual (that is, the product of input and output variables is power) sensor/actuator pair to implement an H_∞ control law by which energy is extracted from the structure at each frequency. The resulting controllers are positive real impedances, and thus could be implemented using a network of passive elements, but with a connection to ground.

One direction that this research has taken, therefore, has been to investigate the theory of positive real systems, with an eye toward fromulating a set of algebraic (state-space domain) constraints on a system (a controller) such that it be passive and space-realizable. The seminal reference is B. D. O. Anderson [2], [3]. His Positive Real Lemma provides a connection between the frequency-domain definition of a positive real system and a state-space-domain representation. Briefly, a positive real system has a transfer function matrix G(s) with the following properties:

   - G(s) has no poles in Re[s] > 0

   - $G^{T*}(s) + G(s)$ is positive semidefinite hermitian in Re[s]>0

The Positive Real Lemma states that for any minimal state-space realization of G(s), call it {A,B,C,D}, there exist matrices P, L, and W with P symmetric positive definite such that

$$PA + A^T P = - LL^T$$

$$PB = C^T - LW$$

$$W^T W = D + D^T \qquad (1)$$

Now for a given {P,L,W} which satisfy these equations one could adjoin these three equations to any cost functional to constrain the resulting closed-loop system, or impedance compensator, to be positive real, and thus

15

implementable passively, though not necessarily space-realizably. The problem is that there are a number of solutions {P,L,W} to the equations above, so the resulting compensator may not be the best optimum.

In *Network Analysis and Synthesis*, Anderson states that the solution {P,L,W} to the positive real lemma equations is used in the synthesis of the passive network represented by G(s). A first step is to determine a set of algebraic constraints which would result in a compensator which is not only positive real but implementable using only resistors and capacitors (or dashpots and springs), allowing connection to ground. I seems possible that the positive real lemma and some knowledge of network synthesis theory may yield these constraints, which would serve as a starting point. (The next step would be to replace the ground with a proof mass and investigate the performance degradation.) A search of the literature for more recent papers in which the principle of positivity is used in designing controllers is in progress, and research in this area is expected to continue in the next six months.

More recently, however, another approach to the design of optimal passive controllers has been formulated. This numerical optimization approach uses a cost-functional approach to get both the matrix necessary conditions for optimality of the absorber damping (C) and stiffness (K) matrices, which are impossible to solve in closed form, and the gradients of the cost functional with respect to each element in the absorber network (each spring and damper) for use in a numerical gradient search. In either case the masses in the network are given a fixed vaue.

The structural plant used is a uniform cantilevered Bernoulli-Euler beam (big surprise) with a unit intensity white noise disturbance force d at the mid-span. The passive controller networks are placed at the beam tip (see Figure 1). The cost functional penalizes the $\mathcal{H}_2$ norm of the sum of the tip displacement and the tip velocity, weighted via a block-diagonal matrix Q to approximate total energy of vibration.
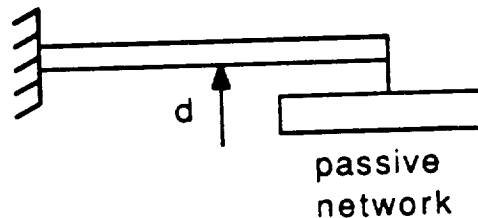

Figure 1: Test Case for numerical Optimization of passive controllers.

The plant model is that of an undamped beam in modal coordinates (i.e., diagonal stiffness matrix and identity mass matrix) rendered in state-space form. The open-loop output vector includes the tip displacement and velocity. The mechanical network, being used as a controller rather than a plant, has an input-output relationship converse to what we're used to in dealing with mass-spring-dashpot systems. That is, its inputs are the beam tip position and velocity and its output is a force. As such, the values of certain springs and dampers appear in the input and output matrices of the controller model. The two models are interconnected just as a generic dynamic controller is connected to any plant, so the closed-loop state vector

includes both the open loop controller and plant states. The disturbance input has closed-loop influence matrix B_C.

To find the matrix necessary conditions for optimality of the controller K and C matrices write the closed-loop cost as

$$J = \text{tr}(PV)$$

$$PA + A^T P + Q = 0 \quad (2)$$

where A is the closed-loop system matrix and $V = E\{d^2\}B_C B_C^T$. Adjoining the Lyapunov equation to the cost in (2) via Lagrange multiplier matrix H and taking matrix partial derivatives with respect to P, H, K, and C yields the necessary conditions. The A matrix is a 4x4 block matrix with C and K in several of its blocks, so the necessary conditions resulting from the derivatives with respect to these matrices are in terms of corresponding blocks of H and P, and are hideously complex. Thus there is no closed-form solution for the optimal K and C matrices.

So finding the optimal values is a numerical optimization problem requiring the gradient of the cost with respect to each of the network elements (each spring and damper). It can be shown that this gradient is, for parameter p

$$\frac{\partial J}{\partial p} = 2tr\left\{HP\frac{\partial A}{\partial p}\right\} \quad (3)$$

where P solves the Lyapunov equation in (2) and H, the Lagrange multiplier referred to above, solves

$$AH + HA^T + V = 0 \quad (4)$$

To find the gradient of A with respect to p requires specifying the topology of the controller network, so that the controller C and K matrices as functions of the individual parameters are known.

Thus far two cases of the above controllers have been investigated, with one mass and two masses, each of value m. The single mass case has only two parameters to be optimized (a single spring and damper), and the two mass case has six, as seen below. All optimizations were performed for a value of m/beam mass = 0.1. Using a matlab function which performs a gradient search given a set of initial parameters several optimizations have been performed to date. In all cases the parameters are constrained to be nonnegative, thus insuring positive definite K and C. In most cases there will be a number (possibly infinite) of local minima of the cost, any number of which can be reached given the proper initial parameter set.
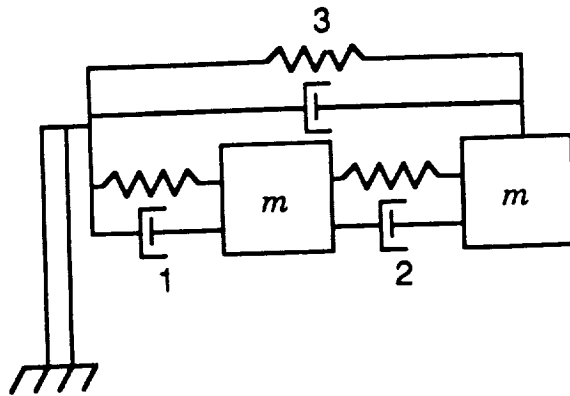
Figure 2: The most general 2 mass passive compensator structure.

Figure 3, the closed-loop transfer function from disturbance to tip velocity, shows the result of this procedure using a single mass network on a ten-mode beam model. Note that the controller has tuned to the first mode, with the result looking very similar to the classical vibration absorber result. It is not exactly the same, as can be seen by optimizing this controller using a single mode beam model, as the minimum energy condition for optimality here differs from the classical problem's minimum of maximum response (really an $\mathcal{H}_\infty$ criterion).

A two mass controller has also been optimized using both a two and a ten mode beam model. In the two mode case several minima have been found which are on the constraints, i.e. in which one or more of the parameter values are zero. A local minimum has also been found using different initial conditions in which two of the parameters (k_2 and c_2) have no effect, remaining at whatever initial value is selected. It is believed there is a better minimum in the interior of the six-dimensional parameter space which has not yet been found. It is probably very sharp, and will be reached from a relatively small set of initial conditions. Several "clever" schemes for identifying this optimum have not yielded results. In the ten mode case the best optimum found is still on the constraints, with $k_2 = 0$. This is shown in Figure 4. Again, it seems possible that a better minimum exists in which all degrees of freedom in the controller are utilized.

It is possible, however, that this is not the case. The $\mathcal{H}_2$ cost over which this passive controller is optimized is certainly contributed to most strongly by the first mode response. It could be the case that doing the best job possible on this mode and ignoring the others yields the optimum. In this case, all degrees of frredom afforded by a two-mass damper are not needed, rather it is the increased mass that is desired. Tuning single mass controllers to modes other than the first and applying them to the multi-mode model has shown that the "closed-loop" cost is still much higher than the more general optima discussed above.

With the above in mind, current efforts are in the area of alternate cost functionals which would lead to more broadband performance of the resulting passive compensators. The most broadband results would be gained by minimizing the $\mathcal{H}_\infty$ norm of the closed loop system matrix, but gradients of this norm are difficult to obtain for use in a numerical procedure. There is a great deal of research being carried out currently, however, in the area of mixed $\mathcal{H}_2/\mathcal{H}_\infty$ control in which a performance criterion is minimized while simultaneously satisfying an $\mathcal{H}_\infty$ norm-bound

18

constraint. Many of these problems become the problem in the limit of a single scalar parameter in the cost functional, but do possess calculable gradients for numerical optimization purposes.

REFERENCES

1)   MacMartin, Douglas, and Hall, Steven, "An H∞ Power Flow Approach to Control of Uncertain Structures," to appear in the Journal of Guidance, Control, and Dynamics.

2)   Anderson, B. D. O., " A System Theory Criterion for Positive Real Matrices," SIAM J. Control, v. 5, no. 2, 1967.

3)   Anderson, B. D. O., and Vongpantilerd, S., Network Analysis and Synthesis: A Modern Systems Theory Approach, Prentice-Hall, Englewood Cliffs, NJ, 1973.
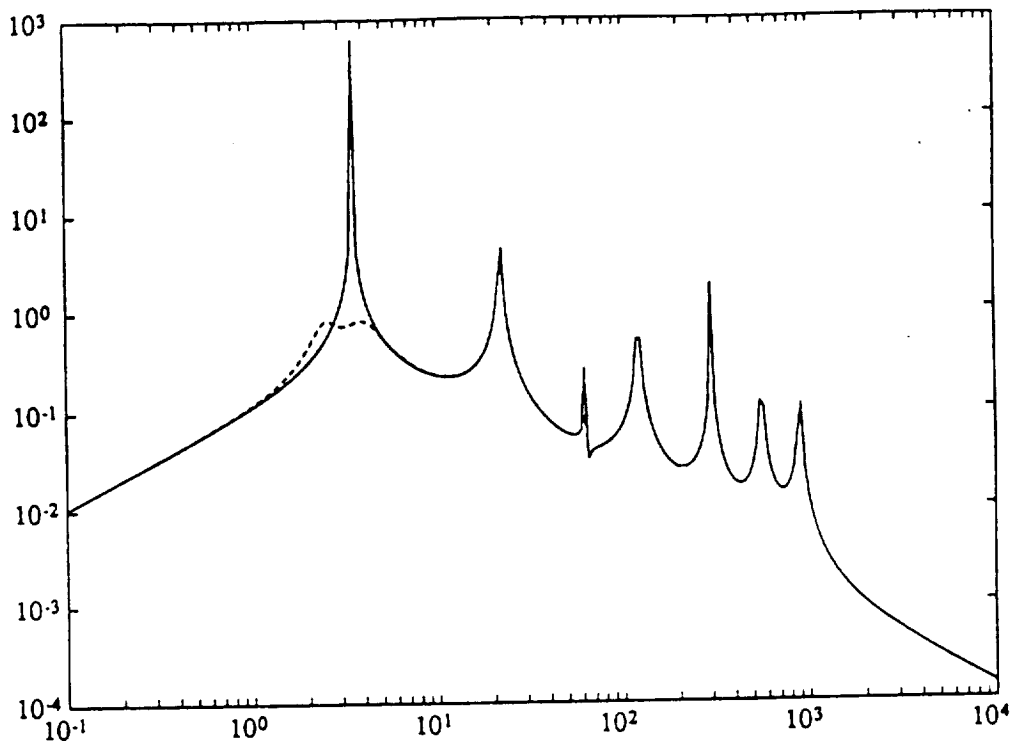
Figure 3: Disturbance to tip velocity transfer functions of the undamped beam (solid) and the passively-compensated beam using a single mass.
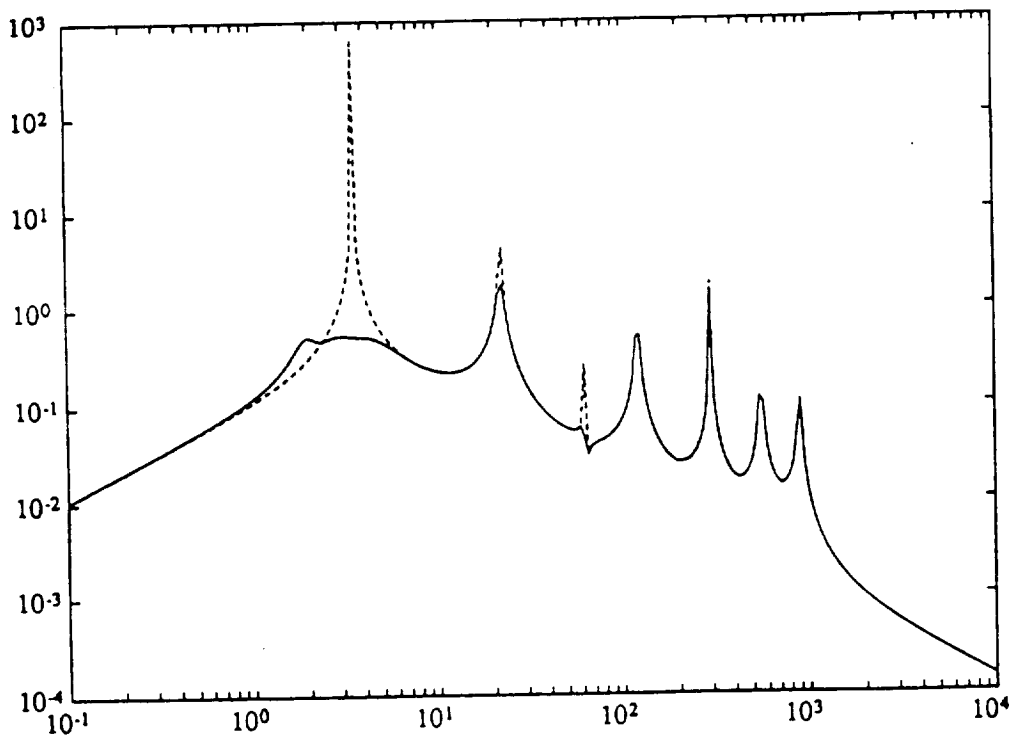
Jstar=9604.3, k2star=0 (may not be global opt)

Figure 5: Transfer functions of the undamped beam (dashed) and the 2 mass compensator with the best optimal cost yet found.

POINTING CONTROL FOR PAYLOADS USING VARIOUS MEASUREMENT TOPOLOGIES

Mr. Mark E. Campbell and Prof. Edward Crawley
(Multibody Testbed)

OBJECTIVE

The objective of this research is to quantify, through analysis and experiment, the performance improvements made by successive relaxation of the constraints on the topology and successive additions to the hardware of the Middeck Active Control Experiment(MACE) model.

APPROACH

The approach will be as follows:

1. Develop a simple two dimensional model of MACE and compare it to typical section models.

2. Develop control schemes for the model by working through a matrix of combining the relaxation of the constraints on the topology and adding hardware to the system. Some of the control schemes to be addressed will be simplification of LQG and LQR, successive loop closures, and interpretation of Mathieu Mercadal's analysis of the finite element model and the full three dimensional system.

3. After selecting a few of the elements of the matrix as the best control approaches, these will be implemented and tested in the lab on the actual MACE test article.

WORK TO DATE

My research began with the investigation of the dynamics of the planar model of MACE. First, the dynamics of a simple rigid bar and payload were derived. There were four degrees of freedom(D.O.F.): three rigid body D.O.F.'s including horizontal and vertical translation of the bus, and rotation of the bus; and the relative angle between the bus and articulating payload. The dynamics were examined for the origin of the various terms, such as coriolis, centripetal, etc.

Two more D.O.F.'s were then added to the model: one flexible vibration mode of the bus and one axial vibration mode of the bus. The system was truncated down to a three D.O.F. model: the rotation of the bus; the flexible vibration mode of the bus; and the relative angle between the bus and articulating payload. The dynamics were also linearized around a nominal state. The basis for the nominal state was the MACE sample problem.

This new model was then compared to the Non-CG mount, flexible model of the typical section models written by David Miller in Linear Closed Loop Analysis, version 1.0. This showed the two models to be very similar.

The immediate future of the research is to begin a linear control analysis of the three D.O.F. model. Classical sequential loop closures will be investigated initially and some MIMO control techniques will be looked into at a later date. The plan is to begin taking the linear model through the matrix of control options in the MACE sample problem. The results of this simplified system could then be used for comparison to the more complicated systems, such as the finite element model.

The order or size of most of the nonlinear terms in the six D.O.F. model will also be investigated, just to know what is being thrown away when the nonlinear system is linearized.

PLANNED RESULTS

The planned results are that we will fully understand the advantages and disadvantages of the matrix control options of the planar model and how this adds to the analysis of the MACE test article. An analogy has already been formulated between the linearized system of the planar model and the typical section models. The plan is to also develop an analogy between the more complicated models of MACE and the simple planar model.

CLOSED-LOOP STABILITY OF MULTIBODY SYSTEMS WITH DISTRIBUTED FLEXIBILITY

Mr. Carlos E. Padilla and Prof. Andreas H. von Flotow

(Multibody Testbed)

In the past few months we have been investigating the problem of closed-loop stability of multibody systems with distributed flexibility (e.g., robotic manipulators, MACE test article). Using existing results for the control of rigid manipulators as a starting point, I am trying to obtain exact stability results for systems whose models are known exactly and for which all the states are available for feedback. (Note that the concept of state feedback for a distributed parameter system needs to be clarified/defined by this research). It can be shown that for independent joint PID control of flexible manipulators stability is guaranteed. This is done using energy considerations independently of the specific model for the distributed parameter system.

Recent literature results attempt to show exponential stability of the tracking control for multi-joint flexible-link manipulators. A generalization of the computed torques approach for flexible manipulators, together with the Positive-Real Lemma, are used to show that stability of the closed loop system is guaranteed when a class of positive real (passive) controllers are used as joint controllers[1]. However, this result depends on both the joint controller and the structure being sufficiently stiff and having enough damping. Further, in order to take into account structural damping to increase the implied performance guarantees, the observability of the modes used to model the flexible members from the joint sensor must be considered. This indicates that both stability and performance may depend on the choice of mode shapes: a modelling choice. I am trying, on the one hand, to generalize this result to the case when full state feedback is

available for control. On the other hand, I would like to investigate further the modelling issues affecting the stability proof and if possible extend the results to practical cases (i.e, non-vanishing regions of convergence).

These issues have become evident in my stability analysis of the MACE test article for "not-quite-independent" joint PD control[2]. Stability results depend on the model and in particular stability bounds seem to depend on the particular choice of mode shapes used to discretize the distributed flexibility. I am at present looking at these and other "modelling for control design" issues and my efforts will be directed towards completing a paper to appear in the 32nd SDM conference: *Further Approximations in Flexible Multibody Dynamics*. Specifically, I want to investigate how far a given set of dynamic equations, for the type of systems under consideration, can be simplified given a set of operational constraints in terms of maximum rigid body displacements and rates. It is foreseen that the degree of simplification will be tied again to the modelling choice of mode shapes. This suggests that some mode shapes capture the "essence" of the physical system better than others. I am interested in finding fundamental conditions (e.g., the satisfaction of certain energy integrals) that will yield the best choice of mode shapes given that only a finite number of them will be used to model the distributed parameter system.

REFERENCES

1) Paden, B., Riedly, B., and Bayo, E., "Exponentially Stable Tracking Control for Multi-Joint Flexible-Link Manipulators," Proceedings of the American Control Conference, May 1990, San Diego, CA, pp. 680-684.

2) Padilla, C., "Nonlinear Modelling, Simulation, and Preliminary Control of the Baseline Test Article," MACE Final Report, First Draft, August 1990.

GRAVITY-SUSPENSION SYSTEM EFFECTS

Mr. Daniel A. Rey and Prof. Harold Alexander

(Multibody Testbed)

Significant progress has been made since the last report towards a comprehensive understanding of the differential stiffening effects of axial, bending and shear loads on a beam in the presence of axial, bending or shear deformations. It was found that axial loads are the only load type which contribute homogeneous stiffening while all other load types are coupled to off-diagonal elastic degrees of freedom. An example of such a coupled stiffening effect to the suspended MACE test article is the increased horizontal plane bending stiffness which arises when a vertical bending moment is applied to the torsionally deformed test article as a payload out of the vertical plane slews towards the longitudinal axis and away from the center of the test article. Contributions to the shear mode of deformation have yet to be determined. This analytical understanding will be complemented by future research which will investigate the extent to which existing finite element software packages capture these effects. A parametric variation analysis will then follow using analytical and numerical modelling techniques to determine how differential stiffening affects the system eigenstructure; tracking also the slope and curvature node positions for the first three flexible modes.

An initial study of the first order effects of a suspension system on a suspended test article has identified the different static and dynamic mechanisms by which a suspension system alters the test article dynamics. Horizontal stiffness is imparted at each attachment point due to the static simple pendulum stiffness and the dynamic impedances of the suspension violin modes. Vertical stiffening occurs as a result of static test article sag and suspension axial stiffness. Compound pendulum effects were stiffen the torsional degree of freedom of the test article while corrupting both the horizontal and vertical bending modes. Modelling techniques or analytical approximations have been found for all of these effects except for the magnitude of the dynamic impedance contributions of the suspension violin modes. It is clear that approximate solution techniques will have to be used for all suspension configurations with three or more cables as the structure becomes overdetermined. The nature of the predicted perturbations to the naked MACE test article with a three point soft spring suspension system were qualitatively confirmed by experiment.

COMMAND SHAPING FOR THE MULTIBODY TESTBED

Mr. James Hyde and Prof. Warren Seering

(Multibody Testbed)

Work in the last six months has concentrated on:

1) Solidifying a M.S. thesis topic,

2) Completing the MACE inertial wheels,

3) Performing and presenting initial modeling and simulation results,

4) Identifying areas for future work.

The thesis title has narrowed to: "Using Input Command Shaping to Minimize Multiple-Mode Vibration in Robotic Systems." This work will extend and expand an earlier Mechanical Engineering Ph.D. thesis by Neil Singer, one of Prof. Seering's former students. Since Seering's group is located in the MIT Artificial Intelligence Laboratory, we have clarified a framework for communicating and working with the SERC laboratory, the main link being the MACE experiment, which will be used to attempt to validate the central concepts of the thesis. Ongoing mechanical design support will augment this cooperation.

A particular recent design effort has been the MACE inertial wheels, which were completed and delivered in mid-summer. The parts were manufactured with some alignment errors, and only after significant modification in the AI Lab shop were they acceptable for inclusion in the experiment hardware. Alignment and stability validation was conducted in the AI Lab, and controller development and construction was completed by SERC personnel.

Specific preliminary thesis research began in February 1990. The first research focus was understanding Singer's Impulse Sequence Input Shaping techniques and working on a new approach to achieve multiple-mode shaping. Singer cancelled multiple-mode vibration by convolving various single mode shapers into a longer sequence; the new method will

yield multiple mode shapers as a direct solution to a set of constraint equations. The new sequences will be shorter than the convolved sequences, thus minimizing system response delays. The major problem with this approach is that the constraint equations are a set of simultaneous, non-linear, transcendental equations, which are very difficult to solve.

Non-linear equation solvers perform well when they are provided with good initial guesses, hence our next step was to linearize the equations, and through an optimization process, generate approximate multiple mode shapers. These approximate shapers were interpreted and fed into a standard non-linear equation solver as initial guesses for the exact solution of the full equations. The exact sequence, theoretically, could be used to eliminate multiple mode residual vibration in a flexible system.

To validate this concept, we employed a finite element MatLab model of MACE. After identifying the system eigenvalues and constructing an input shaping sequence, we conducted simulations of response to shaped and unshaped slewing maneuvers. The input shaper removed about 90% of the vibration in the system, identifying serious potential for the shaping method.

These and similar tests were collected and presented at the 1990 NASA/DoD Controls-Structures Interaction Conference, and also submitted to the 1991 IEEE Conference on Robotics and Automation and the 1991 Automatic Control Conference (see the attached paper for details). The response at the CSI conference was favorable, and several attendees stated intentions of using the technique on some of their test articles - a success considering our major aim of raising the technique's level of familiarity within the aerospace community.

Current work is aimed at increasing the number of vibrational modes that can be eliminated by a single input shaping sequence. We have had success at raising this number to five modes for some of our current models; we hope to develop shapers capable of eliminating vibration in up to ten or fifteen modes. The major obstacle at this point is the robustness of the current non-linear equation solver, and we are going to try various other solvers in the coming weeks.

Future activity will include the use of non-linear models of MACE. The equations defining the shapers are derived from linear flexible system theory, and the exact effects of system non-linearity on the input shaper's effectiveness are unclear. The new models will allow us to identify some of the problems caused by non-linearities, and hopefully assist in developing approaches for dealing with those problems. Sometime in March or April we hope to be conducting tests on the physical MACE experiment, still under construction at SERC.

NONLINEAR ANALYSIS OF COMMAND SHAPING

Mr. Ken Chang and Prof. Warren Seering

(Multibody Testbed)

It was determined that Jim Hyde's work on input shaping required a nonlinear model of MACE. For this purpose, we have been working on installing DISCOS on a SUN Sparc workstation at the AI lab. The rigid and flexible models of MACE developed by Carlos Padilla have been obtained from Cambridge Research and are now being implemented at the lab. Much of our time has been spent modifying the program to function on the AI lab's upgraded UNIX system. The program is now working and resides on the hard disk.

The next logical step in this non-linear modeling work is to include the input shaper in the model. This requires first finding the natural frequencies of the system to any chosen input. Then, these frequencies are used to determine the shaping technique. We will then shape the input and see the effects on residual vibration. Since the shaper works outside of the plant, we can fairly easily implement it by manipulating/shaping the input before it goes into the DISCOS program.

HIGH BANDWIDTH CONTROL OF LOW AREA DENSITY DEFORMABLE MIRRORS

Mr. Eric Anderson, Mr. Jonathan How,

Prof. Steven Hall and Dr. David Miller

(Possible Third SERC Testbed)

INTRODUCTION

A project to investigate the applicability of Controlled Structures Technology to control of large precision optical surfaces has been initiated. The objective of the work is to develop surface shape control technology which will allow the reduction of mirror mass densities around 200 kg/m^2, associated with current techniques, to a more practical 50 kg/m^2. It is understood that such a reduction is not straightforward. A reduction in area mass density will result in relatively low frequency structural resonances and higher open-loop surface inaccuracies which will require the focussed attention of the structural and control designers. Provided such an improvement is successful, active mirror surface control technology should become cheaper and more available to a wider class of applications.

PROBLEM STATEMENT

A brief survey of the available literature shows that designs to control mirror surfaces have existed for over twenty years[1]. A little more analysis shows that a key characteristic of many of these mirrors is that they are very stiff. This is beneficial because the stiffer the mirror, the smaller the deformation for a given disturbance, and the performance can be achieved

26

by controlling the surface in its quasi-static regime. The flexible modes are found at a high frequencies, beyond the required bandwidth. Consequently, for the purposes of the control design, it is possible to treat the mirror as a collection of rigid panels and ignore the flexible dynamics. Many of these designs have been developed using a combination of wavefront and edge sensors, piezoelectric actuators, and a static figure control feedback. This approach assumes that the control roll-off would be such that the flexible modes of the stiff structure would not be destabilized. Very few of the available control approaches discuss the topic of accounting for the effects of control spillover. However, it is recognized that the mass per unit surface area of the mirrors must be reduced from about 200 kg/m^2 to 50 kg/m^2 before the much larger designs envisioned for future space missions become feasible. Weight reduction will result in a much more flexible structure. Future control designs must account for this increased flexibility to avoid spillover destabilization of these modes.

For this work, we will specifically be looking at reducing the weight of the structure even further with an emphasis on reducing the manufacturing (*e.g.* face grinding) costs by actively compensating for long wavelength flaws in the mirror surface. The objective is to use a much cheaper high precision active structure for the mirror combined with a 'large' amount of active control to achieve performance comparable to the previous designs. The resulting mirror will then be better in terms of both cost and weight.

Control systems for current mirrors typically use actuators which push off a backplane which is of comparable stiffness to the mirror. This backplane typically constitutes a significant contribution to the total mass of the mirror structure. Our aim is to develop a self-straining structure (which eliminates the need for the backplane), and the corresponding control architecture to improve the shape performance of a very flexible primary mirror over a wide range of frequencies in the presence of disturbances and modelling errors. The controller will be based on feedback of a combination of structural and optical measurements. A typical representation of the relative control authority of these two feedback loops is shown in Figure 1. Note that there are (at least) two main sets of sensors, but probably only one set of actuators. As shown, the feedback from the structural measurements will be used to control the mirror over a wide frequency range. In particular, it is important to be able to minimize the bandwidth f_1. This will allow for a significant overlap between the two control approaches even when the target object is a faint star and photon limitations result in a very low wavefront sensor update rate. At the higher frequency end, the aim will be to improve the shape performance of the modes which will contribute to the RMS ripple error but typically have a low damping ratio.

OVERALL APPROACH

This research will develop analytical solutions to thE problem which will be verified on an experimental testbed to be designed and constructed. The experimental issues will deal with the final design and lay-up of the test structure, the identification of its properties, and the implementation of the controllers. This work can also be separated into the design of the controller and the structure, but it is recognized that the boundary between the two is not distinct since both will have to deal with issues such as the

sensor and actuator type and architecture. The approaches that will be taken are discussed in the following two sections.

APPROACH TO THE STRUCTURAL DESIGN

The structural design will proceed in close coordination with the control design along both analytical and experimental paths. The concept of an 'active structure,'[2,3,4] which possesses integrated sensing, actuation, and potentially processing, will be employed. The goal of the analytical development is to allow the results obtained to be applied to larger, more complicated flexible controlled structures.

The practical capabilities and limitations of self-straining active structures will be examined with a goal of determining for which problems active structures are best suited. A region of effectiveness compared to the conventional approach of mirror surface control will be established based on such factors as weight savings, processing requirements, reliability, and simplicity of design and manufacture. Performance objectives for precision control will be incorporated in the structural design.

The design will start with a structure with desirable 'passive' properties, including a very low coefficient of thermal expansion, tailored mass and stiffness distributions, and some passive damping. The selection and distribution of active components in the structure will depend strongly on the proposed control architecture, and the expected disturbance environment. The number, placement, and required accuracy of sensors and actuators will be evaluated, with allowance for some redundancy and fault tolerance.

The structure will be modeled well enough to do control design and sensor/actuator placement. The appropriate roles of active isolation and passive damping will be explored in conjunction with ongoing efforts in SERC.

In parallel with the analytical development, an experimental demonstration structure will be tested. Structural sensor and actuator options will be considered and evaluated for accuracy at the submicron displacement level using optical reference measurements. The test structure will then be designed based on results of the initial series of tests and early analytical results. Open loop control to submicron displacements will be demonstrated. The structure will then be actively controlled in the presence of disturbances to the best precision possible.

APPROACH TO THE CONTROL DESIGN

The control design for this testbed will consist of determining the solution to several complex problems which involve modelling, sensor and actuator, implementation, and control architecture issues. The approach will be to perform an analytic evaluation of the best alternatives by performing a trade-off analysis of the implementation costs versus the performance, and then doing an experimental comparison of the final designs.

There are several factors about this problem that will strongly influence the control design. The aim is to control the dynamic motion of a flexible mirror to meet performance objectives which are a fraction of the

wavelength of light. This typically will require a very dense array of both sensors and actuators. Consequently, the number of measurements available to the controller will be very large for any reasonably sized problem, so the control architecture must be designed to efficiently handle this information. Since the aim is also to design a controller for a large frequency range (see Figure 1), either a good model must be developed for the higher frequency regions or the controller must be designed for robustness to parameter uncertainty. Another factor in the tradeoff analysis is that the control commands will be calculated based on the measurements from at least two sets of different sensors, so the controller must be able to combine these in an intelligent fashion.

The approach that will be taken in this work will be to investigate various control architectures, and in the process develop a list of the advantages and disadvantages of each in terms of the issues given above. Other criteria, such as the communication requirements, the flexibility of redesign after failure, and the performance with noisy measurements, will also be addressed. Some of the control architectures that will be investigated are:

I. Centralized design

II. Fully decentralized design

III. Decentralized design with communication allowed between controllers

IV. Multi-level design

where the decentralization will probably be at the mirror segment level. Clearly, each of these designs has some obvious advantages and disadvantages. A centralized design would provide very good overall performance, but will be hard to implement due to the amount of information available. Fully decentralized designs are much simpler to implement, but have performance problems. Multi-level designs combine many of the advantages of these approaches, but there are potential stability problems from control spillover. It is expected that some form of decentralized controller in a multi-level architecture will provide the best overall performance for this type of problem with a large amount of sensor information. Results from previous design studies have certainly indicated that this is the case[5,6,7]. An analysis based on these points should eliminate some potential designs, and further computer simulations will indicate which designs are worth implementing on the final testbed.

Some of the other issues to be addressed during the initial stages of the control design include a determination of the anticipated noise levels in the measurements, since this might require that the controllers include a filter. An algebraic expression for the performance objective will also have to be developed. This could be in the form of compensating the modes of the structure directly, or by controlling the optical modes of the mirror through the use of the Zernike polynomials.[8] Once the final designs are selected, a decision of how to implement the controllers (i.e., digital, analog, or digital analog) will have to be made. The controllers will then have to be redesigned for this specialized implementation case and to include the sensor and actuator dynamics.

NEAR-TERM PLANS

Important tasks to be undertaken early in the project:

I. Modelling issues such as the feasibility of accurately modeling the high frequency modes or the need for the controller to be explicitly designed for robustness will be addressed (mode vs. wave modelling, active vs. passive damping).

II. The type, location for good performance, dynamic range, resolution and dynamics of the sensors and actuators will be evaluated, and the appropriate sensor-actuator matching for efficient control will be studied.

III. Efficient combination of low and high bandwidth control, using wavefront and structural control sensors, will be investigated (where does the break in frequency (Figure 1) occur?).

IV. An algebraic representation of the performance criterion will be expressed.

V. Several control architectures employing dynamic or static feedback approaches will be compared.

VI. The 1D testbed will be constructed using a self-straining beam with distributed sensing and actuation.

VII Mounting of the beam, as well as optimal mass, stiffness, and damping distributions will be addressed.

VIII. An optical reference system will be designed to acquire displacement measurements to judge the control performance (discrete points or continuous surface).

REFERENCES

1) Creedon, J. and Lindgren, A., ``Control of the Optical Surface of a Thin, Deformable Primary Mirror with Application to an Orbiting Astronomical Observatory,'' Automatica, Vol. 6, 1970, pp. 643-660.

2) Fanson, J., Anderson, E., and Rapp, D., ``Active Structures for Control of Large Precision Optical Systems,''Optical Engineering, Nov. 1990.

3) Wada, B. (Editor), ``Adaptive Structures,'' Winter Annual Meeting of the American Society of Mechanical Engineers, San Francisco, California, Volume AD-15, December 1989.

4) N. W. Hagood, E. F. Crawley, J. de Luis, and E. H. Anderson, `Development of Integrated Components for Control of Intelligent Structures,' Smart Materials, Structures, and Mathematical Issues, pages 80-104, Technomic, 1989.

5) Aubrun, J., ``Theory of the Control of Structures by Low-Authority Controllers,'' AIAA Journal of Guidance and Control, Vol. 3, No. 5., 78-1689R, September-October 1980, pp. 444-451.

6) Hall, S., Crawley, E., How, J., and Ward, B., ``A Hierarchic Control Architecture for Intelligent Structures,'' To be published in the AIAA Journal Guidance, Control, and Dynamics, (Space Systems Laboratory Report / #19-88), November 1988.

7)   *How, J.*, Local Control Design Methodologies for a Hierarchic Control
      Architecture, *SM Thesis, MIT Department of Aeronautics and Astronautics, (Space
      Systems Laboratory Report / #14-89), November 1989.*

8)   *Serra, K.*, Adaptive Optics Control using Zernike Modes, *SM Thesis, MIT
      Department of Electrical Engineering and Computer Science, February 1977.*

Objectives and Issues

Objective: Control to $\lambda/20$ at 0.6 μm with the lowest area density.
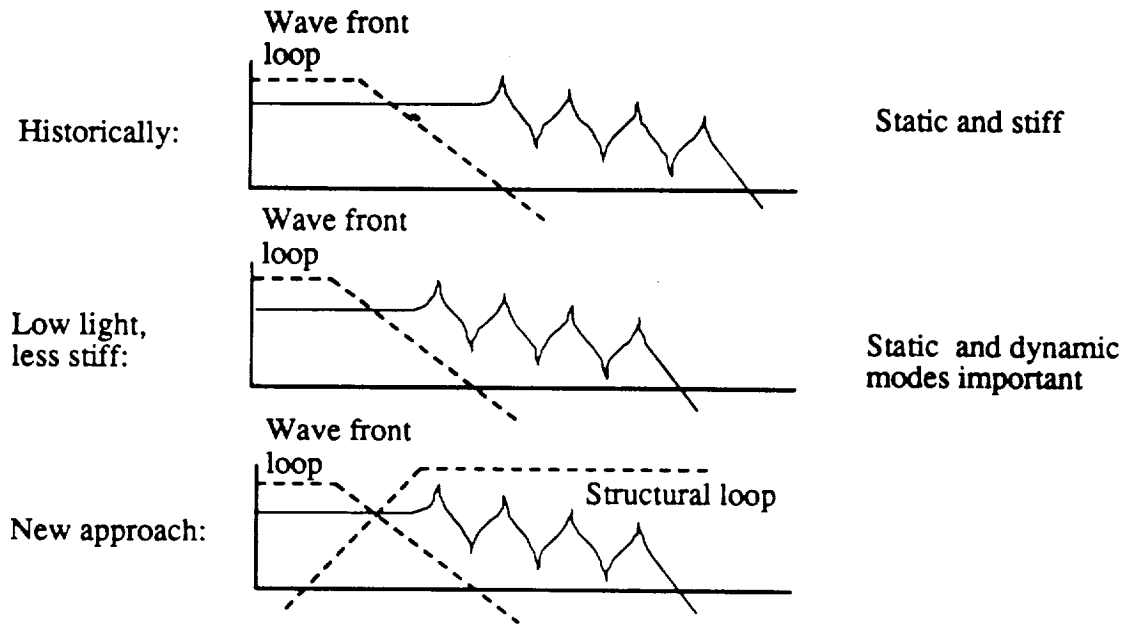
ROBUST PERFORMANCE FOR SYSTEMS WITH PARAMETERIC UNCERTAINTY

Mr. Nesbitt Hagood and Prof. Edward Crawley

(General Affiliation)

There has been much renewed interest in the problem of designing robust control systems for plants which have highly structured, "real parameter" uncertainty. This type of uncertainty can be found in flexible structures were higher modes of the plant can have poorly known natural frequencies and damping. Since the uncertain modes are usually in the critical rolloff region of the structural controller, they can lead to degradation of system stability and performance. Such is the case for the interferometer structure being developed as a testbed for structural controllers. In complicated structures like the interferometer the finite element models rarely represent the structural dynamics to the accuracy needed in conventional Linear Quadratic Gaussian (LQG) design methodologies. The existing design methodologies must be modified and reevaluated in the light of the difficult structural control problem especially in the area of robustness to uncertainty.

In the area of robustness to parametric uncertainty, the particular technique chosen for evaluation is based on considering the average performance of the plant over a set described by the uncertain parameters. It has been shown that if the average performance is finite, then no plant in the set can have an unstable response. This is intuitive since if any plant was unstable it would drive up the average response. This idea can be used to design controllers for uncertain sets of systems by finding controllers which minimize the average quadratic cost. If such a controller can be found it will both guarantee stability and increase the average system performance. The idea of using the average has been used in the past by Bryson, Skelton and others to design robust controllers for aerospace systems. The present work has concentrated on providing a formalism to average cost design.

The difficulty with designing controllers to minimize the average cost lies in computing the average. For systems with many uncertainties, computing the average amounts to performing a high dimensional integration. There are some established ways for approaching this problem such as Monte-Carlo or Fast Probability Integration but they are to computationally intensive for use in control synthesis. The impetus of the present work has been to develop efficient ways to compute approximations to the average which can then be incorporated into the design. One such efficient approximation to the average cost, known as the Bouret equation, was found in the area of random wave propagation, turbulence modelling and Quantum mechanics. It is ideally suited for calculation of the approximate average cost because of its linearity and capability to handle large numbers of uncertainty.

The past six months have been spend developing control methodologies base on the Bouret approximations to the average cost and a related equation which overbounds the average cost. While minimization of the Bouret approximation will provide robustness but not guarantee system

stability *a priori*; minimization of the overbound does guarantee *a priori* stability. While it seems that such guaranteed stability would be desirable for flexible structures, the guarantee caries with it much lower performance and high required control effort. The past six months have been spent quantifying the tradeoff between those controllers which guarantee stability and those which provide robustness but not necessarily stability throughout the set of possible systems. In the coming six months, this trade-off will become more clear as the average based controllers are first simulated and finaly implemented on the SERC interferometer testbed. The two competing controllers, the Bouret approximate average and the average bounding controller will be implemented and compared to existing robust control methodologies such as $\mathcal{H}_\infty$ and LQG/loop transfer recovery. The controllers will be compared on the basis of robustness offered, control cost, and performance.

AREA-AVERAGING SENSORS

Mr. Simon Collins, Dr. David W. Miller and Dr. Marthinus van Schoor

(General Affiliation)

Area-averaging sensors which exhibit magnitude rolloff without associated phase lag have been experimentally demonstrated. This work was published in a paper entitled "Development of Spatially Convolving Sensors for Structural Control Applications" which was presented at the 1990 AIAA Structures, Dynamics and Materials Conference in Long Beach, CA. Achieving magnitude rolloff without phase lag enables gain stabilization without sacrificing phase margin. Future work in this area will first involve demonstrating the advantages of zero phase lag sensor over a point sensor, with or without rolloff dynamics, in an actual closed-loop experiment.

Work during the last six months has focused on the spatial nature of optimal control solutions. In this effort, full state Linear Quadratic Regulator solutions to discrete approximations of distributed parameter systems is formulated. It is realized that the finite set of feedback gains, associated with measurements of structural motion at various locations, are simply discrete approximations of the continuously distributed feedback kernel which convolves with the state function to generate the control command. By observing the discrete gains, this kernel can be inferred. It is then shown that displacement and rotation feedback kernels can be transformed into equivalent curvature feedback kernels. This facilitates implemention using the area-averaging sensor concept. The paper entitled "Formulation of Full State Feedback for Infinite Order Structural Systems" will be presented at the First Joint U.S./Japan Conference on Adaptive Structures in Maui, Hawaii. Future work will involve the experimental implementation of the optimal feedback kernel.

THE NEED FOR PASSIVE DAMPING IN FEEDBACK CONTROLLED STRUCTURE

Prof. Andreas .H. von Flotow

(General Affiliation)

It is well established that an infinite dimensional *mathematical model* of a flexible structure cannot be stabilized with finite bandwidth control; the required gain stabilization beyond the bandwidth model is negated by the infinite structural gain at each resonance. Thus, even a mathematical model with no modeling uncertainty will show that passive damping is critical to enabling active control. What is less well known are the benefits of passive damping for the robust control of *real structures*. There has been a tendency, in the research literature, to define the research problem to consist of developing control approaches for the broadband control (many modes in the control bandwidth) of poorly modeled, lightly damped, modally dense structures. There is ample reason to believe that such control is practically unachievable and that the attribute "lightly damped" is one of the most easily and readily remedied characteristics of such a problem structure.

This paper reports upon the enabling effect of passive damping in the control of uncertain flexible structures, particularly with dislocated actuators and sensors. Quantitative results are all single-input single-output and the benefits of passive damping are then understandable in terms of classical ideas of gain and phase stabilization. The paper derives approximate expressions for the minimum acceptable level of passive damping in terms of modeling uncertainty and desired bandwidth. These relationships can then be interpreted as specifying either a minimum level of passive damping or a minimum level of modeling fidelity. If the requirement is not met, robust control with the bandwidth including uncertain flexible dynamics, is not possible with linear time invariant (LTI) compensation.

These ideas were exploited in the MS thesis of Jim Garcia (June 1990), in which unacceptable interaction of a flexible structure and a low-order control system was limited by passive damping. In this project, a small mirror, fastened to a flexible beam via a piezo-ceramic mount was controlled such that the distance from this mirror to a second mirror statically fastened to the same beam was regulated to remain constant. Commanded motion of the piezo-ceramically mounted mirror excited the beam, influencing the motion of both mirrors and thus the desired distance. This work quantifies the level of passive damping required to enable low-order broadband feedback control of this system.

REFERENCES

1. A.H. von Flotow, D.W. Vos, *The Virtues of Passive Damping in Controlled Structures*, Proceedings of the 61st Shock and Vibration Symposium, Pasadena, CA, October 1990.

2.   *J.G. Garcia, L.A. Sievers, A.H. von Flotow, "Broadband Positioning Control of Small Payloads Mounted on a Flexible Structure," Proceedings of the ASME Winter Annual Mtg., Dallas, TX, November 28, 1990.*

Other SERC Activities

MIDDECK 0-GRAVITY DYNAMICS EXPERIMENT(MODE)

Prof. Edward Crawley, Dr. Marthinus C. van Schoor, Dr. David W. Miller

MODE is an STS middeck flight experiment funded under the NASA In-Step program. MODE was conceived as a dynamics test facility uniquely suited to conducting tests of nonlinear dynamic systems in the zero-gravity environment on the shuttle middeck. During its first flight, tentatively scheduled for September 1991, MODE will test the non-linear dynamics of a fluid volume coupled to a simulated spacecraft mode and jointed truss structure.

The MODE program completed its Critical Design Review (CDR) in March 1990. Construction of flight hardware is proceeding with completion in January, 1991.

MIDDECK ACTIVE CONTROL EXPERIMENT (MACE)

Prof. Edward Crawley and Dr. David W. Miller

MACE was a Phase B study, funded by NASA Langley Research Center, to study the possibility of developing a controlled structure test facility for the shuttle middeck based upon the MODE concept. Recently, this experiment became part of the NASA In-Step program. As presently envisioned, the first flight would involve the testing of a large angle articulating, multibody platform representative of generic multipayload platforms. The objective is to study the effect of gravity perturbations on closed-loop performance. The ground-based engineering model is the SERC multibody testbed.

Government and Industry Interaction

ITEK INVOLVEMENT

As a result of the Center, SERC has become aware of the research and development in active shape control being performed at ITEK and ITEK has become familiar with the research effort in the Center. This has led to the evolution of a joint research program in the development of lightweight, active mirror technology. An actively deformable, precision surface is the third SERC testbed and is presently in the conceptual phase.

JPL INVOLVEMENT

SERC and JPL have continued their close relationship by working on research into active struts, fostered by SERC graduate students residing at JPL during the past year, and through an effort to understand the relationship between certain similar research results achieved at SERC and JPL.

JPL, through Dr. Robert Laskin, has started to participate in the Middeck Active Control Experiment (MACE).

NASA LANGLEY RESEARCH CENTER

While coordination with efforts at NASA LaRC has been good in the past, it was recently suggested that such coordination could be strengthened. The present plan is to better coordinate SERC's multibody testbed and LaRC's evolutionary CSI testbed. The August 1990 Summer SERC Symposium was held at NASA LaRC.

MCDONNELL DOUGLAS SPACE SYSTEMS COMPANY

MDSSC is continuing its participation in the Middeck 0-Gravity Dynamics Experiment (MODE) and is part of the Middeck Active Control Experiment (MACE) team.

LOCKHEED MISSILES AND SPACE COMPANY

LMSC has joined the Middeck Active Control Experiment (MACE) team and supported several undergraduate and graduate students at LMSC during the summer of 1990 to work on MACE component technologies. LMSC plans to significantly increase involvement in MACE in calendar year 1991.

Milestones

PAST

Event	Objective	Date
SERC Symposium	Presented research (held at NASA LaRC).	August 1990
Multibody Testbed Critical Design Review	Formalize design of multibody testbed.	February 1990

FUTURE

Event	Objective	Date
Steering Committee and Technical Representative Meeting	Review the SERC program	January 1991
Science Advisory Committee Meeting	Review the interferometer testbed. Review science issues for multibody testbed.	Spring 1991
SERC Symposium	Present research (to be held at M.I.T.).	June 1991

Publications

N93-25834

Using Input Command Pre-Shaping to Suppress Multiple Mode Vibration

James M. Hyde
Research Assistant
Department of Mechanical Engineering
Massachusetts Institute of Technology
Cambridge, MA 02139

Warren P. Seering
Professor
Department of Mechanical Engineering
Massachusetts Institute of Technology
Cambridge, MA 02139

Abstract

Spacecraft, space-borne robotic systems, and manufacturing equipment often utilize lightweight materials and configurations that give rise to vibration problems. Prior research has led to the development of input command pre-shapers that can significantly reduce residual vibration. These shapers exhibit marked insensitivity to errors in natural frequency estimates and can be combined to minimize vibration at more than one frequency. This paper presents a method for the development of multiple mode input shapers which are simpler to implement than previous designs and produce smaller system response delays. The new technique involves the solution of a group of simultaneous non-linear impulse constraint equations. The resulting shapers were tested on a model of MACE, an MIT/NASA experimental flexible structure.

Introduction

Space-borne robotic systems and vehicles often employ lightweight materials and configurations that result in a high degree of system flexibility. The system's light weight facilitates launching, but chronic vibration problems are a common result. Manufacturing equipment also increasingly utilizes lighter

1

structural elements, a main objective being improving the speed of automated assembly. The combination of a lightweight structure with high performance requirements often leads to serious vibration problems. The growing demand for high accuracy manipulation is in no way aided by these simultaneous attempts to increase speed and decrease weight. Partial or complete suppression of system vibration can improve spacecraft durability and performance, and would allow manufacturing systems to operate faster and more economically.

Attempts to decrease the vibration inherent in flexible systems have enjoyed varied success over the past decade. Cannon and Schmitz [1] experimented with the non-colocated feedback control of a flexible beam. Through the use of accurate system models and optical tip position sensing they achieved significant vibration reduction in their planar test article.

Yurkovich and Tzes [8] reduced vibration in the presence of unknown and/or varying payloads by employing on line system identification and controller tuning. By using frequency domain techniques to examine the system response following a sample input, enough information was gained to adjust the controller gain scheduling to compensate for vibration problems.

Wie [9] employed H_∞ controllers to reduce vibration while providing robustness to modelling errors. This technique displayed solid performance, but was relatively difficult to implement.

Input command shaping is an attractive vibration reduction method because it is essentially "hands off;" inputs can be fed through a shaper and into the system, and ideally the resulting system output will be vibration free. Shapers also usually reside completely outside of a given control system and are thus easily compatible with other vibration schemes (see figure 1). Smith
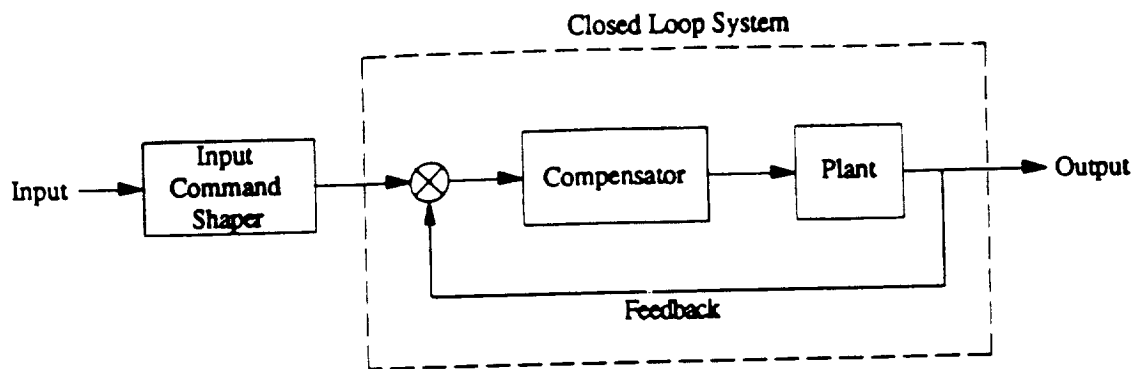
Figure 1: Shaper Position in Control System

[6] conducted early shaping investigations, largely through the use of posicast control.

Meckl [3] examined the use of shaped force profiles to reduce vibration in manufacturing systems. Meckl created profiles by using a versine (1 – cosine) function to modify force commands. When integrated twice, these force profiles became input trajectories that reduced system vibration at a structure's first natural frequency.

A major problem with command shaping is that its success usually depends on solid prior knowledge of plant dynamics. Many attempts at input shaping have been criticized because the shapers exhibited significant dependence on precise system models.

Singer [4] presented a simple shaping algorithm that demonstrated strong insensitivity to modelling errors. The shapers were assembled from impulse sequences and produced only small delays in system response times, on the order of one period of a system's natural frequency. This technique performed notable vibration reduction in tests of a full scale mockup of the Space Shuttle Robotic Manipulator System, conducted at NASA's Manipulator Development Facility at the Johnson Space Flight Center.

Tzes, Englehart, and Yurkovich [7] studied the effects of combining input shaping with a closed loop, acceleration feedback controller. They conducted tests on a flexible beam and proved that each technique can complement the other, resulting in enhanced vibration reduction. This work supports the assertion that input command shaping can be used concurrently with other vibration suppression schemes.

Singer [4] originally assembled shapers designed to cancel single mode vibration and later expanded the algorithm to handle multiple mode problems. The initial multiple mode technique was somewhat cumbersome, however, and the main purpose of this paper is to present an improved method for developing multiple mode shapers. Simpler impulse trains can be assembled by directly solving a full set of multiple mode vibration equations. These new shapers have all the vibration reduction capabilities of the original shapers, and yet exhibit savings in implementation complexity and response time. We present an approach for solving the vibration equations and offer evidence of the new shapers' potential through tests conducted on a model of MACE, an MIT/NASA experimental flexible structure.

Single Mode Shaping

To develop a single mode input shaper, we first note that the second order system response to an impulse input is described by:

$$y_i(t) = A_i \, e^{-\zeta \omega (t - t_i)} \sin((t - t_i)\omega \sqrt{1 - \zeta^2})$$

(1)

where $y_i(t)$ is the output, A_i is the impulse amplitude and t_i is the time at which the impulse occurs. The system's vibration frequency is ω, with damping ζ. If the system is linear, its total response to a series of N impulses

can be expressed as a sum of the the responses to each impulse "i." The magnitude of the total response following the Nth impulse is given by:

$$Amp = \left[\left(\sum_{i=1}^{N} A_i e^{-\zeta\omega(t_N - t_i)} \sin(t_i \omega \sqrt{1 - \zeta^2}) \right)^2 + \left(\sum_{i=1}^{N} A_i e^{-\zeta\omega(t_N - t_i)} \cos(t_i \omega \sqrt{1 - \zeta^2}) \right)^2 \right]^{1/2} \quad (2)$$

A train of properly arranged impulses can suppress residual vibration by forcing Amp to equal zero. This can only happen when both the sine and cosine terms in equation (2) independently equal zero:

$$\sum_{i=1}^{N} A_i e^{\zeta\omega t_i} \sin(t_i \omega \sqrt{1 - \zeta^2}) = 0$$

$$\sum_{i=1}^{N} A_i e^{\zeta\omega t_i} \cos(t_i \omega \sqrt{1 - \zeta^2}) = 0 \quad (3)$$

To construct an impulse sequence that will act as a vibration reducing input shaper, we start by imposing two initial constraints:

$$t_1 = 0 \quad (4)$$

$$\sum_{i=1}^{N} A_i = 1 \quad (5)$$

The first is simply an origin specification, and the second is a normalization constraint. Normalizing a shaper's impulse magnitudes ensures that a shaped input will not exceed limitations imposed on the original input, such as actuator or stress limits. We specify an arbitrary value for A_1, and with $N = 2$, we can use equations (3) to solve for the time and amplitude of the second impulse in a two-impulse shaper.

This shaper will completely cancel residual vibration in a single mode system, as long as the natural frequency and damping ratio are perfectly

known. To account for possible modelling inaccuracies, the shaper should exhibit some insensitivity to errors in natural frequency and damping ratio estimates. By differentiating equations (3) with respect to natural frequency, we generate two additional impulse constraints:

$$\sum_{i=1}^{N} A_i \, t_i \, e^{\zeta \omega t_i} \sin(t_i \omega \sqrt{1 - \zeta^2}) = 0$$
$$\sum_{i=1}^{N} A_i \, t_i \, e^{\zeta \omega t_i} \cos(t_i \omega \sqrt{1 - \zeta^2}) = 0$$

(6)

Setting the partial derivative with respect to natural frequency equal to zero also sets the partial derivative with respect to damping ratio equal to zero [4]. These new constraints require the addition of a third impulse to our sequence; we have four equations, we need two unknown amplitudes and two unknown times. The three impulse sequence will force the residual vibration to be low even if the system parameters are not precisely known.

The standard three impulse, single mode shaper features impulses with a 1-2-1 magnitude configuration and times that are equally spaced. A typical sequence is shown in figure 2.
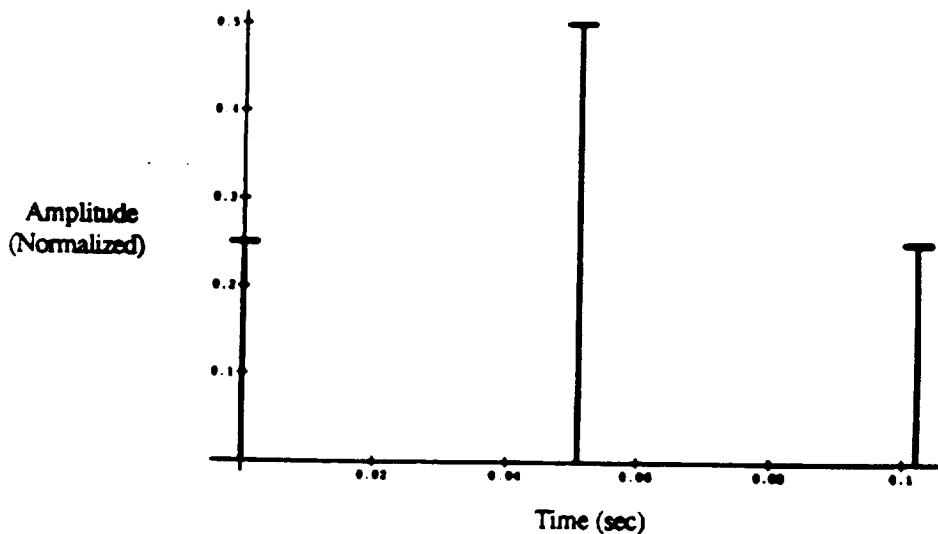
Figure 2: Typical single mode three impulse shaper.

Note: these impulses are constrained to having positive amplitudes. By using negative impulses, the time of a series' final impulse can be decreased, but negative impulses tend to tax a system's actuators and introduce high stress levels. In the remainder of this paper, all shapers will utilize impulses with positive amplitudes. For a full derivation of the above equations, see Singer [4].

Adding Modes

To cancel multiple mode vibration, we can convolve several single mode impulse sequences into longer trains. Convolution results in a sequence whose final impulse is located at a time equal to the sum of the damped periods of the cancelled modes. The value of the final impulse's time will be referred to as the shaper's "length." The number of impulses in the convolved sequence is equal to 3^m, where m equals the number of modes. A standard three mode convolved shaper is shown in figure 3. This sequence was solved for a zero damping case, so the twenty-seven impulses are arranged symmetrically about the center of the pattern.
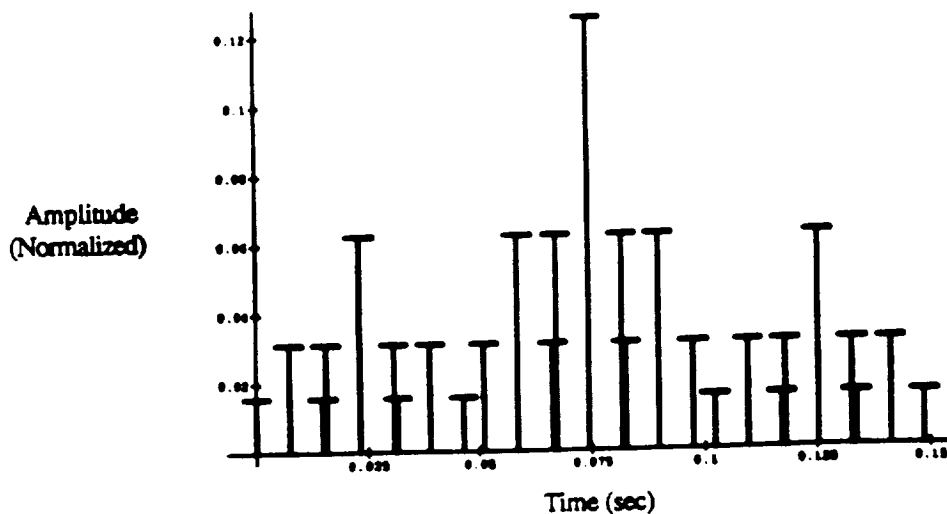
Figure 3: Three mode convolved impulse sequence.

7

The convolved multiple mode sequences are easily generated, but their failings become clear when the cancellation of higher mode vibration is desired. The number of impulses in a convolved shaper increases exponentially with added modes, and by the time the third or fourth mode is added, the sequence has become packed with impulses and can be difficult to implement in real time. Shapers with more impulses increase the time required to modify an input, and might force a decrease in servo rate.

The solution to these problems is to build multiple mode sequences not through convolution of single mode sequences, but through a direct solution of the constraint equations, (3) and (6), as written to include an arbitrary number of modes:

$$\sum_{i=1}^{N} A_i \, e^{\zeta \omega_j t_i} \sin(t_i \omega_j \sqrt{1 - \zeta_j^2}) = 0$$

$$\sum_{i=1}^{N} A_i \, e^{\zeta \omega_j t_i} \cos(t_i \omega_j \sqrt{1 - \zeta_j^2}) = 0 \tag{7a}$$

$$\sum_{i=1}^{N} A_i \, t_i \, e^{\zeta \omega_j t_i} \sin(t_i \omega_j \sqrt{1 - \zeta_j^2}) = 0$$

$$\sum_{i=1}^{N} A_i \, t_i \, e^{\zeta \omega_j t_i} \cos(t_i \omega_j \sqrt{1 - \zeta_j^2}) = 0 \tag{7b}$$

Repeating equations (7) for additional modes "j" generates a set of simultaneous non-linear impulse expressions. Solving these equations can yield shapers with shorter lengths than the convolved shapers. Shorter sequence lengths decrease the delay in system response caused by using the shaper. The direct solution sequences, moreover, use only (2*m) + 1 impulses, m being the number of cancelled modes. This linearly increasing impulse population leads to vastly fewer impulses in higher mode shapers, reducing implementation time.

The savings in length and impulse density that the direct solution sequences support are offset by an increase in sequence generation complexity. The single mode shaper equations, given the constraints of positive impulse amplitudes and shortest possible overall length, had a closed form solution. As written for the multiple mode case, the shaper equations require a strict set of constraints just to limit their infinite solution space, and no general solution has been found.

Solving the Equations

The key to solving the multiple mode equations thus far has been to employ a linear approximation. Equations (7) are non-linear only in terms of impulse time. A straightforward approach is to pick a time for the sequence's final impulse, essentially defining a sequence length, and then divide the length into a fine time mesh. An impulse is placed at each time slot, with unknown amplitude but known time. The equations are now under constrained, but a linear approximation to the exact shaper sequence can be generated through optimization.

The constraints for the optimization problem are the multiple mode equations (7) and the normalization requirement (5). The cost function is the sum of the second derivatives of equations (7a):

$$\text{Cost} = \left| \sum_{j=1}^{M} \sum_{i=1}^{N} A_i\, t_i^2\, e^{\zeta_j \omega_j t_i} \sin(t_i \omega_j \sqrt{1 - \zeta_j^2}) + \sum_{j=1}^{M} \sum_{i=1}^{N} A_i\, t_i^2\, e^{\zeta_j \omega_j t_i} \cos(t_i \omega_j \sqrt{1 - \zeta_j^2}) \right| \tag{8}$$

Minimizing the second derivative expressions forces the impulse sequence to be even more insensitive to modelling errors. With these guidelines, the

9

linear problem becomes "minimize the cost function subject to the stated constraints."

Solution of the linear problem was accomplished using GAMS, a standard optimization package. GAMS utilizes a version of the primal simplex method to perform linear optimization. If M is the number of modes to be cancelled, σ is the length of the sequence, and dt is the value of a single time mesh element, GAMS' constraint matrix consists of:

$$\text{rows: } r = (4 * M) + 1$$

$$\text{columns: } c = \sigma / dt$$

The variable vector is the series of impulse amplitudes, A_i. The simplex method dictates that at least $(c - r)$ amplitudes will equal zero, and additional impulses are occasionally set with zero amplitude. The optimized GAMS output yielded an impulse train with a number of impulses that was less than or equal to r. This train was a linear approximation to the exact multiple mode shaper.

The second phase of the linear work was to find the feasible solution with the smallest possible final impulse time. This was achieved through multiple GAMS runs, systematically reducing the time of the final impulse and using a binary search algorithm that recognized when GAMS returned an infeasible solution, meaning that the time had been reduced too far. This technique ensured that the final GAMS output was the shortest possible approximation. Figure 4 shows a typical final GAMS result from a three mode problem.
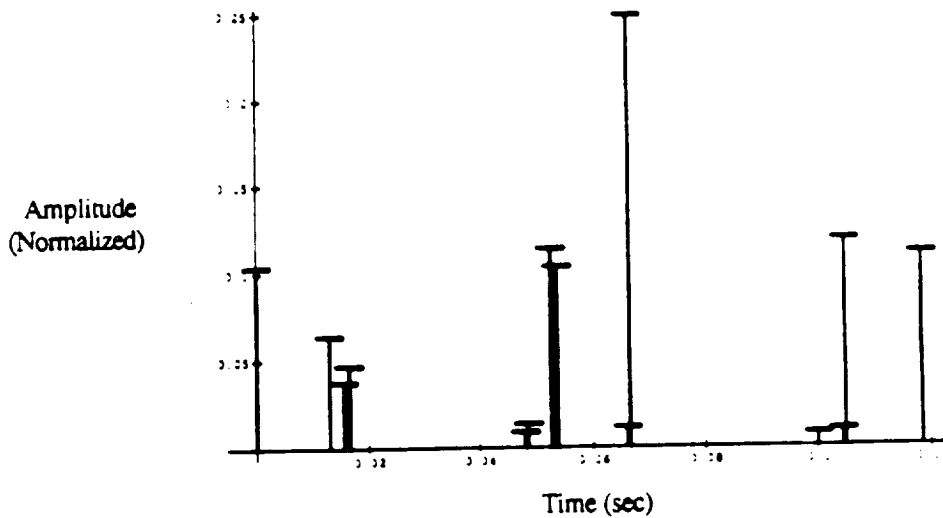
Figure 4: GAMS output for a standard three mode system.

In many cases, this output could stand alone as an effective shaper sequence, especially if the time mesh was set at a digital controller's servo rate. The raw GAMS output, however, had about twice as many impulses as the exact solution demanded. Our goal was to arrive at a sequence with as few impulses as possible, so we used the GAMS output as an initial guess in a non-linear equation solver.

Given the large number of impulses in the final approximate sequence, the GAMS output had to be interpreted to obtain useful guesses of the exact solutions to equations (7). GAMS would often place impulses in adjacent time intervals; these impulses were replaced by single spikes that combined the amplitudes of the neighbors and adopted their exact average time. To further reduce the number of impulses, the interpretation algorithm sought out the closest non-adjacent neighbors. These pairs were combined by summing their amplitudes and taking a weighted average of their times. This set of techniques yielded a sequence whose number of impulses matched that required by the non-linear multiple mode shaper equations (7).

Mathematica™ was used as the non-linear equation solver, mainly because of its additional potential as a programming language that could envelop the entire computational side of the impulse sequence generation. The time and amplitude of the first (i = 1) impulse in equations (7) were held constant, matching the first impulse from the interpreted GAMS output. The remaining times and amplitudes were allowed to vary, with initial guesses of their values provided by the reduced GAMS sequence.

Mathematica employs a Newtonian gradient search algorithm to arrive at its solutions. This method worked quite well, as long as our guesses were sufficiently close to the optimal solutions. As the non-linear equations are continuous and differentiable, adequate gradients are readily available, and points of singularity are usually easy to avoid. The resultant exact impulse sequence, after interpreting the GAMS output in Figure 4 to find initial guesses, is shown in Figure 5. The impulses in the Mathematica result were re-normalized to ensure that the constraint of equation (5) was upheld.
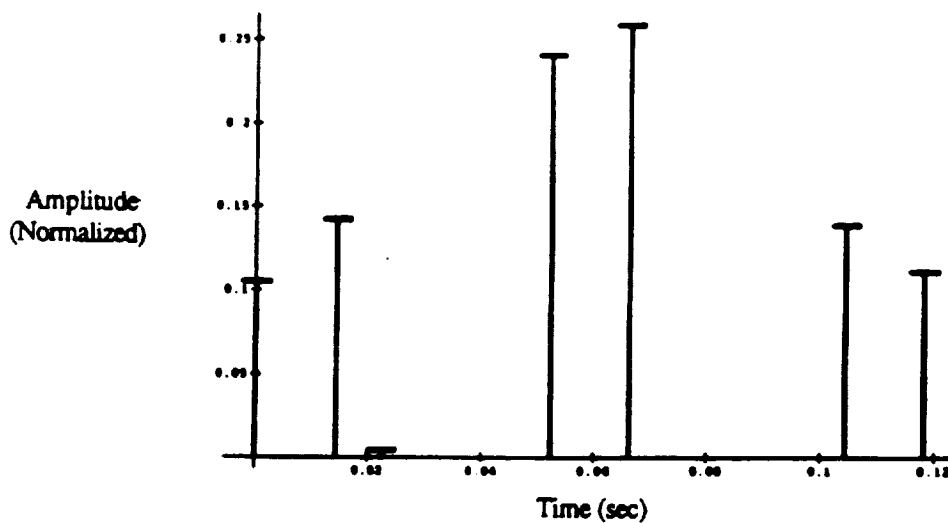
Figure 5: Exact impulse sequence solution, output from Mathematica.

We found that Mathematica could solve the equations only part of the time. A particular structure's absolute modal values and relative modal spacing could disrupt the GAMS program, or Mathematica, or both, resulting in a group of unsolved equations. A variety of different approaches have been used to increase the robustness of the solution process, the ultimate goal being the discovery of a closed form solution. While current work is continuing in this area, the linear approximation/non-linear solution algorithm has successfully generated workable impulse sequences for different groups of three and five modes.

Modeling and Results

The three mode case of particular interest involves a set of frequencies found using a model of an actual flexible system, the MACE test article. The MACE experiment is a joint MIT/NASA project designed to study methods for controlling flexible systems in micro or zero gravity fields. MACE is a flexible structure with two multi-axis pointing payloads residing on either end of a tubular bus. The system incorporates attitude control through a set of three-axis torque wheels, and utilizes inertial position sensing information gained from gyroscope packages mounted at the center of the bus and inside each payload. A simple system schematic is shown in Figure 6.
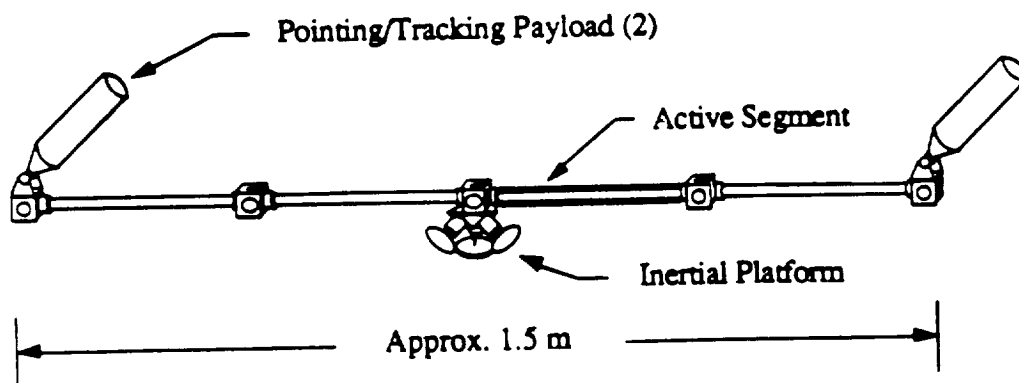
Figure 6: The MACE flexible test article.

The MACE project consists of a Ground Test Article, to reside at MIT, and a Flight Test Article, scheduled for a Space Shuttle launch in 1993. The Ground Test Article is currently being assembled and should be available for testing in December of 1990. The ground article will be actively suspended to emulate a flexible spacecraft in a micro gravity field. This experiment is a prime candidate for practical validation of the command shaper techniques.

While the physical MACE structure has been under construction, personnel at MIT's Space Engineering Research Center (SERC) have developed several computer models of the experiment. The frequencies used in the three mode case mentioned above were found using a linear finite element MatLab model of MACE. The planar model depicted the segmented bus and one of the pointing payloads, as shown in Figure 7.
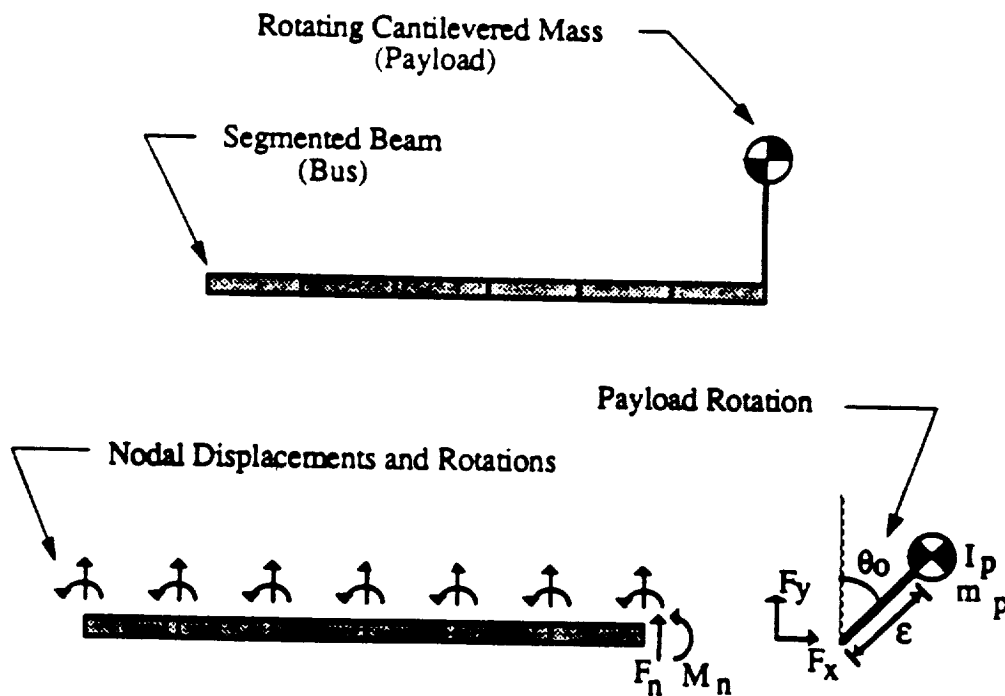
Figure 7: Finite element model of MACE.

The first three eigenvalues of the model were fed into the GAMS / Mathematica routine, generating the shaper sequence shown in Figure 5. Next, simple torque inputs were fed through the shapers and into the modelled payload's gimbal axis, producing the adjusted inputs shown in figure 8. The resulting translation of the beam element on the opposite end of the bus is shown in figure 9, and detailed views of the unshaped and shaped response are provided by figures 10 and 11, respectively. The model had a system of eight modes of vibration, and only the first three were used in forming the input shaper. It is clear from the figures, however, that cancelling these three modes was sufficient to suppress the majority of the structure's vibration.
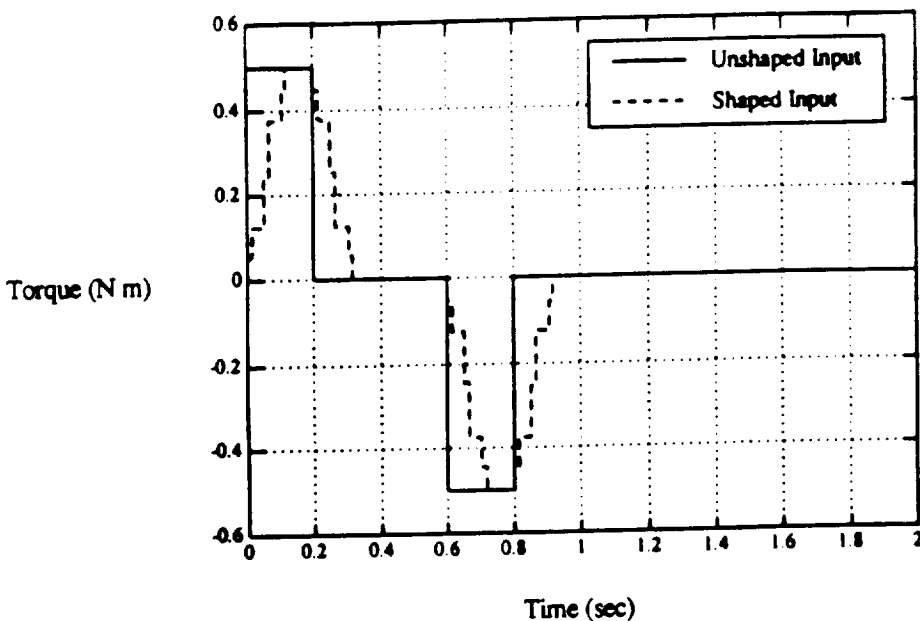
Figure 8: System inputs adjusted by the input shaper.
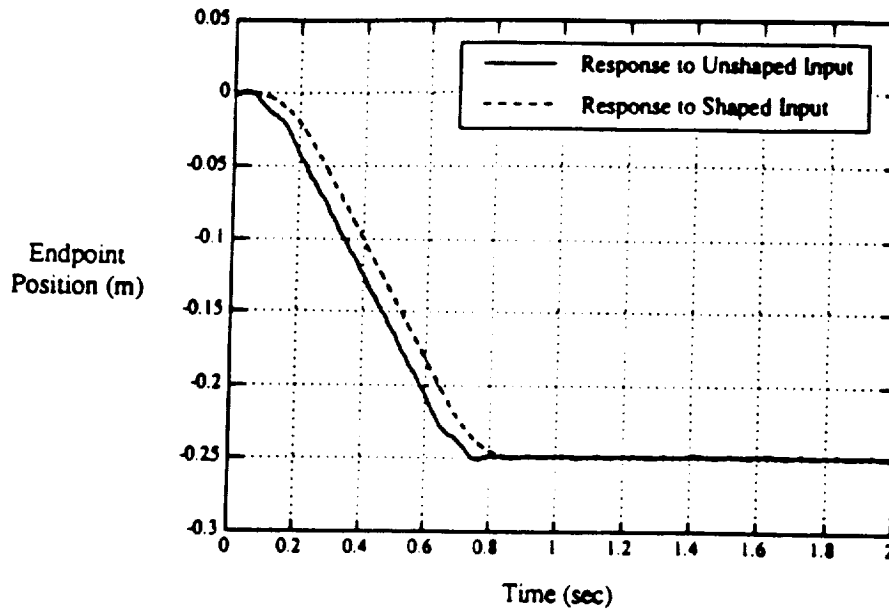
Figure 9: System response to inputs.
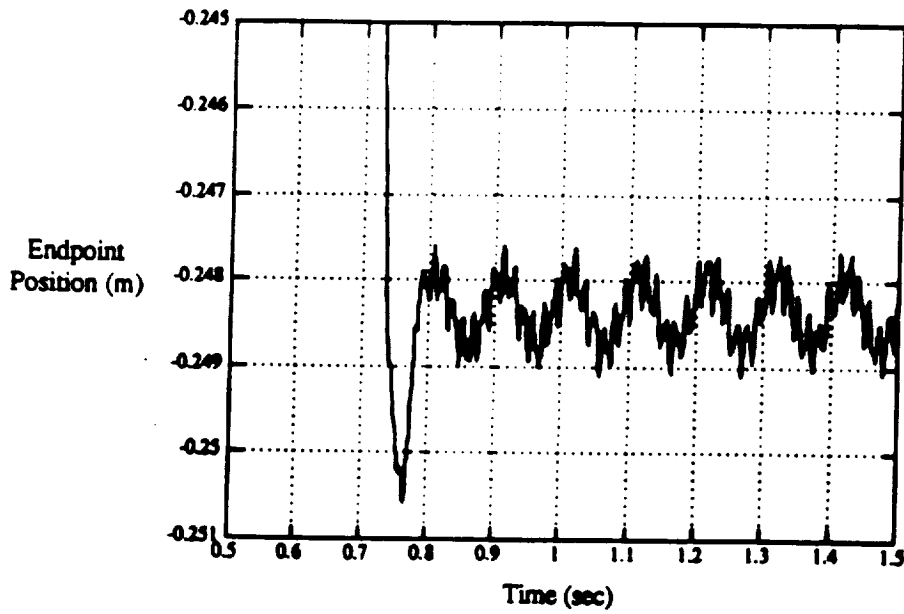
Figure 10: Response to unshaped input (detail).
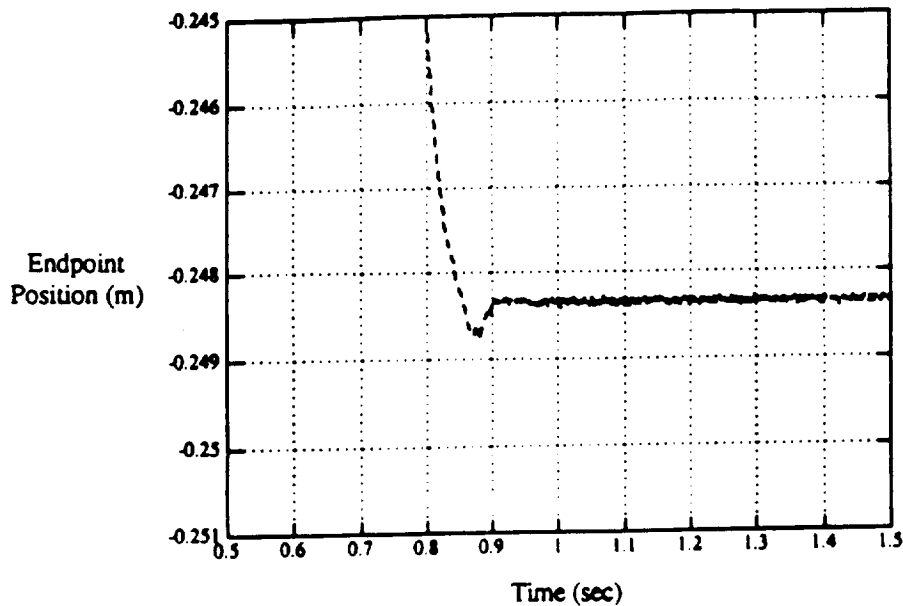
Figure 11: Response to shaped input (detail).

Conclusions

These MatLab results are somewhat predictable. The input shapers are defined by equations that predict the response of linear systems, and the MatLab model was also linear. Cancelling the vibrations of the MatLab model, therefore, served mainly as a confirmation of the proper solution of the constraint equations, and allowed for concrete visualization of what a system experiences when the input shapers are employed. The lessons learned from this initial case will also be valuable when more complex, higher mode shapers are developed.

The next step in this program is to employ more accurate models of MACE. The test article has been simulated non-linearly, using the DISCOS program. This model will likely predict some of the shaper's failings in suppressing vibration in non-linear systems.

The second major future task is to improve the equation solving algorithm to facilitate the construction of higher mode shapers. Sequences

17

that can cancel up to ten or fifteen modes are not out of the question. In addition to increasing the number of cancelled modes, we are devoting effort to decreasing the sequence generation time. We have shown that the direct solution sequences are easier to implement than the convolved sequences, but they are much more difficult to generate. These continued efforts to solve the constraint equations, coupled with the lessons learned from the DISCOS model, will aid in the generation of input shapers capable of effectively reducing vibrations in the actual MACE structure.

Acknowledgements

References

[1] Cannon, Robert H., and Schmitz, Eric,
"Initial Experiments on the End-Point Control of a Flexible One-Link Robot," The International Journal of Robotics Research, Vol. 3, No.3, Fall 1984.

[2] Hollars, Michael G., and Cannon, Robert H,
"Initial Experiments on the End-Point Control of a Two-Link Manipulator with Flexible Tendons," ASME Winter Annual Meeting, November 1985.

[3] Meckl, Peter H. and Seering, Warren P.,
"Controlling Velocity-Limited Systems to Reduce Residual Vibration," IEEE Conference on Robotics and Automation, April 1988.

[4] Singer, Neil C.,
"Residual Vibration Reduction in Computer Controlled Machines," MIT Artificial Intelligence Laboratory Technical Report #1030, February 1989.

[5] Singhose, William E.,
"Shaping Inputs to Reduce Residual Vibration: A Vector Diagram Approach," MIT Bachelor of Science Thesis, February 1990.

[6] Smith, O. J. M.,
Feedback Control Systems, McGraw-Hill Book Company, Inc., New York, N. Y., 1958.

[7] Tzes, A. P., Englehart, M. J., and Yurkovich, S.,
"Input Preshaping With Frequency Domain Information For Flexible-Link Manipulator Control," AIAA Guidance, Navigation, and Control Conference, August 1989.

[8] Yurkovich, S., Pacheco, F. E., and Tzes, A. P.,
"On-Line Frequency Domain Information for Control of a Flexible-Link robot with Varying Payload," Ohio State University Control Research Laboratory Report #CRL-1036-Su88-P, 1989.

[9] Wie, Bong, and Liu, Qiang,
"Feedforward/Feedback Control Synthesis for Performance and Robustness," AIAA Guidance, Navigation, and Control Conference, 1990.

MIT
Space
Engineering
Research
Center

THE MODE FAMILY OF ON-ORBIT EXPERIMENTS:

THE MIDDECK ACTIVE CONTROL EXPERIMENT (MACE)

Prof. Edward F. Crawley — MIT
Dr. David W. Miller — MIT
Dr. Javier de Luis — PSI
Mr. Mel Waldman — LMSC
Dr. Andy Bicos — MDSSC

November 1990

ABSTRACT

A flight experiment entitled the Middeck Active Control Experiment (MACE) proposed by the Space Engineering Research Center (SERC) at the Massachusetts Institute of Technology is described. This is the second in a family of flight experiments being developed at M.I.T. The first is the Middeck 0-Gravity Dynamics Experiment (MODE) which investigates the nonlinear behavior of contained fluids and truss structures in zero gravity. The objective of the MACE program is to investigate and validate the modeling of the dynamics of an actively controlled flexible, articulating, multibody platform free floating in zero gravity. A rationale and experimental approach for the program are presented. The rationale shows that on-orbit testing, coupled with ground testing and a strong analytical program, is necessary in order to fully understand both how flexibility of the platform affects the pointing problem, as well as how gravity perturbs this structural flexibility causing deviations between 1- and 0-gravity behavior. The experimental approach captures the essential physics of multibody platforms, by identifying the appropriate attributes, tests, and performance metrics of the test article, and defines the tests required to successfully validate the analytical framework.

OUTLINE

MODE family of experiments

Overview of the Middeck Zero-Gravity Dynamics Experiment

The Middeck Active Control Experiment (MACE)

Objectives, rationale and focus mission

Science development approach

On-orbit tests

Summary

THE MODE FAMILY OF EXPERIMENTS

The MODE family of experiments is a series of small, relatively inexpensive dynamic and control experiments designed to exploit the interactive, shirt sleeve environment of the STS Middeck. The first facility uses a reusable dynamic test facility to investigate the nonlinear behavior of fluids and truss structures in zero gravity. The second flight modifies the dynamics test facility to include the capability for performing closed-loop active control experiments. This modified, reusable facility is used to investigate the gravity dependent behavior in the closed-loop performance of a flexible, multi-payload platform.

THE MODE FAMILY OF EXPERIMENTS

Fluid Test Article
(FTA)

Coupled Non-Linear
Dynamics of Fluids and
Structures in Zero
Gravity

Structural Test Article
(STA)

Non-Linear Dynamics of
Jointed Truss Structures in
Zero Gravity

Flight # 1:
August 1991

MACE Test Article

Influence of Gravity on the
Active Control of a
Multibody Platform

Flight #2:
September 1993

MACE is part of a logical sequence of cost-effective flight
experiments designed to advance technology of interest to NASA
in the area of controlled structures.

THE MIDDECK 0-GRAVITY DYNAMICS EXPERIMENT (MODE)

MODE consists of two elements: the experiment support module (ESM) containing the equipment typical of a generic dynamic test facility and the two types of test articles. The ESM, which is contained in one Middeck locker, houses the experiment control computer, data acquisition and storage system and sensor and actuator electronics which can be reconfigured to accommodate various test articles. For the first flight of MODE, the test articles will consist of several fluid test articles (FTA's) and several geometries of a structural test article (STA).

THE MIDDECK 0-GRAVITY DYNAMICS EXPERIMENT (MODE)

Experimental Support Module

EXPERIMENT CONTROL

EXCITATION

DATA MEASUREMENT

DATA RECORDER

Test Articles

Fluid Test Article (FTA)

Structural Test Article (STA)
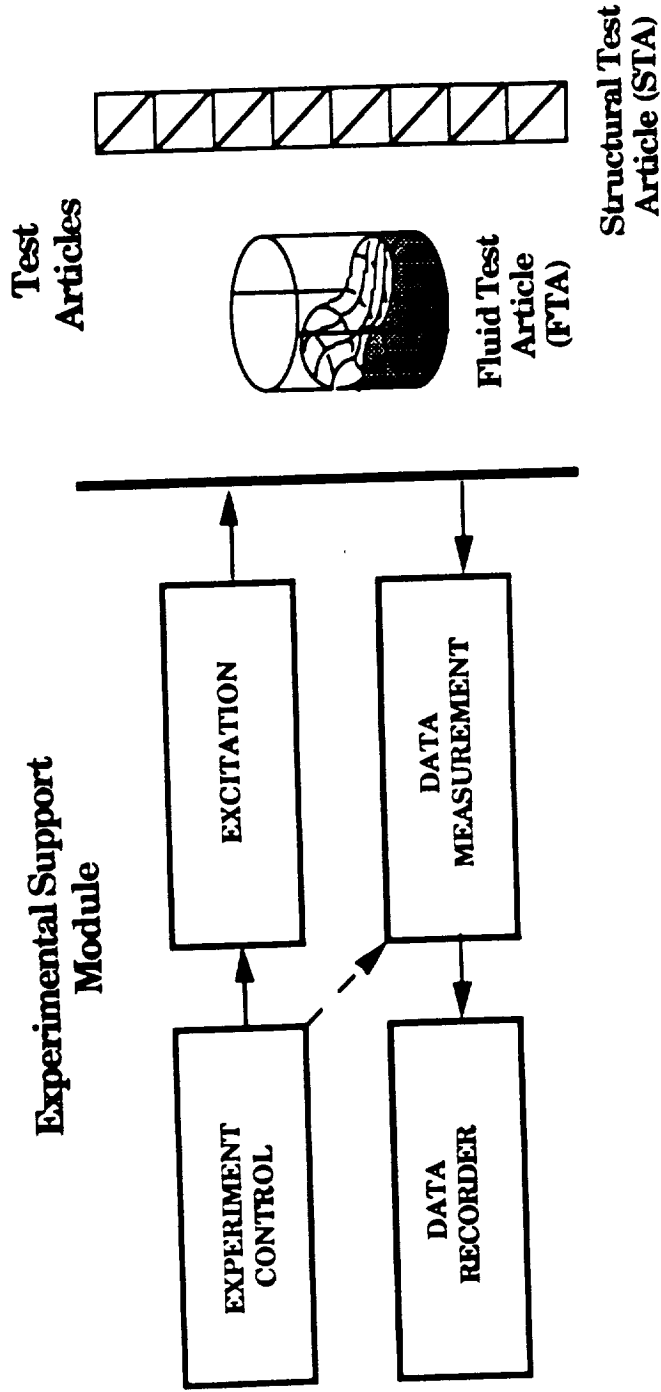
MODE provides a reusable dynamics test facility which will be used on the first flight to test two rather different types of test articles.

FTA OBJECTIVES, REQUIREMENTS AND APPROACH

A rationale justifying the performance of the FTA experiment on-orbit has been developed and is explained on this viewgraph.

FTA OBJECTIVES, REQUIREMENTS AND APPROACH

- Engineering science objective is to characterize fundamental 0-g slosh behavior and obtain quantitative data on slosh force and spacecraft response for correlation of numerical model.

- Requirements

  Scaled tank
  Properly modelled fluid
  Simulation of coupled spacecraft mode
  Harmonic excitation
  Measurement of slosh force

- Modelling approach

  Find fluid flow potential and free surface motion solutions.
  Express kinetic and potential energies in terms of generalized coordinates.
  Derive governing differential equations by applying Lagrange's Principle.
  Solve nonlinear equations subject to harmonic excitation.
  Verify predictions with MODE flight and ground test results.

FTA CONFIGURATION

The FTA assembly, which is stored in a separate locker for launch and landing, is attached to the front panel of the ESM. An umbilical, which is not shown, connects the various FTA sensors and the linear shaker to the ESM electronics. The shaker harmonically excites the force balance, to which the FTA is attached, through both an increasing and decreasing frequency sweep which encompasses the two resonances associated with the slosh motion of the fluid coupled with an electronically synthesized spacecraft mode. This sweep is performed at three different forcing levels to reveal the nonlinear characteristics.

Two geometries of FTA's are used: a flat bottom cylinder and a spherical bottom cylinder. Two different types of fluids will be tested: silicon oil and water. This requires that a total of four FTA's be flown.

Horizontal Rotation: ±60°

Vertical Rotation: ±60°
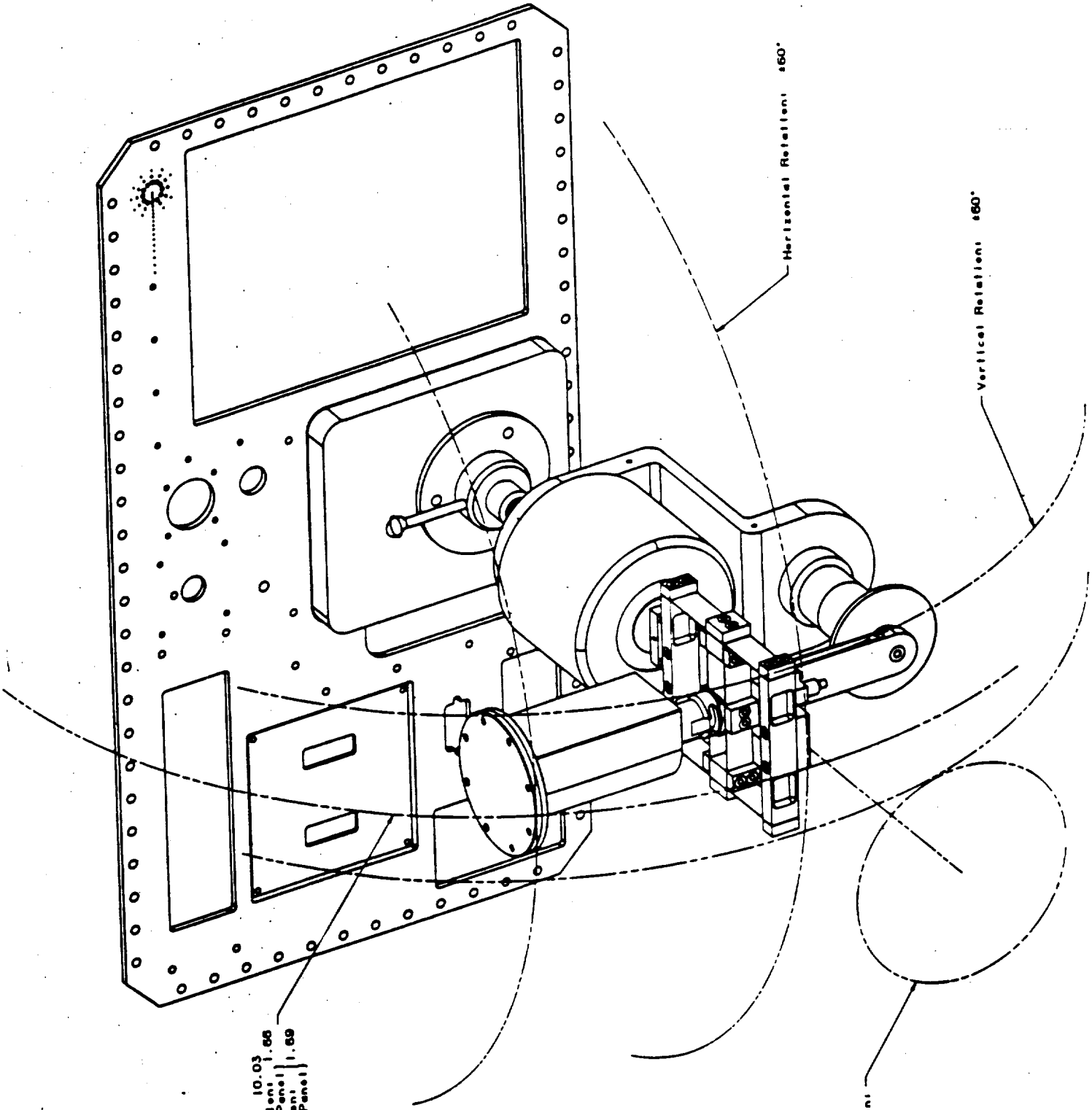
Maximum Radius: 10.03
Center of Rotation: 1.68
   (in Front of Panel)
Maximum Extension: 1.68
   (in Front of Panel)

Axial
Rotation:
±180°

STA OBJECTIVES, REQUIREMENTS AND APPROACH

A rationale justifying the performance of the FTA experiment on-orbit has been developed and is explained on this viewgraph.

STA OBJECTIVES, REQUIREMENTS & APPROACH

- Engineering science objectives are to characterize the fundamental changes in dynamics in 0-g due to absence of gravity on joints, to quantify the changes due to the absence of suspension and gravity load on members, and to obtain quantitative data for correlation with numerical models.

- Requirements

  Truss structure containing elements of future space structures.

  Nonlinear joints with variable pre-load to test nonlinear behavior in several gravity/joint pre-load conditions.

  Reconfigurable truss with deployable and erectable bays.

- Modelling approach

  Develop global linear model using FEM and modal test data.

  Develop Force-State Map of non-linear sub-components.

  Develop describing functions from Force-State Map.

  Insert describing functions into global model and solve for forced response using Harmonic Balance Method.

  Verify predictions with MODE flight and ground test results.

STA CONFIGURATIONS

The STA consists of five types of elements: two four bay deployable truss assemblies; two erectable truss bays; an alpha joint assembly; rigid end masses and a flexible appendage. This viewgraph shows the four different configurations in which the STA will be tested. The ring in three of the four configurations is an alpha joint and the large black dots indicate the nodes of the erectable bays. All deployable bays have preload tension cables. The tension in the cables on one of the deployable bays is adjustable. Testing will involve frequency sweeps at three different forcing levels to identify the nonlinear characteristics of the STA's forced behavior.

STA CONFIGURATIONS
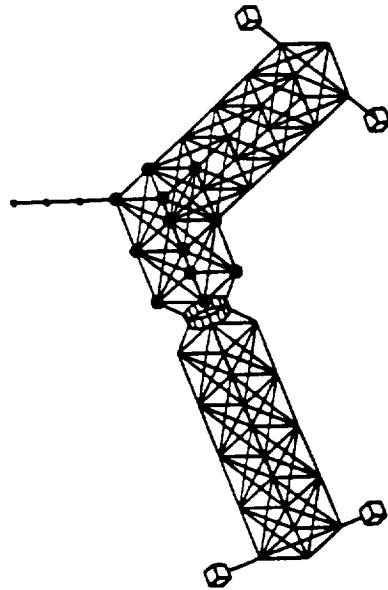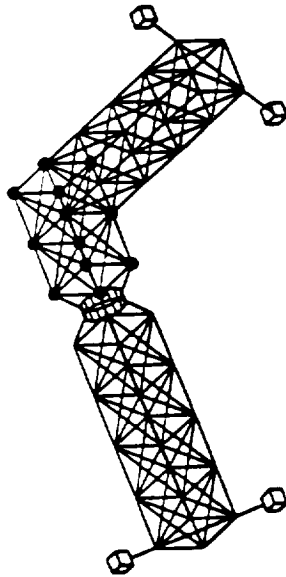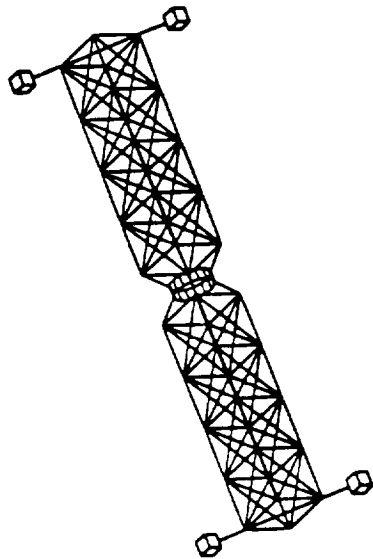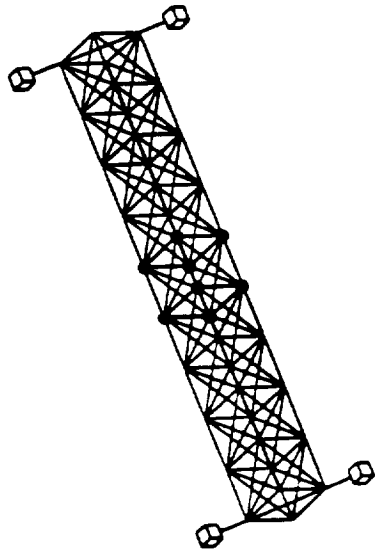
THE MIDDECK ACTIVE CONTROL EXPERIMENT (MACE)

MACE employs the same concept as MODE. An ESM is used to test a multibody platform representative of high mass fraction, multiple payload platforms. The shaded boxes in the ESM are components which also exist in the MODE ESM. The unshaded boxes are components which are unique to the MACE ESM: the realtime feedback control computer and the control actuator drive electronics.

THE MIDDECK ACTIVE CONTROL EXPERIMENT (MACE)

MACE Multibody Platform Test Articl

ESM Experiment Support Module

Experiment Sequencer

Excitation

Actuation

Control Algorithms

Data Measurement

Data Recorder
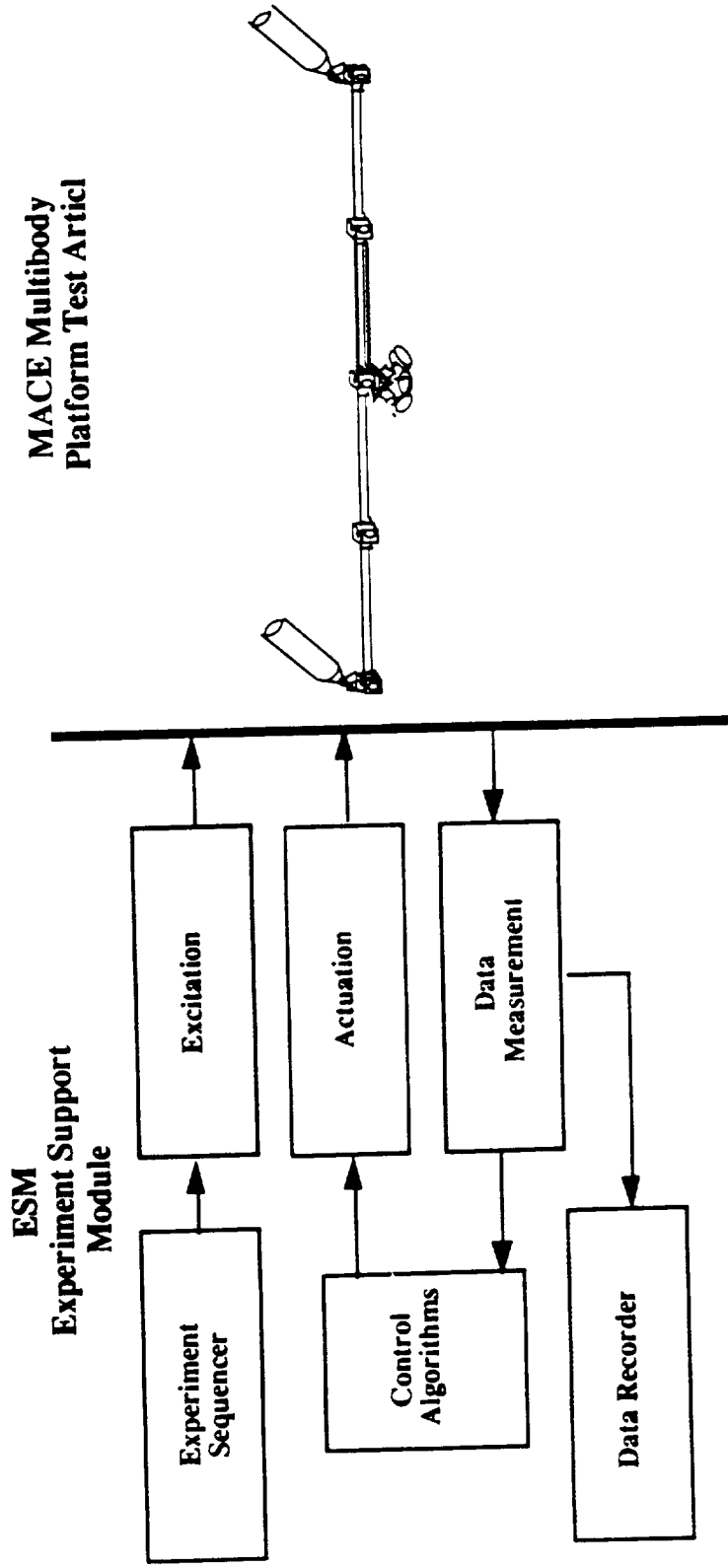
- Substantial commonality of ESM hardware/software

- Significant savings in integration/certification process.

OBJECTIVES AND RATIONALE

MACE differs from MODE in the sense that MACE investigates the accuracy with which the on-orbit closed-loop behavior can be predicted whereas MODE investigates the accuracy with which on-orbit, open-loop behavior can be predicted. The fundamental difference between the two is that no measure of open-loop model accuracy is sufficient to guarantee accurate prediction of closed-loop behavior at arbitrarily large levels of control authority.

OBJECTIVES AND RATIONALE

Objective: to develop a well verified set of tools that will allow designers to either be able to predict on-orbit behavior or allow sufficient versatility in the design to allow identification and tuning of the structure on orbit.

- Since the model fidelity required for stability and performance robustness is intimately related to the level of applied control authority, closed-loop testing is required.

- Vehicle qualification testing will most likely occur on the ground where suspension and direct gravity effects will cause the 1-g and 0-g dynamics to differ.

- Differences between the ground and on-orbit environment cause perturbations which can substantially alter closed-loop behavior.

- Therefore it is essential to perform on-orbit closed-loop testing for comparison with ground testing and analytical predictions to develop these tools.

CAPTURING THE ESSENTIAL PHYSICS: TEST ARTICLE REQUIREMENTS

Several types of proposed mission vehicles were reviewed. These included interferometric telescopes, deformable optical surfaces, multiple payload platforms and robotic devices. Multiple payload platforms were selected as the mission focus for the MACE test article because large angle scanning of multiple payloads presented about the most difficult to test on the ground and therefore accurately predict on orbit. This viewgraph lists some of the essential characteristics of a test article representative of a multiple payload platform.

CAPTURING THE ESSENTIAL PHYSICS: TEST ARTICLE REQUIREMENTS

The simulation of a vehicle with payloads and articulating appendages with pointing and positioning requirements, necessitates a test article with the following attributes:

- appropriately scaled to fit in the middeck while preserving the essential performance requirements.

- two gimballing payloads to enable implementation of multiple interacting control systems with independent objectives.

- two rigid payloads and a flexible appendage, representative of compact high-mass fraction devices and a robotic servicer.

- flexible bus with resonances within the controller bandwidth and to exhibit suspension coupling, gravity stiffening and droop.

- sufficiently complex geometry such that the test article undergoes full 3-D kinematic and coupled flexible motion.

GROUND BASED ENGINEERING MODEL TESTBED

The purpose of the Engineering Model (EM) is to develop science. The EM is presently being fabricated at M.I.T. The segmented bus, which is the structural interconnect between the payloads and the inertial platform, is being dynamically tested. The three torque wheel assembly is completed and the first of two two-axis gimbals is being tested. Fabrication and assembly of the EM should be complete by the beginning of 1991.

GROUND BASED ENGINEERING MODEL TESTBED

Inertial Platform

Active Segment

Active Suspension

Pointing/Tracking Payload (2)

Approx. 1.5 m
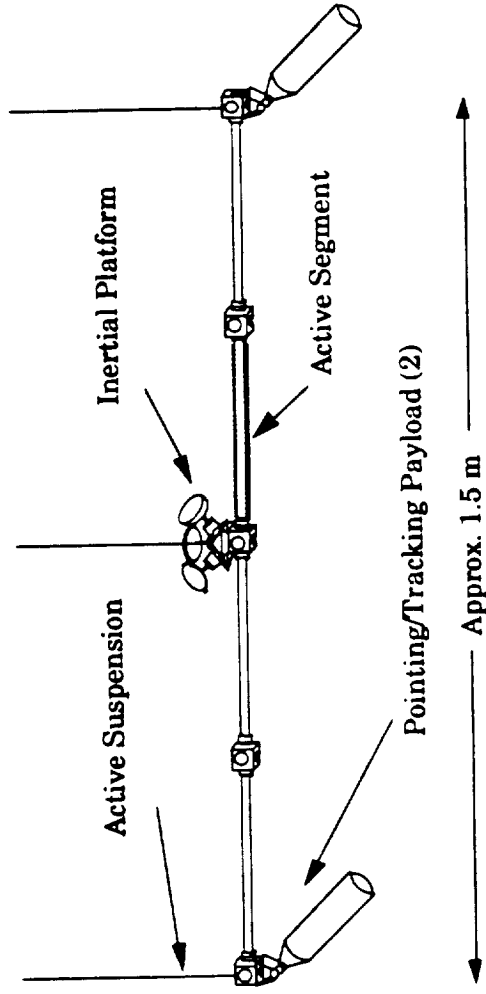
- Three zero spring rate pneumatic/electric suspension devices from CSA engineering with maximum stroke of 63.5 mm.

- AC100 real time control computer from Integrated Systems, Inc.

MACE SCIENCE DEVELOPMENT APPROACH

Six different avenues are being pursued in the development of the MACE science. At first glance, these avenues infer a vast analysis and test matrix. In reality, only a subset will be pursued for the first flight.

1) *Control objectives* refer to studying various combinations of single and multiple payload pointing and scanning.

2) *Control topologies* refers to the feedback paths which are allowed to exist due to different systems integration constraints. *Hardware suites* refers to exploring the performance and robustness improvement obtained as additional suites of hardware become available.

3) *Control approach* refers to the method by which the control algorithms will be derived.

4) *Model complexity* refers to the accuracy and complexity of the models on which these control formulations will be exercised. In other words, the lowest fidelity model provides fundamental insight while the highest fidelity model is used to derive algorithms for implementation.

5) *More complex test article geometries* can be used to further challenge ground testing.

6) Fundamental to the flight experiment is the understanding or *gravity influences* on the problem.

MACE SCIENCE DEVELOPMENT APPROACH

The MACE program will pursue six different avenues in developing controllers for multiple payloads on a flexible bus structure.

1) Control objectives

2) Control topologies and sensor/actuator suites.

3) Control approach to the pointing and scanning problems.

4) Evolution of structural model fidelity.

5) Evolution of structural configuration to more complex geometries.

6) Influence of gravity on closed-loop behavior.

SCIENCE DEVELOPMENT APPROACH:

CONTROL OBJECTIVES

Viewgraph is self-explanatory.

SCIENCE DEVELOPMENT APPROACH:
CONTROL OBJECTIVES

Control Objectives:

- **Pointing** performance of single and multiple payloads.
- **Scanning** performance of single and multiple payloads.

Performance Metrics:

- **Stability**--RMS 2-axis angular position about pointing line of sight or scanning reference profile.
- **Jitter**--RMS 2-axis angular rate about pointing line of sight or scanning reference profile.
- **Slew response time**--time required to complete maneuver.
- **Percent degradation**--reduction from single payload performance associated with addition of an interacting, controlled payload.

SCIENCE DEVELOPMENT APPROACH:

TOPOLOGIES AND HARDWARE SUITES

Four topologies will be investigated. The first called *central* has the payloads clamped to the bus and the torque wheels are used to control the attitude of the assembly. The closed-loop poles are in a Butterworth pattern with a bandwidth equal to one-tenth of the first flexible mode. This "central" topology is used as the low gain baseline against which other designs are compared.

The *localized* topology assumes that payload control design is independent of bus design. Therefore, all payload feedback loops are closed locally and the inertial attitude of the payload is measured locally.

The *centralized* topology requires that the payload infer its inertial attitude from a measurement of the inertial attitude at the center of the bus and other available sensors.

The *global* topology places no constraints on the allowable feedback loops and provides inertial attitude measurements on the bus and on the payload. This topology is used as the high performance scenario for comparison purposes.

First, the control hardware is limited to existing pointing and scanning hardware such as torque wheels, gimbals, rate gyros and angle encoders. Then, sensors whose sole function is to measure the flexibility in the bus become available. Finally, actuators used to control flexibility are added. The purpose of this progression is to investigate the cost/benefit of each additional suite.

SCIENCE DEVELOPMENT APPROACH:
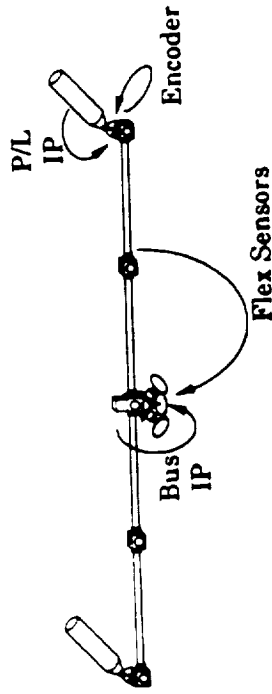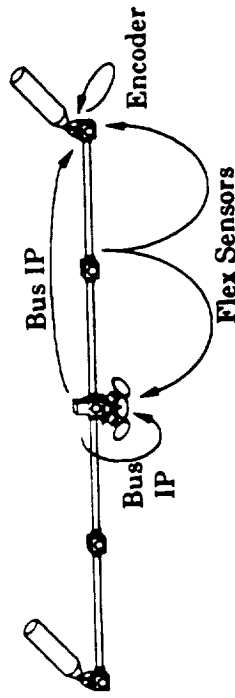## TOPOLOGIES AND HARDWARE SUITES

Localized
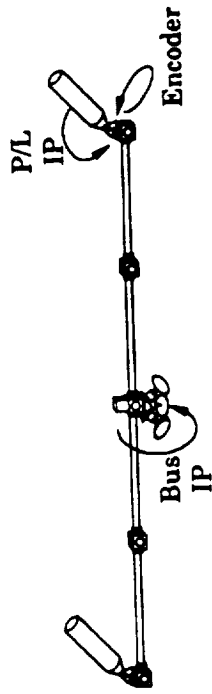
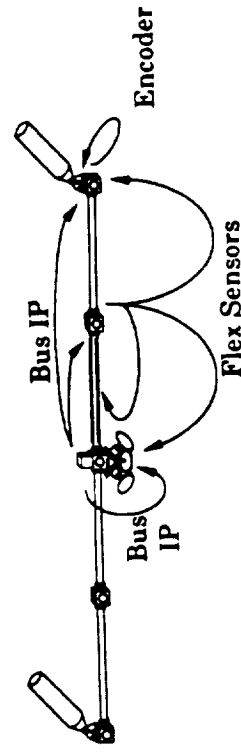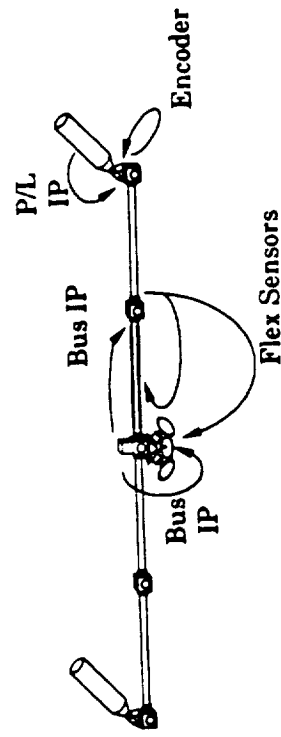### Centralized
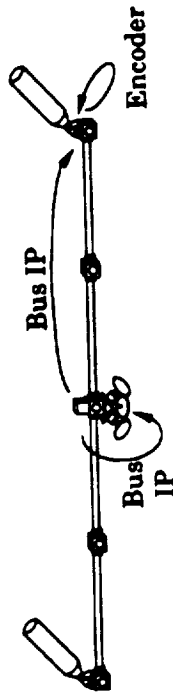
Existing Hardware

Flexibility Sensors

Flexibility Actuators

SCIENCE DEVELOPMENT APPROACH:

CONTROL APPROACH

There are basically two control objectives: pointing and scanning. The pointing problem falls more directly under linear control. Depending on the amount of motion and deformation, the scanning problem may have to be handled with nonlinear techniques.

There already exists some techniques to generate linear control algorithms with simplified structure. Most of these rely on decoupling properties inherent to the system. Such decoupling properties include weak subsystem coupling or time scale separation. Successive loop closure, Nyquist Array, Inverse Nyquist Array and perturbation techniques rely on these decoupling assumptions. Direct optimization is another way to approach the problem. It relies less on understanding the properties of the system and is easier to derive for more complex systems with stronger coupling.

The scanning objective is a classic example of a servomechanism problem. The linear techniques used in the pointing problem may be applicable to this problem. However, the important transformation in the dynamics due to large slews of significant fractions of the spacecraft may render a linear approach inadequate. Therefore, nonlinear control design methods may be required such as gain scheduling, sliding mode control or more generic adaptive control schemes.

SCIENCE DEVELOPMENT APPROACH:
CONTROL APPROACH

- Pointing

  Successive loop closure

  Nyquist Array, Inverse Nyquist Array methods

  Perturbation techniques (weak coupling, connective stability)

  Constrained architecture LQG and other direct optimization techniques

- Scanning

  Linear servomechanism methods (similar to above)

  Nonlinear methods if necessary

  Gain scheduling (slow scanning, wide range)

  Sliding mode control (require numerous, high quality sensors)

  Adaptive control

SCIENCE DEVELOPMENT APPROACH:

MODEL COMPLEXITY

The *typical section* model is used to study the fundamental problem of pointing and scanning a non-center of mass mounted payload attached to a flexible bus. This is a lumped-inertia model of the problem.

The *planar sample problem* is more representative of the actual test article. However, motion is restricted to lie within the plane defined by the model's geometry. This greatly simplifies the complexity of the model allowing easier interpretation of the effectiveness of a particular control architecture. This planar sample problem is available as a document to enable interested researchers to submit control designs.

The *nonlinear three-dimensional model* is a detailed model of the actual EM which has been verified experimentally. This model is used to formulate the control algorithms that are actually implemented on the EM.

SCIENCE DEVELOPMENT APPROACH
MODEL COMPLEXITY

Typical Section

Planar Sample Problem
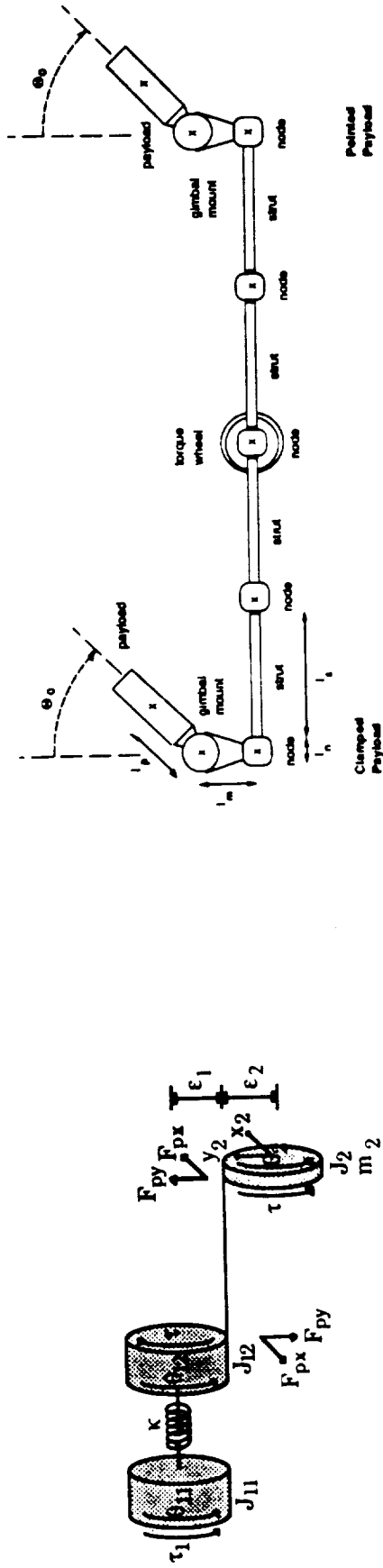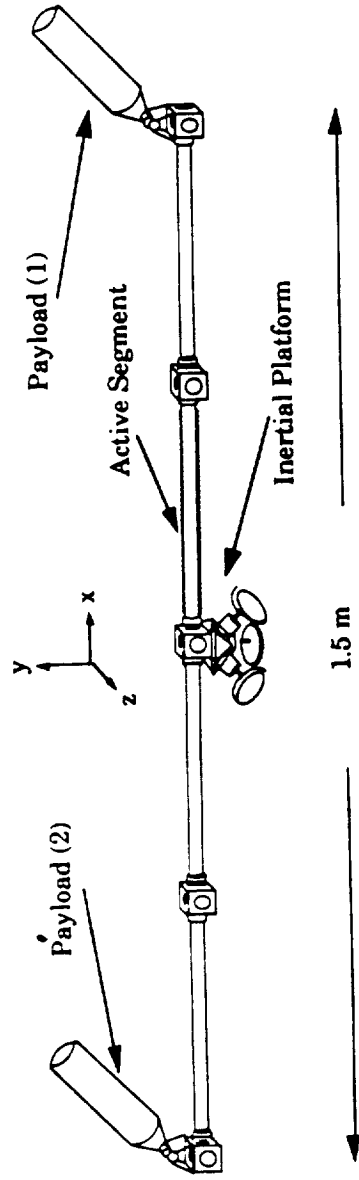
Nonlinear Three-Dimensional Model

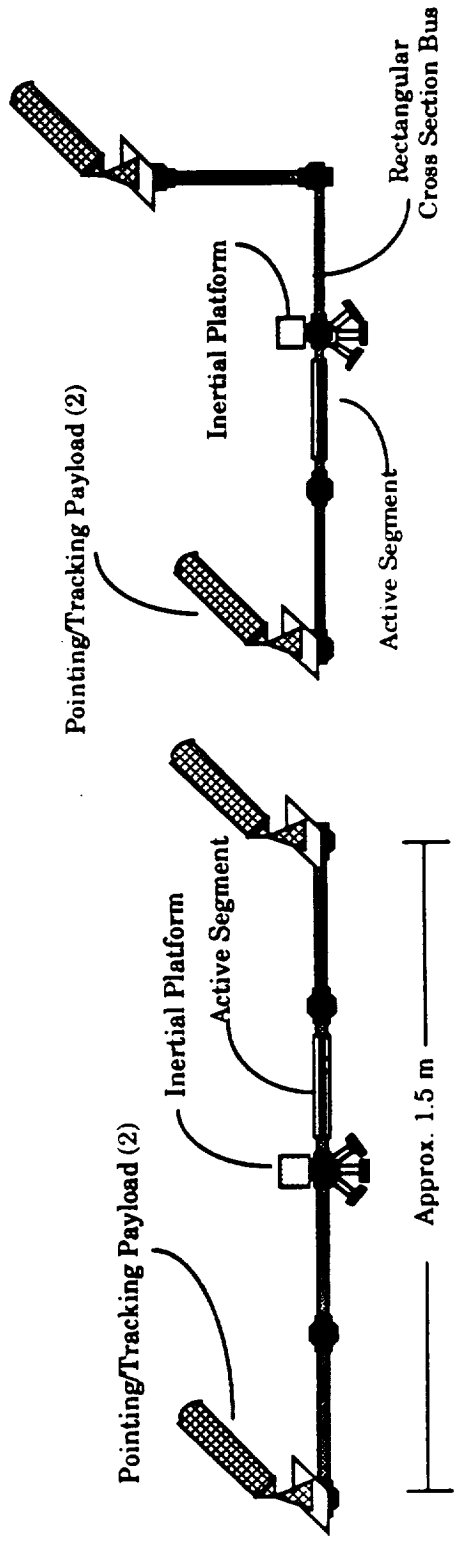# SCIENCE DEVELOPMENT APPROACH:
EVOLUTIONARY CONFIGURATIONS

The EM bus is composed of removable struts and nodes. This enables assembly of the EM in various geometries. More complex geometries are harder to test on the ground because they couple more with the suspension and gravity effects.

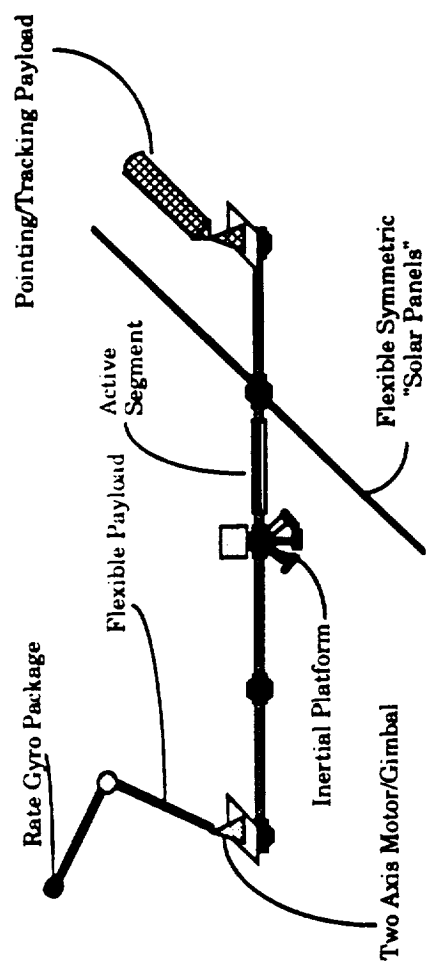The *baseline* configuration is the one that will be studied.

The *three-dimensional* configuration has an 'L' and a rectangular cross-section strut designed to cause bending/torsion coupling and both in- and out-of-plane bending.

The *flexible appendage* configuration includes a flexible articulating payload, representative of a robotic servicer, and two flexible appendages, representative of the roll/bending coupling caused by solar panels.

SCIENCE DEVELOPMENT APPROACH: EVOLUTIONARY CONFIGURATIONS

Pointing/Tracking Payload (2)

Inertial Platform

Active Segment

Approx. 1.5 m

Baseline

Pointing/Tracking Payload (2)

Inertial Platform

Active Segment

Rectangular Cross Section Bus

Three-Dimensional

Pointing/Tracking Payload

Active Segment

Flexible Payload

Rate Gyro Package

Inertial Platform

Two Axis Motor/Gimbal

Flexible Symmetric "Solar Panels"

Flexible Appendage

SCIENCE DEVELOPMENT APPROACH:

GRAVITY INFLUENCES

Viewgraph is self-explanatory.

SCIENCE DEVELOPMENT APPROACH:
GRAVITY INFLUENCES

Objective:

Identify and quantify the magnitude of the perturbation effects of a gravity field and a suspension system on the dynamics of the MACE test article.
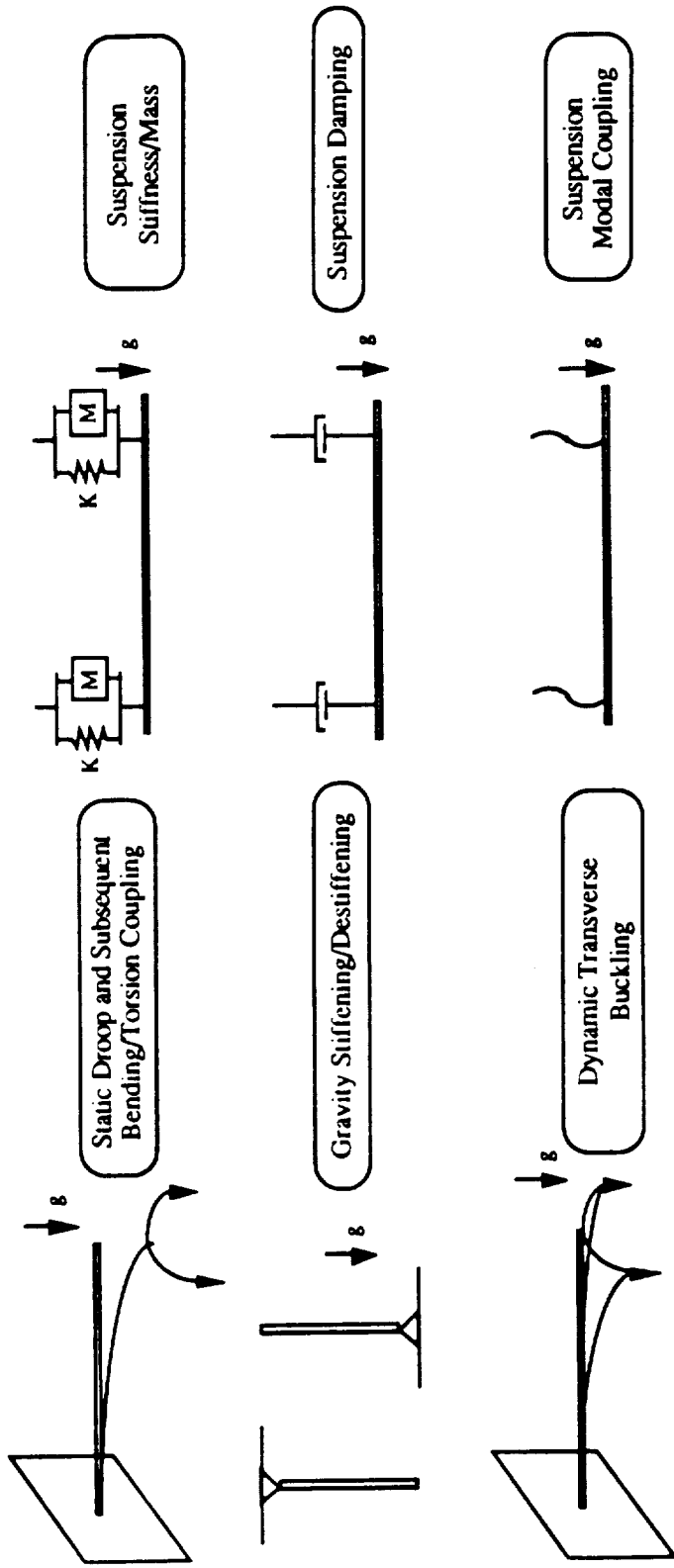
Approach:

- Identify the distinct types of gravity/suspension perturbations.
- Identify a non-dimensional gravity or suspension influence parameter for each important effect and perform a parametric analysis of the effect on the system dynamics.
- Compare analytical results with finite element results.
- Rank the effect types in order of impact on the structural dynamics based on the non-dimensional system parameters.

SCIENCE DEVELOPMENT APPROACH:

GRAVITY INFLUENCES

A gravity effect can be characterized as either a direct gravity effect or an indirect gravity effect. Direct gravity effects are shown in the left column and are characterized by the application of distributed body forces on the structure. Indirect gravity effects are characterized as suspension loads on the structure. These are indirect because the suspension system, which is the influencing factor, is essential in the testing of structures in the one-gravity environment.

SCIENCE DEVELOPMENT APPROACH: GRAVITY INFLUENCES

Suspension Stiffness/Mass

Suspension Damping

Suspension Modal Coupling

Static Droop and Subsequent Bending/Torsion Coupling

Gravity Stiffening/Destiffening

Dynamic Transverse Buckling

THREE CLASSES OF CONTROL ALGORITHMS WILL BE IMPLEMENTED ON ORBIT

The on-orbit tests are designed to achieve the three MACE objectives. First, the gravity effects which most influence the problem will be identified and the level of control authority where they become significant will be determined. Second, the ability to predict on-orbit closed-loop behavior will be determined. Third, the ability to tune the test article on orbit will be tested.

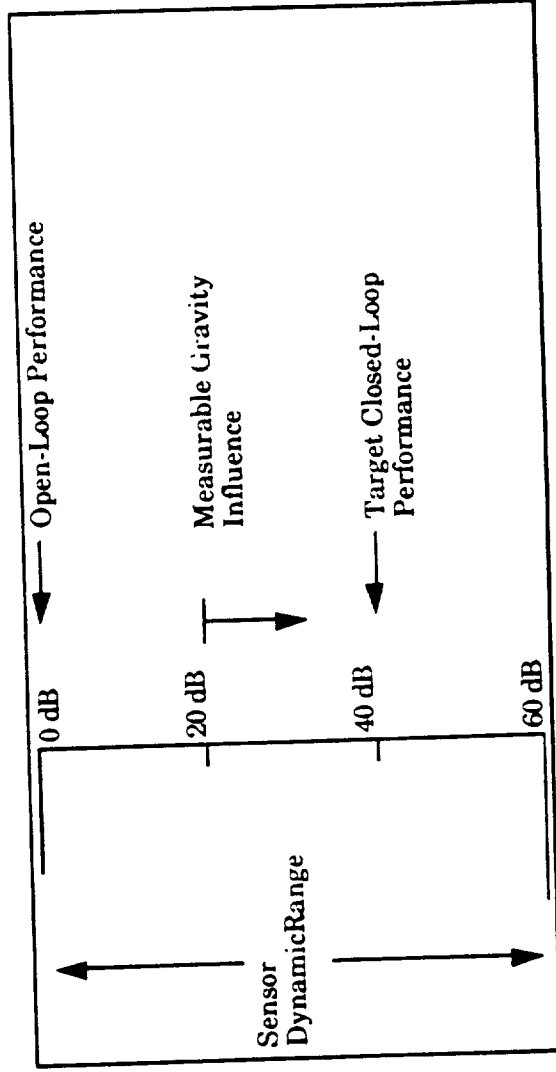# THREE CLASSES OF CONTROL ALGORITHMS WILL BE IMPLEMENTED ON ORBIT

1) Implement same algorithms as implemented on the ground

   - Algorithms based on model which includes gravity and suspension effects.

   - These tests help identify what gravity perturbations are important and when (what gain) they become important.

2) Implement algorithms based on model of predicted 0-g behavior.

   - The gravity parameter in the 1-g model is set to zero and the control algorithms are rederived.

   - These tests determine the accuracy to which 0-g closed-loop performance can be predicted.

3) Implement algorithms based upon on-orbit identified model.

   - First test is an open-loop ID of the structural dynamics.

   - Uplink/downlink capability is being developed to enable downlink of open-loop identification and uplink of associated control algorithms.

   - These tests identify the ability to which the test article's control algorithm can be tuned on orbit.

VALIDATION OF THE ANALYTICAL FRAMEWORK

Three different control algorithms will be implemented on orbit based upon three different models of the test article. The first model is the model of the test article with gravity and suspension effects. Control algorithms based upon this model identify the types of gravity effects which are important and at what level of control authority they become important. The second type of model uses the one-gravity model with gravity terms set to zero. Control algorithms based upon this model identify the ability to predict on-orbit behavior. The third type of model is one that is based upon on-orbit identification of the test article dynamics. Control algorithms based upon this model reveal the ability to tune the test article on orbit.

VALIDATION OF THE ANALYTICAL FRAMEWORK

- Ground testing will include suspension and gravity effects, typical of preflight qualification testing.

- Realistic goal is to improve pointing/scanning performance by 40 dB over open-loop value.

0 dB — Open-Loop Performance

20 dB — Measurable Gravity Influence

40 dB — Target Closed-Loop Performance

60 dB

Sensor Dynamic Range

- Independent of absolute performance level, this demonstrates CST effectiveness.

- Sensor dynamic range of 60 dB is typical.

SUMMARY

Viewgraph is self-explanatory.

SUMMARY

- The MODE family of flight experiments is designed to verify analytical tools developed to predict the gravity dependent behavior of proposed space structures.

- The MODE family of flight experiments uses reusable dynamic and control tests facilities and exploits the unique environment on the STS middeck.

- MACE investigates gravity dependent phenomena pertinent to the closed-loop dynamics of proposed space structures.

  - By comparing performance as a function of control authority between ground and on-orbit testing, perturbations in the dynamics due to the change from 1 to 0-g will be identified.

  - By noting the level of control authority where these performance deviations occur, either analytical predictive capabilities or on-orbit identification procedures can be refined.

M.I.T. SPACE ENGINEERING RESEARCH CENTER

Semi-Annual Report: August 1990

Prof. Edward F. Crawley, Director

Dr. David W. Miller, Research Associate

December 1990   SERC # 17-90-R

MIT's Interferometer CST Testbed

Tupper Hyde*, Ed Kim**, Eric Anderson**, Gary Blackwood**, and Leonard Lublin**

Space Engineering Research Center
Massachusetts Institute of Technology
Cambridge, MA 02139

N93-25836

Introduction

The MIT Space Engineering Research Center (SERC) has developed a controlled structures technology (CST) testbed based on one design for a space-based optical interferometer. The role of the testbed is to provide a versatile platform for experimental investigation and discovery of CST approaches. In particular, it will serve as the focus for experimental verification of CSI methodologies and control strategies at SERC. The testbed program has an emphasis on experimental CST--incorporating a broad suite of actuators and sensors, active struts, system identification, passive damping, active mirror mounts, and precision component characterization.

The SERC testbed represents a one-tenth scaled version of an optical interferometer concept based on an inherently rigid tetrahedral configuration with collecting apertures on one face. The testbed consists of six 3.5 meter long truss legs joined at four vertices and is suspended with attachment points at three vertices (Figure 1). Each aluminum leg has a 0.2m by 0.2m by 0.25m triangular cross-section. The structure has a first flexible mode at 31 Hz and has over 50 global modes below 200 Hz. The stiff tetrahedral design differs from similar testbeds (such as the JPL Phase B) in that the structural topology is closed. The tetrahedral design minimizes structural deflections at the vertices (site of optical components for maximum baseline) resulting in reduced stroke requirements for isolation and pointing of optics. Typical total light path length stability goals are on the order of $\lambda/20$, with a wavelength of light, λ, of roughly 500 nanometers [1]. It is expected that active structural control will be necessary to achieve this goal in the presence of disturbances.

A unique feature of the SERC testbed is the implementation of a multi-axis laser metrology, incorporating complex bends in multiple beam path lengths. At three mock siderostat locations are precision three-axis active mirror mounts. The fourth vertex holds a laser head and other optics. These optical components provide laser interferometric displacement measurements for baseline metrology (six axes define the position of the mock collecting apertures relative to the fourth reference point). We are concerned that the testbed represents a scaled model of an actual scientific observatory as closely as possible. At the same time, we seek to perform CST research which is generic and applicable in different areas.

The structure is instrumented with accelerometers, load cells, strain gages, experimental piezoceramic and piezopolymer sensors, and (initially) three piezoceramic active strut members. The stiffness of the active struts has been selected to approximately match the impedance of structure as seen by the actuator at the active strut mounting location, leading naturally to control designs based on passive shunting, wave impedance, or balanced bridge feedback.

A finite element model of the testbed was constructed and a conventional system identification using an external excitation source will be carried out. The results (frequencies, mode shapes) will be compared and the subsequent roles of each of these models in the control design determined. Because of inherent inaccuracies of the finite element model in representing lightly damped closely spaced modes, the experimentally determined modal model is preferred for control design. Methods for generating uncertainty information from the system identification for application in robust control methodologies, and studies of model reduction techniques are planned.

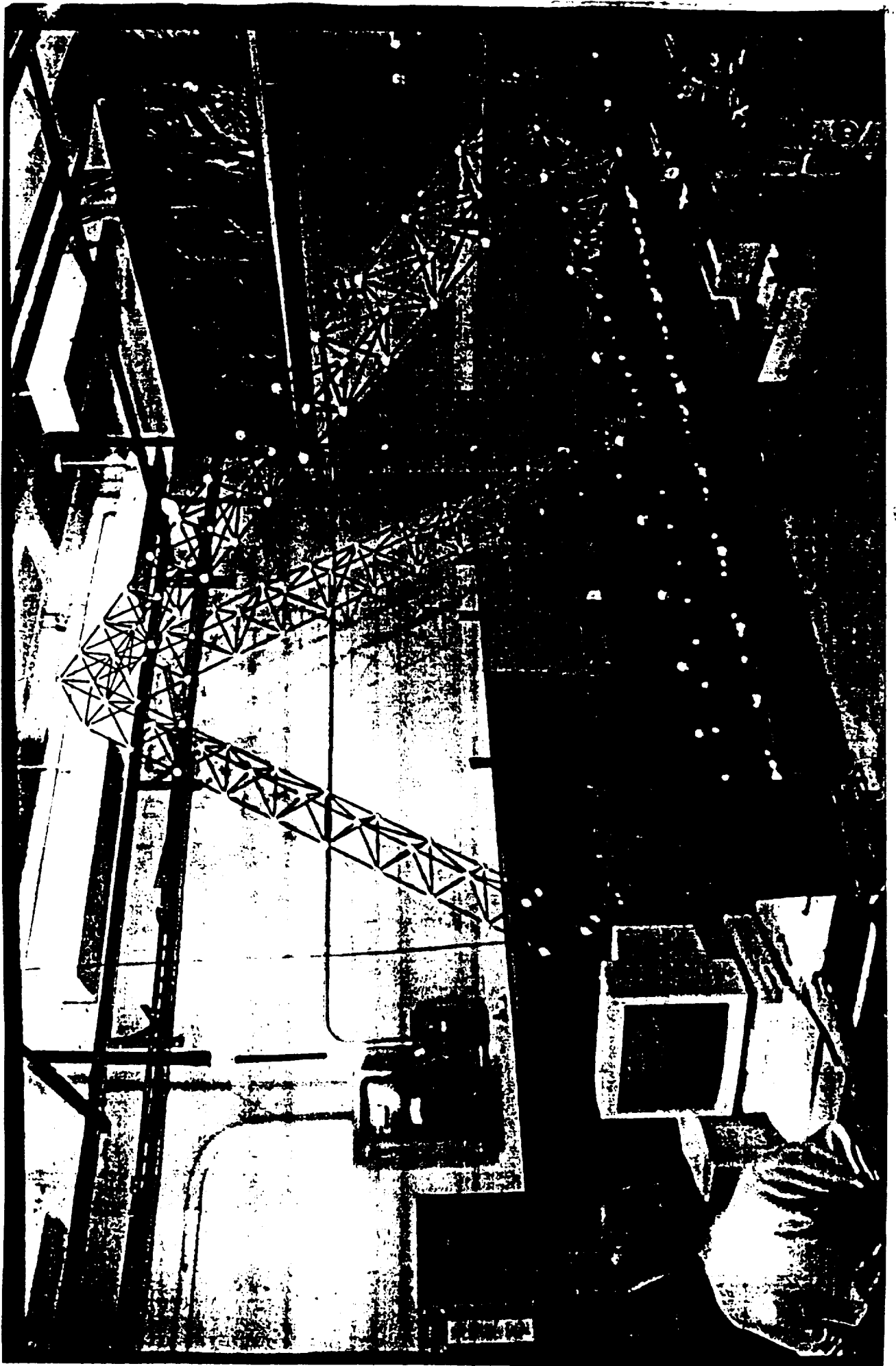* Research Associate   ** Graduate Research Assistant

Figure 1. MIT SERC Interferometer CSI Testbed

Three-axis active mirror mounts have been designed which provide ±3.5 microns of stroke over a frequency range of 500 Hz. Two mounts employ conventional piezoelectric actuators; the third mount utilizes electrostrictive actuators that exhibit superior bidirectional repeatability, a result of greater linearity and reduced hysteresis as compared to piezoelectrics. The moving mirror mass has been sized to reflect the approximate scaled masses of siderostats of the proposed space-based optical interferometer. The actual moving mass of the the mirrors will be varied to determine the level at which interaction with the structural flexibility becomes significant.

The remainder of the paper begins with a description of the optics portion of the testbed. Then the testbed CST program is reviewed with attention focussed in six areas: results from other research closely-related to the testbed, finite element modelling, system identification, passive damping, an axial component tester, and control experiments.

Optics

In this section, the optical components of the testbed are described. The focus here is on the implementation of the on-board metrology system. Functional explanations of space-based interferometry can be found elsewhere in this volume.

Beam-combining coherence requirements for an actual space-based interferometer will require on-board sensing and correction mechanisms capable of controlling path lengths to $\lambda/20$. Multi-aperture non-interferometric imaging instruments with similar baselines and operating wavelengths can have more demanding requirements. The sensing system for orienting the instrument relative to an external reference coordinate frame should have resolution and stability on par with the resolution and stability of the internal metrology system. Our immediate concern is the reduction in errors due to flexibility (Figure 2).

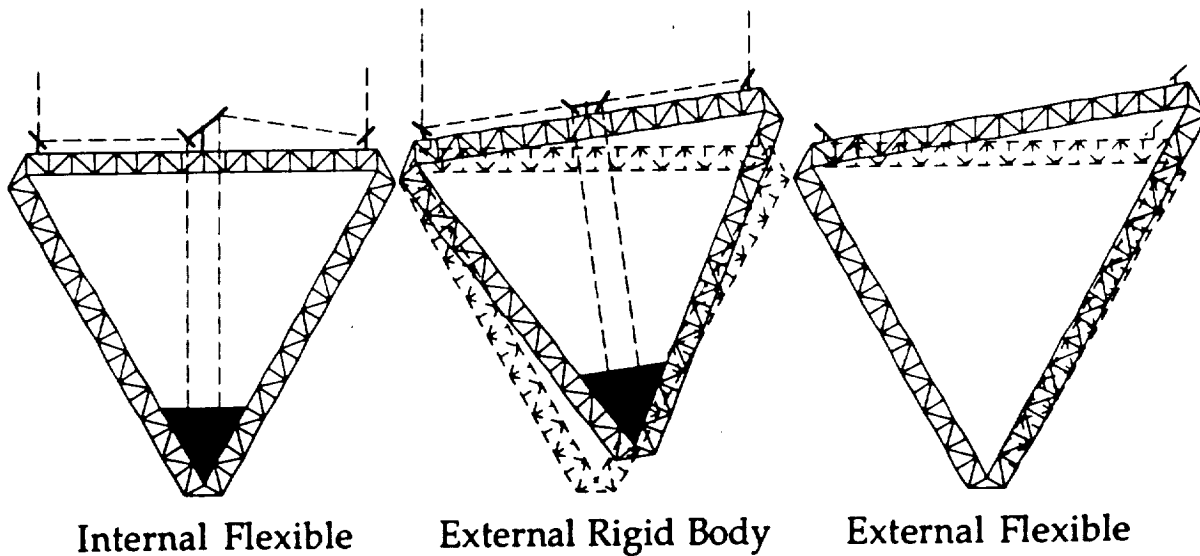Internal Flexible   External Rigid Body   External Flexible

Figure 2: Sources of Path Length Error

The Interferometer CST Testbed under construction at MIT addresses the problem of most direct relevance to CST: control of the instrument geometry in order to control projected baselines and internal path lengths. The testbed control goal is to maintain fixed distances between points on

the structure which represent collecting apertures (mock siderostats) and metrology nodes, since relative motion among these points changes both projected baselines and internal path lengths.

A sample interferometer mission to image a tenth magnitude object at visible wavelengths with one milliarcsecond resolution using one meter apertures leads to path length stability requirements of approximately 80 nm rms. The basic testbed configuration is intended to include enough detail to be representative without being overly complex and costly. Many of the features may be applicable to other spacecraft requiring precision control. Sensing of the external (rigid body) orientation of the testbed and the science optics are not currently addressed, although metrology systems for both of these could be tied directly into the on-board baseline metrology system with little difficulty. Additionally, each mock siderostat mount includes provisions for mounting a small flat mirror with its reflecting surface coplanar with the vertex of the metrology system at that siderostat. Such a mirror might form part of a future science optics chain.

Laser Metrology

A six-axis laser metrology system forming an optical tetrahedron (Figure 3) will provide the primary measure of control effectiveness. One vertex is located at each of the three mock siderostats with the fourth vertex containing the out-of-plane reference point. The outputs of the near and far legs will yield relative displacements among the vertices with the minimum number of laser axes. The vertices of the optical and structural tetrahedrons typically do not coincide since the siderostat locations were chosen to represent non-redundant baselines without necessarily requiring rigid body tilting of the entire instrument. In the initial configuration, one siderostat plate will be located near one structural vertex; the others are roughly 1/2 and 1/3 of the distance down two different legs. The relative angles between the actively-mounted cat's eyes will be less than 96.5 degrees, which is within the cone of operation.
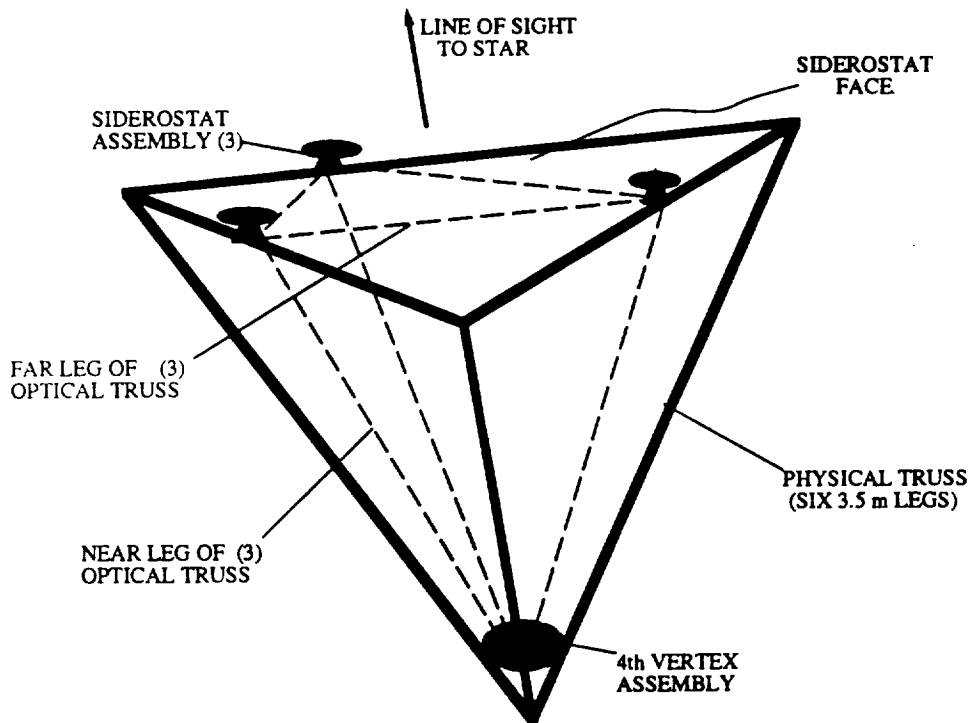

Figure 3: Illustration of the Structural and Optical Tetrahedral Trusses

The power required to operate six axes, instead of the nine that would be needed to determine $\Delta x, \Delta y, \Delta z$ for the three siderostats, permitted the use of a commercially available laser measurement system using a single laser head mounted on the testbed. We are using a dual-frequency stabilized laser head (670 μW total power), detectors, and fringe counting electronics manufactured by Hewlett-Packard Corporation. A lens and 45-degree polarizer assembly plus a short length of optical fiber allow the detector electronics packages to be located out of the way of

the measurement optics and associated mounting fixtures. The VME-based fringe counting electronics provide a seamless link to our real-time control computer.

Figure 4 details one measurement axis. The measurement resolution is limited by the HP-supplied electronics to $\lambda/64$ at $\lambda = 633$ nm, or approximately 10 nm. Greater resolution can be obtained with alternate electronics, such as the VME modules developed by Mike Shao's group at JPL. For operation in air without wavelength tracking over short time scales and in a laboratory disturbance environment, we feel that 10 nm resolution will be adequate. Our closed loop control frequency range is 2-200 Hz, so changes in the refractive index of air and other sources of error with long time constants will not pose any problem. A preliminary error budget suggests that measurement resolution will be ~ 17 nm.
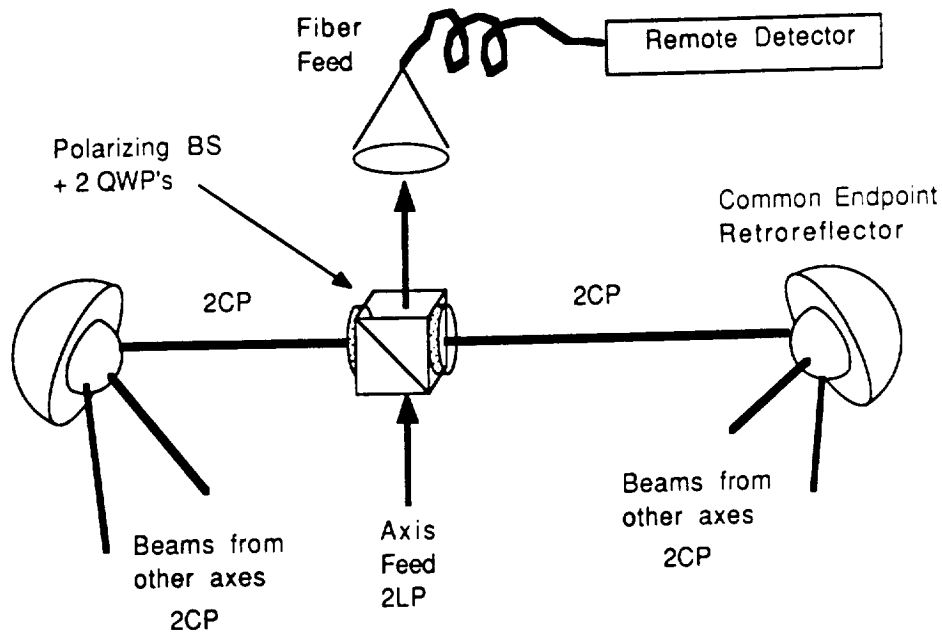

Figure 4: One Axis of the Laser Metrology System

Cat's Eye Retroreflectors

Cat's eye retroreflectors will be used to provide wide fields of view at the vertices of the optical tetrahedron. These are similar to cat's eyes used by C. Townes (UC Berkeley 10μm interferometer) and D. Hutter (US Naval Observatory Astrometric Interferometer) although in this application there is no siderostat slew range to contend with. The minimum size of the cat's eye for a given amount of spherical aberration is a function of the laser beam diameter and the refractive index of the cat's eye glass. The metrology laser beam diameter of 6 mm at the laser head led to a cat's eye size and mirror mass which was unnecessarily cumbersome for implementation on a moving platform. Reducing the beam diameter permits the cat's eye size to be reduced while maintaining the same spherical aberration performance. Lenses reduce the collimated beam diameter to 4 mm without reducing the available power. The cat's eye parameters are:

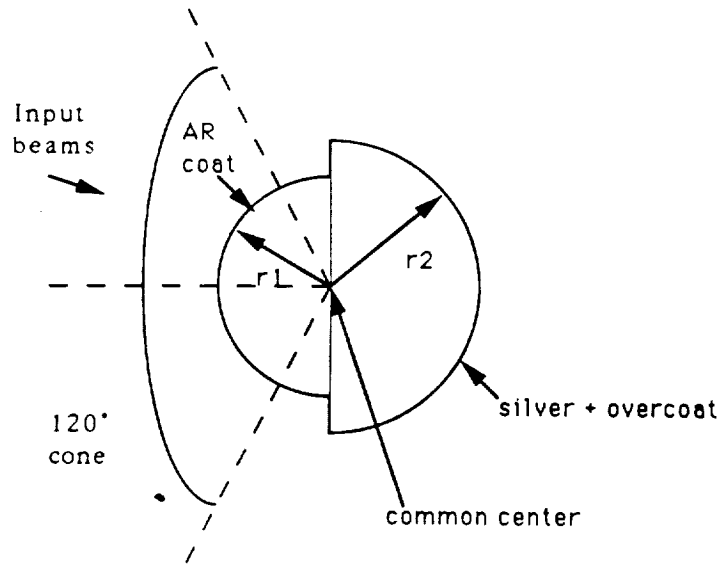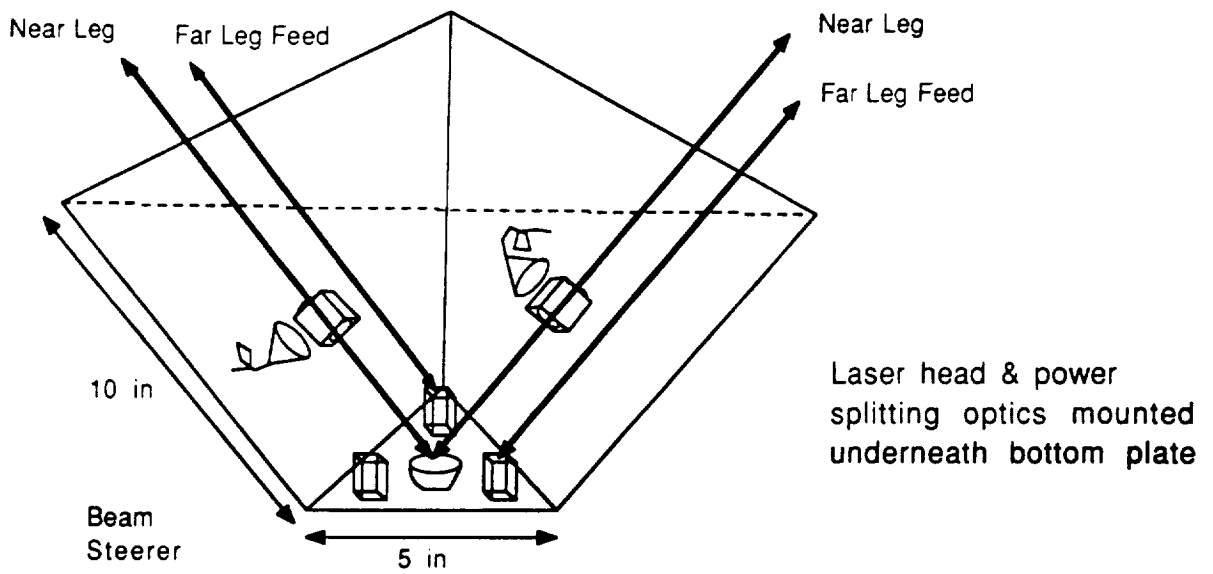|	
glass index at 633 nm	1.72 (Schott SF 10)
radius of small hemisphere	25 mm
radius of large hemisphere	34.7 mm
max. ΔOPL across beam cross section	$\lambda/10$
mass	511 g
usable field of view:	+/- 60 degree cone (see Figure 5)

Figure 5: Cat's Eye Retroreflector

Figure 6: Layout of Fourth Vertex

Modifying the radii to generate a small amount of focusing will help counteract the increased divergence of the smaller beam diameter and produce better overlap at the detectors. The curved surface of the large hemisphere will have a silver reflective coating with a protective overcoat. The curved surface of the small hemisphere will be coated with a broadband anti-reflective coating targetted to be the proper thickness for $\lambda = 633$ nm at half the cone angle. Anti-reflective performance at other angles will depend on the spectral response of the coating. The hemispheres will be aligned after coating and joined by optical contacting.

Other Optics
The remainder of the optics for each measurement leg consists of a polarizing beamsplitter cube with crystal quartz quarter wave plates cemented to opposite faces, plus the associated feed optics. Each beamsplitter-waveplate assembly is mounted in a semi-custom mount which provides the adjustment degrees of freedom needed to align the measurement beam with respect to its retroreflector endpoints. Three of these mounts are rigidly attached to an open pyramidal "bucket" that is itself rigidly attached to the main fourth vertex optics plate (Figure 6). The remaining three mounts are rigidly attached to the siderostat optics plates (Figure 7) in the far leg measurement paths. These rigid mounts are designed to prevent motion of the beamsplitter optics from appearing as motion of the retroreflectors. The feed optics must maintain the orthogonality of the laser polarizations through complex bends in order to minimize errors due to polarization mixing.
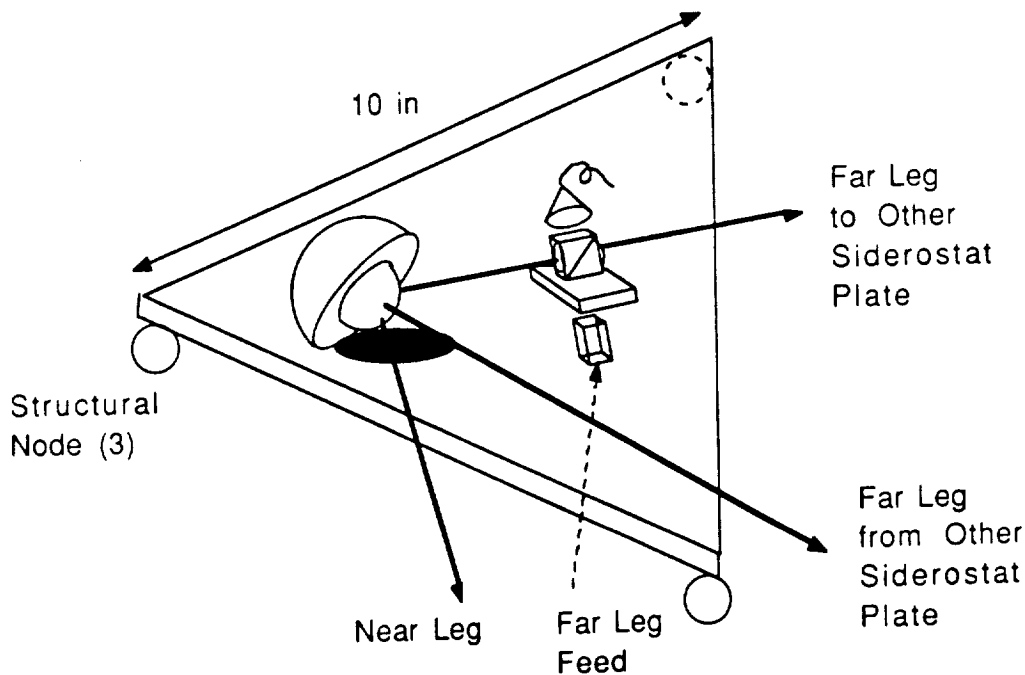

Figure 7: Layout of Siderostat Plate

Results from Recent Testbed-Related Research

In conjunction with the development of the testbed, several other areas of research are being pursued. Three studies have been completed, and are documented elsewhere [1-3]. Some relevant results are summarized below.

Systems Level Disturbance Minimization Using Controlled Structures Technology

Disturbances present on a typical large space-based observatory are detailed. The spectrum of disturbances is divided into those which depend on the space (Earth orbital) environment and those which are internal. Various CST techniques for minimizing the effect of disturbances on mission requirements are reviewed. These include passive structural tailoring, passive damping, vibration isolation, and active structural control. The full-scale 35-meter baseline version of the interferometer testbed is used as a case study for evaluating the flowdown of systems level information to the structural requirements. The power, attitude control, and interferometer and metrology subsystems are discussed with respect to their role as disturbance sources. Finally, an approach for systems level disturbance minimization is outlined.

Experimental Characterization of Damping at Nanostrain Levels

In light of the increasing trend towards nanometer-level requirements on structural stability, it was considered beneficial to characterize damping at extremely small displacement and strain levels. There has been discussion in the CSI community recently regarding dynamic behavior of structures at extremely low vibration levels. In particular, it was not known whether there was a radical change in properties below a particular vibration or displacement floor. In this study, damping was measured in aluminum and graphite/epoxy material specimens in air and in vacuum, and in the bare interferometer testbed truss. It was demonstrated that material damping was independent of strain from ten microstrain down to one nanostrain. Excellent correlation with thermoelastic material models was obtained. Damping in the testbed was found to be independent of strain below one microstrain (Figure 8). The linearity can be exploited by doing system identification at micron displacement levels instead of nanometer levels. The results were immediately instrumental in allowing the use of relatively inexpensive accelerometers for system identification on the testbed, rather than the extremely accurate high cost sensors.
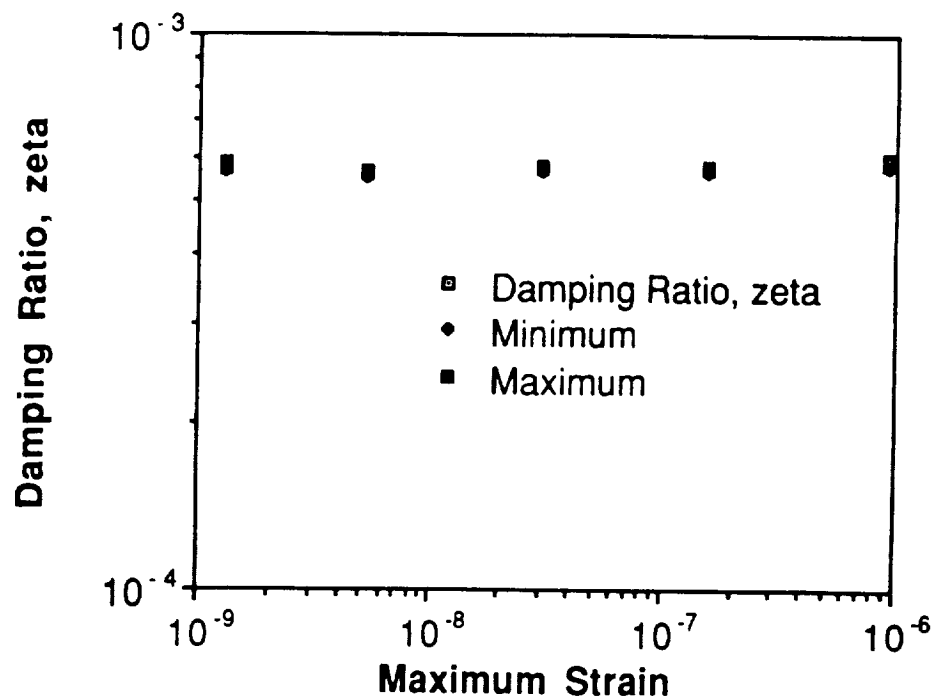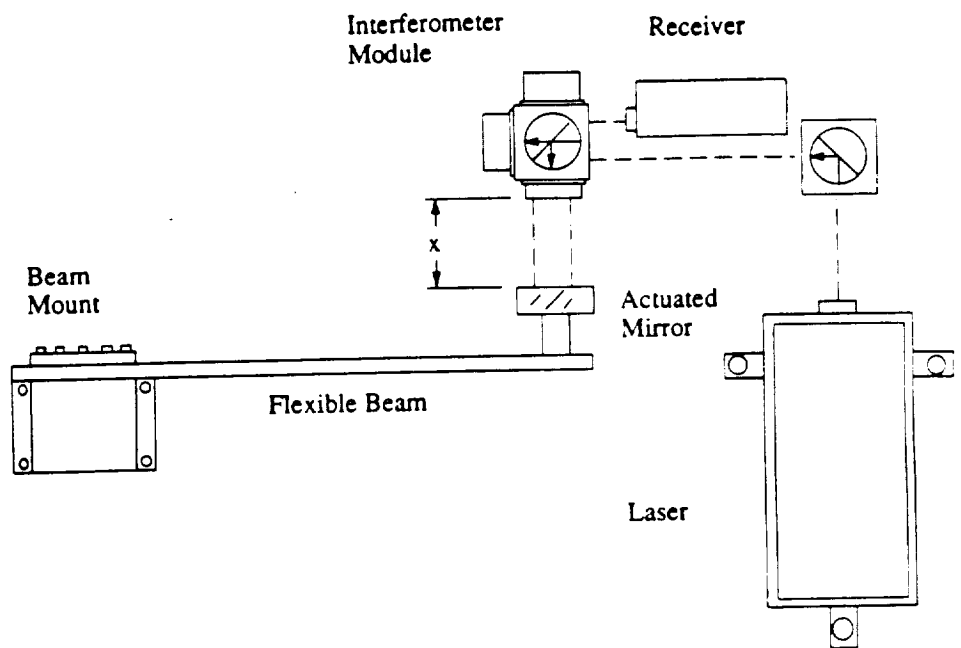

Figure 8: Experimentally Determined Damping in 44 Hz Testbed Mode

Interferometer Module   Receiver

Beam Mount

x

Actuated Mirror

Flexible Beam

Laser

a)   Collocated Sensor-Actuator Set-up

Fold Mirror   Interferometer Module   Receiver

Sensing Mirror

Differential Position

Actuated Mirror

Flexible Beam

Laser
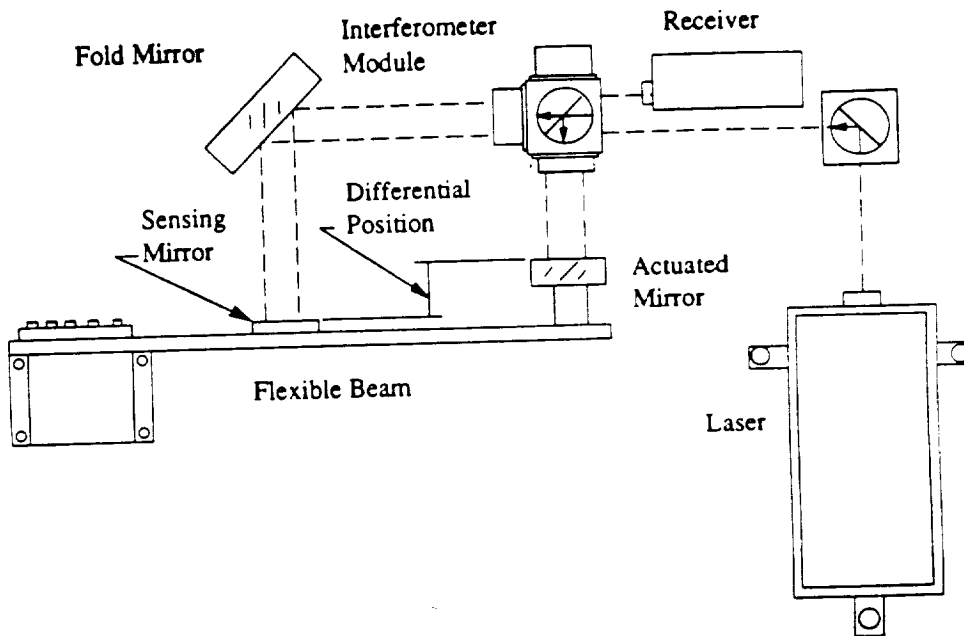
b)   Non-Collocated Sensor-Actuator Set-up

Figure 9: Experimental Approach for Investigating Path Length Control

Experimental Demonstration of Nanometer-level Active Control of a Flexible Beam

In this approach to structural control, the flexibility of the structure is ignored to the greatest extent possible. Instead of controlling the structure, a mirror mass was moved to maintain an optical path length in the presence of disturbances propagating through the structure (Figure 9) using a control strtegy that ignored the structural dynamics of the flexible base structure. The approach was successful provided that the actuated mass was small compared to modal masses of the structure. The effect of damping was investigated and quantified. An order of magnitude

reduction in vibration levels was demonstrated (Figure 10). This concept--implemented only for a single input single output case--will be extended to the interferometer testbed, where active mirror mounts will be used to position the cat's eye retroreflectors in three displacement degrees of freedom. Preliminary analysis of the finite element model suggests that the ratio of the moving mirror mass to the modal masses of the structure are small enough to allow the design of a high performance stable controller without further considerations of the structural dynamics. Research into active isolation will focus on the extension of this approach to cases involving noncollocation, multiple flexible modes, and multi input multi output systems.

	Motion (rms) (0-20,000 Hz)	Attenuation	Motion (peak) (0-20,000 Hz)
Fixed Block			
Uncontrolled	17 nm		16 nm
Controlled	0.77 nm	-27 dB	5 nm @ piezo mode
Collocated			
Uncontrolled	77 nm		250 nm @ 1st mode
Controlled	3.1 nm	-26.8dB	11 nm @ piezo mode
Non-Collocated (x=0.5)			
Uncontrolled	45nm		190 nm @ 1st mode
Controlled	3.9 nm	-21.2 dB	10 nm @ piezo mode

Figure 10: Results from Path Length Control Experiment

Finite Element Model

The purpose of the finite element model is to provide a basis for analytical studies of structural modification, and to serve as one basis for control design. The accuracy of the finite element model is verified by comparison of frequencies and mode shapes with an experimentally derived modal model. It is not likely that the model will be used for control design if experimental models are available. The effort in finite element modelling is outlined in Figure 11.

Two finite element models have been constructed using ADINA: a continuum beam model and a model which contains separate elements for each strut. The continuum model has sufficient accuracy to make it useful for examining various approaches to control. Some features of the models are described below.

Continuum Model
- Equivalent continuum cross-sectional properties for each leg of the truss were derived. (The six legs have identical cross-sections.)
- Each of the six legs was then modeled with 14 Timoshenko beam elements.
- The first flexible mode is at 38 Hz.
- The low mode shapes are characterized by 1st and 2nd bending and the torsion of individual legs.

Continuum Model	Full Struts Model	Correlation with Modal Model	Parametric Studies
equivalent beam properties	strut stiffness and joint mass	ADINA-matlab link	disturbance-to-performance metric t.f's
geometry	geometry	frequencies, mode shapes	system i.d. shaker location/direction search
frequencies, mode shapes	frequencies, mode shapes	iteration	passive damping location search
documentation	iteration on properties		active member location search
adjustment based on system id	modelling of additional hardware (vertices,optics), iteration		point impedance calculation
	choose strut locations		
	testbed global damping measurement		

Figure 11: Near Term Efforts on Testbed Finite Element Model

Full Struts Model
- There are 228 nodes representing the aluminum joints.
- Each of the 696 struts is modeled with a Timoshenko beam.
- The first flexible mode is at 34.56 Hz.
- The model runs in under 2 minutes on the Cray II.
- The low mode shapes are characterized by 1st and 2nd bending and torsion of the individual legs.
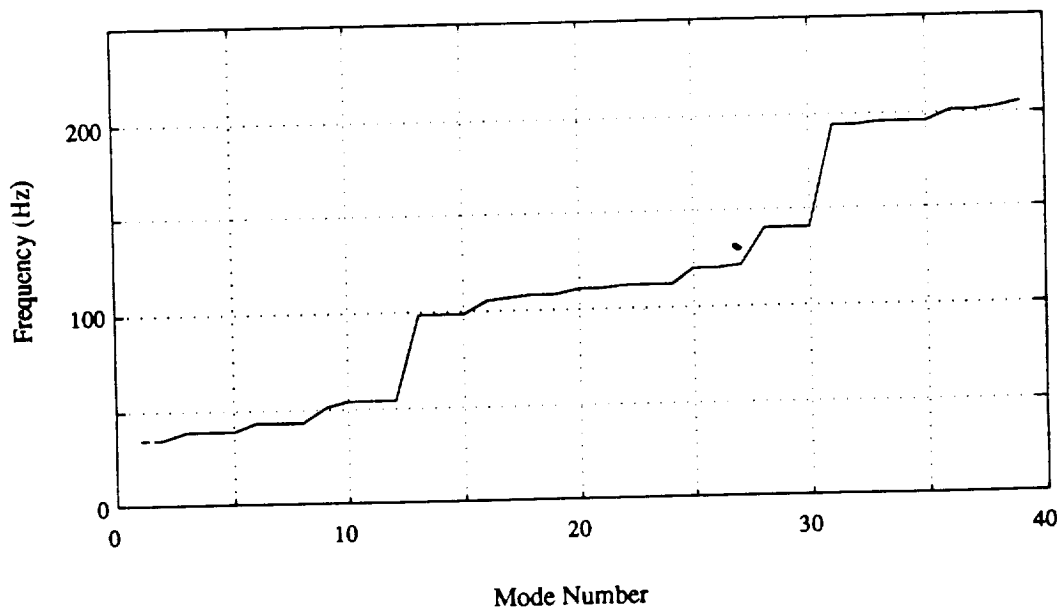- There are 35 flexible modes below 200 Hz.

Figure 12: Frequency Distribution of First 39 Finite Element Modes

Distribution of Modes

Figure 12 shows the frequency vs. mode number for the first 39 modes based on the full struts model. Because of the inherent symmetry of the structure, there are repeated eigenvalues (multiplicity 2 or 3) present. Further, there is a separation between clumps of modes from 54-98 Hz and from 142-194 Hz. The repeated roots and clumping of modes will disappear once concentrated mass of the three siderostats and the fourth vertex are added. Also, the added mass will drop the frequencies further so that there will be more than 50 modes below 200 Hz.

Matlab Postprocessing

The eigenvectors from the full struts model have been used to calculate strain energy distributions for each mode. The elements can be ranked from most to least strain energy by mode or sum of modes. This information will be used to choose passive damping element locations, and later as an initial criterion for active member location selection. With an improved model (including optics) we will be able to calculate a rough optical path performance metric to rank locations on an 'open loop' controllability basis (*i.e.* without simulating performance of the closed loop system).

In separate work, a two-dimensional truss model has been used as a sample problem to develop necessary tools for control based on state-space models from the ADINA output. Implications of the close modal spacing and light damping are being studied.

Addition of Damping

The finite element model will be augmented with experimentally determined damping values. In addition, damping will be added in select elements in conjunction with the viscoelastic struts experiment. A more careful study optimizing passive damping locations will be carried out later.

Role of the Finite Element Model

The finite element model in its current form is a useful tool for parametric studies, mode shape visualization, calculation of strain energy distributions, and selection of system ID accelerometer locations. We have improved the accuracy of the model, but it is still not perfect. With initial ID data we will be able to make a direct comparison between finite element and experimental data.

At some point a broader discussion of the role of finite element models in CST may be in order. There are several points which must be addressed. From the academic perspective at SERC, these include:

- The 'need' to develop a highly accurate finite element model because it is standard practice in industry.
- The value of a finite element model for laying out identification and control architectures
- The inadequacy of finite element models as a basis for control in a complex lightly damped structure
- The relative value of finite element models and experimental system identification
- The realistic potential for on-orbit system identification
- The need for an accurate finite element model if system identification is not possible
- The role of a hybrid approach which could include subscale and component identification

System Identification

A system identification is routinely performed on controlled structure testbeds as a prelude to control experiments. To date, the interferometer testbed is the most complex structure to be identified in SERC. The experimental model derived from the system ID will serve two purposes. First, it will allow verification of the finite element model. Second, it will provide a modal model for control design.

Because of the complexity of the optics, the testbed will not reach its 'final' configuration for some time (late fall 1990). However, an initial ID will be performed in order to provide verification of the naked truss finite element model. The structure and model will be sufficiently complicated later so that tracing sources of error will be difficult. In addition, the initial ID will allow us to become familiar with the recently-purchased software and hardware systems. The ID will be done with an external shaker and roughly 32 or more accelerometers. Later, active members installed in the truss will be used for system ID.

Initial tests show several interesting results. The first flexible mode was measured at 31.34 Hz, compared with a finite element prediction of 34.56 Hz. This 10% error indicates a need to revise the finite element model, with input from a subcomponent stiffness test on the struts. The effect of gravity is apparent in the structure. Modes which are nominally the same frequency differ by typically 0.3 Hz. Also, pendulum and bounce suspension modes have been measured (below 4 Hz). Finally, typical damping ratios of 0.04% to 0.07% have been recorded for the flexible truss modes, with minimal intrumentation and cabling on the structure.

Frequency Resolution

Due to memory limitations of the identification computer, frequency resolution is currently at best 0.0125 Hz. This may not be acceptable for lightly damped modes present in the testbed.

Generation of the Modal Model

The Structural Measurement Systems STAR software will provide frequency domain fits over limited frequency ranges. These will be assembled in Matlab where the full modal model will be constructed. This model will initially contain roughly 100 states.

Passive Damping

Viscoelastic	Shunted Piezoelectric	Viscous Dashpot	Proof Mass
material properties (Poron, Scotchdamp)	small truss experiment	survey available hardware	Hardware available in lab
design	active member impedance selection	confer with Honeywell	Harris precision device
construction	analysis (resistive, resonant)	evaluate inexpensive design concepts	select locations
test in small truss	electrical components		testbed damping measurements
component tester	component tester		
choose strut locations	choose strut locations		
testbed global damping measurement	testbed global damping measurement		

Figure 13: Near Term Efforts on Passive Damping Augmentation

A passive-as-possible approach is preferred in achieving a spacecraft which must meet stringent shape or pointing requirements. However, in an environment which will include several

potential disturbance sources, some sort of vibration alleviation will also be necessary. The introduction of an active control system can greatly improve performance at the expense of complexity, cost, and the possibility of instability. Passive damping augmentation is a far less glamorous, but nevertheless effective alternative. When an active structural control system is considered necessary, passive damping can only be beneficial. It does not make sense to implement aggressive structural control on a plant with only 0.05% inherent damping. Our initial goal is to conduct enough tests to establish the basis for later comprehensive experimental studies of passive damping schemes to be carried out in the future. The program has been broken into four areas representing different approaches to passive damping. These are shown in Figure 13.

Viscoelastic

Constrained layer viscoelastic struts have been tested in a small cantilevered truss. Poron and Scotchdamp materials were compared, and Scotchdamp was found to be more effective. The effectiveness of different Viscoelastic layer thicknesses has been judged based on ringdown experiments in a first bending mode. A significant component of the strain energy of the structure is in the damper strut. This allowed high loss factors (25 %), and large drops in frequency.

Twelve of these simple highly effective struts have been manufactured. With information from the component tester, it will be possible to model the struts with equivalent axial stiffness and viscous damping. This information will be integrated into the finite element model where a prediction of the added global damping due to several viscoelastic struts is possible. A repeat of the ID experiments will yield a measured value for damping.

Shunted Piezoelectrics

A resistively-shunted strut [4] was built and tested in a small cantilevered truss. The initial results were discouraging, with damping values below those expected. Subsequent re-engineering of the strut yielded no improvement. The use of a commercial Physik Instrumente actuator in the strut gave no better results. Although the experiment was designed to concentrate a large amount of strain energy in the piezoceramic material, this was apparently not the case. A careful test of the strut in the component tester will provide an accurate accounting of strain energy distribution. The active member actuator stiffnesses were selected with consideration of appropriate stiffness properties for the shunting application in the large testbed.

Concerns

The difficult problem we face in adding significant global damping is the large number of struts (696) in the testbed. The damping members must be selectively placed, perhaps near critical payloads. At this point, the constrained layer Viscoelastic struts are by far the least expensive and easiest to make. Drawbacks include the frequency-dependent loss factor and material propertytemperature sensitivity. The shunted piezoceramics are potentially more effective than we have demonstrated to date, but are expensive. A device based on the Honeywell D-Strut design, which is capable of broadband viscous damping and is relatively temperature-independent is desirable, but is at this point prohibitively expensive to incorporate into the testbed.

Component Tester

An axial component tester has been constructed and is operational on an optics bench. This facility includes a Physik Instrumente piezoceramic strut to drive various test articles which represent subcomponents of the testbed. Mainly, these are passive or active replacements for the aluminum struts. Load and displacement are measured, the latter with a Zygo Axiom 2/20 interferometer system. The tester will be used in the 0.1-200 Hz frequency range, with displacements from 1 nm to 60 µm. Initial measurements to be conducted are:

- stiffness of truss longerons and diagonals
- stiffness of active struts
- voltage/deflection plots of active struts
- viscoelastic strut characterization

The facility will be available in the future for characterization of other passive or active components.

Control Experiments

We do not forsee having the capability to do absolute shape control in the near future, since that requires rigid body control of the testbed. The initial effort involves separation of the structural control and optical metrology path length control loops. Capabilities will be established in each through simple closed-loop experiments. Figure 14 shows the near term goals for control experiments.

Software		Structural Control	Optical Path Control
Integration with hardware	User environment	number of actuators	mirror mount dynamics
interface to laser metrology	streamlining	active member characteristics	accelerometer measurements
integration of vector processor	matlab links (pseudo-autocode)	actuator locations	interferometer measurements
tradeoffs between number of states vs. speed (benchmarks)	input/output displays	control design	single axis piston
data storage capability	input/output saturation flags	collocated velocity	multi-mirror, multi-axis
matlab links	internal state displays	collocated force and strain	
	documentation	optical performance measure	

Figure 14: Near Term Efforts on Control Experiments

Model Basis for Control Design

There are several methods for generating a model which is a suitable basis for control design. These include finite element models (usually augmented with experimental damping values), measured models based on modal models from system identification, and measured models based on direct information from input-output actuator-sensor pairs. The third approach is preferred if the proper measurements can be made. For all these designs model reduction may be necessary in the plant and controller.

Real Time Software

The software to do linear, constant coefficient, digital control is functionally complete. The code is called *MatCon* for matrix control. The user interface is through Matlab, where a typical continuous control design is discretized. The discrete matrices and some other constants (number of inputs, outputs, and states, scaling factors, and the sampling period) are saved in a standard Matlab *.mat* file. The real-time computer then reads this data and starts the controller. The following algorithm is used.

$$input \ vector \ y \ from \ A/D$$
$$x_{n+1} = F_{11}x_n + F_{12}y_n$$
$$u_n = F_{21}x_n$$
$$output \ vector \ u \ to \ D/A$$
$$wait \ for \ next \ sample \ time$$

While the controller is running the user can stop and start the controller, record states, inputs, and outputs, and scale inputs and outputs. The data file of input vectors is stored in on-board memory, until a set number of samples has been saved. The controller is then stopped and the data transferred to the hard disk on a Sun Sparcstation, where it can be read back into Matlab. States and outputs can be reconstructed from the saved input data for full analysis. There is a direct interface to the six HP laser measurement boards. Four-pole Bessel anti-alias filters with a corner frequency set by digital input-output from the real-time computer are used. The filter cards also provide a digitally programmed gain of 1,2,4,8,or 16 to help amplify low-level sensor signals. We will have the capability to process 16 inputs, 10 outputs, 32 states at 1kHz. The control bandwidth is not expected to exceed 150 Hz.

Active Struts

The active strut design is shown in Figure 15. In addition to the load cell and internal strain gage measurements, two accelerometers are mounted to the strut to provide an inertial collocated measurement and to permit system identification using the active struts. Three struts are currently available, and an additional homemade unit will initially be used as a disturbance source generator.
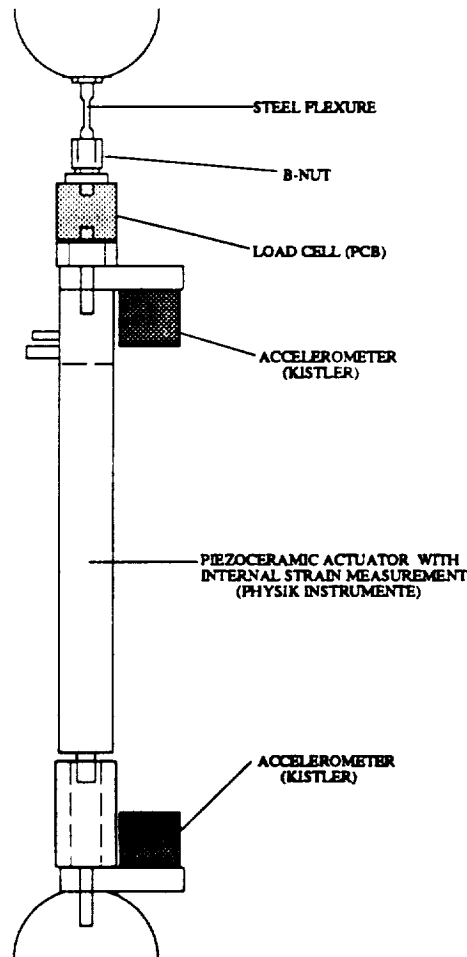

Figure 15: Active Strut Configuration

Active Mirror Mounts

Active mirror mounts will be used to maintain to $\lambda/20$ the linear positions of the cat's eye retroreflectors, which are located at the three mock siderostat locations shown in Figure 3. Output position control will be achieved by moving the cat's eye and mounting table using three microactuators: 0.7" piezoelectric stacks for two of the active mirror mounts and 0.4" electrostrictive stacks for the third, as shown in Figure 16. The actuators will be run in common mode to actuate piston, or z, motion of the point M of the cat's eye. In differential mode, the cat's eye and table will be tilted; resulting in x and y displacements through the lever arm and flexure assembly. The rotations and lateral displacements cannot be controlled independently, but this constraint will not be a problem for the envisioned set of control experiments in the near to medium term. Simultaneous displacements of +/- 3.5 µm can be achieved in all three directions. The mirror mount design includes the flexibility to introduce additional mass to simulate the scaled mass of the retroreflectors. Additionally, the mounts can later be modified to incorporate mass reactuation, where the he effect of moving the mass of the cat's eye is reduced or even cancelled. The result will be a reduction in the interaction between the mirror control system and the truss flexibility.
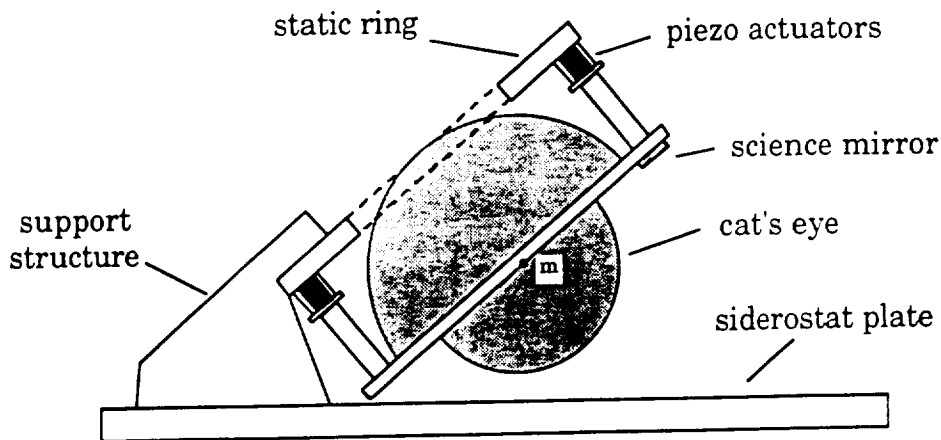

Figure 16: Active Mirror Mount Functional Drawing

The active mirror mount is a small stroke device intended to control only path length errors in the flexible truss. These errors will result from disturbance sources that are introduced intentionally to simulate space disturbances and from disturbances present in the ambient noise environment of the laboratory. Figure 17 shows the ambient acceleration power spectral density (PSD) in the worst-case direction measured by a triax of moderate-sensitivity accelerometers (1V/g) at a proposed active mirror mount location on the truss. In this very preliminary study, the structural dynamic response, starting at 30 Hz, is also corrupted by electrical noise and various lower frequency suspension modes. A displacement PSD is calculated by scaling the acceleration PSD by $1/\omega^4$, which leads to an estimate of rms displacement of 22 nm in the frequency band of 20-100 Hz. Assuming that a point corresponding to a siderostat on another leg experiences the same disturbance and vibrates out of phase with the first point throughout this frequency range, an ambient path length error of 44 nm rms can be expected. The actual error may be less once electrical noise is removed and the additional mass of the active mirror mounts is added to the truss.

Electrostrictive Actuators

In separate work [5], electrostrictive ceramic PMN:BA, a material of interest to structural control engineers, was characterized for test parameters of frequency, amplitude, and temperature. Results indicate that at room temperature the material strain response is quite linear with almost
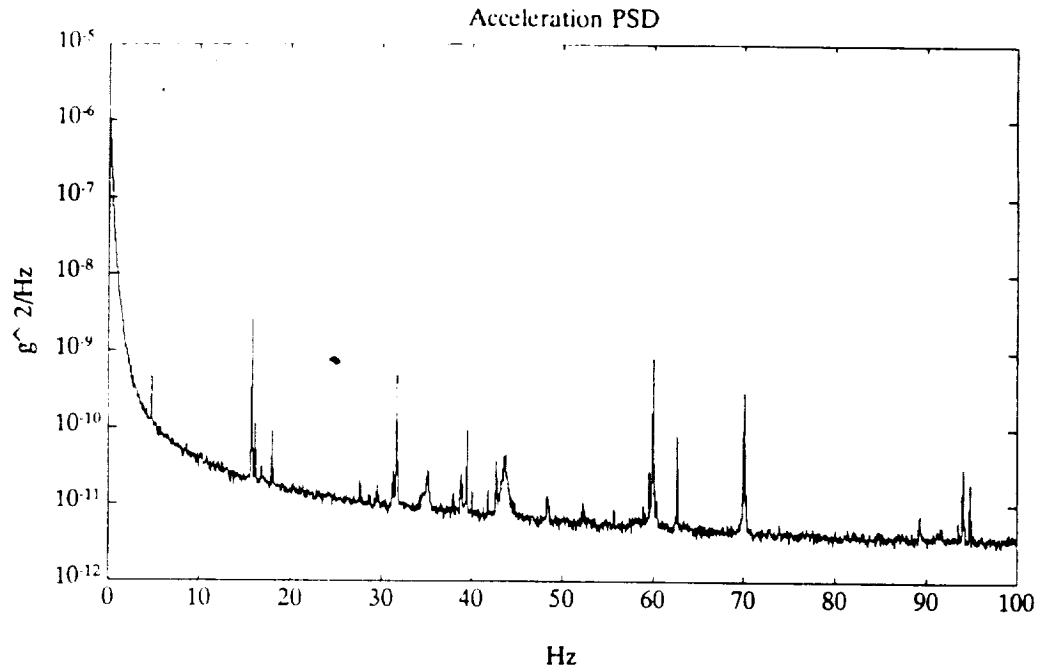

Figure 17 Acceleration Power Spectral Density in Worst-case Direction at Proposed Active Mirror Mount Location
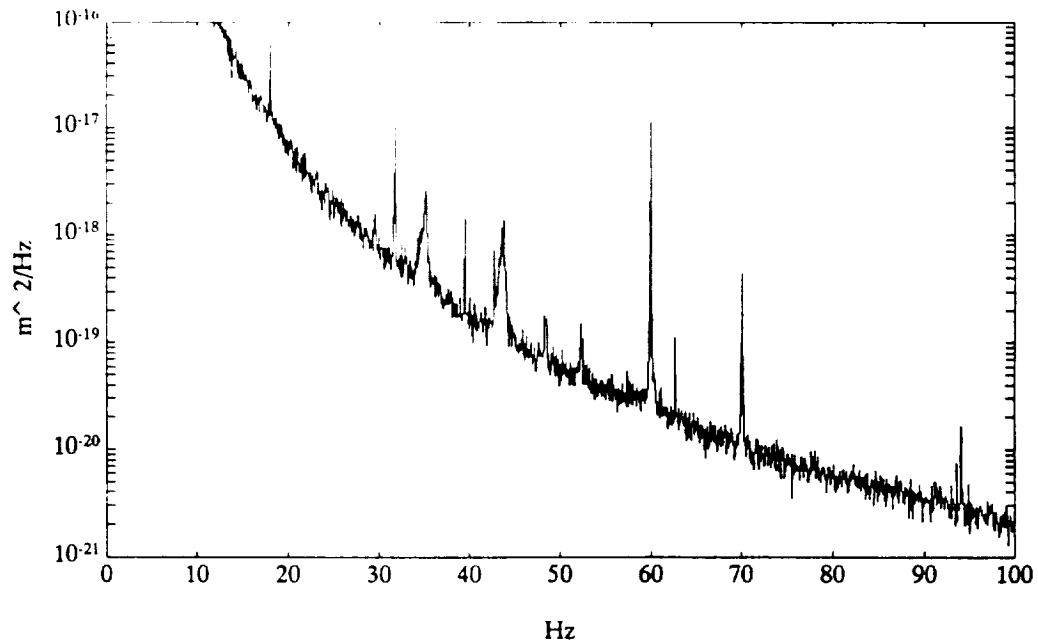
Figure 18 Displacement Power Spectral Density in Worst-case Direction at Proposed Active Mirror Mount Location (Derived from Acceleration Measurement)

no phase due to hysteresis, unlike piezoelectrics, and is constant with frequency. However, the induced strain sensitivity is highly dependent on temperature, and hysteresis increases rapidly below room temperature. Since electrostrictive actuators will be used in one of the three active

mirror mounts, the operating temperature of the actuators will need to be monitored during calibration and usage.

Summary

The SERC interferometer CST testbed will soon be fully operational. The facility will address concerns regarding extremely tight constraints imposed on structural motion in future space observatories. At the same time, the testbed will serve as a platform for exploration of a broad range of controlled structure technologies and approaches.

References

[1] Eyerman, C.E., A Systems Engineering Approach to Disturbance Minimization for Spacecraft Utilizing Controlled Structures Technology, MIT Dept. of Aeronautics and Astronautics,S.M. thesis, May, 1990, SERC Report 2-90.

[2] Ting, J., Characterization of Damping of Materials and Structures at Nanostrain Levels, MIT Dept. of Aeronautics and Astronautics,S.M. thesis, May, 1990, SERC Report 1-90.

[3] Garcia, J.G., Stability of an Actuated Mirror on a Flexible Structure as a Function of Mass and Structural Damping, MIT Dept. of Mechanical Engineering, S.M. thesis, June, 1990.

[4] Hagood, N.W. and von Flotow, A.H., 'Damping of Vibrations with Piezoelectric Materials and Passive Electrical Networks,' accepted for publication in *Journal of Sound and Vibration*.

[5] Blackwood, G.H. and Fleming, F.M., Characterization of Transverse Field-Induced Strain in PMN:BA Electroceramic Plates, MIT Space Engineering Research Center Report #7-90, July, 1990.

August 8, 1990

Dr. Stephen Synnott
M.S. 301-125L
Jet Propulsion Laboratory
4800 Oak Grove Drive
Pasadena, CA 91109

Dear Steve:

I have enclosed the paper based on our presentation at the Workshop on Technologies for Space Interferometry held at JPL last spring for inclusion is the volume you are assembling. Please contact me at 617/253-6685 or Tupper Hyde at 617/253-5243 with any questions.

Sincerely,

Eric Anderson

On a Cost Functional for $\mathcal{H}_2/\mathcal{H}_\infty$ Minimization

Douglas G. MacMartin, Steven R. Hall*
Space Engineering Research Center
Department of Aeronautics and Astronautics
Massachusetts Institute of Technology
Cambridge MA 02139

Denis Mustafa[†]
Laboratory for Information and Decision Systems
Massachusetts Institute of Technology
Cambridge MA 02139

Abstract

A cost functional is proposed and investigated which is motivated by minimizing the energy in a structure using only collocated feedback. Defined for an $\mathcal{H}_\infty$-norm bounded system, this cost functional also overbounds the $\mathcal{H}_2$ cost. Some properties of this cost functional are given, and preliminary results on the procedure for minimizing it are presented. The frequency domain cost functional is shown to have a time domain representation in terms of a Stackelberg non-zero sum differential game.

Introduction

This paper examines the properties, evaluation algorithm, and an optimization approach for a cost functional for combined $\mathcal{H}_2/\mathcal{H}_\infty$ control. Combined $\mathcal{H}_2$ and $\mathcal{H}_\infty$ control is of interest since it combines the problems of nominal performance and robust stability. Related work includes $\mathcal{H}_2$ optimization with an $\mathcal{H}_\infty$ constraint [1-4], minimum entropy $\mathcal{H}_\infty$ control [4,5], and mixed $\mathcal{H}_2$ and $\mathcal{H}_\infty$ control [6,7]. The cost functional of interest to us is defined as follows.

Definition 1 *Consider a system* $H(s) = [H_0(s)\ H_1(s)]$ *and a number* $\gamma \in \mathbb{R}$, *with* $H_0 \in \mathcal{RH}_2$, $H_1 \in \mathcal{RH}_\infty$, *and* $\|H_1\|_\infty < \gamma$. *Then the cost* $L(H,\gamma)$ *is defined by*

$$L(H,\gamma) := \frac{1}{2\pi} \int_{-\infty}^{\infty} \text{trace} \left\{ (I - \gamma^{-2} H_1 H_1^*)^{-1} H_0 H_0^* \right\} d\omega \quad (1)$$

The specific form of this cost is motivated by minimizing the total vibrational energy of a structure with only a model of the local dynamics near an actuator and collocated sensor. Previous work with this type of model has used $\mathcal{H}_2$ [8] and $\mathcal{H}_\infty$ [9] optimizations of the power flow. Briefly, the fraction of the input power flow that is reflected into the structure at the actuator location is a quadratic at each frequency, and can be represented by a transfer function HH^*. The fraction of the power that is dissipated is then $(I - HH^*)$, and the total power dissipated is $(I - HH^*)E$ where E is the structural energy as a function of frequency. If the power flow into the structure from external disturbance sources is given by $\Phi(j\omega)$, then a power balance yields that the total energy in the structure is given by $L([H\ H\Phi], 1)$. A more detailed explanation may be found in [10].

In [7], a framework for mixed $\mathcal{H}_2/\mathcal{H}_\infty$ control problems is considered. There the cost functional is motivated in an input/output sense. The system is subject to two inputs, one of bounded spectrum, and the other with bounded power. For the case where the first input signal is white and the second is causal, necessary and sufficient conditions are given for the existence of a controller which minimizes the cost. The non-white and non-causal case is

described but not solved (see Section 3.3.) This case is, however, of particular interest as the cost then equals $L(H,\gamma)$, revealing a close relationship between the present approach and the approach taken in [7]. This connection is currently under investigation.

The final section of this paper gives a third interpretation of this cost in terms of a Stackelberg non-zero sum differential game.

Properties

The following basic properties of $L(H,\gamma)$ will be stated without proof, and can be easily shown to hold.

Proposition 2 *Let* $H(s)$ *and* γ *satisfy the conditions in Definition 1. Then*

(i) $L(H,\gamma)$ *is well defined.*

(ii) $L(H,\gamma) \geq 0$, *and* $L(H,\gamma) = 0 \iff H_0 = 0$.

(iii) $L(UHV,\gamma) = L(H,\gamma)$ *for any* $U, V \in \mathcal{RL}_\infty$ *with* $U^*U = I$, $VV^* = I$.

In the case where $H_1 = H_0$, further properties of the cost $L(H,\gamma)$ can be established by relating it to the entropy $I(H,\gamma)$ of a system defined, for example, in Reference [5].

Definition 3 *For* $H \in \mathcal{RH}_2$, $\gamma \in \mathbb{R}$, *and* $\|H\|_\infty < \gamma$, *the entropy at infinity is defined by*

$$I(H,\gamma) := -\frac{\gamma^2}{2\pi} \int_{-\infty}^{\infty} \ln \left| \det \left(I - \gamma^{-2} H^* H \right) \right| d\omega \quad (2)$$

Also let $C(H)$ be the usual $\mathcal{H}_2$ cost associated with the system H;

$$C(H) := \frac{1}{2\pi} \int_{-\infty}^{\infty} \text{trace} \{ H^* H \} d\omega \quad (3)$$

Proposition 4 *For* $H = [H_0\ H_0]$, *with H_0 and γ satisfying the conditions in Definition 3, consider the cost* $L(H,\gamma)$, *the entropy* $I(H_0,\gamma)$, *and the $\mathcal{H}_2$ cost* $C(H_0)$. *Define* $\xi = \gamma^{-2}$, *then*

(i) $L(H,\gamma) = \frac{\partial}{\partial \xi} (\xi I(H_0,\gamma))$

(ii) $L(H,\gamma) \geq I(H_0,\gamma) \geq C(H_0)$.

Proof: The first assertion follows directly from the proof of Proposition 2.3.2 in Reference [5]. The first inequality in (ii) follows from $L(H,\gamma) = I(H_0,\gamma) + \frac{\partial}{\partial \xi}(I(H_0,\gamma))$ and the result from Proposition 2.3.2 in [5] that $\frac{\partial}{\partial \xi}(I(H_0,\gamma)) \geq 0$. The final inequality is obtained from the result that $I(H_0,\gamma)$ itself bounds the $\mathcal{H}_2$ cost. □

That $L(H,\gamma)$ overbounds an $\mathcal{H}_2$ cost can also be shown to hold for the case $H_1 \neq H_0$.

Proposition 5 $L(H,\gamma) \geq C(H_0)$.

Proof: Since $\|H_1\|_\infty < \gamma$, $(I - \gamma^{-2}H_1H_1^*) < 1$ and $(I - \gamma^{-2}H_1H_1^*)^{-1} < 1$. The result then follows directly from the definition of $L(H,\gamma)$ in Equation (1). □

Finally, note that relaxing the $\mathcal{H}_\infty$-norm bound completely recovers the $\mathcal{H}_2$ cost.

Proposition 6 $\lim_{\gamma\to\infty} L(H,\gamma) = C(H_0)$.

Proof: This follows directly from the definition of $L(H,\gamma)$ in Equation (1) and the Dominated Convergence Theorem. □

Evaluation of the Cost

Consider a state space representation for a strictly proper system $H = [H_0 \; H_1]$,

$$H = \left[\begin{array}{c|cc} A & B_0 & B_1 \\ \hline C & 0 & 0 \end{array}\right] = C(sI - A)^{-1}[B_0 \; B_1] \qquad (4)$$

The aim is to evaluate $L(H,\gamma)$ in terms of the state space data. Note that a non-zero term D_1 could be included; H_1 is made strictly proper only to simplify the results.

Lemma 7 Let $H = [H_0 \; H_1]$ be given by Equation (4), $\gamma \in \mathbb{R}$, and $\|H_1\|_\infty < \gamma$. Then

$$L(H,\gamma) = \text{trace}\left\{CQC^T\right\} \qquad (5)$$

where P, Q satisfy $(A + \gamma^{-2}B_1B_1^TP)$ stable and

$$PA + A^TP + \gamma^{-2}PB_1B_1^TP + C^TC = 0 \qquad (6)$$

$$(A + \gamma^{-2}B_1B_1^TP)Q + Q(A + \gamma^{-2}B_1B_1^TP)^T + B_0B_0^T = 0 \qquad (7)$$

Proof: Since $H_1H_1^* < \gamma^2 I \; \forall\, \omega$, then $\exists\, M^{\pm 1} \in \mathcal{RH}_\infty$ given by

$$M^*M = H_0^*(I - \gamma^{-2}H_1H_1^*)^{-1}H_0 \qquad (8)$$

A state space representation for M^*M can be found by noting that M^*M is the transfer function of the feedback system shown in Figure 1. So

$$M^*M = \left[\begin{array}{cc|c} A & \gamma^{-2}B_1B_1^T & B_0 \\ -C^TC & -A^T & 0 \\ \hline 0 & B_0^T & 0 \end{array}\right] \qquad (9)$$

With P given by Equation (6), then

$$M = \left[\begin{array}{c|c} A + \gamma^{-2}B_1B_1^TP & B_0 \\ \hline C & 0 \end{array}\right] \qquad (10)$$

is the stable factor of M^*M above [11]. Substituting Equation (8) into (1), it is clear from (3) that the cost $L(H,\gamma)$ is then given by $\|M\|_2$, where $\|M\|_2 = \text{trace}\left\{CQC^T\right\}$ and Q satisfies the Lyapunov equation (7) [13]. □
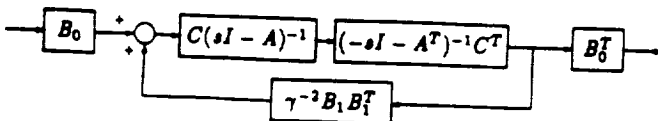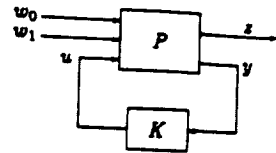
Figure 1: Block Diagram for M^*M

Figure 2: Feedback System

Optimization

The goal of this section is to present an approach for solving for the optimum controller that minimizes a cost functional of the form (1). Linear time-invariant controllers will be assumed throughout, but this form is not proven to yield minimal cost. The necessary conditions that an optimal compensator must satisfy are presented. Conditions for the existence of such a controller are not discussed here.

The system can be described by the block diagram in Figure 2. P can be realized in state space as

$$P = \left[\begin{array}{c|ccc} A & B_0 & B_1 & B_2 \\ \hline C_1 & 0 & 0 & D_{12} \\ C_2 & D_{20} & D_{21} & 0 \end{array}\right] \qquad (11)$$

and H is then given by the lower linear fractional transformation,

$$H = \mathcal{F}(P,K) = [P_{10} \; P_{11}] + P_{12}K(I - P_{22}K)^{-1}[P_{20} \; P_{21}] \qquad (12)$$

Admissible compensators K will be those which stabilize P, and satisfy $\|H_1\|_\infty < \gamma$. The problem statement is then

$$\min_K \{L(H,\gamma) : K \text{ admissible}\} \qquad (13)$$

By a scaling of H, without loss of generality consider the case $\gamma = 1$.

The full state feedback problem is examined first, with normalized control weighting, so that $C_1^T = [C^T \; 0]$ and $D_{12}^T = [0 \; I]$.

Theorem 8 Consider the problem statement (13), with $A_{CL} := A + B_2F$. If F is a static feedback matrix that solves Equation (13), then:

$$F = -B_2^T(P\check{Q} + \check{P}Q)(Q + \check{Q})^{-1} \qquad (14)$$

where P, Q, $\check{P}$, and $\check{Q}$ satisfy $A_{tmp} = (A_{CL} + B_1B_1^TP)$ stable and

$$PA_{CL} + A_{CL}^TP + PB_1B_1^TP + C^TC + F^TF = 0 \qquad (15)$$

$$A_{tmp}Q + QA_{tmp}^T + B_0B_0^T = 0 \qquad (16)$$

$$\check{P}A_{tmp} + A_{tmp}^T\check{P} + C^TC + F^TF = 0 \qquad (17)$$

$$A_{tmp}\check{Q} + \check{Q}A_{tmp}^T + Q\check{P}B_1B_1^T + B_1B_1^T\check{P}Q = 0 \qquad (18)$$

Proof: The closed loop system is $H = \left[\begin{array}{c|cc} A_{CL} & B_0 & B_1 \\ \hline C & 0 & 0 \\ F & 0 & 0 \end{array}\right]$. From Proposition 7, the cost is $J = \text{trace}\left\{CQC^T + FQF^T\right\}$, where Q solves the Lyapunov equation (16), and P satisfies the Riccati equation (15). Appending these two equations to the cost as constraints with Lagrange multipliers $\check{P}$ and $\check{Q}$ respectively yields the equations for $\check{P}$, $\check{Q}$ and F upon differentiating with respect to Q, P and F.

Preliminary results indicate that an iterative approach to solving these equations converges rapidly to the optimal feedback law F. Given an initial guess for F (say, from the minimum entropy control problem [5]), P, Q, $\check{P}$, and $\check{Q}$ can be computed sequentially as the solution of Riccati and Lyapunov equations. Equation (14) can then be evaluated for F, and the process repeated.

For a system of order n and a fixed order compensator of order n_c, the necessary conditions for the optimum can be found again using a Lagrange multiplier approach, in terms of 4 order $n + n_c$ matrix equations similar to Equations (15)–(18). Work currently in progress to simplify and interpret these results for the dynamic compensation problem. Note that there is no a priori reason to expect that no improvement in the cost can be achieved for $n_c > n$.

Time Domain Interpretation

The form of the augmented cost for the linear control problem leads to an interesting differential games interpretation. It is well known that the central controller in the $\mathcal{H}_\infty$ problem can be found as the solution to a zero-sum differential game [14], where for minimizing $\|T_{zw}\|_\infty$, the control u and noise w solve the optimization problems:

$$u = \text{argmin} \int_0^\infty z^T z - \gamma^2 w^T w \, dt \qquad (19)$$

$$w = \text{argmin} \int_0^\infty -z^T z + \gamma^2 w^T w \, dt \qquad (20)$$

u has some information y about the state, and w has full information.

With the current cost functional, and under the assumption of linear feedback, the optimization problem is again equivalent to a differential game, but it is no longer a zero-sum game. Whether the two problems are equivalent when both are allowed nonlinear feedback is unknown.

Proposition 9 *If an optimal linear compensator exists for problem (13), then it is the same as that of a Stackelberg differential game with u as leader, w_1 as follower and w_0 as unit intensity white noise, where u and w_1 solve the following optimization problems:*

$$u = \text{argmin} \lim_{t \to \infty} E\left\{ z^T z \right\} \qquad (21)$$

$$w_1 = \text{argmin} \lim_{t \to \infty} E\left\{ -z^T z + \gamma^2 w_1^T w_1 \right\} \qquad (22)$$

u has some information y about the state, and w has full information.

Proof: Assuming a linear control law for u, the optimization problem for w_1 is easily solved with a single Riccati equation (which is Equation (15) for the state feedback case.) Appending this as a constraint for the optimization problem (21) results in an identical problem formulation to that of problem (13). □

This game seems to be a more natural problem to pose than the pure $\mathcal{H}_\infty$ differential game, since the control does not benefit from the use of noise, but instead optimizes an $\mathcal{H}_2$ type of cost functional, while the deterministic noise w_1 solves the same optimization problem as before. In addition, the plant is subject to a white noise input w_0. This looks similar to the framework of [6,7] since a single output is minimized in the presence of two disturbance inputs, one of which is associated with the $\mathcal{H}_2$ nature of the problem while the other is associated with the $\mathcal{H}_\infty$ nature.

Note that for a non-zero sum differential game, the solution depends on how the optimality is defined. For the Stackelberg or leader-follower solution [15–17], one player (here the control u) acts as leader and announces a strategy, and knowing this strategy, the follower (here the noise w_1) solves its optimization problem. Also note that in general, the optimal control for the Stackelberg problem is known to be nonlinear [17]. Similar equations to (15)–(18) have been reported in [16], where the optimal linear state feedback law for a Stackelberg problem was found. The nonlinear, team optimal strategy obtained, for example, in [17] does not apply to this problem since the leader u cannot increase the follower w_1's cost indefinitely, and therefore cannot induce w_1 to follow a strategy desirable to u.

The differential games representation of problem (13) allows the matrices of Equations (15)–(18) to be given an interpretation. $-P$ and $+\check{P}$ correspond to the optimal cost-to-go for the costs associated with w_1 and u respectively, Q is the covariance of the state, and $\check{Q}$ is the sensitivity of the cost for u to changes in the cost for w_1.

References

[1] Bernstein, D. S. and Haddad, W. M., "LQG Control with an $\mathcal{H}_\infty$ Performance Bound: A Riccati Equation Approach," *IEEE Trans. Auto. Control*, Vol. 34, No 3, March 1989, pp. 293-305.

[2] Haddad, W. M. and Bernstein, D. S., "On the Gap Between $\mathcal{H}_2$ and Entropy Perfomance Measures in $\mathcal{H}_\infty$ Control Design," *Proceedings, 28th IEEE Conf. on Decision and Control*, Dec. 1989, pp. 1506-1508.

[3] Rotea, M. A., and Khargonekar, P. P., "Simultaneous $\mathcal{H}_2/\mathcal{H}_\infty$ Optimal Control with State Feedback," *Proceedings, 1990 Am. Control Conference*, San Diego, CA, May 1990, pp. 2380-2384.

[4] Mustafa, D. "Relations Between Maximum-entropy/$\mathcal{H}_\infty$ Control and Combined $\mathcal{H}_\infty$/LQG Control," *Systems and Control Letters*, Vol. 12, 1989, pp. 193-203.

[5] Mustafa, D. *Minimum Entropy $\mathcal{H}_\infty$ Control*, PhD Thesis, University of Cambridge, 1989.

[6] Doyle, J., Zhou, K., and Bodenheimer, B., "Optimal Control with Mixed $\mathcal{H}_2$ and $\mathcal{H}_\infty$ Performance Objectives," *Proceedings, 1989 Am. Control Conference*, Pittsburgh, PA, pp. 2065-2070.

[7] Zhou, K., Doyle, J., Glover and Bodenheimer, B., "Mixed $\mathcal{H}_2$ and $\mathcal{H}_\infty$ Control," *Proceedings, 1990 Am. Control Conference*, San Diego, CA, May 1990, pp. 2502-2507.

[8] Miller, D. W., Hall, S. R. and von Flotow, A. H., "Optimal Control of Power Flow at Structural Junctions," *J. of Sound and Vibration*, Vol. 140, No. 2, 1990.

[9] MacMartin, D. G. and Hall, S. R., "An $\mathcal{H}_\infty$ Power Flow Approach to Control of Uncertain Structures," *Proceedings, 1990 Am. Control Conference*, San Diego, CA, May 1990, pp. 3073-3080, to appear in *AIAA J. of Guidance, Control, and Dynamics*.

[10] MacMartin, D. G. and Hall, S. R., "Applications of Statistical Energy Analysis to Control," *preprint*, June, 1990.

[11] Francis, B. A., *A Course in $\mathcal{H}_\infty$ Control Theory*, Springer-Verlag, 1987.

[12] Kwakernaak, and Sivan, *Linear Optimal Control Systems*, Wiley-Interscience, 1972.

[13] Doyle, J. C., Glover, K., Khargonekar, P. P., and Francis, B. A., "State-Space Solutions to Standard $\mathcal{H}_2$ and $\mathcal{H}_\infty$ Control Problems," *IEEE Trans. Auto. Control*, Vol. 34, No. 8, Aug. 1989, pp. 831-847.

[14] Rhee, I., and Speyer, J. L., "A Game Theoretic Controller and its Relationship to $\mathcal{H}_\infty$ and Linear-Exponential-Gaussian Synthesis," *Proceedings, 28th IEEE Conf. on Decision and Control*, Dec. 1989, pp. 909-915.

[15] Simaan, M., and Cruz, J. B., "On the Stackelberg Strategy in Nonzero-Sum Games," *J. Opt. Theory and Applications*, Vol. 11, No. 5, 1973, pp. 533-555.

[16] Medanic, J., "Closed-loop Stackelberg Strategies in Linear-Quadratic Problems," *IEEE Trans. Auto. Contr.*, Vol. AC-23, No. 4, Aug. 1978, pp. 632-637.

[17] Basar, T., and Selbuz, H., "Closed-Loop Stackelberg Strategies with Applications in the Optimal Control of Multilevel Systems," *IEEE Trans. Auto. Contr.*, Vol. AC-24, No. 2, April 1979, pp. 166-179.
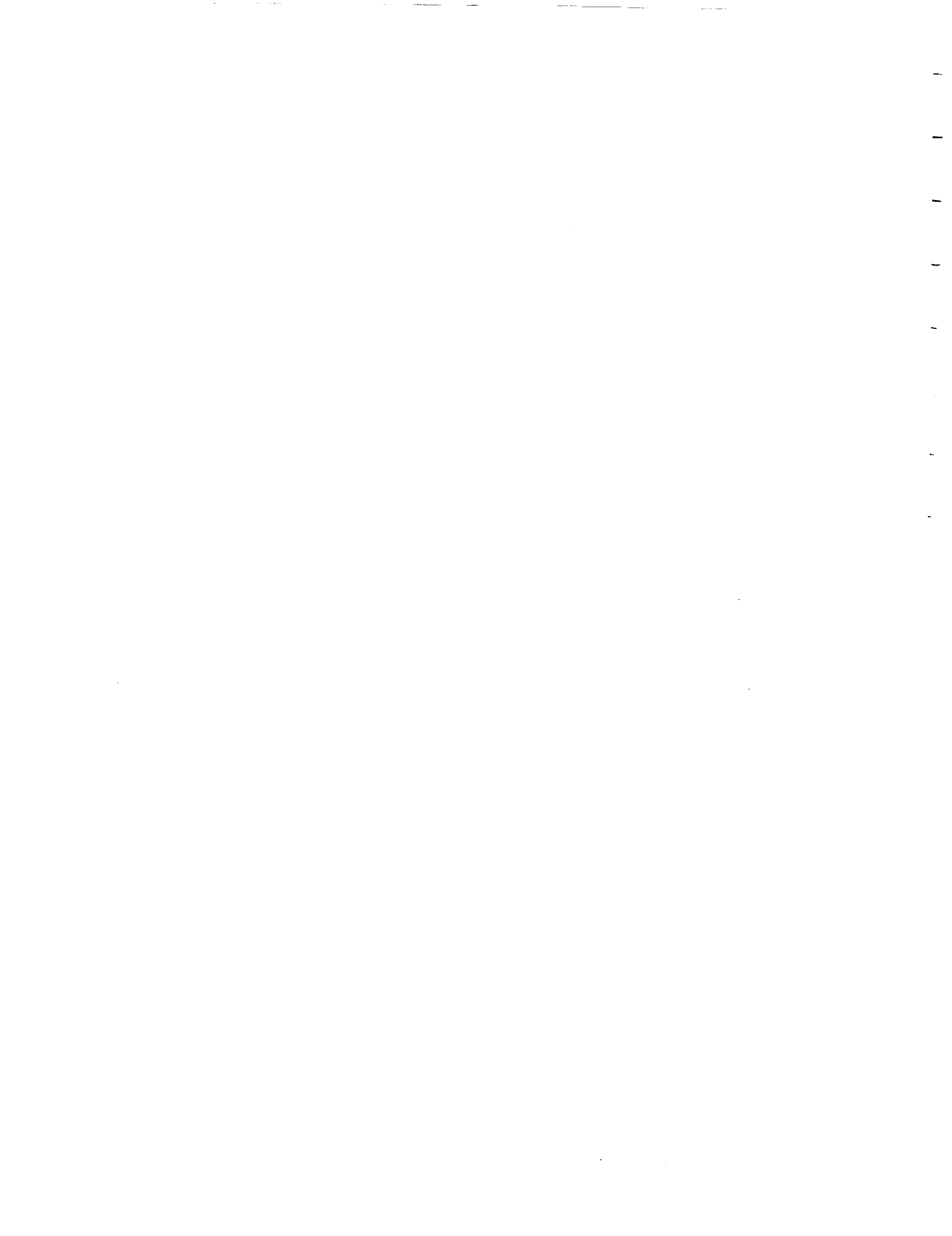
Fixed-Order Multi-Model Estimation and Control

Douglas MacMartin and Steven R. Hall[*]

Dept. of Aeronautics and Astronautics

Massachusetts Institute of Technology

Cambridge, MA 02139

(617) 258-8747

Dennis S. Bernstein[†]

Harris Corporation

MS 22/4842

Melbourne, FL 32901

(407) 729-2140

September 17, 1990

Abstract

In certain applications modeling uncertainty can be represented by a finite number of plant models. This paper considers the problems of determining a feedback controller or estimator that optimizes an $\mathcal{H}_2$ performance criterion involving a collection of plant models. The approach is based upon fixed-structure optimization in which the estimator or controller order are fixed prior to the development of optimality conditions.

1 Introduction

The goal of robust control design is to obtain controllers that maintain desirable performance in the face of modeling uncertainty. In certain cases modeling uncertainty can be adequately represented by means of a finite number of plant models. This multi-model problem arises for example, if the plant can undergo sensor or actuator failure modes. A finite set of models has also been used to design for robustness to an infinite set of models, as in the case of parametric uncertainty [1], high frequency uncertainty [2], or parameter variations (e.g. for different flight regimes) [3].

A fundamental issue in multi-model problems is the *simultaneous* or *reliable* stabilization problem. Here the goal is to design controllers that stabilize each model in a finite collection of plant models. Considerable progress has been made in solving this problem [4–10].

The goal of the present paper is to consider a multi-model optimization problem. Specifically, we consider a quadratic ($\mathcal{H}_2$) performance criterion involving a collection of plant models controlled by a single feedback compensator. The approach we take involves fixing the order of the compensator and optimizing over the feedback gains. This approach is similar to that of [11] where static output feedback controllers were considered.

One of our principal objectives in considering the Multi-Model Control Problem is to examine the issue of compensator order. In [6] it is shown that simultaneous

stabilization of a pair of plants of bounded degree may require a compensator of arbitrarily high order. In the present paper we show how this issue manifests itself in the structure of the necessary conditions for optimality.

To further elucidate the role of compensator order we also consider two related problems that are simpler in structure but that involve analogous issues. The objective of the Multi-Model Approximation Problem is to determine a single model that simultaneously approximates a finite collection of models. For a collection of r models each of order n_i, $i = 1, \ldots, r$, the maximal-order solution is given by a model of order $\sum_{i=1}^{r} n_i$, which is larger than the order of each of the given plant models.

In a related vein we also consider the Multi-Model Estimation Problem wherein we seek an estimator for each model in a given collection of plant models. As in the Multi-Model Approximation Problem the maximal-order solution has order greater than the individual plant models.

The fixed-structure approach applied to the multi-model problems is a direct extension of the technique utilized in [12–14]. Indeed, by specializing these results to the case of a single model, the results of [12–14] are immediately recovered.

2 Multi-Model Approximation

Consider the following problem.

Problem 1 (Optimal Multi-Model Approximation Problem) *Given a set of r controllable and observable systems H_i, $i = 1 \ldots r$, with state space representations*

$$H_i = \left[\begin{array}{c|c} A_i & B_i \\ \hline C_i & 0 \end{array} \right] = C_i(sI - A_i)^{-1}B_i \tag{1}$$

and a set of r numbers $\alpha_i \in \mathbb{R}$, $\alpha_i > 0$, $i = 1 \ldots r$, find a single approximation model of fixed order n_m, with state space representation

$$H_m = \left[\begin{array}{c|c} A_m & B_m \\ \hline C_m & 0 \end{array} \right] \tag{2}$$

2

that minimizes the weighted $\mathcal{H}_2$ model-approximation criterion,

$$J(H_m) = \sum_{i=1}^{r} \alpha_i \|H_i - H_m\|_2^2 \qquad (3)$$

To guarantee finite cost J, assume that each H_i is stable, and also restrict the optimization to the set of stable approximation models H_m. Furthermore, since the value of J is independent of the internal realization of H_m, assume that the realization in Equation (2) is controllable and observable. Thus require that $(A_m, B_m, C_m) \in \mathcal{R}$ where

$$\mathcal{R} = \{(A_m, B_m, C_m) : A_m \ stable, \ (A_m, B_m) \ controllable, \ (A_m, C_m) \ observable\}$$

Without loss of generality, the weightings α_i can be assumed to be normalized so that

$$\sum_{i=1}^{r} \alpha_i = 1$$

With this normalization, the weighting α_i can then be associated with the probability that H_i accurately models the dynamics of the system.

The necessary conditions for an optimal solution to this problem are given in Theorem 4. The approach used to obtain them is presented briefly here for comparison with the approach required for the multi-model estimation and control problems in Sections 3 and 4, and for the single model problems in [12–14].

The model approximation error transfer function $H_i - H_m$ can be represented in state space as

$$H_i - H_m = \left[\begin{array}{cc|c} A_i & 0 & B_i \\ 0 & A_m & B_m \\ \hline C_i & -C_m & 0 \end{array} \right] = \left[\begin{array}{c|c} \bar{A}_i & \bar{B}_i \\ \hline \bar{C}_i & 0 \end{array} \right] \qquad (4)$$

The cost J is then

$$J(H_m) = \sum_{i=1}^{r} \mathrm{tr} \left\{ \alpha_i \bar{C}_i \bar{Q}_i \bar{C}_i^T \right\} \qquad (5)$$

where each $\bar{Q}_i$ satisfies a Lyapunov equation

$$\bar{A}_i \bar{Q}_i + \bar{Q}_i \bar{A}_i^T + \bar{B}_i \bar{B}_i^T = 0 \qquad (6)$$

3

Appending these constraints to the cost with Lagrange multipliers $\tilde{P}_i$ yields first order necessary conditions for a solution upon differentiation with respect to $\tilde{Q}_i$, A_m, B_m, and C_m. Each matrix $\tilde{P}_i$ and $\tilde{Q}_i$ has dimension $(n_i + n_m) \times (n_i + n_m)$ and can be partitioned into $n_i \times n_i$, $n_i \times n_m$, $n_m \times n_i$ and $n_m \times n_m$ blocks as

$$\tilde{P}_i = \begin{bmatrix} \tilde{P}_{i_{11}} & \tilde{P}_{i_{12}} \\ \tilde{P}_{i_{21}} & \tilde{P}_{i_{22}} \end{bmatrix} \qquad \tilde{Q}_i = \begin{bmatrix} \tilde{Q}_{i_{11}} & \tilde{Q}_{i_{12}} \\ \tilde{Q}_{i_{21}} & \tilde{Q}_{i_{22}} \end{bmatrix} \tag{7}$$

The necessary conditions are then Equations (6), and

$$\frac{\partial J}{\partial \tilde{Q}_i} = \tilde{P}_i \tilde{A}_i + \tilde{A}_i^T \tilde{P}_i + \tilde{C}_i^T \tilde{C}_i = 0 \quad \forall i \tag{8}$$

$$\frac{\partial J}{\partial B_m} = \sum_{i=1}^{r} \alpha_i \tilde{P}_{i_{22}} B_m + \sum_{i=1}^{r} \alpha_i \tilde{P}_{i_{12}} B_i = 0 \tag{9}$$

$$\frac{\partial J}{\partial C_m} = C_m \sum_{i=1}^{r} \alpha_i \tilde{Q}_{i_{22}} - \sum_{i=1}^{r} \alpha_i C_i \tilde{Q}_{i_{12}} = 0 \tag{10}$$

$$\frac{\partial J}{\partial A_m} = \sum_{i=1}^{r} \alpha_i (\tilde{P}_{i_{22}} \tilde{Q}_{i_{22}} + \tilde{P}_{i_{21}} \tilde{Q}_{i_{12}}) = 0 \tag{11}$$

The equation obtained from differentiation with respect to A_m is of particular importance in simplifying and understanding the structure of the necessary conditions. In the case of a single model ($r = 1$), Equation (11) yields

$$I_{n_m} = \underbrace{(-\tilde{P}_{22}^{-1} \tilde{P}_{21})}_{\Gamma} \underbrace{(\tilde{Q}_{12} \tilde{Q}_{22}^{-1})}_{G^T} \tag{12}$$

A projection operator $\tau = G^T \Gamma = \tau^2$ is then used to simplify the equations [12].

For the multi-model approximation case, from Equation (6) each $\tilde{Q}_{i_{22}}$ satisfies an identical equation,

$$A_m \tilde{Q}_{i_{22}} + \tilde{Q}_{i_{22}} A_m^T + B_m B_m^T = 0 \tag{13}$$

Hence the $\tilde{Q}_{i_{22}}$ satisfy $\tilde{Q}_{i_{22}} = \tilde{Q}_{22}$, $i = 1 \ldots r$. Similarly, each $\tilde{P}_{i_{22}}$ satisfies

$$\tilde{P}_{i_{22}} A_m + A_m^T \tilde{P}_{i_{22}} + C_m^T C_m = 0 \tag{14}$$

and hence $\tilde{P}_{i_{22}} = \tilde{P}_{22}$, $i = 1 \ldots r$. Furthermore, from Equations (13) and (14), $\tilde{Q}_{22}$ and $\tilde{P}_{22}$ are the controllability and observability grammians, respectively, of the system H_m. With these simplifications Equation (11) can be written as

$$\tilde{P}_{22}\tilde{Q}_{22} + \sum_{i=1}^{r} \alpha_i (\tilde{P}_{i_{21}} \tilde{Q}_{i_{12}}) = 0 \tag{15}$$

This immediately gives the following result:

Proposition 2 *Given a fixed order model that is optimal for Problem 1, of order $n_m > N = \sum_{i=1}^{r} n_i$, there exists a model of order N with the same cost. Hence with no fixed order constraint, the optimal system for multi-model approximation has order no larger than N.*

Proof: $\forall i$, $\operatorname{rank}\left\{\tilde{P}_{i_{21}} \tilde{Q}_{i_{12}}\right\} \leq n_i$, hence $\operatorname{rank}\left\{\sum_{i=1}^{r} \alpha_i \tilde{P}_{i_{21}} \tilde{Q}_{i_{12}}\right\} \leq N$. So, from Equation (15), $\operatorname{rank}\left\{\tilde{P}_{22}\tilde{Q}_{22}\right\} \leq N$. If $n_m > N$, either $\tilde{P}_{22}$ or $\tilde{Q}_{22}$ or both must not be full rank, and thus the representation of H_m must have states which are either uncontrollable or unobservable. (The maximum number of states which are both observable and controllable is N.) Removing any uncontrollable or unobservable states yields a system with identical cost and at most N states. □

With the controllability and observability assumptions on the representation of H_m, $\tilde{P}_{22}$ and $\tilde{Q}_{22}$ must be positive definite, and thus Equation (15) can be written

$$I_{n_m} = \sum_{i=1}^{r} \underbrace{(-\alpha_i \tilde{P}_{22}^{-1} \tilde{P}_{i_{21}})}_{\Gamma_i} \underbrace{(\tilde{Q}_{i_{12}} \tilde{Q}_{22}^{-1})}_{G_i^T} \tag{16}$$

Define

$$\Gamma = \begin{bmatrix} \Gamma_1 & \cdots & \Gamma_r \end{bmatrix} \tag{17}$$

$$G = \begin{bmatrix} G_1 & \cdots & G_r \end{bmatrix} \tag{18}$$

$$\tau = G^T \Gamma \tag{19}$$

$$\tau_\perp = I_N - \tau \tag{20}$$

5

Then τ is again an oblique projection operator, that is $\tau^2 = \tau$. Note that in general, τ is oblique rather than orthogonal, since it need not be symmetric.

The following lemma from [12] is required for the statement of the main theorem.

Lemma 3 *Suppose $\hat{Q}$, $\hat{P} \in \mathbb{R}^{N \times N}$ are positive semi-definite. Then $\hat{Q}\hat{P}$ is nonnegative semisimple (has non-negative eigenvalues). Furthermore, if $\mathrm{rank}\{\hat{Q}\hat{P}\} = n_m$, then there exist $G, \Gamma \in \mathbb{R}^{n_m \times N}$ and positive semisimple $M \in \mathbb{R}^{n_m \times n_m}$ such that*

$$\hat{Q}\hat{P} = G^T M \Gamma \tag{21}$$

$$\Gamma G^T = I_{n_m} \tag{22}$$

Matrices G, Γ, and M satisfying the conditions of the lemma will be referred to as a projective factorization of $\hat{Q}\hat{P}$.

It will be convenient to compile the state space information about all of the models into a single set of matrices $(\hat{A}, \hat{B}, \hat{C}_\alpha)$, where

$$\hat{A} = \begin{bmatrix} A_1 & 0 & \cdots & 0 \\ 0 & A_2 & & \\ \vdots & & \ddots & \\ 0 & & & A_r \end{bmatrix} \qquad \hat{B} = \begin{bmatrix} B_1 \\ B_2 \\ \vdots \\ B_r \end{bmatrix} \tag{23}$$

$$\hat{C}_\alpha = \begin{bmatrix} \alpha_1 C_1 & \alpha_2 C_2 & \cdots & \alpha_r C_r \end{bmatrix}$$

The subscript α on $\hat{C}_\alpha$ indicates that it depends on α_i.

Theorem 4 *Suppose (A_m, B_m, C_m) solves the optimal multi-model approximation problem (1). Then there exist positive semi-definite matrices $\hat{Q}$, $\hat{P} \in \mathbb{R}^{N \times N}$ such that, for some projective factorization of $\hat{Q}\hat{P}$, A_m, B_m, and C_m are given by*

$$A_m = \Gamma \hat{A} G^T \tag{24}$$

$$B_m = \Gamma \hat{B} \tag{25}$$

$$C_m = \hat{C}_\alpha G^T \tag{26}$$

6

and such that the following conditions are satisfied:

$$\text{rank}\left\{\hat{Q}\right\} = \text{rank}\left\{\hat{P}\right\} = \text{rank}\left\{\hat{Q}\hat{P}\right\} = n_m \qquad (27)$$

$$\hat{A}\hat{Q} + \hat{Q}\hat{A}^T + \hat{B}\hat{B}^T - \tau_\perp \hat{B}\hat{B}^T \tau_\perp^T = 0 \qquad (28)$$

$$\hat{P}\hat{A} + \hat{A}^T\hat{P} + \hat{C}^T\hat{C} - \tau_\perp^T \hat{C}_\alpha^T \hat{C}_\alpha \tau_\perp = 0 \qquad (29)$$

Proof: Define $\hat{Q} = G^T \tilde{Q}_{22} G$ and $\hat{P} = \Gamma^T \tilde{P}_{22} \Gamma$, and note that $\tau\hat{Q} = \hat{Q}$, and $\hat{P}\tau = \hat{P}$. Pre- and post-multiplying the Lyapunov equations (13) and (14) for $\tilde{Q}_{22}$ and $\tilde{P}_{22}$ by either $I_{n_m} = \Gamma G^T$ or $I_{n_m} = G\Gamma^T$ yields the following equations:

$$\tau\left[\hat{A}\hat{Q} + \hat{Q}\hat{A}^T + \hat{B}\hat{B}^T\right] = 0 \qquad (30)$$

$$\left[\hat{P}\hat{A} + \hat{A}^T\hat{P} + \hat{C}_\alpha^T\hat{C}_\alpha\right]\tau = 0 \qquad (31)$$

The $(1,2)$ sub-blocks of the Lyapunov equations (6) and (8) yield identical equations. Equation (30) is equivalent to Equation (28) since Equation (28)=(30)+(30)^T−(30)τ, and Equation (30)=τ(28). Similarly, Equations (31) and (29) are equivalent. Note that only two Lyapunov equations are required for the necessary conditions because the $(1,1)$ sub-blocks of both Equation (6) and Equation (8) are superfluous.

Equations (25) and (26) follow directly from (9) and (10). Equation (24) for A_m is obtained from the $(2,2)$ block of either $\left(\sum\limits_{i=1}^{r} \alpha_i(\text{Eq'n 8})\tilde{Q}_i\right)$ or $\left(\sum\limits_{i=1}^{r} \alpha_i\tilde{P}_i(\text{Eq'n 6})\right)$, either of which yield that $\sum\limits_{i=1}^{r}\left(\alpha_i\tilde{P}_i\tilde{A}_i\tilde{Q}_i\right)_{22} = 0$. $\qquad\square$

Because the form of the equations is identical to that of the single model case, the discussion in [12] applies for this problem as well. As in [12], the form is a result of optimality, and not fixed beforehand. If (A_m, B_m, C_m) satisfies the necessary conditions, so does $(TA_mT^{-1}, TB_m, C_mT^{-1})$ for an arbitrary nonsingular transformation matrix T. Further, there exists a similarity transformation which diagonalizes $\hat{Q}\hat{P}$ and τ simultaneously. Representing τ in terms of $\hat{Q}\hat{P}$ as in [12] leads to numerical algorithms for the optimal multi-model approximation problem.

7

Remark 5 *In the "full order" case $n_m = N$, then $\tau = G = \Gamma = I_N$, giving $A_m = \hat{A}$, $B_m = \hat{B}$, and $C_m = \hat{C}_\alpha$. Thus $H_m = \sum_{i=1}^{r} \alpha_i H_i$. This is exactly the expected result; the best possible approximation is simply the weighted average of all the models.*

Remark 6 *For a single model ($r = 1$), the equations clearly collapse to the equations of [12].*

3 Multi-Model Estimation

Consider the following problem.

Problem 7 (Optimal Multi-Model Estimation Problem) *Given a set of r systems H_i, $i = 1 \ldots r$, with state space representations*

$$H_i = \left[\begin{array}{c|c} A_i & \bar{B}_i \\ \hline C_{i_1} & 0 \\ C_{i_2} & \bar{D}_i \end{array} \right] = \left[\begin{array}{c} C_{i_1} \\ C_{i_2} \end{array} \right] (sI - A_i)^{-1} \bar{B}_i + \left[\begin{array}{c} 0 \\ \bar{D}_i \end{array} \right] \tag{32}$$

and a set of r numbers $\alpha_i \in \mathbb{R}$, $\alpha_i > 0$, $i = 1 \ldots r$, find a single estimator of fixed order n_e, with state space representation

$$H_e = \left[\begin{array}{c|c} A_e & B_e \\ \hline C_e & 0 \end{array} \right] \tag{33}$$

that minimizes the weighted $\mathcal{H}_2$ model-estimation criterion,

$$J(H_e) = \sum_{i=1}^{r} \alpha_i \| H_{i_1} - H_e H_{i_2} \|_2^2 \tag{34}$$

where H_i is partitioned into H_{i_1} and H_{i_2} according to the two outputs.

The estimation problem can be illustrated by the block diagram as shown in Figure 1.

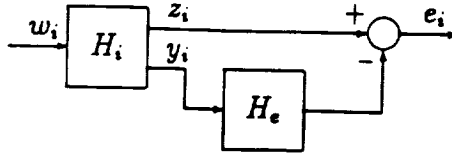The following assumptions about the problem will be made:

8

Figure 1: Estimation problem for each system.

(i) Each H_i is stable, and each (A_i, C_{i_2}) is detectable.

(ii) $\sum\limits_{i=1}^{r} \alpha_i = 1$

(iii) For clarity in understanding the form of the equations, the process and measurement noise for each model will be assumed to be uncorrelated, so $\bar{B}_i \bar{D}_i^T = 0$. Without loss of generality, assume $\bar{B}_i = [B_i \ 0]$ and $\bar{D}_i = [0 \ D_i]$.

(iv) Require that the measurement noise have no singular directions common to all models, so $\sum\limits_{i=1}^{r} \alpha_i D_i D_i^T > 0$. This is a generalization of the usual single model assumption of nonsingular measurement noise, $DD^T > 0$.

It is interesting to note that each D_i need not have full row rank, hence the estimation problem for each individual model may be singular without the multi-model problem being singular.

As in the multi-model approximation case, require $(A_e, B_e, C_e) \in \mathcal{R}$.

The model estimation error transfer function $H_{i_1} - H_e H_{i_2}$ can be represented in state space as

$$H_{i_1} - H_e H_{i_2} = \left[\begin{array}{cc|cc} A_i & 0 & B_i & 0 \\ B_e C_{i_2} & A_e & 0 & B_e D_i \\ \hline C_{i_1} & -C_e & 0 & 0 \end{array} \right] = \left[\begin{array}{c|c} \tilde{A}_i & \tilde{B}_i \\ \hline \tilde{C}_i & 0 \end{array} \right] \quad (35)$$

The cost J can again be written in the form of Equation (5),

$$J(H_e) = \sum\limits_{i=1}^{r} \text{tr} \left\{ \alpha_i \tilde{C}_i \tilde{Q}_i \tilde{C}_i^T \right\} \quad (36)$$

9

where each $\tilde{Q}_i$ satisfies a Lyapunov equation identical to Equation (6)).

Necessary conditions can again be obtained using a Lagrange multiplier approach. The Lyapunov equations for $\tilde{P}_i$ are identical to Equations (8). The equation obtained by differentiating with respect to A_e is the same as Equation (11), and once again this will be the key equation for understanding the structure of the necessary conditions. For this problem, each $\tilde{Q}_{i_{22}}$ satisfies

$$A_e\tilde{Q}_{i_{22}} + \tilde{Q}_{i_{22}}A_e^T + B_eC_{i_2}\tilde{Q}_{i_{12}} + \tilde{Q}_{i_{21}}C_{i_2}^TB_e^T + B_eB_e^T = 0 \qquad (37)$$

Each $\tilde{Q}_{i_{22}}$ now satisfies a distinct equation, and thus $\tilde{Q}_{i_{22}} \neq \tilde{Q}_{j_{22}}$, $i \neq j$. The critical observation for this problem, however, is that each $\tilde{P}_{i_{22}}$ still satisfies Equation (14). Thus it is still true that $\tilde{P}_{i_{22}} = \tilde{P}_{22}$, $i = 1 \ldots r$. This is sufficient to obtain the elements of a projection operator from Equation (11), and to prove the following result, analogous to Proposition 2.

Proposition 8 *Given a fixed order model that is optimal for Problem 7, of order $n_m > N = \sum_{i=1}^{r} n_i$, there exists a model of order N with the same cost. Hence with no fixed order constraint, the optimal system for multi-model estimation has order no larger than N.*

Proof: As in the Multi-Model Approximation case, rank $\left\{\sum_{i=1}^{r} \alpha_i \tilde{P}_{i_{21}}\tilde{Q}_{i_{12}}\right\} \leq N$. From Equation (11), rank $\left\{\tilde{P}_{22} \sum_{i=1}^{r} \alpha_i \tilde{Q}_{i_{22}}\right\} \leq N$. If $n_m > N$, either $\tilde{P}_{22}$ or $\sum_{i=1}^{r} \alpha_i \tilde{Q}_{i_{22}}$ or both must not be full rank. $\tilde{P}_{22}$ is the observability grammian of the system (A_e, B_e, C_e), and thus is not full rank if and only if (A_e, C_e) is unobservable. Also, $\sum_{i=1}^{r} \alpha_i \tilde{Q}_{i_{22}}$ is not full rank if and only if (A_e, B_e) is not controllable. This result will be proven in Proposition 13. Proposition 8 then follows in the same manner as the proof of Proposition 2. $\qquad \square$

Remark 9 *The estimator must obtain all the information possible about the state from the output y. Since all state information from all the models has a finite dimension N, there is an estimator state vector of dimension N that contains the most*

information possible about the state vectors of the H_i. *Any additional estimator states must be redundant.*

As noted earlier, $\tilde{P}_{22}$ is the observability grammian for H_e and therefore must be positive definite. Proposition 13 proves that $\sum_{i=1}^{r} \alpha_i \tilde{Q}_{i_{22}}$ must also be positive definite. Hence for the multi-model estimation problem, Equation (11) can be written as

$$I_{n_{\mathbb{P}}} = \sum_{i=1}^{r} \underbrace{(-\alpha_i \tilde{P}_{22}^{-1} \tilde{P}_{i_{21}})}_{\Gamma_i} \underbrace{(\tilde{Q}_{i_{12}} \left(\sum_{i=1}^{r} \alpha_i \tilde{Q}_{i_{22}} \right)^{-1})}_{G_i^T} \tag{38}$$

With G, Γ, and τ defined as in Equations (17–19), τ is again a projection operator, satisfying $\tau^2 = \tau$.

In addition to the definitions of $\hat{A}$ and $\hat{B}$, given in Equation (23), this problem requires $\hat{C}_{\alpha_1}$ and $\hat{C}_{\alpha_2}$, defined analogously to $\hat{C}_{\alpha}$, and

$$\hat{V}_1 = \begin{bmatrix} B_1 B_1^T & 0 & \cdots & 0 \\ 0 & B_2 B_2^T & & \\ \vdots & & \ddots & \\ 0 & & & B_r B_r^T \end{bmatrix} \tag{39}$$

$$V_2 = \sum_{i=1}^{r} \alpha_i D_i D_i^T \tag{40}$$

Theorem 10 *Suppose* (A_e, B_e, C_e) *solves the optimal multi-model estimation problem (7). Then there exist positive semi-definite matrices* Q, $\hat{Q}$, $\hat{P} \in \mathbb{R}^{N \times N}$ *such that, for some projective factorization of* $\hat{Q}\hat{P}$, A_e, B_e, *and* C_e *are given by*

$$A_e = \Gamma \hat{A} G^T - B_e \hat{C}_{\alpha_2} G^T \tag{41}$$

$$B_e = \Gamma Q \hat{C}_{\alpha_2}^T V_2^{-1} \tag{42}$$

$$C_e = \hat{C}_{\alpha_1} G^T \tag{43}$$

and such that the following conditions are satisfied:

$$\hat{A}Q + Q\hat{A}^T + \hat{V}_1 - Q\hat{C}_{\alpha_2}^T V_2^{-1} \hat{C}_{\alpha_2} Q + \tau_\perp Q \hat{C}_{\alpha_2}^T V_2^{-1} \hat{C}_{\alpha_2} Q \tau_\perp = 0 \tag{44}$$

11

$$\hat{A}\hat{Q} + \hat{Q}\hat{A}^T + Q\hat{C}_{\alpha_2}^T V_2^{-1}\hat{C}_{\alpha_2}Q - \tau_\perp Q\hat{C}_{\alpha_2}^T V_2^{-1}\hat{C}_{\alpha_2}Q\tau_\perp = 0 \qquad (45)$$

$$\hat{P}(\hat{A} - Q\hat{C}_{\alpha_2}^T V_2^{-1}\hat{C}_{\alpha_2}) + (\hat{A} - Q\hat{C}_{\alpha_2}^T V_2^{-1}\hat{C}_{\alpha_2})^T \hat{P} + \hat{C}_{\alpha_1}^T \hat{C}_{\alpha_1} - \tau_\perp \hat{C}_{\alpha_1}^T \hat{C}_{\alpha_1}\tau_\perp = 0 \quad (46)$$

Proof: The derivation of these equations is similar to that for the necessary conditions for the multi-model approximation problem. Define $\hat{Q} = G^T \left(\sum_{i=1}^r \alpha_i \tilde{Q}_{i_{22}} \right) G$, $\hat{P} = \Gamma^T \tilde{P}_{22} \Gamma$, and $Q = \text{diag}\left\{ \alpha_i^{-1} \tilde{Q}_{i_{11}} \right\} - \hat{Q}$. Substituting into the Lyapunov equations defining $\tilde{Q}_i$ and $\tilde{P}_i$ yields Equations (45) and (46) from both the $(1,2)$ and $(2,2)$ sub-blocks. The $(1,1)$ sub-block of the $\tilde{Q}_i$ Lyapunov equation can be used to obtain Equation (44), and the $(1,1)$ sub-block of the $\tilde{P}_i$ equation is superfluous. Equations (42) and (43) follow directly from the equations obtained by differentiating the augmented cost with respect to B_e and C_e. Equation (41) for A_e is obtained in an analogous fashion to the approximation problem. □

As in the multi-model approximation case, the necessary conditions obtained here are similar in form to those for the single model case [13]. Again, the necessary conditions hold for any non-singular state transformation of the estimator. Numerical algorithms developed for solving the equations in [13] can be applied to this problem as well.

Remark 11 *In the "full order" case $n_e = N$, then $\tau = G = \Gamma = I_N$, giving $A_e = \hat{A} - B_e\hat{C}_{\alpha_2}$, $B_e = Q\hat{C}_{\alpha_2}^T V_2^{-1}$, and $C_e = \hat{C}_{\alpha_1}$. Only the Riccati equation for Q needs to be solved, and this has the same form as the Kalman filter equation. Because of the coupling of the multiple models in Q, the full order estimator is not simply a weighted average of the individual model estimators.*

Remark 12 *For a single model ($r = 1$), the equations clearly collapse to the equations of [12]. For $r = 1$ and $n_e = N$, the equations collapse to the standard Kalman filter result.*

Finally, the proposition used in the proof of Proposition 8 needs to be proven.

Proposition 13 $\bar{Q} = \sum_{i=1}^r \alpha_i \tilde{Q}_{i_{22}}$ *is full rank if and only if (A_e, B_e) is controllable.*

Proof: $\bar{Q}$ satisfies the Lyapunov equation

$$(A_e + B_e \hat{C}_{\alpha_2} G^T)\bar{Q} + \bar{Q}(A_e + B_e \hat{C}_{\alpha_2} G^T)^T + B_e V_2 B_e^T = 0 \qquad (47)$$

This follows from summing Equations (37) and representing $\bar{Q}_{i_{12}}$ in terms of G and $\bar{Q}$. $\bar{Q}$ is therefore a controllability grammian, and is full rank if and only if $(A_e + B_e \hat{C}_{\alpha_2} G^T, B_e)$ is controllable. This system is controllable if and only if (A_e, B_e) is controllable. $\qquad \square$

4 Multi-Model Control

A simple form of the necessary conditions for the multi-model control problem is significantly harder to obtain than for either of the two previously considered problems. A form of the equations similar to the single model case has not yet been obtained. The problem will be set up here, and the critical issues discussed. In particular, the question of controller order is investigated.

Consider the following problem.

Problem 14 (Optimal Multi-Model Control Problem) *Given a set of r systems H_i, $i = 1 \dots r$, with state space representations*

$$H_i = \left[\begin{array}{c|cc} A_i & \bar{B}_{i_1} & B_{i_2} \\ \hline \bar{C}_{i_1} & 0 & \bar{D}_{i_{12}} \\ C_{i_2} & \bar{D}_{i_{21}} & 0 \end{array} \right] \qquad (48)$$

and a set of r numbers $\alpha_i \in \mathbb{R}$, $\alpha_i > 0$, $i = 1 \dots r$, find a single compensator of fixed order n_c, with state space representation

$$H_c = \left[\begin{array}{c|c} A_c & B_c \\ \hline C_c & 0 \end{array} \right] \qquad (49)$$

that minimizes the weighted $\mathcal{H}_2$ model-control criterion,

$$J(H_c) \;=\; \sum_{i=1}^{r} \alpha_i \, \|H_{i_{sw}}\|_2^2 \qquad (50)$$

13

$$= \sum_{i=1}^{r} \alpha_i \left\| H_{i_{11}} + H_{i_{12}} H_c (I - H_{i_{22}} H_c)^{-1} H_{i_{21}} \right\|_2^2 \qquad (51)$$

H_i *is partitioned into* $H_{i_{11}}$, $H_{i_{12}}$, $H_{i_{21}}$ *and* $H_{i_{22}}$ *according to the two inputs and two outputs. The closed loop transfer function* $H_{i_{zw}}$ *is obtained from the lower linear fractional transformation,* $H_{i_{zw}} = \mathcal{F}(H_i, H_c)$.

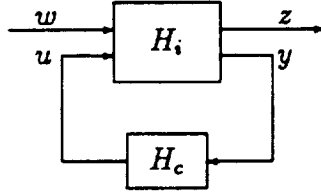The control problem can be illustrated by the block diagram as shown in Figure 2.

Figure 2: Control problem for each system.

The following assumptions about the problem will be made.

(i) Each system H_i must satisfy (A_i, B_{i_2}) stabilizable and (A_i, C_{i_2}) detectable.

(ii) $\sum_{i=1}^{r} \alpha_i = 1$

(iii) For a compensator H_c to exist which gives finite cost J, the set of systems H_i must be simultaneously stabilizable. Conditions for simultaneous stabilization have been studied by Ghosh and Byrnes [6].

(iv) As in the estimation problem, assume uncorrelated process and measurement noise, so $\bar{B}_{i_1} \bar{D}_{i_{21}}^T = 0$. Without loss of generality, again take $\bar{B}_{i_1} = [B_{i_1} \ 0]$ and $\bar{D}_{i_{21}} = [0 \ D_{i_{21}}]$. Further, require that the measurement noise have no singular directions common to all the models, so $\sum_{i=1}^{r} \alpha_i D_{i_{21}} D_{i_{21}}^T > 0$.

(v) The dual assumptions to (iv) will also be made. That is, $\bar{C}_{i_1}^T \bar{D}_{i_{12}} = 0$, $\bar{C}_{i_1} = \begin{bmatrix} C_{i_1} \\ 0 \end{bmatrix}$, $\bar{D}_{i_{12}} = \begin{bmatrix} 0 \\ D_{i_{12}} \end{bmatrix}$, and $\sum_{i=1}^{r} \alpha_i D_{i_{12}} D_{i_{12}}^T > 0$. Note that for any individual H_i, the control weighting $D_{i_{12}} D_{i_{12}}^T$ may be singular.

14

The optimization will be restricted to the (non-empty) set of simultaneously stabilizing compensators H_c, with controllable and observable realizations.

The closed loop transfer function $H_{i_{zw}}$ can be represented in state space as

$$H_{i_{zw}} = \left[\begin{array}{cc|cc} A_i & B_{i_2}C_c & B_{i_1} & 0 \\ B_cC_{i_2} & A_c & 0 & B_cD_{i_{21}} \\ \hline C_{i_1} & 0 & 0 & 0 \\ 0 & D_{i_{12}}C_c & 0 & 0 \end{array} \right] = \left[\begin{array}{c|c} \tilde{A}_i & \tilde{B}_i \\ \hline \tilde{C}_i & 0 \end{array} \right] \tag{52}$$

The cost J can again be written in the form of Equation (5),

$$J(H_c) = \sum_{i=1}^{r} \text{tr} \left\{ \alpha_i \tilde{C}_i \tilde{Q}_i \tilde{C}_i^T \right\} \tag{53}$$

and again, each $\tilde{Q}_i$ satisfies a Lyapunov equation identical to Equation (6).

Necessary conditions can again be obtained using a Lagrange multiplier approach. The Lyapunov equations for $\tilde{P}_i$ are identical to Equations (8). Once again, the equation obtained by differentiating with respect to A_c is the same as Equation (11). However, for the control problem, there is a crucial difference. Each $\tilde{Q}_{i_{22}}$ and $\tilde{P}_{i_{22}}$ satisfy, respectively,

$$A_c\tilde{Q}_{i_{22}} + \tilde{Q}_{i_{22}}A_c^T + B_cC_{i_2}\tilde{Q}_{i_{12}} + \tilde{Q}_{i_{21}}C_{i_2}^TB_c^T + B_cB_c^T = 0 \tag{54}$$

$$\tilde{P}_{i_{22}}A_c + A_c^T\tilde{P}_{i_{22}} + \tilde{P}_{i_{21}}B_{i_2}C_c + C_c^TB_{i_2}^T\tilde{P}_{i_{12}} + C_c^TC_c = 0 \tag{55}$$

Thus for this problem, every $\tilde{Q}_{i_{22}}$ and every $\tilde{P}_{i_{22}}$ is different, that is $\tilde{Q}_{i_{22}} \neq \tilde{Q}_{j_{22}}$, $i \neq j$, and $\tilde{P}_{i_{22}} \neq \tilde{P}_{j_{22}}$, $i \neq j$. As a result, Equation (11) is difficult to factor, and this also has serious implications on the order of the compensator.

Proposition 15 *There is no a priori* **bound on the order of a compensator which is** *optimal for Problem 14.*

Proof: Ghosh and Byrnes [7] give an example of two second order systems, parameterized by λ, which require an arbitrarily high order compensator for simultaneous stabilization as λ tends to some limit. Since any optimal compensator must be simultaneously stabilizing, it also may be of arbitrarily high order. □

15

Remark 16 *The result in Proposition 15 has been shown before; the purpose of re-stating it here is to illustrate how the result manifests itself in the present context.*

For all three of the problems investigated in this paper, $\sum_{i=1}^{r} \alpha_i \tilde{P}_{i_{21}} \tilde{Q}_{i_{12}}$ has at most rank N. Equation (11) then yields that $\sum_{i=1}^{r} \alpha_i \tilde{P}_{i_{22}} \tilde{Q}_{i_{22}}$ has rank less than or equal to N. For controllable and observable systems H_m, H_e, and H_c, each term in this last sum has rank n_m, n_e, or n_c. In the approximation case, this sum can be factored as $P_{22} Q_{22}$, and in the estimation case, it can be factored as $P_{22} \sum_{i=1}^{r} \alpha_i \tilde{Q}_{i_{22}}$. Sylvester's inequality [15] can then be used to show that this second sum has rank equal to n_m or n_e. From this, the conclusion that $n_m \leq N$, and $n_e \leq N$ follows. In the multi-model control problem, the sum $\sum_{i=1}^{r} \alpha_i \tilde{P}_{i_{22}} \tilde{Q}_{i_{22}}$ may have maximum rank N while the individual terms in the sum can have larger rank n_c. That is, the optimal compensator may be both observable and controllable for arbitrarily large order n_c.

Theorem 17 *Suppose (A_c, B_c, C_c) solves the optimal multi-model control problem (14). Then there exist positive semi-definite matrices $\tilde{Q}_i$, $\tilde{P}_i \in \mathbb{R}^{(n_i + n_c) \times (n_i + n_c)}$ such that A_c, B_c, and C_c are the solutions of*

$$\sum_{i=1}^{r} \alpha_i \left(\tilde{P}_{i_{22}} A_c \tilde{Q}_{i_{22}} + \tilde{P}_{i_{21}} A_i \tilde{Q}_{i_{12}} + \tilde{P}_{i_{22}} B_c C_{i_2} \tilde{Q}_{i_{12}} + \tilde{P}_{i_{21}} B_{i_2} C_c \tilde{Q}_{i_{22}} \right) = 0 \qquad (56)$$

$$\sum_{i=1}^{r} \alpha_i \left(\tilde{P}_{i_{22}} B_c D_{i_{21}} D_{i_{21}}^T + (\tilde{P}_{i_{21}} \tilde{Q}_{i_{11}} + \tilde{P}_{i_{22}} \tilde{Q}_{i_{21}}) C_{i_1}^T \right) = 0 \qquad (57)$$

$$\sum_{i=1}^{r} \alpha_i \left(D_{i_{12}}^T D_{i_{12}} C_c \tilde{Q}_{i_{22}} + B_{i_2}^T (\tilde{P}_{i_{12}} \tilde{Q}_{i_{22}} + \tilde{P}_{i_{11}} \tilde{Q}_{i_{12}}) \right) = 0 \qquad (58)$$

where $\tilde{Q}_i$ and $\tilde{P}_i$ satisfy Equations (6) and (8) respectively, with the appropriate partitioning given by Equation (7).

Proof: Equations (57) and (58) are the necessary conditions obtained directly from differentiating the augmented cost with respect to B_c and C_c. Equation (56) for A_c is obtained in the same manner as for the approximation and estimation problems. $\square$

16

Remark 18 *Equation (56) can be solved for A_c using Kronecker algebra [16];*

$$\text{vec}\{A_c\} = \left(\sum_{i=1}^{r} \alpha_i \tilde{Q}_{i_{22}}^T \otimes \tilde{P}_{i_{22}}\right)^{-1} \times$$

$$\sum_{i=1}^{r} \alpha_i \left(\left(\tilde{Q}_{i_{12}}^T \otimes \tilde{P}_{i_{21}}\right) \text{vec}\{A_i\} + \text{vec}\left\{\tilde{P}_{i_{22}} B_c C_{i_2} \tilde{Q}_{i_{12}} + \tilde{P}_{i_{21}} B_{i_2} C_c \tilde{Q}_{i_{22}}\right\}\right) \quad (59)$$

Note that the inverse in Equation (59) exists. To see this, note that each $\tilde{P}_{i_{22}}$ and $\tilde{Q}_{i_{22}}$ are positive definite, and their Kronecker product is therefore positive definite [16]. The sum of these products is therefore nonsingular.

Remark 19 *If $D_{i_{21}} = \mu_i D_{21}$, $i = 1 \ldots r$ (which may not be an unreasonable assumption,) then Equation (57) can be written as*

$$B_c = \left(\sum_{i=1}^{r} \alpha_i \tilde{P}_{i_{22}}\right)^{-1} \left(\sum_{i=1}^{r} \alpha_i (\tilde{P}_{i_{21}} \tilde{Q}_{i_{11}} + \tilde{P}_{i_{22}} \tilde{Q}_{i_{21}}) C_{i_1}^T\right) V_2^{-1} = 0 \quad (60)$$

where

$$V_2 = \left(\sum_{i=1}^{r} \alpha_i \mu_i\right) D_{21} D_{21}^T \quad (61)$$

In general, B_c can be solved using Kronecker algebra. Similar comments apply to the calculation of C_c.

5   Conclusions

The simultaneous optimal approximation, estimation and control problems for multiple models has been investigated. In each problem, the order of the system to be found is fixed, and the necessary conditions that an optimal solution must satisfy are found. For both the approximation and estimation cases, the optimal model can be written as an optimal projection of a "full order" model with order $N = \sum_{i=1}^{r} n_i$. There is no improvement in the optimal cost that can be obtained by using a model with order larger than N. In the control case, there is no such *a priori* bound in terms of the individual model orders n_i that can be placed on the optimal compensator order.

References

[1] Ashkenazi, A., and Bryson Jr., A. E., "Control Logic for Parameter Insensitivity and Disturbance Attenuation," *AIAA J. Guidance*, Vol. 5, No. 4, July 1982, pp. 383–388.

[2] Miyazawa, Y., "Robust Flight Control System Design with Multiple Model Approach," *Proceedings, AIAA Guid., Nav. and Control Conf.*, Portland, OR, Aug. 1990, pp. 874-882.

[3] Gangsaas, D., Bruce, K. R., Blight, J. D., and Ly, U. "Application of Modern Synthesis to Aircraft Control," *IEEE Trans. Autom. Contr.*, Vol. AC–31, No. 11, Nov. 1986, pp. 995–1014.

[4] R. Saeks and J. J. Murray, "Fractional representation, algebraic geometry and the simultaneous stabilization problem," *IEEE Trans. Autom. Contr.*, Vol. AC–27, No. 4, Aug. 1982, pp. 895–903.

[5] M. Vidyasagar and N. Viswanadham, "Algebraic design echniques for reliable stabilization," *IEEE Trans. Autom. Contr.*, Vol. AC–27, No. 5, Oct. 1982, pp. 1085–1095.

[6] B. K. Ghosh and C. I. Byrnes, "Simultaneous stabilization and simultaneous pole placement by non-switching dynamic compensation," *IEEE Trans. Autom. Contr.*, Vol. AC–28, No. 6, June 1983, pp. 735–741.

[7] ____, "Simultaneous partial pole placement – a new approach to multi-mode system design," *IEEE Trans. Autom. Contr.*, Vol. AC–31, (1986), pp. 440–443.

[8] ____, "An approach to simultaneous system design, Part I: Semialgebraic Geometric Methods," *SIAM J. Contr. Optim.*, Vol. 24, No. 3, May 1986, pp. 480–496.

18

[9] ____, "Transcendental and interpolation methods in simultaneous stabilization and simultaneous partial pole placement problems," *SIAM J. Contr. Optim.* Vol. 24, No. 6, Nov. 1986, pp. 1091–1109.

[10] B. K. Ghosh, "An approach to simultaneous system design, Part II: Nonswitching gain and dynamic feedback compensation by algebraic geometric methods," *SIAM J. Contr. Optim.*, Vol. 26, No. 4, July 1988, pp. 919-963.

[11] P. M. Makila, "Multiple models, multiplicative noise and linear quadratic control-algorithm aspects," *preprint.*

[12] Hyland, D. C., and Bernstein, D. S., "The Optimal Projection Equations for Model Reduction and the Relationships Among the Methods of Wilson, Skelton, and Moore," *IEEE Trans. Auto. Contr.*, Vol. AC–30, No. 12, Dec. 1985, pp. 1201-1211.

[13] Bernstein, D. S., and Hyland, D. C., "The Optimal Projection Equations for Reduced Order State Estimation," *IEEE Trans. Auto. Contr.*, Vol. AC–30, No. 6, June 1985, pp. 583-585.

[14] Hyland, D. C., and Bernstein, D. S., "The Optimal Projection Equations for Fixed-Order Dynamic Compensation," *IEEE Trans. Auto. Contr.*, Vol. AC–29, No. 11, Nov. 1985, pp. 1034-1037.

[15] Chen, C., *Introduction to Linear System Theory*, Holt, Rinehart & Winston, 1984.

[16] Graham, A., *Kronecker Products and Matrix Calculus: with Applications*, Ellis Horwood Limited, 1981.

FORMULATION OF FULL STATE FEEDBACK FOR INFINITE ORDER STRUCTURAL SYSTEMS

Dr. David W. Miller and Dr. Marthinus C. van Schoor

Space Engineering Research Center
Massachusetts Institute of Technology
Cambridge, MA 02139

ABSTRACT

The exact Linear Quadratic Regulator solution for infinite order structures is the convolution of spatially distributed feedback kernels with spatially continuous state functions. For structures, several state functions exist that completely describe the state of the structure at any given point in time. The continuous control function is then the convolution of one of these state functions with an appropriate feedback kernel. If another state function is selected, a new feedback kernel can be derived that will yield identical closed-loop performance. The appropriate state function should be selected based upon the ease with which it can be measured.

This paper discusses the estimation of exact displacement and displacement rate feedback kernels from finite dimensional control solutions based on finite element structural models. These kernels are then transformed to equivalent curvature and curvature rate feedback kernels. These curvature kernels are augmented with single point displacement and rotation feedback to account for rigid body motions. The curvature and curvature rate state functions can be measured using a growing class of sensors known as area averaging sensors. The output of area averaging sensors equals the convolution of all structural curvature states with the spatial sensitivity function of the sensor. Transforming the discrete feedback gains into continuous feedback kernels and using area averaging sensors enables the implementation of full state feedback for infinite order structural systems.

INTRODUCTION

Rationale

Structures are infinite order systems. To obtain a mathematically exact structural model requires the use of a set of partial differential equations subjected to the appropriate boundary conditions. However, in practice it is difficult or impossible to find the exact closed-form Linear Quadratic Regulator[1] (LQR) solution for most structures. Therefore, structures are often modelled by discretization of the structure. This is even true for some very simple structures. The most common method of discretization is finite elements. When the structure is discretized, the order of the model is reduced. Instead of being modelled by an infinite order system, the structure is now modelled with a finite number of degrees-of-freedom. The result is a matrix ordinary differential equation which will approximate the temporal and spatial behavior of the structure.

Given the possibility to model a structure as an infinite order system or as a discrete finite dimensional model, it is prudent to define the terminology used in this paper. A **state function** corresponds to a motion variable which is a continuous function of both space and time. **Discrete states** or **degrees-of-freedom** correspond to point motion variables, which are functions only of time, at a finite number or locations throughout the structure (Fig. 1). The feedback of spatially discrete structural states involves feedback **gains**, whereas the feedback of a spatially continuous state function involves feedback **kernels**.

For control design, Linear Quadratic Regulator (LQR) methods exist that can be used to formulate optimal structural control solutions for these matrix ordinary differential descriptions. Given that model truncation is one of the major contributors to the control spillover problem, it is desirable to include as many degrees-of-freedom as possible in the control model. This is a costly approach, both in terms of money and in implementation since the increased

Figure 1. Graphical representation of state vector and state function description of a structure
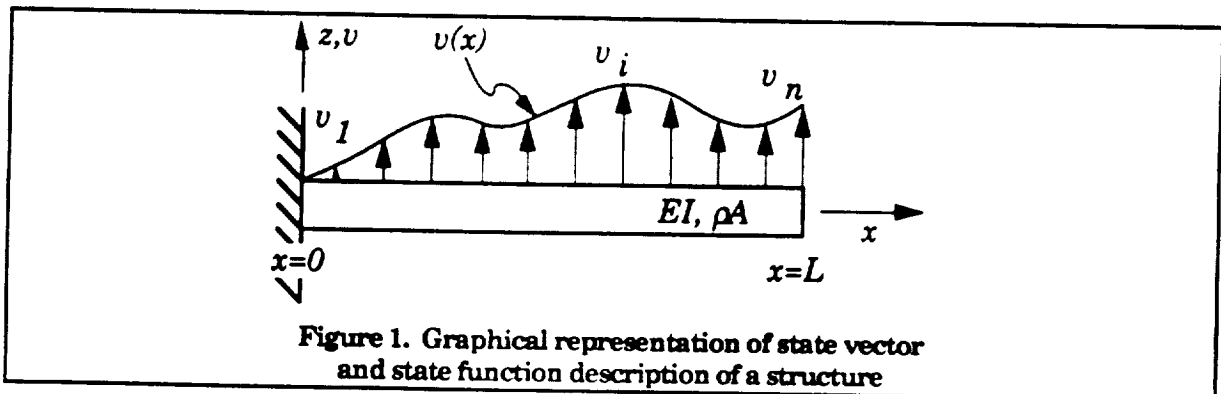
number of degrees-of-freedom requires more state sensors and the controller needs to multiply state feedback gains with the increased number of state measurements to obtain the feedback command. However, the derivation and implementation of a LQR solution, based on a infinite order model, that convolves a spatially distributed feedback kernel(s) with a spatially continuous state function(s) would completely avoid the model truncation, spatial aliasing and cost of implementation problems.

This approach contradicts two common beliefs that stems from the use of approximate, reduced order structural models. A common belief is that that the feedback architecture is typically the multiplication of gains with discrete point measurements (or estimates) of the structural motion. These measurements typically correspond to degrees-of-freedom in a finite element model. The second belief is that the type of degrees-of-freedom (displacement, rotation and their rates) used in the reduced order model are the appropriate state variables to measure.

It is also important to realize that the feedback kernels can be transformed as desired to accommodate measurements other than the states variables used in the model. Such a transformation can allow the use of not only displacement or rotation but also curvature as measurements for the infinite order controller. This paper discusses the estimation of exact feedback kernels from finite dimensional control solutions and the transformation of these kernels to accommodate the measurement of curvature. Posing the feedback in terms of curvature allows the use of a growing class of sensors known as area averaging sensors. These sensors can provide the spatially continuous measurement of the curvature required by the infinite order controller.

Implementation issues associated with these sensors are also discussed in order to demonstrate one technique for realizing the use of these feedback kernels. In this sense, the continuous kernel represents the full state feedback solution for infinite order structural systems, and the availability of at least one implementation technique makes this solution more than just a mathematical exercise.

Background

The description that is obtained of a structural system from a finite element model is a set of second order, matrix ordinary differential equations of the form

$$M\ddot{x}(t) + C\dot{x}(t) + Kx(t) = f(t) \qquad (1)$$

where M, C and K are the mass, damping and stiffness matrices, respectively. The vectors x and f contain discrete point degrees-of-freedom and force inputs, respectively. This system can be placed in first order, state-space form

$$\dot{z}(t) = Az(t) + Bu(t) \qquad (2a)$$

where

$$\begin{Bmatrix} \dot{x} \\ \ddot{x} \end{Bmatrix} = \begin{bmatrix} 0 & I \\ -M^{-1}K & -M^{-1}C \end{bmatrix} \begin{Bmatrix} x \\ \dot{x} \end{Bmatrix} = \begin{Bmatrix} 0 \\ M^{-1} \end{Bmatrix} f$$

(2b)

The Linear Quadratic Regulator minimizes a cost

$$J = \frac{1}{2} \int_0^\infty \left\{ z^T Q z + u^T R u \right\} dt$$

(3)

for this system by formulating a feedback gain matrix G such that

$$u(t) = -R^{-1} B^T P z(t) = -G z(t)$$

(4)

where P is the solution to the steady-state matrix Riccati equation

$$PA + A^T P + Q - PBR^{-1} B^T P = 0$$

(5)

The feedback form in Eq. 4 consists of multiplying the feedback gains contained in G by the state vector in z, whose entries correspond to the temporal motions of spatially discrete points throughout the structure. The resultant products are summed to arrive at the appropriate control actions which are placed in the vector u. This feedback architecture is simply an artifact of the need to use a finite dimensional (reduced order) structural model to implement the control design.

In actuality, structures do not undergo motion only at discrete points corresponding to the model's nodes but also deform continuously throughout the region between nodes (See Fig. 1). The exact motion of the structure is described by state functions which are continuously distributed along the length of the structure. Therefore, for infinite order structural systems, the mathematically exact control inputs are not the sum of products of discrete gains with discrete motions but the general form of the control is the spatial convolution of the state function with a feedback kernel.

In order to demonstrate the concept of using infinite order structural models for control, a simple structural beam can be used as an example. The partial differential equation description of a uniform beam is

$$EI \frac{\partial^4 v(x,t)}{\partial x^4} + \rho A \frac{\partial^2 v(x,t)}{\partial t^2} = f(x,t)$$

(6)

This description can be placed into state-space, spatial operator form[2]

$$\frac{\partial}{\partial t} z(x,t) = a(x) z(x,t) + b(x) u(x,t)$$

(7)

by choosing the state functions as those which determine the potential (strain) and kinetic energy in the beam (curvature and transverse velocity)

$$\left\{ \begin{array}{c} \dfrac{\partial^3 v}{\partial x^2 \partial t} \\[2mm] \dfrac{\partial^2 v}{\partial t^2} \end{array} \right\} = \left[\begin{array}{cc} 0 & \dfrac{\partial^2}{\partial x^2} \\[3mm] -\dfrac{EI}{\rho A}\dfrac{\partial^2}{\partial x^2} & 0 \end{array} \right] \left\{ \begin{array}{c} \dfrac{\partial^2 v}{\partial x^2} \\[2mm] \dfrac{\partial v}{\partial t} \end{array} \right\} + \left\{ \begin{array}{c} 0 \\[1mm] \dfrac{1}{\rho A} \end{array} \right\} f \tag{8}$$

The parameter E is the modulus of elasticity, I is the area moment of inertia, A is the cross-sectional area and ρ is the volumetric mass density.

The cost is defined by

$$J = \frac{1}{2} \int\limits_{0}^{\infty} \int\limits_{-\infty}^{\infty} (<qz,z> + <ru,u>) dx dt \tag{9}$$

where the matrices q and r are matrix operators penalizing the state and control functions, respectively. Note that q and r are not constants but are spatial operators and that the inner integral indicates that the beam is assumed to be of infinite extent. An infinite extent beam was chosen to facilitate the acquisition of a closed-form, exact solution. However, the operator form for a finite extent beam can also be posed, although the solution will probably require numerical techniques.

The feedback structure is found from the solution pz to the functional Riccati equation

$$0 = paz + a^* pz + qz - pbr^{-1}b^* pz \qquad \forall z \tag{10}$$

where the symbol "*" signifies the adjoint operator. The feedback is the spatial convolution of a kernel matrix κ with the state function z

$$u(x,t) = -r^{-1}b^* (pz)(x,t) = -\int\limits_{-\infty}^{\infty} \kappa(x-w)z(w,t)dw \tag{11}$$

where x corresponds to the location on the structure where control is applied and w indicates where states are measured. Equation 11 is the general solution because it represents the control action at any location as a function of the state functions along the entire extent of the structure. This feedback is analogous to that in Eq. 4 in the sense that it represents the continuous sum of gains times the states of the structure.

The implementation of these continuously distributed feedback kernels requires the use of a continuously distributed sensor. Several researchers have demonstrated the use of continuously distributed curvature sensors and actuators. C.K. Lee[3,4], S.E. Miller[5], S. Collins[6] and D. Miller[7] have worked on the development of area averaging sensors. These authors use spatially distributed sensors to achieve certain measurement characteristics. C.K. Lee[3,4] and S. Collins[6] used sensors shaped as particular mode shapes to obtain a measurement of the generalized coordinate of that mode. S. Collins[6] and D. Miller[7] developed sensors which roll off with frequency without exhibiting phase lag. It will be shown in this paper that area averaging sensors can be used to implement the feedback solution to a partial differential equation description of a finite extent structure.

Approach

An over optimistic goal for this research would have been to attempt to solve the infinite dimensional structural control problem. This goal is not realistic because first it would require the exact partial differential equations (PDE) and boundary conditions (BC's) that describe the dynamics of the structure and second it would be impossible in most cases to find the LQR solution even if an exact model existed. de Luis[2], for example used an infinite extent beam in solving the infinite dimensional control problem in order to find a closed-form, exact control solution. The same infinite dimensional control problem can also be posed for a finite extent beam[8]. However, this problem is much more difficult to solve due to the existence of boundary conditions.

A more realistic approach is to model the structures with the more familiar finite reduced order models (Eqs. 2 through 5) and to hope that by increasing the fidelity (number of degrees-of-freedom) of the model, the continuous feedback kernel can be inferred from the distribution of the discrete gains.

The following section discusses the derivation and implementation of continuously distributed feedback kernels. Several important steps are involved in this derivation. First, spatially discrete displacement and rotation gains derived using standard matrix Riccati techniques on finite element structural models must be converted into spatially continuous feedback kernels. Second, these kernels must be transformed into feedback of distributed curvature to facilitate implementation using area averaging sensors. An alternative approach, also discussed in the next section, is to first convert discrete displacement and rotation gains into discrete curvature gains and then to convert these gains into a spatially continuous curvature feedback kernel. Numerical examples are interspersed with these formulations to demonstrate these techniques. After the section on feedback kernel formulation, a discussion of general control issues of interest is presented along with an additional numerical examples.

Reference Example

Throughout the rest of this paper, these techniques are formulated for the cantilevered beam of length L shown in Figure 2. A control moment is applied to a point on the beam $1/10^{th}$ of the distance from the clamped root to the free tip. This moment actuator is used to represent an equivalent piezoelectric actuator at the cantilevered end. de Luis *et al*[2] demonstrate that one valid way of modelling the influence of a piezoelectric curvature actuator is to derive equivalent moments at the two ends of the actuator, which are of equal magnitude but of opposite sign. In this problem, if it is assumed that the piezoelectric actuator runs from the root, the companion moment at the clamped end of the beam does not enter the problem and is therefore not shown. The pertinent parameters of the problem are listed in Table 1. The performance metric is the transverse displacement of the tip of the beam (v_{tip}). The entry in the state penalty matrix (Q) corresponding to this displacement is

6

assumed to be unity. This state penalty in equation form, from Eq. 3, is

$$z^T Q z = v_{tip}^2 \qquad\qquad (12)$$

Figure 2. Cantilevered, Bernoulli-Euler beam.
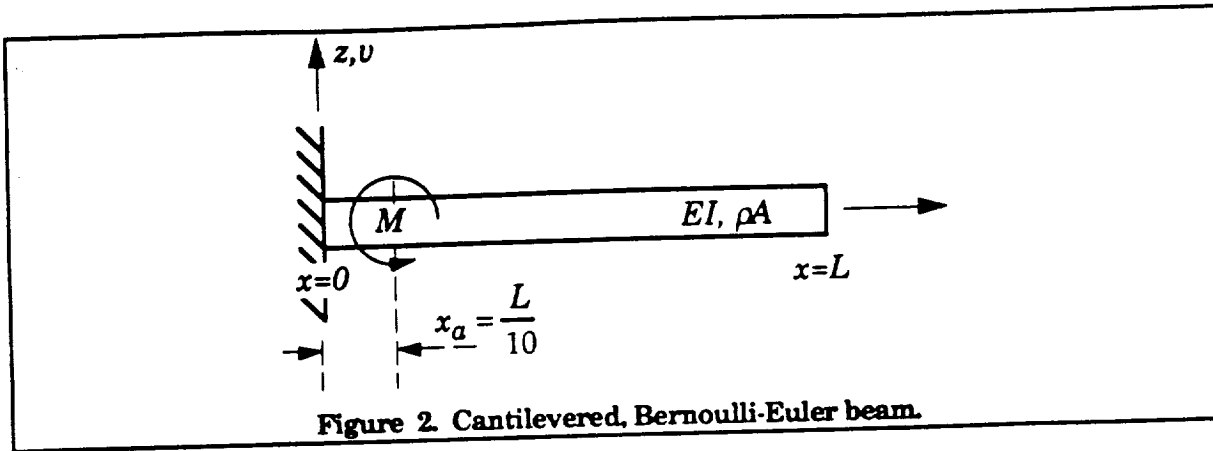
FEEDBACK KERNEL FORMULATION

This formulation process is shown in Figure 3. The upper left box represents the formulation of discrete displacement and rotation gains using classical finite element models. The objective is to evaluate the continuous curvature kernel represented by the bottom, right box. Two paths (1 and 2) can be followed to obtain the curvature kernel from the displacement and rotation gains. Following either path involves the same three steps but in different order. In either case, the first step is to evaluate the discrete displacement and rotation gains. For brevity, reference to displacement, rotation and curvature rate gains and kernels are omitted from the discussion although they are an integral part of any control design. However the evaluation of these rate gains and kernels are identical to the processes shown for the displacement, rotation and curvature gains and kernels.

Following path one, the second step involves calculating the continuous displacement kernel from the discrete displacement and rotation gains (Path 1a in Fig.3). This displacement kernel completely describes the feedback. The evaluation of a rotation kernel is redundant since it would simply be derived using the same gains that were used in deriving the displacement kernel. The third step (1b) involves transforming the displacement kernel into a curvature kernel which convolves with distributed curvature to generate the control action. This path is discussed in detail in the rest of this section.

Table 1. Parameters for cantilevered beam example.

Bending stiffness	EI	1.0 Nm^2
Mass per unit length	ρA	1.0 kg/m
Length	L	1.0 m
Actuator location	x_a	0.1 m
Control effort penalty	R	0.001

7

Figure 3. Matrix of feedback options.
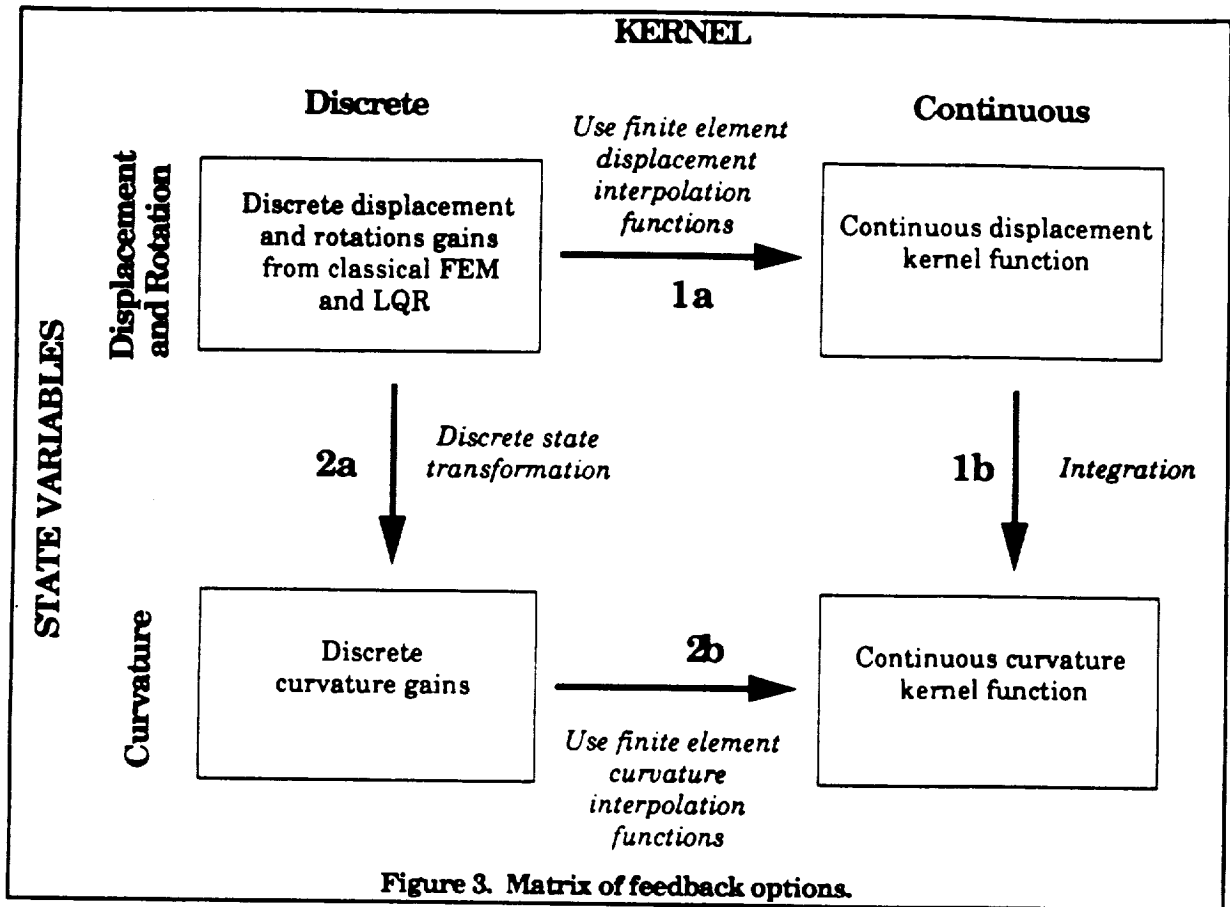
Following path two, the second step involves transforming the discrete displacement and rotation gains into discrete curvature gains (**2a**). The third step then involves using these gains to find the continuous curvature kernel (**2b**). This path is used, in the following discussion, as a check of the first path since both paths should yield approximately the same curvature kernel.

Evaluation of the Discrete Displacement and Rotation Gains

The first step in evaluating the discrete displacement and rotation gains is to develop a finite element model of the cantilevered beam. The mass and stiffness finite elements that are used in the following analysis are

$$
m_{ele} = \frac{\rho A l}{420} \begin{bmatrix} 156 & 22l & 54 & -13l \\ 22l & 4l^2 & 13l & -3l^2 \\ 54 & 13l & 156 & -22l \\ -13l & -3l^2 & -22l & 4l^2 \end{bmatrix} \quad k_{ele} = \frac{EI}{l^3} \begin{bmatrix} 12 & 6l & -12 & 6l \\ 6l & 4l^2 & -6l & 2l^2 \\ -12 & -6l & 12 & -6l \\ 6l & 2l^2 & -6l & 4l^2 \end{bmatrix}_{(13)}
$$

8

with the corresponding finite element nodal degrees-of-freedom

$$v_{ele}^T = \begin{bmatrix} v_i & \dot{v}_i & v_{i+1} & \dot{v}_{i+1} \end{bmatrix}$$ (14)

where l is the element length and is equal to the total length of the beam (L) divided by the number of elements. The other parameters are listed in Table 1. It is assumed that the model is undamped. The entry in the state penalty matrix Q corresponding to this displacement is set equal to one.

Using a ten element model of the beam, the gains obtained from the LQR solver are shown in Figure 4. The gains in the upper left window are the displacement gains at discrete locations along the structure. The lower left window shows the rotation gains. Notice that no discernable spatial distribution can be seen in these gains. The windows in the upper and lower right display the displacement rate and rotation rate gains, respectively.

(a)

(b)

(c)

(d)

Figure 4. Discrete gains at nodal positions along the structure for controlling tip displacement. The individual windows show gains for (a) displacement, (b) displacement rate, (c) rotation and (d) rotation rate.

9
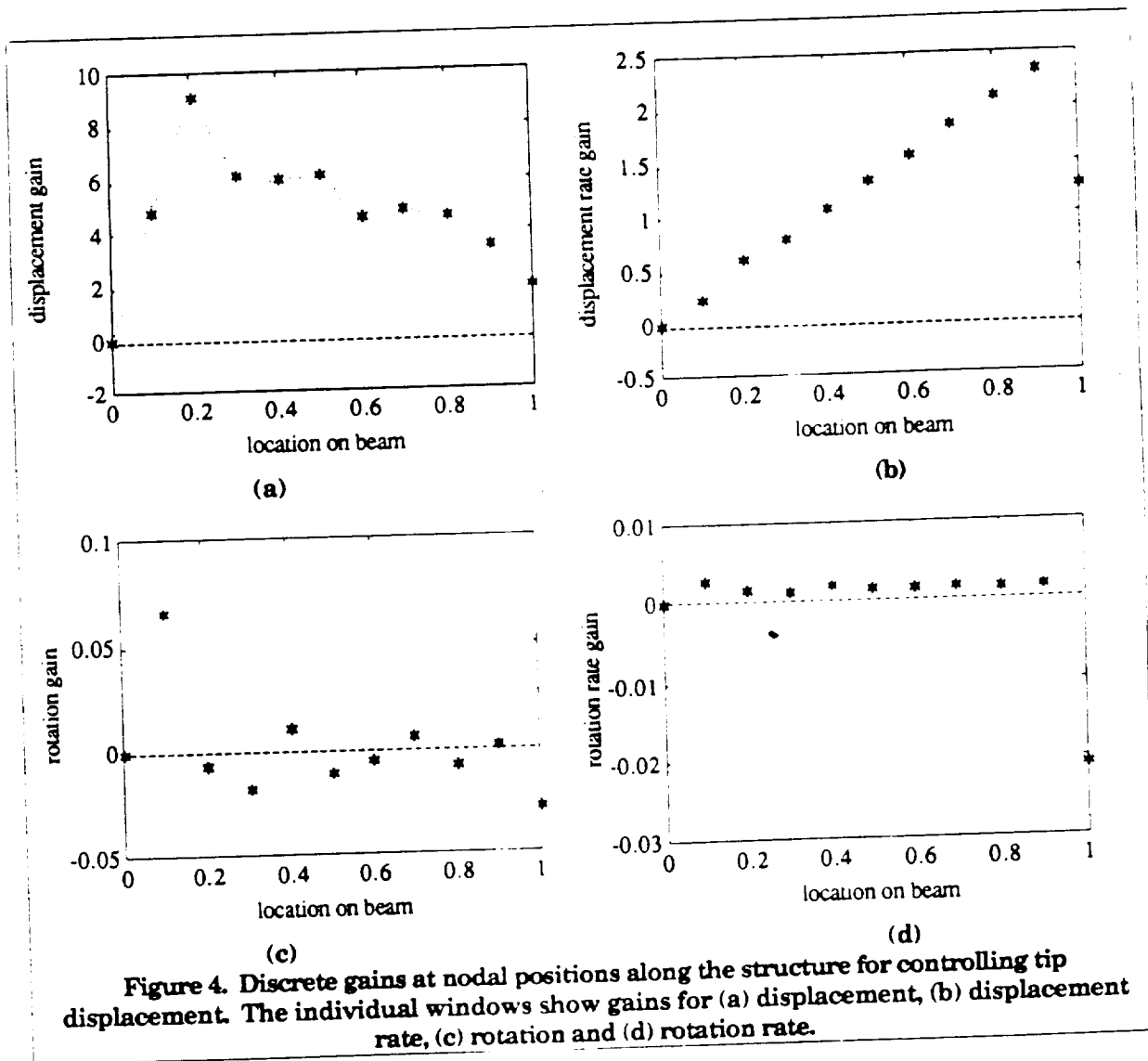
These displacement and displacement rate gain distributions indicate the shape that the respective continuous kernels will have, but not the magnitudes. This is only an approximate indication of the continuous shapes since the displacement kernel combines the information from both the discrete displacement and rotation gains. In other words, a single kernel contains all of the gain information displayed in a single column of Figure 4.

Evaluation of the Spatially Continuous Feedback Kernel

The next objective in the analysis is to find the spatially continuous feedback kernel from the spatially discrete gains evaluated in the previous section (Path 1a in Fig. 3). To this end, the beam finite element displacement and rotation gains will be used to derive the continuous displacement feedback kernel which convolves with the displacement state function. Since the reference example has a point actuator, the feedback convolution in Eq. 11 degenerates to the integral of a kernel times the state function. It is also convenient to use a kernel that is defined over the length of the beam, rather than having the kernel be defined, as in Eq. 11, in terms of the actuator location (x_a). Using this kernel transformation, the feedback is given by

$$u(t) = -\int_o^L \kappa(w)z(w,t)dw = -\int_0^L [\kappa_C \quad \kappa_{DR}](w) \left\{ \begin{array}{c} \dfrac{\partial^2 v}{\partial w^2} \\ \dfrac{\partial v}{\partial t} \end{array} \right\}(w,t)dw$$

$$= -\int_o^L \kappa_C(w)\frac{\partial^2 v}{\partial w^2}(w,t)dw - \int_o^L \kappa_{DR}(w)\frac{\partial v}{\partial t}(w,t)dw$$

$$= -\int_o^L \kappa_D(w)v(w,t)dw - \int_o^L \kappa_{DR}(w)\frac{\partial v}{\partial t}(w,t)dw$$

$$= u_D(t) + u_{DR}(t) \tag{15}$$

Note that the state functions shown in Eq. 8 include the curvature of the beam. Eq. 15 shows part of the feedback to be the integral of curvature times a curvature kernel. Alternatively, this can equivalently be expressed as the integral of the displacement state functions times a displacement kernel. This displacement kernel is derived in the next paragraph.

The integration over the entire length of the beam can be divided into the sum of integrals over segments of the structure corresponding to the finite element domains as shown in Fig. 5.

Figure 5. Graphical representation of integration of kernel with state function
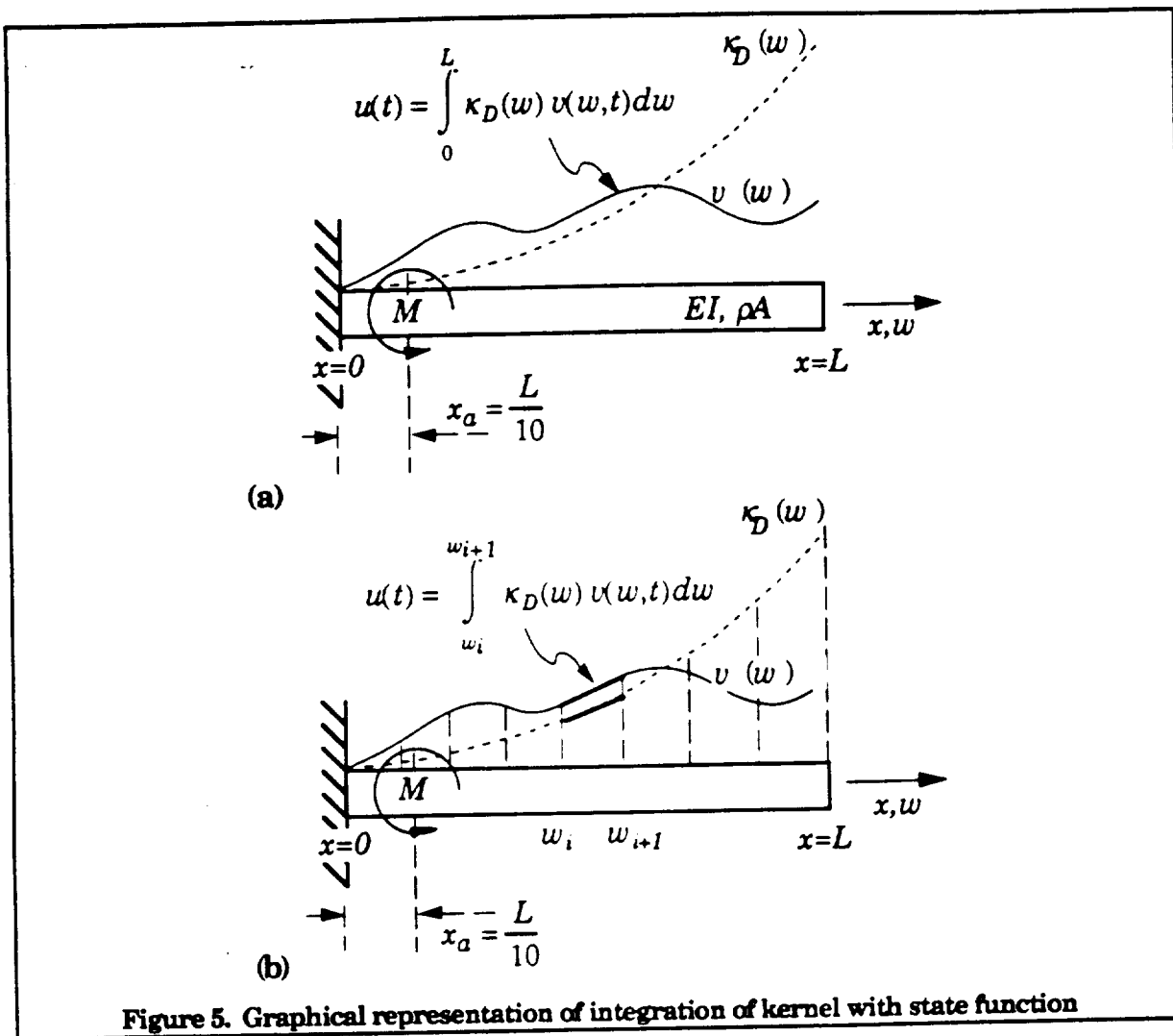
The first half of Eq. 15 then becomes

$$u_D(t) = -\int_0^L \kappa_D(w)v(w,t)dw$$

$$=\ldots- \int_{w_i}^{w_{i+1}} \kappa_D(w)v(w,t)dw - \int_{w_{i+1}}^{w_{i+2}} \kappa_D(w)v(w,t)dw-\ldots$$

$$=\ldots u_{D_i} + u_{D_{i+1}} +\ldots \tag{16}$$

The element interpolation function description of the displacement anywhere within the element located between w_i and w_{i+1}

$$v(\xi,t) = \left(1 - 3\frac{\xi^2}{l^2} + 2\frac{\xi^3}{l^3}\right)v_i(t) + \left(\frac{\xi}{l} - 2\frac{\xi^2}{l^2} + \frac{\xi^3}{l^3}\right)lv_i'(t)$$

$$+ \left(3\frac{\xi^2}{l^2} - 2\frac{\xi^3}{l^3}\right)v_{i+1}(t) - \left(\frac{\xi^2}{l^2} - \frac{\xi^3}{l^3}\right)lv_{i+1}'(t) \qquad for \quad 0 \le \xi \le l \tag{17}$$

11

can be substituted into each of these element convolutions. Then, the control action associated with an element is a function of that element's nodal degrees-of-freedom

$$
u_{D_i}(t) = - \int_{w_i}^{w_{i+1}} \kappa_D(w) \left\{ \left(1 - 3\frac{\xi^2}{l^2} + 2\frac{\xi^3}{l^3} \right) v_i(t) + \left(\frac{\xi}{l} - 2\frac{\xi^2}{l^2} + \frac{\xi^3}{l^3} \right) l\dot{v}_i(t) + \right.
$$

$$
\left. \left(3\frac{\xi^2}{l^2} - 2\frac{\xi^3}{l^2} \right) v_{i+1}(t) - \left(\frac{\xi^2}{l^2} - \frac{\xi^3}{l^2} \right) l\dot{v}_{i+1}(t) \right\} dw \quad \text{where} \;\; \xi = w - w_i
$$

(18)

If the form for κ_D were known, then the integral in Eq. 18 could be evaluated to find the the gains for the nodal degrees-of-freedom. Conversely, in this case these gains are known from the solution to the matrix Riccati equation and instead it is the form of the kernel κ_D that is being sought. To estimate this kernel, a form for the kernel, containing unknown parameters, can be selected so that the spatial integral in Eq. 18 can be evaluated. Then, these parameters can be found by equating the elements of this integration to the discrete gains. A cubic form for the kernel is chosen

$$
\kappa_{D_i}(w) = a_i(w - w_i)^3 + b_i(w - w_i)^2 + c_i(w - w_i) + d_i \quad \text{for} \; w_i \le w \le w_{i+1}
$$

(19)

Given the polynomial order (cubic) assumed for the four degree-of-freedom finite element, a cubic polynomial for the internal curvature distribution is the highest order polynomial for which the unknown coefficients can be uniquely found.

If the form in Eq. 19 is inserted into Eq. 18, and the integral is evaluated, the result will be the contribution that the continuous kernel across that element makes to the gains associated with that element's nodal degrees-of-freedom. In other words, at one of the element's nodes, Eq. 18 yields partial gains for the nodal degrees-of-freedom which, if summed with the gain contributions from the adjacent element, will give the total gains associated with that node's degrees-of-freedom. Thus, the gain contributions from the elements neighboring a shared node can be used to find the total displacement and rotation gains associated with that shared node

$$
g_{v_i} = \int_0^l \left(a_i\xi^3 + b_i\xi^2 + c_i\xi + d_i \right) \left(3\frac{\xi^2}{l^2} - 2\frac{\xi^3}{l^2} \right) d\xi +
$$

$$
\int_0^l \left(a_{i+1}\xi^3 + b_{i+1}\xi^2 + c_{i+1}\xi + d_{i+1} \right) \left(1 - 3\frac{\xi^2}{l^2} + 2\frac{\xi^3}{l^3} \right) d\xi
$$

(20a)

$$g_{v_i'} = \int\limits_o^l \left(a_i\xi^3 + b_i\xi^2 + c_i\xi + d_i\right)\left(-\frac{\xi^2}{l^2} + \frac{\xi^3}{l^2}\right)l\,d\xi +$$

$$\int\limits_o^l \left(a_{i+1}\xi^3 + b_{i+1}\xi^2 + c_{i+1}\xi + d_{i+1}\right)\left(\frac{\xi}{l} - 2\frac{\xi^2}{l^2} + \frac{\xi^3}{l^3}\right)l\,d\xi \qquad (20b)$$

where g_{v_i} and $g_{v_i'}$ are that node's displacement and rotation gains, respectively, as shown in Fig. 4.

These two relations give two conditions for finding for the elemental kernel coefficients a_i, b_i, c_i and d_i. Two more conditions are required in order to ensure a unique solution. These two additional conditions are found by requiring continuity of the kernel magnitude and slope at a shared node. These are found by using Eq. 19 to evaluate the magnitude and slope at the right end of the ith kernel and equating that to the magnitude and slope of the $(i+1)$th kernel at its left end yielding

$$a_i l^3 + 2b_i l^2 + c_i l + d_i - d_{i+1} = 0 \qquad (21)$$

$$3a_i l^2 + 2b_i l + c_i - c_{i+1} = 0 \qquad (22)$$

These four conditions can be expressed in matrix form as

$$\begin{bmatrix} \dfrac{3l^4}{14} & \dfrac{4l^3}{15} & \dfrac{7l^2}{20} & \dfrac{l}{2} & \dfrac{l^4}{28} & \dfrac{l^3}{15} & \dfrac{3l^2}{20} & \dfrac{l}{2} \\[2mm] -\dfrac{l^5}{42} & -\dfrac{l^4}{30} & -\dfrac{l^3}{20} & -\dfrac{l^2}{12} & \dfrac{l^5}{105} & \dfrac{l^4}{60} & \dfrac{l^3}{30} & \dfrac{l^2}{12} \\[2mm] l^3 & l^2 & l & 1 & 0 & 0 & 0 & -1 \\[1mm] 3l^2 & 2l & 1 & 0 & 0 & 0 & -1 & 0 \end{bmatrix} \begin{Bmatrix} a_i \\ b_i \\ c_i \\ d_i \\ a_{i+1} \\ b_{i+1} \\ c_{i+1} \\ d_{i+1} \end{Bmatrix} = \begin{Bmatrix} g_v \\ g_{v'} \\ 0 \\ 0 \end{Bmatrix} \qquad (23)$$

where the first two rows are found by evaluating the integrals in Eqs. 20a and 20b. A global matrix can be assembled, using Eq. 23 as the sub-matrices, to yield a linear equation relating the coefficients of the cubic-fitted kernel functions to the discrete gains

$$Tc = g \qquad (24)$$

The desired coefficients are then given by

$$c = T^{-1}g \tag{25}$$

The approximate shape of the spatially continuous displacement feedback kernel can be calculated by evaluating this piecewise cubic kernel along the length of the structure. This evaluation is made by using the coefficients in c which are appropriate for the given segment of the structure within which the kernel is being evaluated.

Using the discrete gains of the ten element finite element model (shown in Fig. 4) to evaluate the coefficients in Eq. 19 of the piecewise cubic displacement and displacement rate kernels, the functions in Figure 6 are found. These functions are the piecewise cubic kernels combined into a single curve.

Notice the erratic shape of the displacement kernel. This erratic shape may correspond to some weighted sum of mode shapes. Given that the tip displacement (performance metric) can be represented as a sum of displacement mode shapes, and that the applied moment (control input) can be represented by the sum of curvature mode shapes, the shapes in Figure 6 could correspond to some combination of the displacement and/or curvature mode shapes. In other words, these shapes may correspond to some type of mode shape 'feedthrough' from the control input to the performance metric.
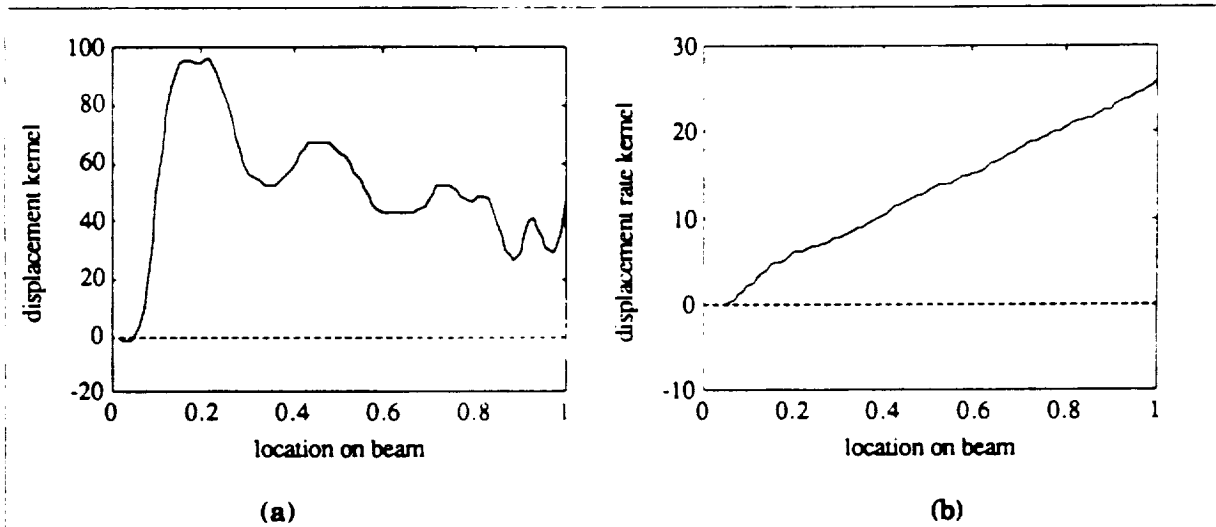
Figure 6. Spatially continuous feedback kernels as a function of location along the beam for controlling tip displacement. The individual windows show the kernels for (a) displacement and (b) displacement rate.

14

Equivalent Feedback Using Alternative State Functions

The feedback architecture using the kernel derived in the previous section has the form in Eq. 16. This involves the spatial integral of the kernel times the displacement state function. However, the continuously distributed displacement state function may not be a measurable quantity. Therefore, it may be convenient to express the same control in terms of another, more measurable state function.

Extensive work in the area of area averaging sensors[4,5,6,7,8] has shown that continuously distributed measurements of curvature-induced strain can be made using polyvinylidene flouride (PVDF). Therefore, the displacement feedback kernel of Eq. 16 must be transformed into equivalent feedback of the curvature state function.

Integration by parts can be used to transform the feedback form in Eq. 16 into equivalent feedback of the curvature state function plus point measurements of rotation and displacement, in order to retain rigid body control. This transformation is given by

$$
u_D(t) = \int_0^L \kappa_D(w) v(w,t) dw
$$

$$
= v(0,t) \int_0^L \kappa_D(w) dw + \frac{\partial v(L,t)}{\partial x} \int_0^L \int_w^L \kappa_D(\gamma) d\gamma dw -
$$

$$
\int_0^L \int_0^w \int_\gamma^L \kappa_D(\tau) d\tau d\gamma \frac{\partial^2 v(w)}{\partial w^2} dw
$$

(26)

While the point measurements of displacement and rotation must be made in order to retain rigid body measurement, the actual location on the structure where these measurements are made is arbitrary. The displacement or rotation of a point on the structure can be related to the displacement or rotation of any other point by integrating the intervening strain appropriately. For example,

$$
\frac{\partial v(L,t)}{\partial x} = \frac{\partial v(0,t)}{\partial x} + \int_0^L \frac{\partial^2 v(w,t)}{\partial w^2} dw
$$

(27)

15

Substituting this translation of the rotation measurement into Eq. 26 gives the equivalent feedback as

$$u_D(t) = v(0,t) \int_0^L \kappa_D(w)dw + \frac{\partial v(0,t)}{\partial x} \int_0^L \int_w^L \kappa_D(\gamma)d\gamma dw +$$

$$\int_0^L \int_w^L \int_\gamma^L \kappa_D(\tau)d\tau d\gamma \frac{\partial^2 v(w,t)}{\partial w^2} dw \qquad (28)$$

Notice that in this equation, the first two terms, representing the feedback gains associated with point displacement and rotation measurements, can be evaluated directly from the displacement feedback kernel. The outer integral in the third term corresponds to the integration of the distributed curvature kernel with the curvature state function. The inner two integrals evaluate the curvature kernel from the displacement kernel. This curvature kernel is given by

$$\kappa_C(w) = \int_w^L \int_\gamma^L \kappa_D(\tau)d\tau d\gamma \qquad (29)$$

The boundary conditions in the reference example were conveniently chosen to exclude rigid body motion thereby eliminating the need for any point displacement or rotation measurements. The motion of the structure is completely describable by the curvature state function because

$$v(0,t) = \frac{\partial v(0,t)}{\partial x} = 0 \qquad (30)$$

Substituting Eq. 30 into Eq. 28 yields

$$u_D(t) = \int_0^L \int_w^L \int_\gamma^L \kappa_D(\tau)d\tau d\gamma \frac{\partial^2 v(w,t)}{\partial w^2} dw \qquad (31)$$

as the feedback law in terms of the displacement kernel. To calculate the shape of the continuous curvature kernel, Eq. 29 is employed. Equation 31 can also be used to evaluate the curvature rate kernel if the displacement rate kernel (κ_{DR}) is used in place of the displacement kernel (κ_D).

Figure 7 depicts the resulting curvature and curvature rate kernels for the ten node finite element model (Figure 4 and 6). Notice that, unlike the displacement kernel, the curvature kernel is smoother. This is predominantly due to the smoothing process inherent in the double integration of Eq. 31. Also notice that the magnitude of the kernels in Fig. 7 are largest where the cantilevered beam tends to exhibit the largest curvature: the root. In Fig. 6, the magnitude of the displacement kernel is not the largest where the beam tends to exhibit maximum displacement; namely the tip.
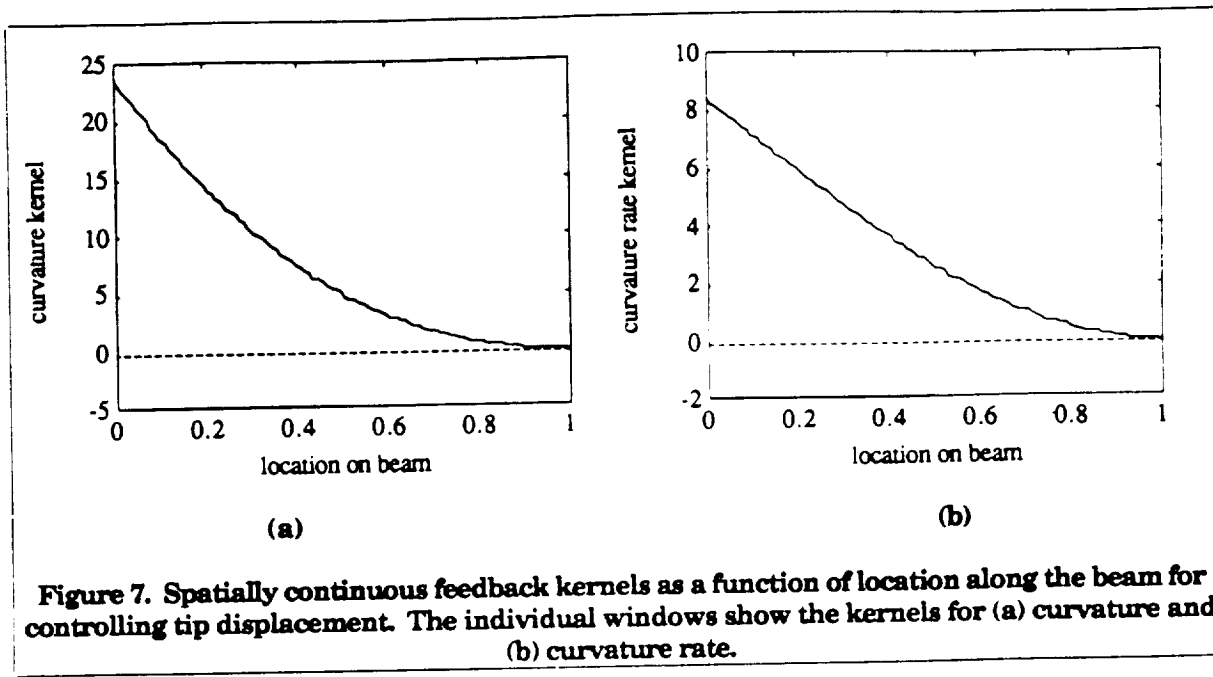
Figure 7. Spatially continuous feedback kernels as a function of location along the beam for controlling tip displacement. The individual windows show the kernels for (a) curvature and (b) curvature rate.

Although not shown, for this reference example, increasing control authority by decreasing the control effort penalty (R) does not change the kernel shapes. Instead, it changes the absolute and relative magnitudes of the kernels. A change in the shape of the kernel will be achieved by a change in the spatial nature of the problem such as moving the actuator or selecting a different performance metric. This observation is supported by an additional example presented later in the paper. Actual implementation of these sensors is the topic of a follow-on paper.

The results in Fig. 7 correspond to the objective represented by the lower, right box in Figure 3. The next step would be to implement these two kernel shapes using area averaging sensors. The details of this process will be discussed in the section on implementation issues. Prior to that, the next section discusses the alternate path in Fig. 3; namely path number **2**.

Equivalent Feedback Gains using Curvature States

An alternative procedure to evaluating the continuous curvature kernel is to first derive the discrete curvature gains from the discrete displacement and rotation gains, as shown by path **2a** in Fig. 3. This can be done in two ways. The first involves using the transformation matrix given by de Luis et al[2]

$$\left\{\begin{array}{c} v_i^{''} \\ v_{i+1}^{''} \end{array}\right\} = \left[\begin{array}{cccc} -\dfrac{6}{l^2} & -\dfrac{4}{l} & \dfrac{6}{l^2} & -\dfrac{2}{l} \\ \dfrac{6}{l^2} & \dfrac{2}{l} & -\dfrac{6}{l^2} & \dfrac{4}{l} \end{array}\right] \left\{\begin{array}{c} v_i \\ v_i^{'} \\ v_{i+1} \\ v_{i+1}^{'} \end{array}\right\} \tag{32}$$

This elemental sub-matrix can be assembled into a global state transformation matrix. The number of degrees-of-freedom are not reduced by this transformation because now there exist two independent curvatures at each node. Remember, curvature is not constrained to be continuous in the beam finite element formulation because applied point moments can induce discontinuous curvature. Originally, displacement and rotation were the two nodal DOFs. Now, a node has two curvatures, one associated with the left and one with the right-hand element.

The 'o' symbols in Figure 8 indicate the net curvature gains at each node as derived using this transformation. The net curvature gain at a particular node is found by summing the individual curvature gains at that node. This procedure is justified at nodes where external moments are not applied because the two curvature gains correspond to the feedback of curvature measurements acquired an infinitesimal distance to either side of the node. Without an externally applied moment, it can be assumed that these curvature measurements are identical and therefore the net gain is the sum of the two gains.

The second approach to deriving discrete curvature gains is to integrate the displacement and rotation gain vectors to get the curvature vector. Unlike Eq. 29, this integration process involves both the displacement and rotation gains. This integral can be approximately evaluated element by element by summing the products of the gains with the element width. Other standard numerical integration techniques can also be used.

The '*' symbols in Fig. 8 represent the curvature and curvature rate gains found using this integration approach.
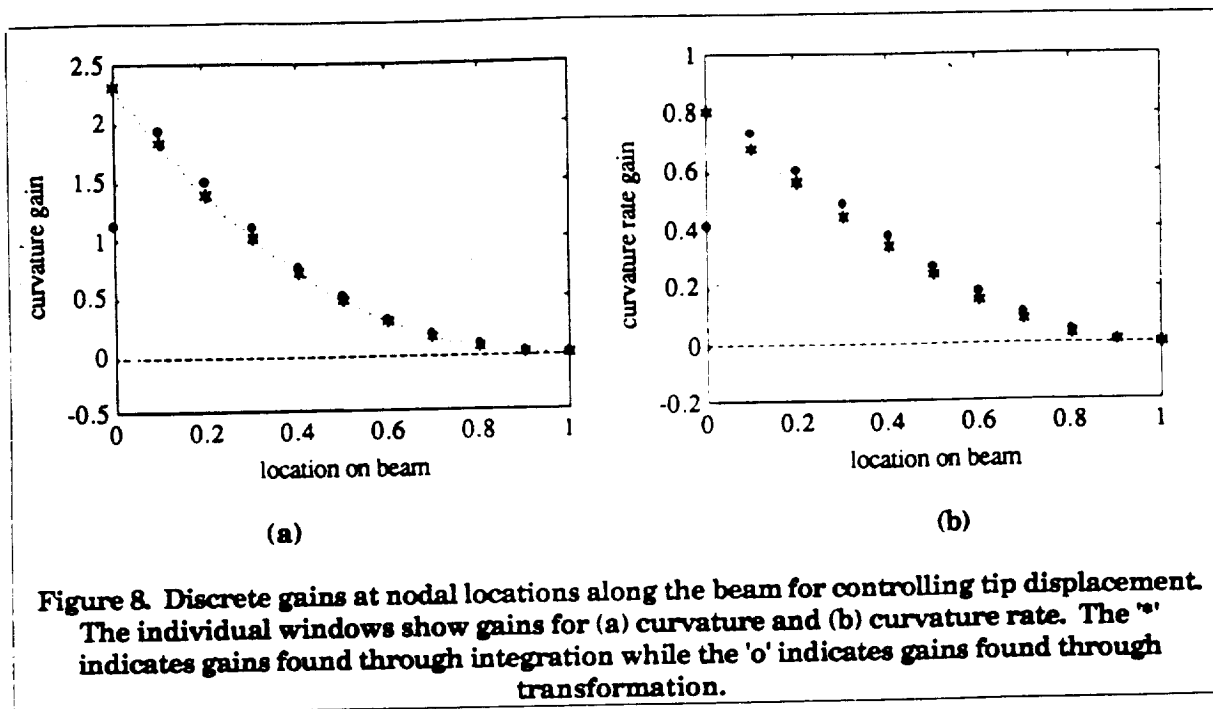
Figure 8. Discrete gains at nodal locations along the beam for controlling tip displacement. The individual windows show gains for (a) curvature and (b) curvature rate. The '*' indicates gains found through integration while the 'o' indicates gains found through transformation.

Notice the good agreement between the curvature and curvature rate gains found using the transformation and integration techniques. The agreement may seem to improve near the tip of the beam but when calculated it was found that the relative error is more less constant along the beam.

The final step in Figure 3 (**2b**) involves calculating the curvature and curvature rate kernels from the discrete curvature and curvature rate gains. Rather than using the technique in Eqs. 15 through 25, it can be observed that each of the discrete gains at a node roughly represents the area under the continuous kernel for the region between the midpoints of that node's neighboring elements Therefore, if the gain is divided by the length of an element, the result should be approximately equal to the magnitude of the kernel at the nodal location.

Figure 9, when compared with Fig. 7, shows that this is the case. Furthermore, Fig. 9 shows the overlay of the gains divided by respective element lengths for different fidelity models. This reveals that the magnitude of the kernel is captured quite well at nodal locations for rather coarse models for this simple reference example. This is an important result since in practice it would be generally impossible to find the exact feedback kernel from a continuous model. However, Fig. 9 illustrates that as the order of the model is increased the kernel shape is asymptotically approaching some shape. It is this shape that represents the infinite order solution and that must be implemented.
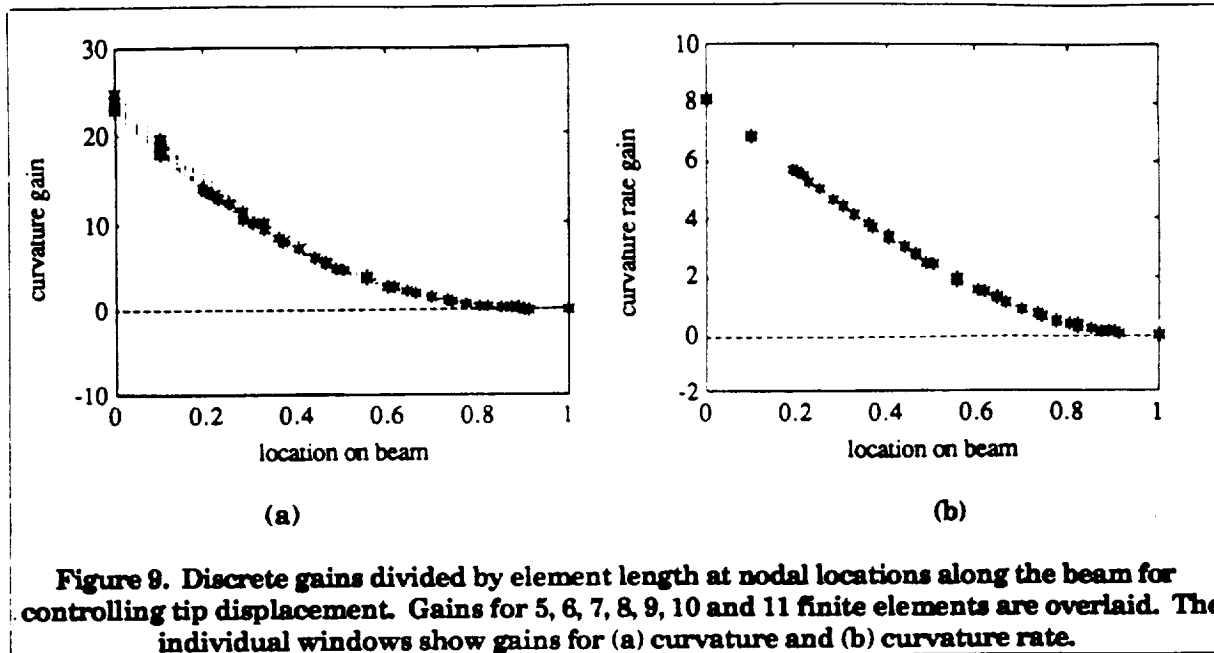
Figure 9. Discrete gains divided by element length at nodal locations along the beam for controlling tip displacement. Gains for 5, 6, 7, 8, 9, 10 and 11 finite elements are overlaid. The individual windows show gains for (a) curvature and (b) curvature rate.

Implementation Issues

The possibility of implementing infinite order structural controllers is made possible by the existence of area averaging sensors such as those described in References 4,5,7 and 8. Once the curvature kernel is obtained, it is a simple calculation to alter the kernel for equivalent feedback of curvature-induced surface strain. This simply requires knowledge of the distance of the surface mounted sensor from the centroidal axis in the structure. Once this kernel is found, the sensor can be built.

Polyvinylidene flouride (PVDF)[9] is suggested for this sensor for several reasons. First, PVDF is a strain sensitive material which can be continuously distributed along the surface of a structure and whose accumulated charge on a surface electrode equals the integral over the length of the PVDF of the electrode width times the surface strain in the structure. Second, PVDF has an elasticity which is relatively small when compared to the elasticity of conventional structural materials. This allows the sensor to be rather non-intrusive into the dynamics of the structure. Third, the shape of the electrode can be easily altered to equal that of the kernel while leaving the actual PVDF material uniformly distributed. This achieves the strain sensitivity appropriate for implementing the kernel while keeping the small dynamic influence that the PVDF does exert on the structure uniformly distributed. In addition, removal of electrode from near the edge of the PVDF greatly reduces the possibility of the sensor shorting its bottom and top surface electrodes. A fourth and final reason for using PVDF is its high strain sensitivity which provides an excellent signal to noise ratio for control purposes.

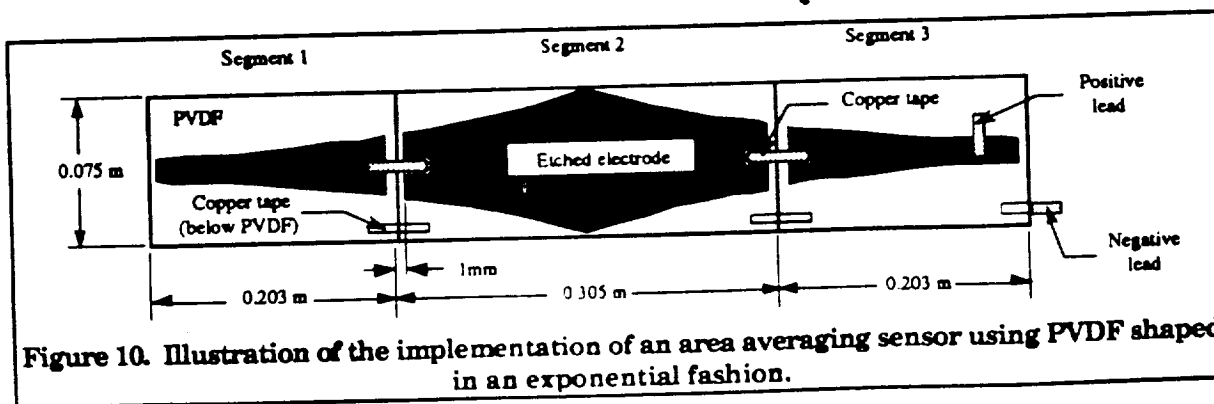One drawback of implementing the feedback kernel through the shaping of the

electrode is that once the electrode is shaped and the material is mounted on the structure, the kernel is effectively fixed and cannot be altered. Feedback gains which reside in a computer can be readily altered if alteration is required. However, C. K. Lee in Reference 4 has developed a method which could be used to circumvent this inflexibility in the gains. He uses an area averaging sensor whose electrode is segmented into numerous squares and the voltages on these squares are summed as appropriate for a particular gain distribution. If the gain distribution needs to be altered, the manner in which these voltages are summed can be changed.

Throughout the discussion of full state feedback for infinite order systems, there was an implicit assumption that high frequency dynamics in the structure consisted solely of additional modes which would be properly modelled given the use of a sufficient number of finite elements. However, this is seldom, if ever, the case in actual structures. Often, torsion or out-of-plane bending modes exist irrespective of whether only in-plane bending was modelled. These dynamics may feed through to the output of the sensor. Therefore, the spatial wavenumber filtering concepts presented in Reference 8 could be used to roll off, without phase lag, the frequency response of the spatially continuous sensor.

Figure 10 illustrates the way in which a PVDF area averaging sensor was implemented in Reference 8. The electrode is shaped as a decreasing exponential in two directions. Note that the sensor may have to be segmented if the PVDF sheet is not as long as the kernel. Given that PVDF is a polarized material, a negative part of the kernel can be implemented by either flipping that segment of the PVDF or reversing leads (see Reference 8).

For the reference example discussed thus far, two PVDF electrodes could be shaped: one each as shown in Figs. 7a and 7b. Bonding these two sensors to either side of the cantilevered beam, one sensor for the curvature kernel and one for the curvature rate kernel, the two sensor voltages can be summed appropriately and used to drive the control moment.

The unique feature of this technique is that the processes of multiplying the gains times the curvature measurements and accumulating these products is performed by the sensor. This feature significantly reduces the control implementation effort associated with numerous point sensors.

Figure 10. Illustration of the implementation of an area averaging sensor using PVDF shaped in an exponential fashion.

Issues associated with controllers based on classical beam finite elements

The previous section has shown how PVDF sensors can be used to implement infinite order controllers. It was also shown in Figure 9, that finite elements models can be used to predict the shape of the infinite order feedback kernel. The hope is that by progressively increasing the order (accuracy or fidelity) of the finite element model, the shape of the feedback kernel will approach some asymptotic shape. It is this shape that represents the infinite order feedback kernel and that must be implemented with PVDF.

Classical finite elements are the obvious elements to be used in such a model refinement process. This study has identified two implementation problems that are uniquely associated with these classical beam finite elements. The first is that the stiffness matrix obtained with these classical beam elements becomes ill-conditioned as the element size decreases. Decreasing the element size is typically associated with increasing model fidelity. This is illustrated by looking at the conditioning number of the stiffness matrix of a cantilevered beam obtained by using the following classical beam finite element:

$$k_{ele} = \frac{EI}{l^3} \begin{bmatrix} 12 & 6l & -12 & 6l \\ 6l & 4l^2 & -6l & 2l^2 \\ -12 & -6l & 12 & -6l \\ 6l & 2l^2 & -6l & 4l^2 \end{bmatrix}$$

(33)

The conditioning number for a matrix is the ratio obtained by dividing the largest eigenvalue by the smallest eigenvalue of the matrix. The higher the conditioning number of a matrix, the more ill-conditioned the matrix is and the more likely that matrix will be susceptible to computer round-off errors. It can be shown[10] that the conditioning number is proportional to:

$$Cond \propto \frac{1}{l^2}$$

(34)

Thus as more elements are used and the element length (l) decreases, the matrix becomes ill-conditioned and results from the LQR routine will become less reliable.

A second problem associated with classical finite element models is a problem of non-uniqueness. From finite difference theory it is known that rotation can be estimated from discretized displacements as:

$$v_i^{'} = \frac{v_{i+1} - v_{i-1}}{2l} + O\left(l^2\right)$$

(35)

In Eq. 35, $v_i^{'}$ is the nodal rotation and v_i's is the nodal deflection. The truncation error, which is of order l^2, will decrease as the element size (l)
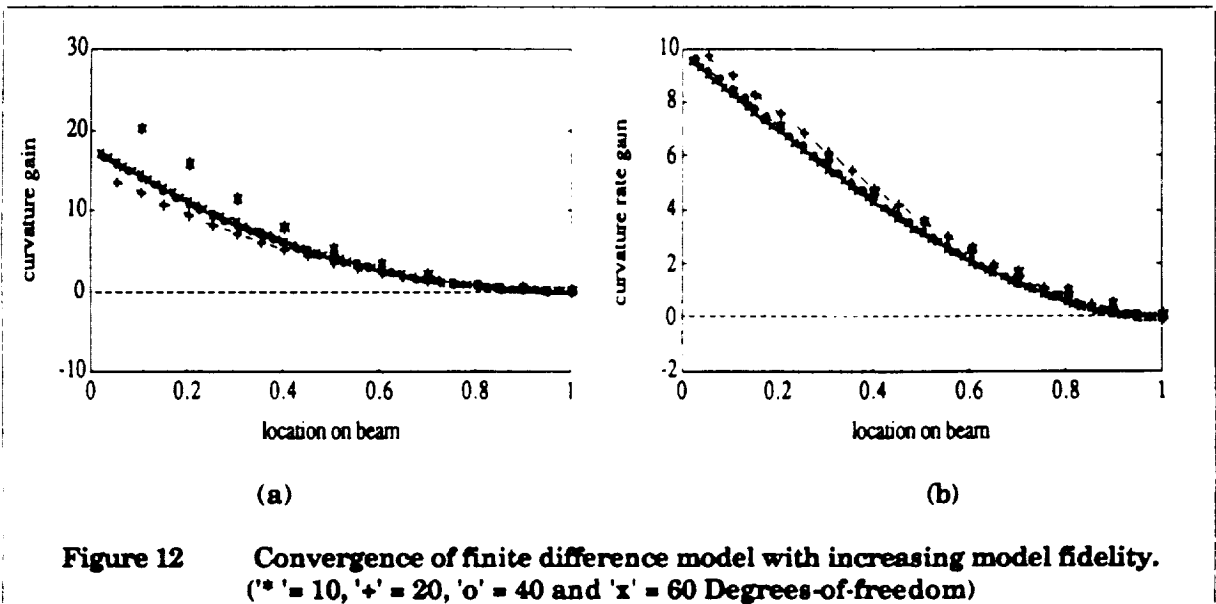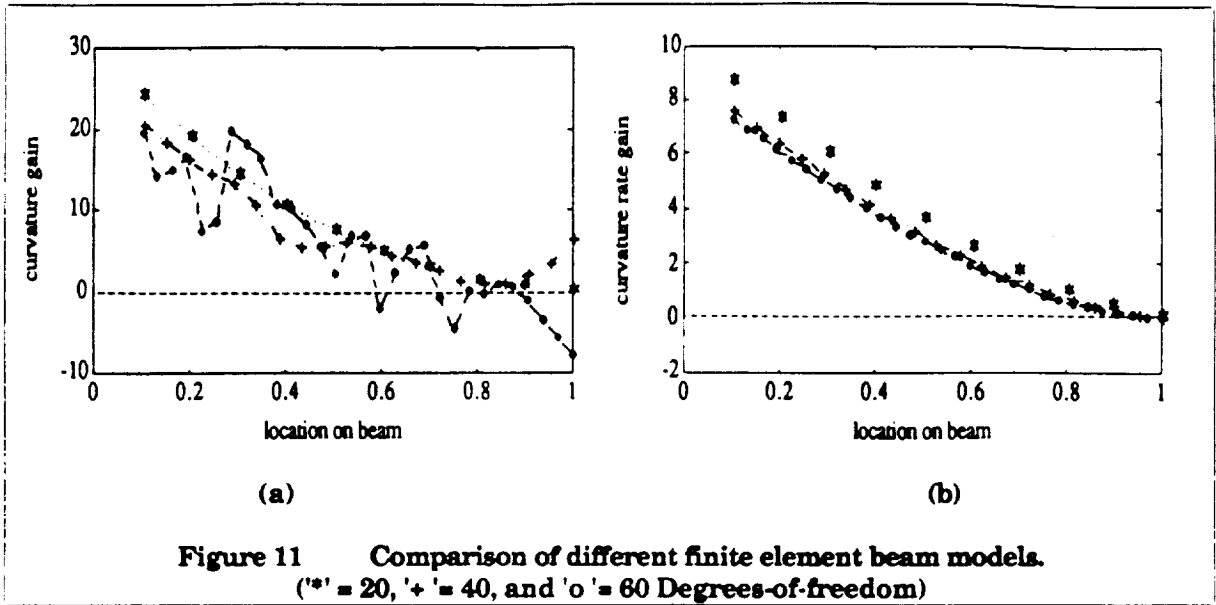
decreases, indicating that the finite element nodal rotations (v_i') can be expressed as linear combinations of the nodal displacements (v_i) with increasing accuracy. The manifestation of this problem lies in the interpretation of the feedback gains calculated by the LQR algorithm. Given that the nodal rotations may become linearly dependent on the nodal displacements (or vice versa), the gains obtained by the LQR algorithm may yield an optimal solution but the displacement and rotation gains may not be unique.

These two problems are investigated by comparing the results of two discretized models used to solve the reference cantilevered beam example. The first model is the classical finite element beam model, while the second is a second order accurate finite difference model. In the finite difference mode, the stiffness term in the governing differential equation (Eq. 6) is approximated by:

$$EIv_i^{'''} = EI\left[\frac{v_{i+2} - 6v_{i-1} + 4v_i - 6v_{i-1} + v_{i-2}}{l^4}\right] + O\left(l^2\right) \tag{36}$$

The effects of ill-conditioning and non-uniqueness are investigated by comparing the results of models in which the fidelity of the model is increased by increasing the number of nodes. Both these models should exhibit the ill-conditioning problem since the finite difference model also has a conditioning number that will increase (deteriorate) as the element size decreases since the conditioning number is approximately $1/(l^2)$ [10]. The finite difference model, however, should not exhibit the non-uniqueness problem associated with the finite element model. These conclusions are supported by the results of the investigation. Although not shown, both the models exhibit ill-conditioning problems and the Riccati solver failed to yield a solution for a model with 40 nodes (or 80 degrees-of-freedom) for the finite element model and 80 degrees-of-freedom for the finite difference model. However, the finite element model may exhibit the non-uniqueness problem as the fidelity of the model is increased. In Fig. 11 the distribution of curvature gains becomes erratic as the number of nodes are increased above 10. The finite difference model on the other hand, as shown in Fig. 12 does not exhibit this behavior. Even with these erratic gains, the closed loop finite element models are stable with identical closed loop poles for the first five modes. This observation leads to the conclusion that this behavior may be due to the non-uniqueness problem associated with these elements.

Note that the slow convergence to the "infinite" shape of the finite difference model is due to the method in which the point moment is applied to the structure. An applied point moment is achieved by applying appropriate forces to nodes neighboring the node to which the moment must be applied.

(a)

(b)

Figure 11 Comparison of different finite element beam models.
(' * ' = 20, '+ '= 40, and 'o '= 60 Degrees-of-freedom)

(a)

(b)

Figure 12 Convergence of finite difference model with increasing model fidelity.
(' * '= 10, '+' = 20, 'o' = 40 and 'x' = 60 Degrees-of-freedom)

24

An Additional Numerical Example

An additional numerical example involves the control of the relative transverse displacement between the tip and the middle of the beam. This state penalty has the form

$$q\left(v_{tip} - v_{middle}\right)^2 = q\left(v_{tip}^2 - 2v_{tip}v_{middle} + v_{middle}^2\right) \tag{37}$$

For this example, the scalar q is unity.

Figure 13 shows the discrete gains. Again, the displacement and rotation gains are rather erratic. However, the curvature and curvature rate gains are smooth. Figure 14 shows the continuous feedback kernels. While the curvature rate kernel has a shape similar to that in the previous example, the curvature kernel now undergoes a change in sign. All the curves seem to have an inflection point near the midpoint of the beam $(x=0.5)$.

CONCLUSIONS

A technique has been presented for inferring the exact, spatially continuous LQR feedback solution to the control of structures from the discrete feedback gains derived using finite dimensional structural descriptions. These feedback kernels possess several unique attributes. First, it has been shown that feedback of the state functions can be transformed to equivalent feedback of other state functions. This aids in implementation because the feedback can be derived in terms of the state function that is most easily measured. Area averaging sensors provide one means for implementing these spatially continuous feedback kernels. Second, these continuous sensors can eliminate spatial aliasing. Spatial aliasing is one of the primary causes of spillover in structural control. Third, all of the feedback computation can be effectively performed by an area averaging sensor.

The research presented in this paper must be seen as the first step in an attempt to formulate and implement full state feedback for infinite order structural systems. Several issues must be resolved before this approach can be considered a viable alternative to reduced order controllers. For example: the accuracy with which the area averaging sensors must match the desired kernel must be investigated. Robustness of this control approach must be determined and the theory must be demonstrated in the laboratory. The researchers are presently working on these topics and plan to implement an infinite order controller on a cantilevered beam using the actuator and performance metric presented in the reference example.
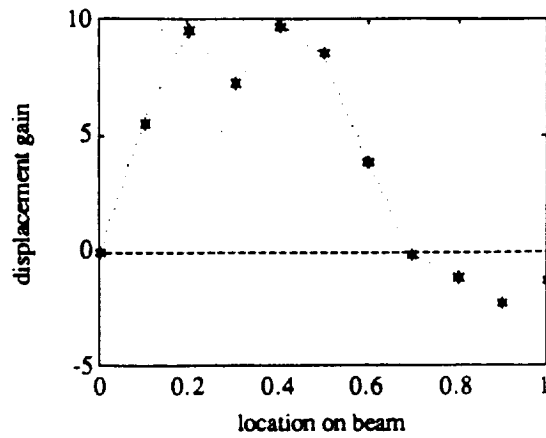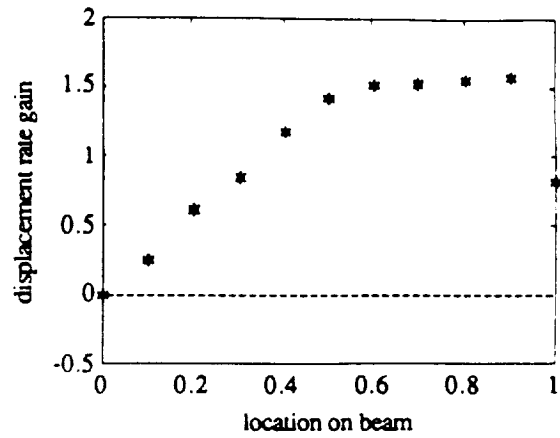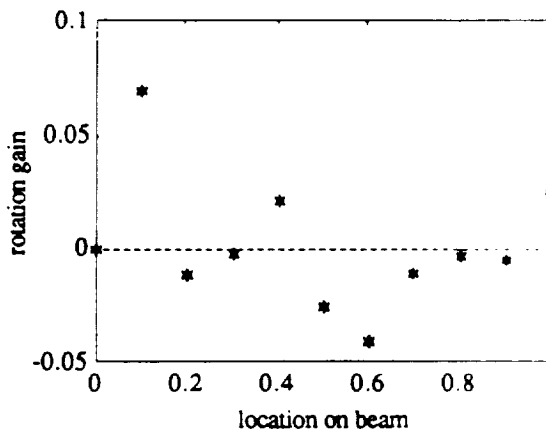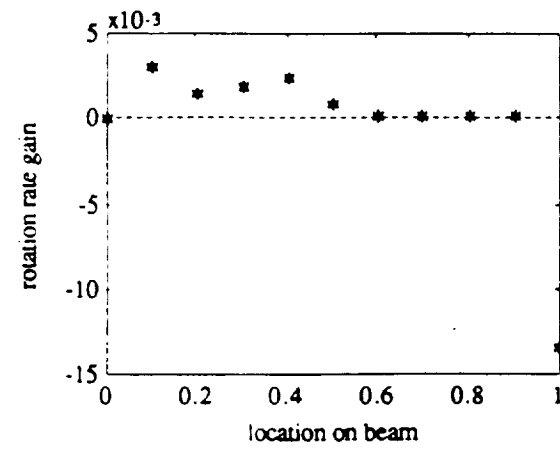
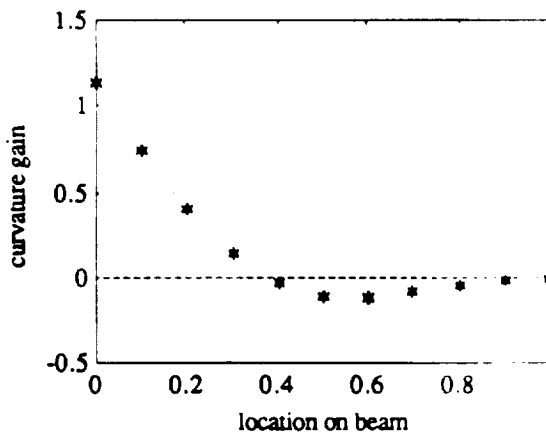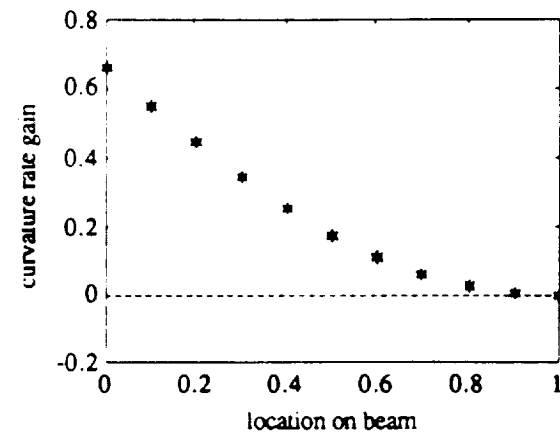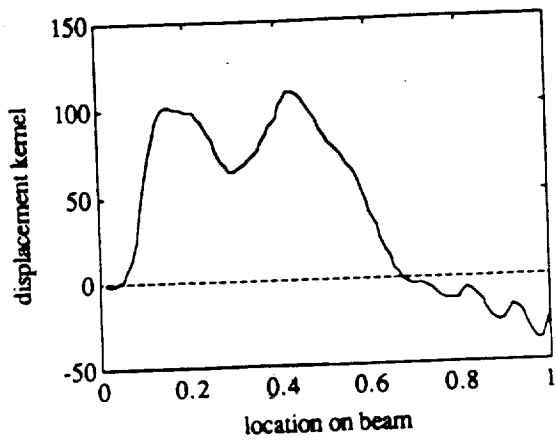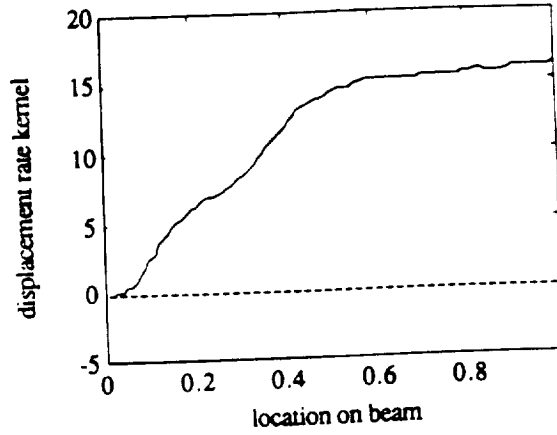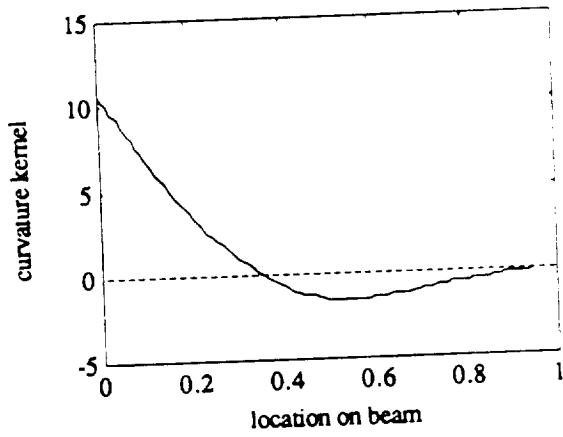Figure 13. Discrete gains at nodal positions along the structure for controlling relative displacement between the tip and midpoint. The individual windows show gains for (a) displacement, (b) displacement rate, (c) rotation, (d) rotation rate, (e) curvature and (f) curvature rate.
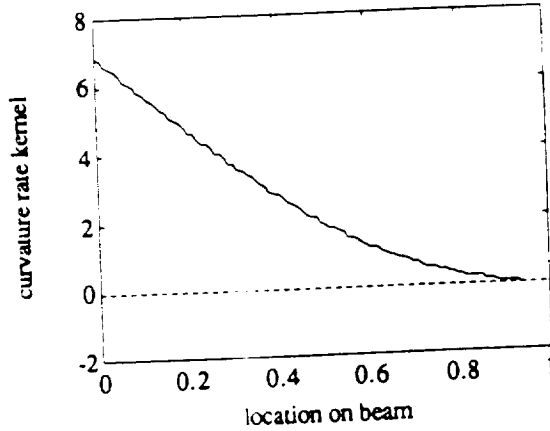
Figure 14. Spatially continuous feedback kernels as a function of location along the beam for controlling relative tip displacement. The individual windows show the kernels for (a) displacement, (b) displacement rate, (c) curvature and (d) curvature rate.

REFERENCES

1. Kwakernaak, H and Sivan, R., *Linear Optimal Control Systems*, John Wiley and Sons, Inc., New York, 1972.
2. de Luis, J., Crawley, E.F. and Hall, S.R., "Design and Implementation of Optimal Controllers for Intelligent Structures Using Infinite Order Structural Models," Space Systems Laboratory Report No. 3-89, M.I.T., Cambridge, MA, 1989.
3. Lee, C. K., "Piezoelectric Laminates for Torsional and Bending Modal Control: Theory and Experiment," PhD Dissertation, Cornell University, Ithaca, NY, 1987.
4. Lee, C. K., Chiang, W. W. and O'Sullivan, T.C., "Piezoelectric Modal Sensors and Actuators Achieving Critical Damping on a Cantilever Plate," *Proc. of the AIAA/ASME/ASCE/AHS/ASC 30th Structures, Structural Dynamics and Materials Conference*, Mobile, AL, April 3-5, 1989, pp. 2018-2026.
5. Miller, S.E., Hubbard, J., "Theoretical and Experimental Analysis of Spatially Distributed Sensors on a Bernoulli-Euler Beam," Charles Stark Draper Laboratory Report C-5953, Cambridge, MA, 1987.
6. Collins, S.A., Notestine, R.J., Padilla, C.E., Ramey, M., Schmitz, E. and von Flotow, A.H., "Design, Manufacture, and Application to Space Robotics of Distributed Piezoelectric Film Sensors," Proceedings of the 31st AIAA/ASME/ASCE/AHS/ASC Structures, Structural Dynamics and Materials Conference, Long Beach, CA, April 2-4, 1990, Paper No. AIAA-90-0949, pp. 1899-1906.
7. Miller, D. W., Collins, S. A. and Peltzman, S. P., "Development of Spatially Convolving Sensors for Structural Control Applications," Paper # AIAA-90-1127, Proceedings of the 31st AIAA/ASME/ASCE/AHS Structures, Structural Dynamics, and Materials Conference, Long Beach, CA., April 1990, pp. 2283-2297.
8. Bailey, T., Hubbard, J. E., "Distributed Piezoelectric-Polymer Active Vibration Control of a Cantilevered Beam," *Journal of Guidance, Control and Dynamics*, Volume 8, Number 5, Sept. 1985, pp. 605-611.
9. *KYNAR Piezo Film Technical Manual*, Pennwalt Corp., Valley Forge, PA, 1987.
10. Strang, G., *Linear Algebra and Its Applications*, Second Edition, Academic Press, New York, 1980.

on a structure in order to modify its dynamic behavior to meet its performance requirements. Unfortunately, active control introduces the possibility of exciting the structure in an unstable manner making it critical that either confidence in the prediction of on-orbit behavior be improved or the types of tests required for *qualification* be identified.

Before proceeding with a discussion of the experimental approach to *developing* qualification procedures, it is necessary to present the rationale that lead to MACE. After all, conducting experiments on-orbit, even those which are performed on the STS middeck, is technically risky, expensive, requires extensive planning, and produces less data than would be obtained in a comparable ground experiment. The program must clearly exploit the unique aspects of the on-orbit environment in order to justify its conduct.

The objective of this paper is to portray the rationale for conducting this type of flight experiment and to pose the scientific questions to be addressed through this research. Additionally, the test article will be described, along with the ground and on-orbit experiment support equipment. This paper concludes with a discussion of planned on-orbit activities.

OBJECTIVES AND RATIONALE

The goal of MACE is to develop a well verified set of CST tools that will allow designers to either be able to predict on-orbit behavior or allow sufficient versatility in the design to allow identification and tuning of the structure on-orbit. A number of different options exist for deriving this set of tools. The first and least expensive is to rely on analysis for the design and qualification of spacecraft which incorporate CST. Unfortunately, this approach is far less than satisfactory. The scientific literature is riddled with examples of both closed and open-loop experiments whose performance varied greatly from that predicted by state-of-the-art analytical methods. The reasons behind this are varied. Often the structural or sensor/actuator characteristic which contributes to this performance degradation is not the next detail that would have been included in the analytical model. Its existence is usually not predicted but instead is discovered through experimentation. This experience illustrates that analysis alone is not sufficient.

The question that next arises is what sort of testing needs to be performed, along with analysis, in order to *develop* an effective and efficient spacecraft *qualification* procedure. Four different options exist. Listed in ascending order from lowest to highest cost and complexity, they are: ground-based open-loop experiments, ground-based closed-loop experiments, on-orbit open-loop experiments and on-orbit closed-loop experiments.

Ground-based open-loop testing is the simplest type of experimental program that can be carried out to verify the validity of analytical models. It is an absolutely necessary step, since the quantities that are most required for closed-loop control design are exactly those which are hard to predict analytically. For example, structural modal frequencies can be predicted using numerical methods with a relatively high degree of accuracy. Conversely, modal damping values are extremely hard to predict analytically on large complex structures where many energy dissipation mechanisms are present. Unfortunately, closed-loop controllers for

structures usually require accurate knowledge of the modal damping because damping determines stability margins and therefore performance. This problem is exacerbated in structures that are lightly damped, such as LSS.

It is easily concluded, therefore, that ground-based open-loop testing is essential to quantify the accuracy of analytical models. However, these tests by themselves are not sufficient to validate the appropriateness of an analytical model or the performance of a closed-loop system. Skelton[3] has demonstrated that no measures of accuracy of the open-loop model are sufficient to guarantee stability of a closed-loop system at arbitrarily high gain. This implies that the acquisition of the open-loop model can never be sufficient to predict closed-loop performance. Therefore, ground-based closed-loop testing is absolutely necessary for the successful application of CST to realistic structures.

Since CST structures will be used in the space environment, it is important to investigate whether those characteristics that are present on-orbit and cannot be adequately simulated on earth affect the open and closed-loop tests. In Table 1 various vehicle parameters are listed along with four significant differences that occur between on orbit and ground-based tests. The table indicates that these differences do affect the vehicle parameters.

Table 1   The various structural, kinematic and dynamic parameters that can differ between on-orbit and ground tests.

	Aero/ Acoustic	Suspension	Gravity	Thermal/ Radiation
Stiffness	no	yes	yes	yes
Damping	yes	yes	yes	yes
Mass	yes	yes	no	no
Forcing	yes	yes	no	no
Kinematics	no	yes	yes	no

The important issue is whether the differences in Table 1 cause *regular* or *singular* perturbations to the problem. A regular perturbation is one whose affect on the vehicle parameter disappears as the perturbation is allowed to approach zero. This is in contrast with a singular perturbation whose presence substantially modifies the vehicle parameter even as the perturbation approaches zero. If the perturbations are regular, then they can be modelled and the results from the ground-based tests can be more easily used to predict on-orbit behavior. However, they may still have a very substantial, although predictable effect on the structural parameter. For example, small changes in the plant can often lead to large changes in the modal damping or in the mode shapes, two quantities that have a direct effect on closed-loop stability and actuator and sensor performance. Therefore, if the plant is highly sensitive to regular perturbations due to influences listed in Table 1, it is probably necessary to conduct open-loop on-orbit testing. If the perturbations are singular, it is essential to conduct open-loop testing on-orbit in order to identify and adjust for these perturbations.

The only issue that now remains to be addressed is whether on-orbit closed-loop testing is still required. The answer to this question depends on whether any singular perturbations are identified during the on-orbit open-

loop experiments, or whether any regular perturbations cause significant unpredictable changes in the plant. If the answer to either of these questions is "yes", then on-orbit closed-loop testing is essential.

A preliminary analysis does not reveal any singular perturbations arising from one of the four sources shown in Table 1. Non-convective potential aeroacoustic equations do not give rise to singularities, nor do conservative fields such as gravity. So long as suspension devices are passive or collocated active, they do not introduce singularities. Since the thermal/radiation terms only affect otherwise symmetric stiffness and damping parameters, they also do not give rise to singular perturbations.

However, a situation in which a regular perturbation can have significant effect on the closed-loop performance of the structure can be easily imagined. The stiffness added by a suspension system, even if small, can change the modal structure. Additionally, for an articulated test article, a suspension system could introduce an unexpected kinematic constraint. Gravity can change preload on a joint, and hence damping. Gravity will also cause otherwise straight members to curve, causing significant changes in the modal structure, such as nonplanar coupling of modes. Therefore, while no singular perturbations have been identified, there are a number of regular perturbations which can cause significant changes in the plant that could result in control performance being degraded.

Therefore, the conclusion that is reached is that ground-based open and closed-loop testing is not sufficient for the verification of CST technology. At a minimum, on-orbit open-loop testing would need to be conducted to test for the presence of any singular perturbations, or any significant regular perturbations. If these perturbations are found to exist, then on-orbit closed-loop testing becomes essential as argued by Skelton. If they are not present, then the closed-loop tests might still be needed if a suitable ground-based performance metric or disturbance environment is unobtainable, or, more likely, if the additional cost of conducting the closed-loop experiments were incremental.

Having demonstrated the likely necessity of on-orbit closed-loop testing, a test article on which to perform the experiments must now be selected. A survey of proposed future spacecraft was undertaken and an evaluation was made on which type of spacecraft exhibit the most requirements for CST and which were most limited by earth-bound testing.[4,5] Some of the spacecraft types that were considered included two point alignment occulting instruments, multipoint alignment interferometric devices, shape control of reflective surfaces, flexible manipulators, and multipayload platforms. This latter type was selected because the large angle motions of the payloads stress state-of-the-art suspension devices and because of its applicability to missions of near term interest.

Proposed missions which will use this type of spacecraft include low and geosynchronous platforms in the Mission to Planet Earth, the evolutionary International Space Station, and the planetary orbiting platforms of the Exploration Initiative. As these platforms become larger and more complex, the propensity for individual on-board controllers to interact

with each other and with the bus attitude control system will grow. This propensity is exacerbated by increasing payload mass fraction associated with larger instruments and robotic devices, decreasing structural bus stiffness associated with larger platforms, increasing authority of the controllers associated with tighter pointing and positioning requirements, and the increasing need to reject disturbances which originate at other payloads. This rationale makes clear the need to develop a well verified set of CST tools. This development must include:

1. The development of a comprehensive analytical CST framework for the design and analysis of controlled multibody platforms. This analysis begins with an understanding of how flexibility influences the pointing and tracking performance of multibody platforms, and must be able to include the influences of suspension and gravity for use in correlating with ground test results, and to exclude the influence of suspension and gravity for use in predicting on-orbit results.

2. The validation of the analytical framework by comparison with a set of ground based experiments with a test article which incorporates the essential physical characteristics of a multibody platform. This test will, of necessity, include the influence of gravity and suspension, and will be typical of the preflight ground testing of an actual platform.

3. The validation of the analytical framework by comparison with a set of on-orbit zero gravity experiments which eliminate the influence of gravity and suspension.

The specific criteria which will determine experiment success of MACE are the identification of the regular (and, if they exist, singular) perturbations in the dynamics which occur as a result of the change from one to zero gravity, and the production of the data for the final validation of the analytical framework. The ultimate result of MACE will be a well verified modelling capability for the controlled structures design and qualification of future multibody platforms, and a detailed understanding of the parametric tendencies in vehicle dynamics, geometry and performance requirements, which cause the zero gravity closed-loop behavior to differ from the one gravity results. This capability can be exploited by future spacecraft designers to either obtain confidence in the on-orbit performance of their CST spacecraft before they are deployed, or to design enough versatility into the spacecraft in order to accommodate any unexpected deviation between ground and on-orbit behavior.

EXPERIMENTAL APPROACH

The fulfillment of the basic objective of the MODE 2 program requires two steps. First, the research must validate the analytical framework for the design and analysis of controlled multibody platforms by comparison with a set of *ground based* experiments on a test article which incorporates the essential physical characteristics of envisioned multibody platforms. Second, the research must also validate the analytical framework by comparison with a set of *zero gravity* experiments with a test article similar to that used in the ground tests. These objectives necessitate two aspects of the experimental approach: the capture of the essential physical characteristics of multibody platforms in the design of the MACE test article, and the performance of

3

meaningful tests which validate the analytical framework through a coherent on-orbit and ground test program.

Capturing the Essential Physics

To arrive at the essential physical characteristics of multibody platforms, one must consider the vehicle architecture of the missions which are envisioned by the international space community.[6] In such platforms, the payloads and articulating appendages each have pointing or positioning requirements, and corresponding attitude sensors, pointing gimbals and control systems. The spacecraft structural bus is flexible and has its own attitude control system. The simulation of this vehicle architecture, in its associated operational environment, necessitates a test article with the following attributes:

- a test article designed with the appropriate multiple scaling laws to allow it to fit in the middeck, yet preserve the essential performance requirements of a full scale test article,
- the incorporation of at least two gimballing payloads to enable the implementation of multiple interacting control systems with independent objectives,
- the incorporation of two rigid payloads, representative of compact but high mass fraction devices, and a flexible appendage, interchangeable with one payload, representative of an articulating appendage such as a robotic servicer,
- a sufficiently flexible structural bus such that flexible resonances lie within the controller bandwidth,
- a sufficiently flexible structural bus which, when suspended even from state-of-the-art suspension devices, exhibits a degree of suspension coupling, gravity stiffening and droop,
- a sufficiently low structural damping so that the test article is representative of structures incorporating typical aerospace materials,
- and a sufficiently complex geometry so that the test article undergoes full 3-D kinematic and coupled flexible motion further stressing state-of-the-art suspension systems.

In order to develop the appropriately refined CST tools, representative test objectives with appropriate disturbances and performance metrics must be used.[7] The tests that will be carried out as part of MACE include pointing and tracking of single and multiple payloads. For each experiment run, performance will be measured in the presence of random broadband disturbances, which originate on the structural bus, and narrowband disturbances due to the planar and non-planar slewing of a second payload.

The performance metrics of all the closed-loop tests will be derived from inertial angular rate data obtained from bi-axis gyroscope packages mounted on the payloads. Specifically, the performance metrics for the various tests are stability (i.e., RMS 2-axis angular position about pointing line of sight or tracking reference profile), jitter (i.e., RMS 2-axis angular rate about pointing line of sight or tracking reference profile), slew response time (i.e., time required to complete maneuver) and percent degradation of stability and jitter from single payload performance (i.e., quantification of multiple interacting control performance).

Different types of controllers, both linear and nonlinear, will be implemented on the MACE test article depending on the performance objective and payload amplitude. Three families of controllers will be used during the on-orbit test. One family will be identical to those used in the ground test. This family will explicitly identify the differences in one-gravity and zero-gravity performance. The second family will be those which analytically corrected beforehand for the absence of suspension and gravity effects. This family will explicitly verify the ability to model the known differences between ground and flight and identify the importance of unexpected perturbations. The third family will be based upon on-orbit identification of the test article. Between these three families, the objectives of MACE will be met.

Validation of the Analytical Framework

Given a test article which captures the essential physical characteristics of the generic class of multibody platforms, a test program which validates the analytical CST tools must be formulated. Such a program must incorporate both ground-based and zero-gravity testing.

Based upon SERC's previous experience in laboratory active structural control experiments, it was concluded that a challenging yet realistic goal for MACE would be to attempt to improve closed-loop pointing/tracking performance by 40 dB over its open-loop value (Fig. 2). Independent of the absolute level of performance, this level of performance improvement will demonstrate the effectiveness of the controlled structures technology.
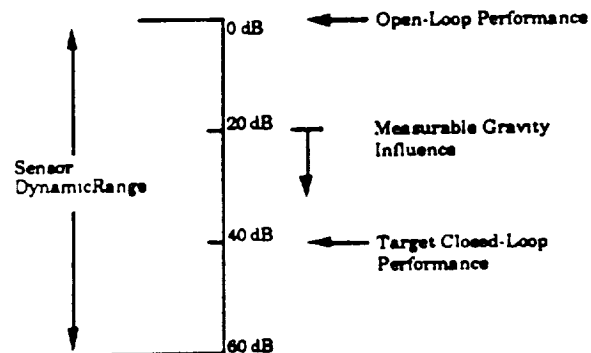
Figure 2   MACE Test Article Requirement

Both the ground testing and on-orbit testing will begin by measuring the open-loop performance. Then the authority of the controller will be increased, and closed-loop performance in the presence of scaled disturbances will be measured. By comparing closed-loop performance as a function of control authority between ground and on-orbit testing, regular (and if they exist, singular) perturbations in the dynamics which occur as a result of the change from one to zero gravity will be identified. To extract maximum benefit from the on-orbit data, it is desirable for these perturbations to begin to manifest themselves at the level of control authority which achieves half of the performance in the 1-g environment (i.e., at 20 dB). In this way, there is a series of tests (i.e., 0 to 20 dB) where ground and orbital results should be similar, and a series of tests (i.e., 20 to 40 dB) where significant deviation might be expected.

Singular perturbations could cause significant deviations throughout the 0 to 40 dB range.

This experimental approach is formulated to study the levels of control authority where the gravity perturbations become important (*i.e.*, the *transition regime*). Testing only at levels below this *transition regime* does not justify an on-orbit experiment. Testing only at levels above this *transition regime* may not yield meaningful data. Valuable information can only be uncovered by testing at levels which span the *transition regime* because these tests gradually reveal the fundamental ways in which the pertinent gravity dependent phenomena perturb the control problem.

Thus the MACE test article and associated tests are representative of an important class of future NASA, ESA, and NASDA missions, and they are designed to exhibit gravity dependent characteristics which become important to closed-loop performance as control authority is increased. By its design, the program exhibits mission applicability, technical relevancy and a fundamental exploitation of the environment unique to the STS system.

POINTING ON A FLEXIBLE STRUCTURAL BUS

A preliminary analysis of the linear pointing problem is presented to illustrate the research approach. In this section, performance degradation due to unmodelled flexibility will be investigated. There are two fundamental questions that need to be answered for the problem of pointing while mounted on a flexible structural bus. They are:

1) *How does unmodelled flexibility degrade payload pointing performance?* and

2) *How are controllers designed and implemented on a modelled flexible bus?*

The first identifies the problem and the second identifies the solution. The actual control analysis tasks that will be used as this research progresses are:

Task 1. Design a controller assuming the structural bus is rigid.

Task 2. Evaluate the performance of this controller on an evaluation model which incorporates flexibility in the structural bus.

Task 3. Use a flexible model to design the active controller using existing pointing and tracking hardware.

Task 4. Allow the flexible model controller to use additional sensors which measure flexible motion of the bus.

Task 5. Allow the flexible model controller to also use actuators to control this flexible motion.

The first two tasks address the first question. The control algorithm derived using the rigid design model in task 1 will be applied, in task 2, to a flexible evaluation model using two different sensor configurations referred to as *localized* and *centralized*, which are depicted in Fig. 3.

In the localized configuration, the inertial attitude of the payload is measured directly by an inertial platform (IP). In the centralized configuration, the inertial attitude of the payload is inferred from the inertial attitude of the structural bus at the IP and a measure of the relative angle at the gimbal. Now, flexibility lies between the payload and the inertial measurement. If the structural bus were rigid the performance using the centralized and localized configurations would be equivalent. In the centralized configuration, however, flexibility in the structural bus can introduce an additional angle between the IP and the end of the structural bus where the gimbal is located. Left unmeasured, this flexibility induced angle can degrade pointing performance.
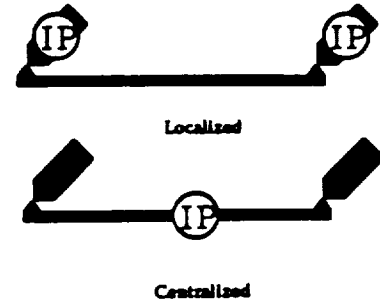

Figure 3 Localized and centralized configurations for impinging design model control laws on the flexible evaluation model

In this paper, only typical section analyses[6] will be dealt with to investigate the manner in which structural bus flexibility degrades payload pointing performance (tasks 1 and 2). The typical section models employ lumped masses and inertias to capture the fundamental physics embedded in the linear pointing problem. Ultimately, these various control design and analysis tasks will be performed on models of increasing complexity.

There are two basic classes of rigid payloads: center of gravity (CG) mounted payloads and non-CG mounted payloads. As will be shown, CG mounted payloads exhibit certain desirable characteristics which make their control significantly easier.

The simplest model which captures the fundamentals of CG mounted payload pointing is the two inertia model shown in Fig. 4. The inertia J_1 represents a structural bus on which an attitude control torque τ_1 is applied. The inertia J_2 represents the pointed payload with the torque τ representing the gimbal torque between the payload and the structural bus. The two angle coordinates θ_1 and θ_2 are the inertial rotations of the structural bus and payload, respectively. This model is used as the rigid control design model.

In the Linear Quadratic Regulator (LQR) formulation the inertial angle of the payload can be penalized to improve payload pointing stability as

$$ J = \tfrac{1}{2}\int_0^\infty \left(x^T Q\, x + u^T R\, u\right)dt \tag{1} $$

$$ x = \begin{Bmatrix} \theta_1 \\ \theta_2 \\ \dot\theta_1 \\ \dot\theta_2 \end{Bmatrix},\ Q = \begin{bmatrix} 0 & 0 & 0 & 0 \\ 0 & v & 0 & 0 \\ 0 & 0 & 0 & 0 \\ 0 & 0 & 0 & 0 \end{bmatrix},\ u = \begin{Bmatrix} \tau_1 \\ \tau \end{Bmatrix} \text{ and } R = \begin{bmatrix} \alpha & 0 \\ 0 & \beta \end{bmatrix} \tag{2} $$

where J is the cost, x is the state vector, Q is the state penalty matrix, u is the control input vector, and R is the

control effort penalty matrix. The feedback solution to the steady-state Riccati equation gives

$$\begin{Bmatrix} \tau_1 \\ \tau \end{Bmatrix} = -\begin{bmatrix} 0 & 0 & 0 & 0 \\ 0 & \sqrt{\dfrac{v}{\beta}} & 0 & \sqrt{2J_2}\sqrt[4]{\dfrac{v}{\beta}} \end{bmatrix}\begin{Bmatrix} \theta_1 \\ \theta_2 \\ \dot\theta_1 \\ \dot\theta_2 \end{Bmatrix} = -Gx \qquad (3)$$
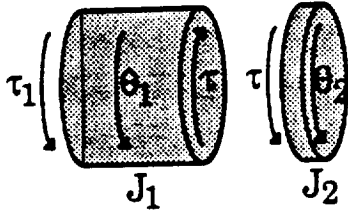

Figure 4 Rigid design model for CG mounted payload.

Notice that this control only feeds the inertial payload angle and angular rate to the gimbal torque. No attitude control or measurement of the structural bus attitude are required. The control stiffens and damps the payload motion with respect to a particular orientation in inertial space by using the structural bus as a reaction inertia. The closed-loop eigenvalues are

$$s = 0, 0, \frac{1}{\sqrt{2J_2}}\sqrt[4]{\frac{v}{\beta}}(-1 \pm i) \qquad (4)$$

As might be expected, the pointing mode is in a Butterworth pattern with damping equal to 70.71% of critical.

The closed-loop variance of the payload inertial angle about its nominal line-of-sight can be calculated assuming a steady-state additive white noise disturbance. This disturbance is assumed to be present either at the attitude control location or at the payload gimbal. Other work has looked at stability bounds associated with unmodelled flexibility.[9]

The variance is found by solving the closed-loop Lyapunov equation relating the driving noise covariance matrix V to the state covariance matrix X.

$$XA_{cl}^T + A_{cl}X = -V \qquad (5)$$

where A_{cl} is the closed-loop state dynamics matrix of the plant. The variance of the payload inertial angle is

$$\frac{\Phi_{\tau_g \tau_g}}{2\sqrt{2J_2}\left(\dfrac{v}{\beta}\right)^{3/4}} \qquad (6)$$

Notice that the variance is only a function of the additive gimbal torque noise ($\Phi_{\tau_g\tau_g}$). If there is no gimbal torque noise, the variance is zero. The attitude control noise does not disturb the payload because the motion of the payload is decoupled from the motion of the structural bus. The cost is proportional to the gimbal torque noise and decreases with increasing payload inertia and increasing control authority (v/β).

Having derived the controller using the design model, it is now possible to investigate how unmodelled flexibility degrades the pointing performance by impinging the control law (Eq. 3) upon a flexible evaluation model (Fig 5).
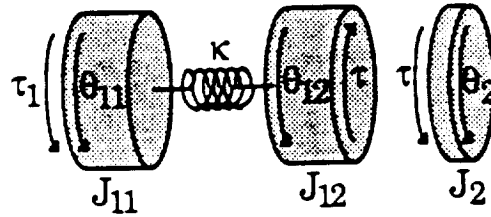

Figure 5 Flexible evaluation model for CG mounted payload

Assuming that θ_2 can be measured directly (the localized configuration), the closed-loop eigenvalues are given by

$$s = 0, 0, \frac{1}{\sqrt{2J_2}}\sqrt[4]{\frac{v}{\beta}}(-1 \pm i), \pm i\sqrt{\frac{J_{11}+J_{12}}{J_{11}J_{12}}\kappa} \qquad (7)$$

Notice that the rigid body mode is unaffected since the attitude control torque is not used. The poles associated with the pointing mode are equivalent to the poles for the system without flexibility (Eq. 4). The remaining poles are identical to the flexible mode poles of the open-loop system.

Control spillover exists because the gimbal torque disturbs the structure. However, there is no observation spillover because there is no measurement of any motion associated with the mismodelled structure. The measurement of the payload inertial motion is reconstructed exactly and therefore eliminates spillover. The closed-loop variance of the payload angle is identical to that in Eq. 6. Therefore, flexibility does not degrade the pointing performance when local inertial measurements are fed back to a CG mounted payload.

In the centralized configuration, the inertial angle of the payload equals the inertial angle of J_{12} (θ_{12}) plus the gimbal angle (θ_G). However, the inertial angle of the structural bus is assumed to be measured at the attitude control location on J_{11}. Therefore, the flexibility induced rotation $\theta_{12} - \theta_{11}$ is not measured.

The closed-loop variance of the payload's inertial angle is shown in Fig. 6a (for gimbal noise) and Fig. 6b (for attitude control noise). The horizontal axis represents the ratio v/β as the cost of the control (β) is decreased. The solid line in Fig. 6a is the variance, from Eq. 6, for the rigid design model subject to gimbal noise. The dashed line represents the variance associated with the flexible evaluation model. Notice that feedback from inertial measurements at the attitude control location to the gimbal, across the flexibility, couples the flexible motion to the payload angle causing performance degradation which increases with increasing control authority (v/β).

In the case of attitude control noise (Fig. 6b), only the variance associated with the evaluation model is shown because the variance associated with the rigid design model (Eq. 6) is zero. This variance is now nonzero because the centralized configuration fails to account for the flexibility induced angle between the inertial platform and the location where the gimbal is attached
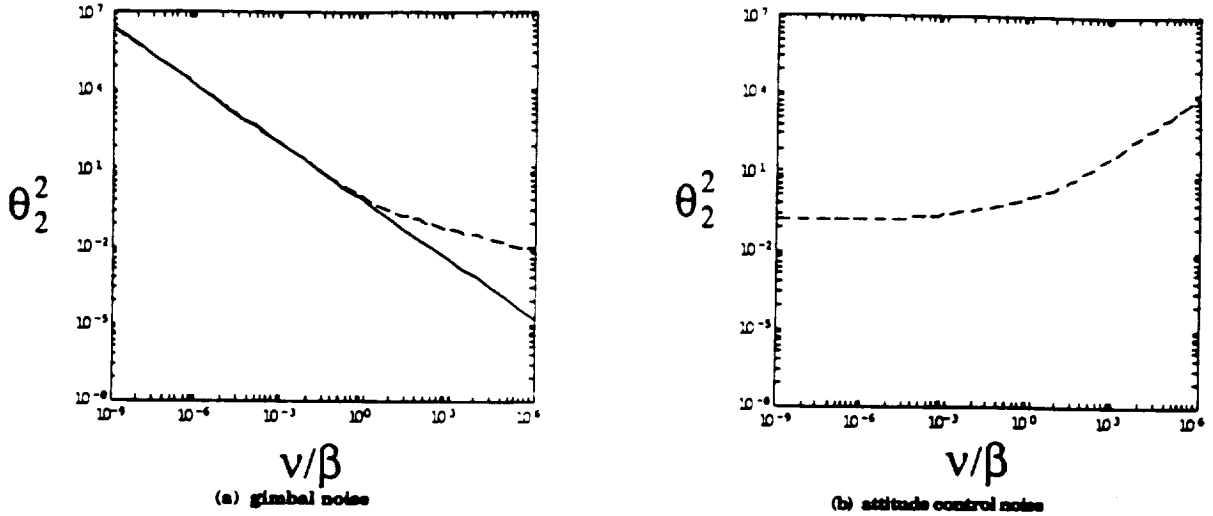
6

$$\theta_2^2 \qquad \theta_2^2$$

$$\nu/\beta \qquad \nu/\beta$$

(a) gimbal noise   (b) attitude control noise

Figure 6 Variance of CG mounted payload under white noise applied at the gimbal and attitude control location for centralized configuration. The values of $J_1=1$, $J_2=0.5$ and $\kappa=1$ were used.

$(\theta_{11}\text{-}\theta_{12})$. This flexibility-induced angle corrupts the estimate of the payload inertial angle. Since the payload attempts to track this estimate, this error causes a degradation in pointing performance.

Multibody platforms can also have non-CG mounted payloads attached to the structural bus. The non-CG mount couples rotation (θ_1) of the structural bus with rotation θ_2 of the payload. The rigid control design model is shown in Fig. 7.
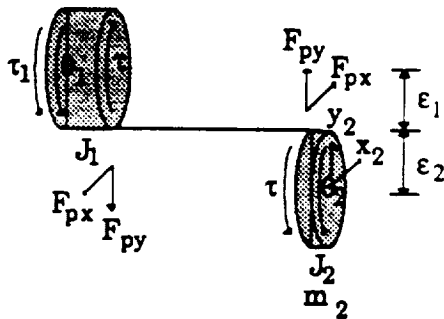
Figure 7 Rigid design model for non-CG mounted payload

Penalizing the inertial angle of the payload gives the feedback as

$$\begin{Bmatrix} \tau_1 \\ \tau \end{Bmatrix} = - \begin{bmatrix} 0 & \frac{1}{\alpha}b_{32}\sqrt{\frac{\nu}{\mu}} & 0 & b_{32}\sqrt{\frac{2}{\mu}}\sqrt[4]{\frac{\nu}{\mu}} \\ 0 & \frac{1}{\beta}b_{33}\sqrt{\frac{\nu}{\mu}} & 0 & \frac{1}{\beta}b_{33}\sqrt{\frac{2}{\mu}}\sqrt[4]{\frac{\nu}{\mu}} \end{bmatrix} \begin{Bmatrix} \theta_1 \\ \dot{\theta}_2 \\ \dot{\theta}_1 \\ \dot{\theta}_2 \end{Bmatrix} = -Gx$$

(8)

where

$$\mu = \frac{1}{\alpha}b_{32}^2 + \frac{1}{\beta}b_{33}^2$$

(9)

$$b_{32} = -\frac{m_1 m_2 \varepsilon_1 \varepsilon_2}{den}$$

$$b_{22} = \frac{(m_1 + m_2)J_1 + m_1 m_2 (\varepsilon_1 + \varepsilon_2)}{den}$$

(10)

$$den = (m_1 + m_2)J_1 J_2 + (J_1 \varepsilon_2^2 + J_2 \varepsilon_1^2)m_1 m_2$$

(11)

Notice that while both the attitude control and gimbal actuators are used, only the inertial states of the payload are measured. The closed-loop poles are given by

$$s = 0, \ 0, \ \frac{1}{\sqrt{2}}\sqrt[4]{\nu\mu}(-1\pm i)$$

(12)

Again, the Butterworth pattern exists. The control now requires feedback to the structural bus' attitude control torque since angular motion of the structural bus and payload are coupled in open-loop.

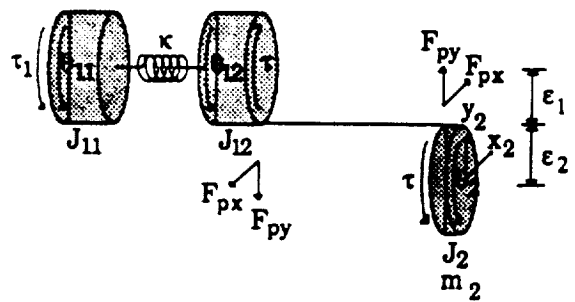This control can be impinged upon a flexible evaluation model such as the one shown in Fig. 8.

Figure 8 Flexible evaluation model for non-CG mounted payload.

Flexible motion of the structural bus, caused by gimbal and attitude control torque noise, perturbs the angle of the payload. This results in both control and observation spillover.

Impinging the feedback in Eq. 8 on the evaluation model in Fig. 8, using the localized configuration, gives the results shown in Figs. 9a and 9b. The overlaid solid and dashed lines in Fig. 9a show that the level to which gimbal noise disturbs the payload angle barely changes

between the design and evaluation models. The solid curve in Fig. 9b shows the variance of the payload angle associated with the design model (Fig. 7) in the presence of attitude control torque noise. Notice that since structural bus rotation couples with payload rotation, attitude control noise now disturbs the payload in the design model. The dashed line in Fig. 9b shows the variance associated with the evaluation model. Excitation of the flexible motion couples with payload rotation to cause performance degradation, even though a localized configuration is used. The evaluation model is more susceptible to performance degradation as a function of control authority when the noise is introduced at the attitude control location than when it is introduced at the gimbal. This is because the unmodelled flexibility lies between the disturbance and the payload thereby frequency shaping the disturbance on the payload in the former case, while the disturbance is impinged directly upon the payload in the latter.

Figures 9c and 9d show the variance caused by the two different noise sources for the non-CG mounted systems when a centralized configuration is used. In both figures, the solid curves represent the variance associated with the design model. The dashed curves are the variances of the evaluation model. Notice in Fig. 9c

that the variance associated with gimbal noise deviates from that for the design model at high levels of control authority. This was not the case for the localized configuration (Fig. 9a). For the case of attitude control noise (Fig. 9d), deviation again occurs between the variance of the design and evaluation models. Note, however, that for either noise source the variance eventually increases with increasing control authority and that the level of control authority which minimizes the variance depends on which noise source exists.

The above analysis has served to illustrate the degradation in performance that can occur when controllers designed using rigid models are applied to flexible spacecraft. The open-loop coupling of the unmodelled flexibility to the payload angle makes the non-CG systems more susceptible to performance degradation than the CG system. Centralized configurations exhibit more deviation from the expected rigid body performance than localized configurations because the feedback paths are closed across the flexibility thereby coupling the unmodelled flexibility to payload motion. However, centralized configurations are programmatically advantageous because the various payloads share an expensive common resource, the IP.
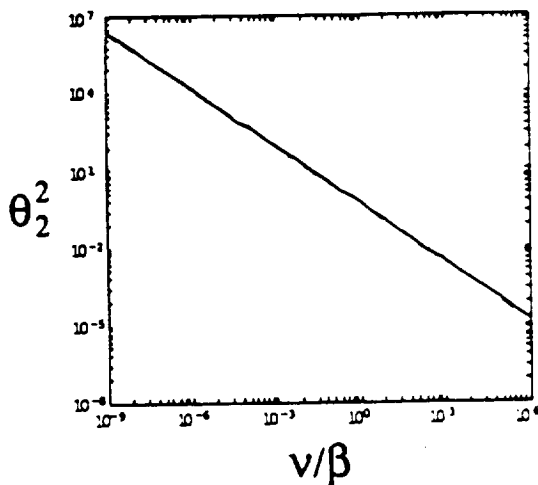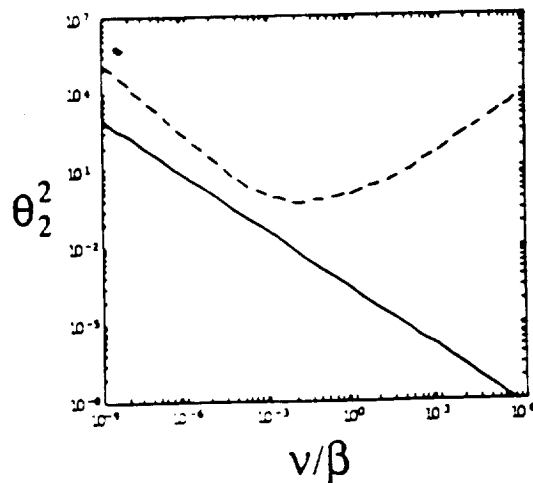

(a) localized config. gimbal noise
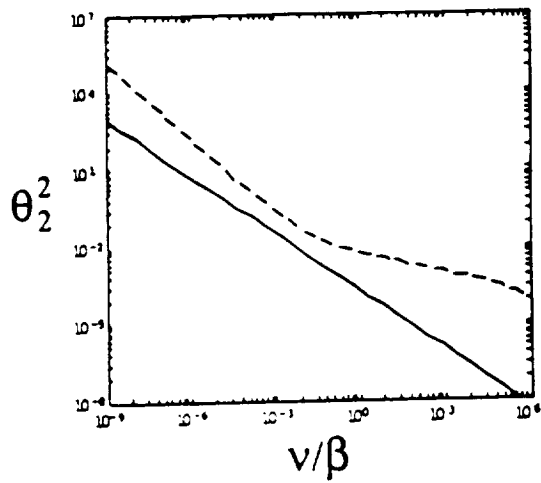
(b) localized config. attitude control noise
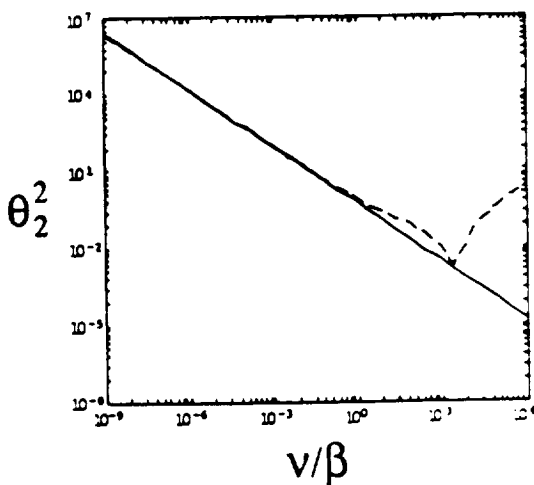
(c) centralized config. gimbal noise

(d) centralized config. attitude control noise

Figure 9   Variance of non-CG mounted payload under white noise applied at the gimbal and attitude control location for localized and centralized configurations. $J_1=1, J_2=5, \alpha=1, c_1=2, c_2=1, m_2=1$

C-2

EFFECT OF GRAVITY ON THE POINTING AND TRACKING PROBLEMS

Multibody platforms were chosen as the reference mission configuration not only because they characterize many proposed missions but also because they are arguably the most susceptible to gravity influences. The essence of the on-orbit phase of the MACE program is to identify and characterize these influences. To this end, a set of sample problems was selected each of which captures a different type of gravity perturbation. The objective of this line of research is to analytically predict the manner and degree to which these influences perturb the closed-loop control problem.

Gravity will cause changes between dynamics measured on the ground and on-orbit. These perturbations can be grouped in two broad categories: those resulting directly from the presence of the gravity field, and those which are a result of the mechanical suspension system required for 1-g tests. These are illustrated in Fig. 10. The first category includes: modal coupling which occurs due to the static sag of a structural member, gravity stiffening (in tension) or destiffening (in compression) of structures along the gravity vector, and dynamic buckling which occurs when the structural members deform transversely to the gravity vector. The second category of problems includes: added stiffness and mass of the suspension system, added damping of the suspension system, and modal coupling of the suspension dynamics with the test article. All of these influences result in perturbations of the system frequencies, damping and mode shapes which can fundamentally alter the stability and performance of a controller, and must be taken into account in design.

GROUND-BASED ENGINEERING MODEL TESTBED

The initial configuration of the MACE test article is shown in Fig. 11. It consists of a segmented straight tubular bus with a two axis pointing/tracking payload at each end. An active, strain-inducing segment is located along the bus. The MACE test article will have a closely coupled set of flexible modes with a fundamental bending frequency below 2 Hz. This is done through the choice of material (Lexan) and geometry of the bus.

A segmented design of tubular members connected by universal joints was chosen as the bus structure for a number of reasons. First, it provides an evolutionary test article since it is straightforward to modify its geometry to represent more complex structures. It is also possible to add and change the locations of passive and active members. These include piezoelectric members and members with a high level of passive damping. Discrete devices such as torque wheels, accelerometers and proof mass actuators can be attached at the joints.

The overall length of the test article is approximately 1.5 m. The MACE engineering model (EM) node provides for attachment of the members through the MACE joint and provides a standard hole pattern for attachment of the payloads, inertial platforms and other instrumentation. Each member is .4 m in length and 25.4 mm in diameter. Four members are used in the MACE initial configuration.

Two types of payloads are currently envisioned:

- *Pointing/tracking.* These payloads are mounted to the bus through a two axis motorized gimbal mount. The payloads are rigid, and capable of 120° motion in two axes.

- *Flexible appendage.* This payload consists of a flexible, instrumented boom mounted on a two axis motorized gimbal. The gimbal is capable of 120° motion in two axes, and the fundamental frequency of the flexible boom is less than the fundamental frequency of the bus structure (<2 Hz).

The DC torque actuators in the gimbals will be used to align the payloads or to sweep them through a pre-determined tracking profile. Rate gyroscopes located on the rigid pointing/tracking payloads and the flexible appendage will provide a measure of the inertial angular rate of the payloads for feedback and performance measure. The gimbal motors will have integrated encoders.

In addition to the sensors and actuators located on the payloads, the following sensors and actuators will also be used:

- *Torque Wheels.* A set of three torque wheels is situated at the center node of the structural bus. The purpose of these torque wheels is to provide both three axis attitude control and structural control.
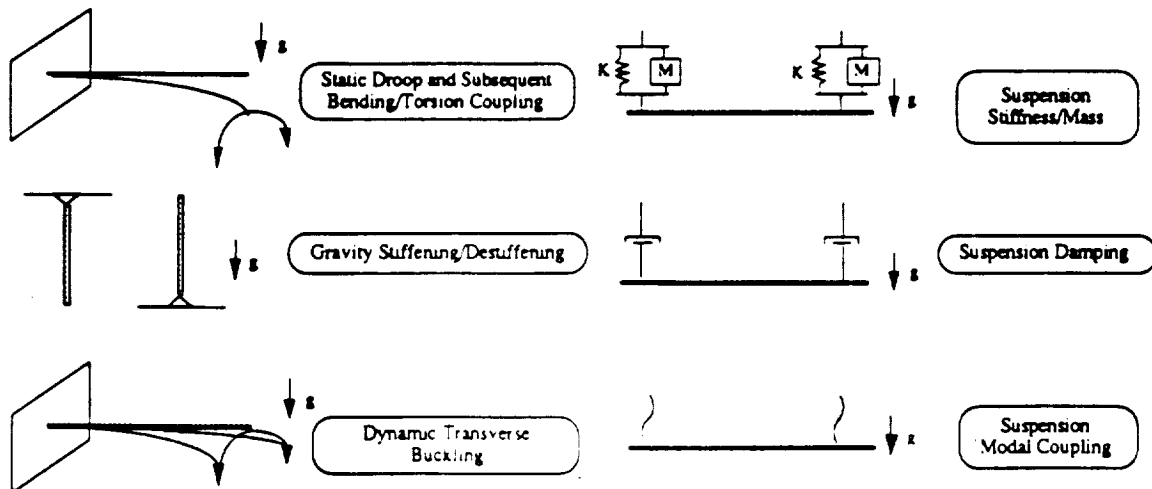

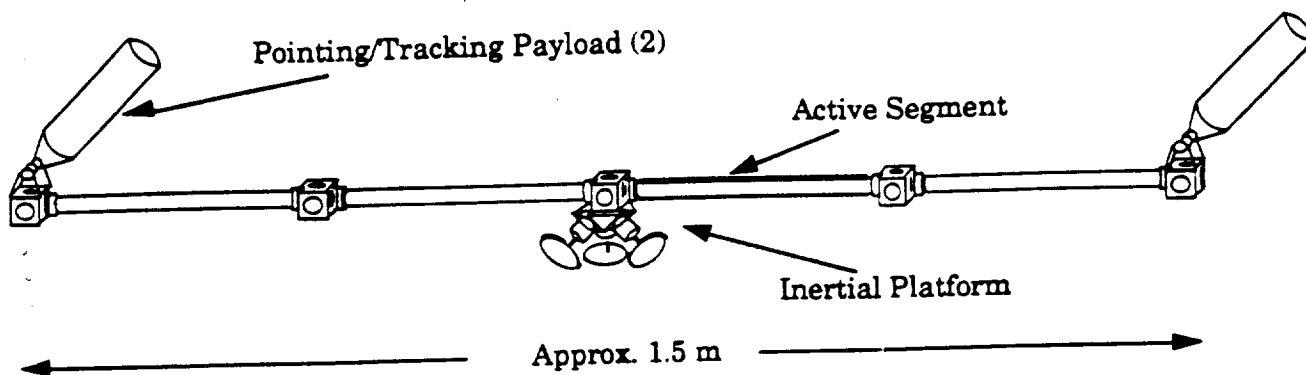Figure 10 Sample problems illustrating the effect of gravity on structures

Pointing/Tracking Payload (2)

Active Segment

Inertial Platform

Approx. 1.5 m

Figure 11   Initial configuration for multibody platform test article

* *Active Member.*   The MACE active member consists of a square Lexan rod with piezoelectric ceramics mounted on the sides. It will be capable of bending about two axes. The member will be instrumented with surface bonded strain gauges.

* *Rate Gyroscopes.*   A set of three rate gyroscopes will be collocated with the torque wheels forming an inertial attitude control platform.

Additional sensors such as strain gauges, accelerometers, *etc.* can be placed along the test article as required by the various control algorithms.

Given the recognized need to perform closed-loop ground-based tests, the question arises as to how does one best approximate the boundary conditions of space. Required is a system which will support the payload weight while having a minimal impact on the test article dynamics.   A zero spring rate pneumatic/electric suspension device from CSA Engineering Inc. of Palo Alto, California will be used to support the test article in 1-g.   The suspension system will have a 63.5 mm maximum vertical stroke, a maximum payload of 17.4 kg, and will use displacement and acceleration feedback.

FLIGHT TESTBED

The MACE flight testbed consists of (1) the Experiment Support Module (ESM), which contains all experiment electronics in one standard middeck locker, and (2) the MACE test article which is stowed in a second middeck locker (Fig. 12).[10]   The primary difference between the ground-based EM and the flight testbed will be the manner in which the various active components of the test article will be connected to each other and to the ESM.   Electrical connections along the bus will be accomplished by modifying the EM joint to provide simultaneous electrical and mechanical connections. This will be accomplished by inserting a multipin electrical connector inside the joint. Wiring will run inside the hollow Lexan members. Finally, the test article will be connected to the ESM through a single umbilical which will also attach to a test article node. This greatly simplifies on-orbit assembly time thereby maximizing testing time.

Experiment Support Module (ESM)

Much of the MODE 2 ESM will be identical to the MODE 1 ESM, utilizing many similar or identical components. These will include the ESM support frame, data storage device, analog circuit card cage, and the

majority of the computer system.   Modifications will include the addition of a real time high speed control computer, and downlink/uplink capability.   All MACE data acquisition, storage, signal processing and signal generation will be performed by Payload Systems SensorNet Experiment Computer.

The purpose of the downlink/uplink is to allow on-orbit identification, downlink of identified parameters and uplink of new control algorithms in the event that unexpected behavior occurs.   Downlink will be accomplished through data interleaving on the STS video channel. Uplink will be accomplished through the STS Text and Graphics System (TAGS).

Required Resources

MACE resource requirements are summarized in Table 2 below.

Table 2   MACE Resource Requirements Summary Table

ESM		
Weight	54 lbs.	
Volume, operational	1 Middeck Locker	
Volume, stowed	1 Middeck Locker	
Power requirement	113 Watts @ +28 VDC	
Telemetry	Downlink/uplink	
Crew activities	Set-up, operations	
Data processing	Performed by ESM	
MACE Test Article		
Weight	54 lbs.	
Volume, operational	30" x 8" x 60"	
Volume, stowed	1 Middeck Locker	
Power requirement	15 Watts	
Crew activities	Set-up, operations	

Flight Operations

MODE-2 calls for operation by the crew on two separate days.   Procedures require configuration, activation and operation of MODE-2 by one crew member during a normal eight hour work period. If the test sequence proceeds flawlessly, the crew task for all the MACE tests will involve assembling the test article in a predetermined configuration, running open-loop identification tests over a specified frequency range, and beginning closed-loop operations. The probable testing scenario would be to excite the structure using a pre-determined excitation profile with one of the on-board actuators, then, after steady-state has been achieved, to
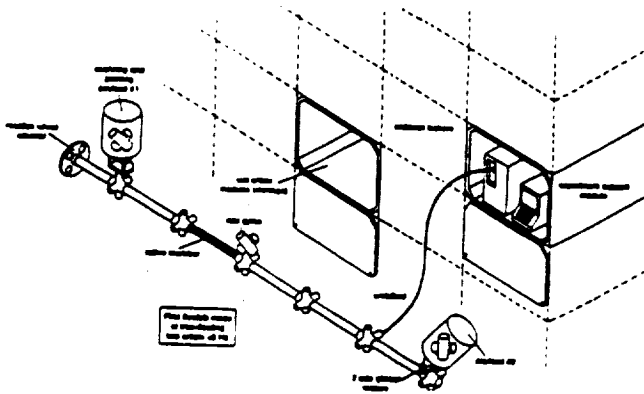
10

Figure 12. The MACE test article deployed on the STS Middeck

initiate the active control using low gain values. Assuming no instabilities are found, the performance metric and sensor outputs will be recorded and the experiment can be repeated with higher gain values, until all the predetermined gains have been implemented or an instability is reached. Testing would proceed to additional configurations or control algorithms as time permits. This procedure is illustrated in Fig. 13.
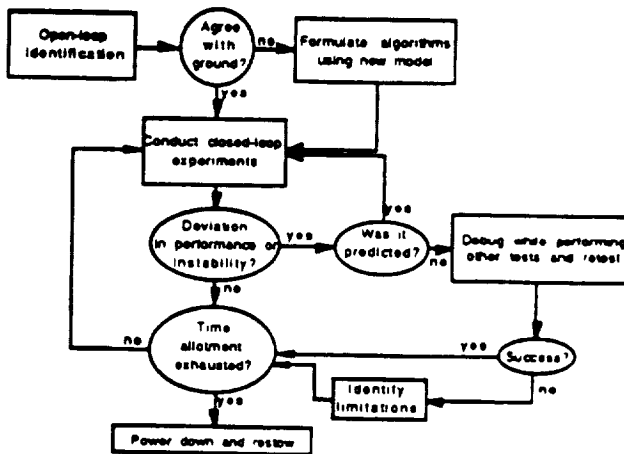

Figure 13 Testing procedure decision flowchart

After the first day, video and video encoded data will be transmitted to the ground to be analyzed by the PI team and new control algorithms, if necessary, will be uplinked to the crew prior to the second day's operation. While no real time communications, audio or video, are required, this infrequent access to the STS video and TAGS system will be necessary for up/down link activities.

CONCLUSIONS

There is a clear need to develop an effective and efficient analytical and test procedure for qualifying CST spacecraft. The goal is to determine the degree to which gravity perturbs the closed-loop performance of Large Space Structures which cannot be fully or accurately tested on the ground.

The MODE-2 program, using the MACE test article, is designed to develop this qualification procedure by formulating a set of CST design and qualification tools and validating these tools through extensive ground and on-orbit testing. By conducting these open and closed-loop tests using a relatively inexpensive test article, a cost effective preliminary search can be performed to identify the presence of gravitational perturbations to the control problem. The specific criteria which will determine experiment success are the identification of the regular (and, if they exist, singular) perturbations in the dynamics which occur as a result of the change from one to zero gravity, and the development of validated analytical and experimental CST tools needed to insure the operational success of a CST spacecraft.

REFERENCES

1. Crawley, E.F., Miller, D.W., van Schoor, M., de Luis, J., "Middeck 0-Gravity Dynamics Experiment (MODE): Project Plan," Massachusetts Institute of Technology Space Systems Laboratory Report # SSL 9-89, 1989.

2. Crawley, E.F., de Luis, J., Miller, D.W., "Middeck Active Control Experiment (MACE): Phase A Final Report," Massachusetts Institute of Technology Space Systems Laboratory Report # SSL 7-89, 1989.

3. Skelton, R.E., "A Tutorial on Model Error Concepts in Control Design," to appear in International Journal of Control.

4. NASA Space Systems Technology Model, NASA TM 88176, Prepared for the Office of Aeronautics and Space Technology, June 1985

5. Space Station Engineering Design Issues: Report of a Workshop, Irvine, CA Nov. 1988, National Academy Press, Washington, DC, 1989

6. Proceedings of the Workshop on Multibody Simulation, JPL D-5190, Jet Propulsion Laboratory, April 1988.

7. Laskin, R.A., Sirlin, S.W., "Future Payload Isolation and Pointing System Technology," Journal of Guidance, Control and Dynamics, Vol. 9, No. 4, pp 469-477.

8. Miller, D.W., Jacques, R.N., de Luis, J., "Typical Section Problems for Structural Control Applications," Paper # AIAA-90-1225, presented at the Dynamics Specialist Conference, Long Beach, CA, April 1990.

9. Spanos, J.T., "Control-Structure Interaction in Precision Pointing Servo Loops," J. of Guidance, Control, and Dynamics, Vol. 12, No. 2, pp. 256-265, March-April 1989.

10. MACE Hardware Design Document, MACE-1-900, MIT Space Engineering Research Center, May, 1990.